The Fabrication Of High Packing Density Ceramic Powder Beds For The Three Dimensional Printing Process

by

Michael Anthony Caradonna

B.S., Mechanical Engineering
The University of Notre Dame, 1995

Submitted to the Department of Mechanical Engineering in
Partial Fulfillment of the Requirements for the Degree of

Master of Science in Mechanical Engineering

at the

Massachusetts Institute of Technology

June 1997

Signature of Author _____
Department of Mechanical Engineering
May 23, 1997

Certified by _____
Emanuel M. Sachs
Professor of Mechanical Engineering
Laboratory for Manufacturing and Productivity
Thesis Supervisor

Accepted by _____
Ain A. Sonin
Chairman of Graduate Committee

The Fabrication Of High Packing Density Ceramic Powder Beds For The Three Dimensional Printing Process

by

Michael A. Caradonna

Submitted to the Department of Mechanical Engineering on May 23, 1997 in Partial Fulfillment of the Requirements for the Degree of Master of Science in Mechanical Engineering

ABSTRACT

Three Dimensional Printing is a solid freeform fabrication process which can be used to create parts directly from CAD models. In the past, the 3DP process has been used to create structural ceramic parts using spray dried powders. Although fully dense parts have been made, it has been necessary to use an iso-static pressing step before sintering. Such a step has many disadvantages such as causing anisotropic shrinkage, warping, and lower part yields. In order to eliminate the iso-static pressing step, an improved process which uses slurries instead of dry powders makes it possible to fabricate green parts with high enough packing density that printed parts can be sintered directly.

The main effort on the slurry-based 3DP process focused on fabricating powder beds which had high packing density and good surface finish. Three possible approaches were investigated: repeated tape-casting, spray deposition, and ink-jet printing of slurry.

The repeated tape-casting approach was able to produce powder beds with excellent surface finish (4 μm peak-to-peak roughness), high packing density (60-65% of theoretical), and small pore size (typically 0.3 μm or less). Such powder beds can also be fabricated relatively quickly since a layer is produced in a single pass. However, this approach can be difficult to control.

The spray deposition approach was determined to be a poor candidate for layer fabrication. Besides having relatively rough surface finish, nozzle performance problems make it impossible to build thick powder beds with good dimensional control.

The ink-jet printing approach has produced large powder beds up to 8.5 mm in height. For such powder beds, good surface finish (8 μm local peak-to-peak roughness) and dimensional control was evident. Ink-jet printed powder beds also have good packing density (55-62% of theoretical) and pore size distribution. One problem with powder beds which have been printed is that velocity ripple in the fast-axis shows up as a height ripple on the powder bed surface (typically 4.5% peak-to-peak). This can be eliminated with improved machine design. The ink-jet printing approach appears to be the leading method of fabricating complex ceramic parts with the slurry-based 3DP process.

Thesis Supervisor: Emanuel M. Sachs
Title: Professor of Mechanical Engineering

Acknowledgments

This thesis is dedicated to my parents, Monika and Francis Caradonna, who have always provided me with the encouragement and support to attain my professional and personal goals. Thank you both for everything.

Although there is one name listed as the author of this work, this document would not have been possible without the help of many people. Although it would be impossible to list everyone who contributed to this work, several people deserve special thanks:

Ely Sachs, for providing guidance and support for the project. I feel that I have learned much more working on 3DP under your tutelage than a mere assemblage of facts. I have learned a great deal about problem solving and that is something I will take with me forever.

Michael Cima, for being a very helpful reference for materials related problems. I know so much about ceramics processing now that maybe I should submit my thesis to the materials science department for a second degree!

Jason Grau deserves special mention. He provided help designing and running experiments, taught me a great deal about ceramics processing, and graciously provided important data and photos for this document. Good luck with finishing your own thesis!

Without the help of the support staff (Dave Brancazio, Jim Serdy, Laura Zaganjori, Fred Cote, John Centorino, Lenny Rigione, and Barbara Layne), this work would have been impossible. Thanks for all your help.

The following students helped run experiments, discuss ideas, or played some other role which helped further my research and deserve special thanks: Satbir Khanuja, Jaedeok Yoo, Bugra Giritlioglu, Scott Uhland, Jooho Moon, John Santini, Ben Wu, P.J. Baker, Jérôme Terrazzoni, and Vedran Knezevic.

Lastly, I would like to thank the students of the 3DP lab who have always been a great help and source of support—in particular, the graduating crowd (P.J., Javier, Gabriel, Jeannie, and Jérôme) whose companionship over the past two years I have enjoyed tremendously. Good luck to you all in your future endeavors.

Support for this project was provided by the DARPA Solid Freeform Fabrication (SFF) program and the 3DP Industrial Consortium.

Table of Contents

List of Figures

List of Tables

Chapter 1 : Introduction

1.1: Introduction

Almost all machines rely on common engineering materials such as aluminum or steel for structural or high temperature applications. They are easy to machine and process, relatively inexpensive, and they have been studied extensively so their behavior and limits are well understood. However, as increasing demands are made on reducing weight, increasing efficiency, or decreasing thermal expansion, the physical properties of these common materials can be a limiting factor in designs. Many designers are now seeking other materials which offer improved properties such as increased strength, lower weight, or higher temperature resistance. Although there is no such thing as a "super" material which offers improved performance in all areas, a specialized material might have excellent properties which are critical for a particular application. Ceramics are one class of materials which promise to offer many advantages in certain applications.

For instance, jet aircraft engines currently use steel ball bearings. However, to get increased thermal efficiency, higher temperatures are required. The use of steel can limit designs both because of its relatively high thermal expansion coefficient and relatively low melting temperature. As a result, there has been interest in using ceramic ball bearings which are lighter, can withstand higher temperatures, higher compressive stresses, and have a lower thermal expansion coefficient.

There is also interest in using ceramics for wear applications. One such application of ceramics is as a bearing surface in semiconductor manufacturing equipment. Semiconductor manufacturing processes are very sensitive to any dust or particulates because any foreign matter can disturb the very fine features which are used in integrated circuits (as of this writing, 0.18 μm is state-of-the-art). As a result, designers need to be careful that the machines do not generate wear particles. Traditional metal-on-metal bearings can generate a relatively large amount of wear particles. However, using ground ceramic raceways and steel balls, particle generation can be reduced significantly. The reason for the reduction in particles is the fact that ceramics have a surface which has negative skewness (for comparison, steel has positive skewness). This effectively means that there are no sharp asperities on the surface to break off and generate particles. As the feature size of integrated circuits continues to drop, wear particle generation will become an increasing concern. In the future, increased use of ceramic parts for wear applications is one possible way of meeting this increasingly difficult design requirement.

Although structural ceramic parts can offer improved properties over more traditional engineering materials such as steel and aluminum, they have been slow to gain widespread acceptance. This is largely due to the increased difficulty in fabricating structural ceramic parts. Because metals are ductile and are resistant to shock, they can processed using many common manufacturing processes such as machining, stamping, casting, and forming [Kalpakjian, 1992]. Conversely, ceramics are fairly brittle and cannot be processed by any of the previously mentioned techniques. They are typically fabricated using powder metallurgy techniques (dry pressing, powder injection molding, and extrusion), slip casting, iso-static pressing, and tape casting [Reed, 1988].

Most complex structural ceramic shapes are generated using powder metallurgy techniques. In this case, the desired material is ground or chemically processed to create a fine powder. Typically this powder is processed to enhance flowability. This can include operations such as spray drying or adding lubricants to the powder. The powder is then put into a die and pressed to form a green compact. This green compact is then sintered to full density in a furnace to create the final part. The method of using green-pressing dies has a number of drawbacks. The first of these is their expense both in terms of time and money. A complex multi-part pressing mold can take months to build and cost tens to hundreds of thousands of dollars. This is acceptable if large numbers of the desired part are to be built such that the cost of the tool is amortized over thousands of parts. However, if the desired quantity of parts is just one such as when building a special tool or prototype, the fabrication cost is quite significant. A second disadvantage of using green-pressing dies to make ceramic parts is that the geometries which can be made are limited. A third disadvantage of dies is the fact that complex geometries can result in non-uniform densification of the powder during the pressing process. This can result in uneven shrinkage, warping, and porosity in the final part during the sintering stage.

A new process recently developed at MIT called the Three Dimensional Printing Process (3DP) offers the ability to sidestep some of the manufacturing difficulties which have limited the use of structural ceramics. The main advantage of 3DP over traditional powder metallurgy techniques is that it makes it possible to create complex ceramic green parts without a green-pressing die or mold. By eliminating the need for green-pressing dies, the 3DP process makes it possible for designers to consider using structural ceramics in applications both where only a few parts will be needed (such as on a custom machine) and where a complex geometry is necessary (such as a turbine blade with internal cooling passages).

1.2: The Three Dimensional Printing Rapid Prototyping Process

The Three Dimensional Printing process is a solid freeform fabrication (SFF) process which allows parts to be created directly from computer models. Other SFF processes which are commonly used include stereolithography (SLA), selective laser sintering (SLS), laminated object manufacturing (LOM), and fused deposition modeling (FDM) [Yoo, 1996]. These processes all differ from traditional machining since material is added to the desired part as opposed to material removal in milling, turning, and boring. The 3DP process begins with the definition of a three-dimensional geometry using computer-aided design (CAD) software. This CAD data is then post-processed with software which slices the model into many thin layers which are essentially two-dimensional. A real part is then created by the successive printing of these layers to recreate the desired geometry. An individual layer is printed by first spreading a thin layer of powder and then printing binder to glue the powder together in selected regions to create the desired layer pattern. This process is repeated until all the layers have been printed. After printing is complete, the unbound powder is removed leaving a green part with the desired geometry. A diagram which illustrates the 3DP process is shown below in Figure 1.1.

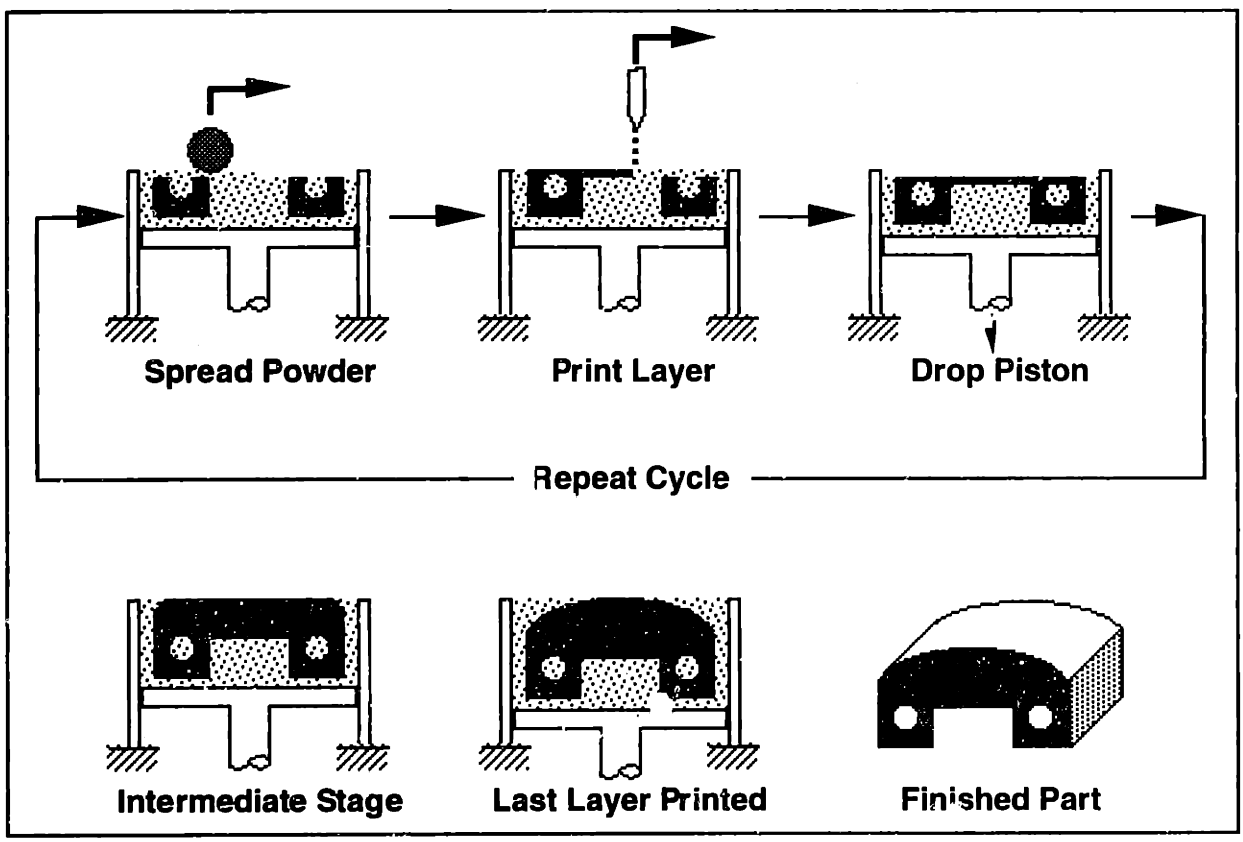

Figure 1.1: The 3DP manufacturing process

Because 3DP is an additive manufacturing process, many geometries are possible which are not feasible with traditional machining such as undercuts and internal cavities. Furthermore, many materials can be used in the 3DP process as long as they can be obtained in the powder form. Currently, work has been done using metals [Michaels, 1992], polymers [Cima, Sachs, Cima, Yoo, Khanuja, Borland, Wu, Giordano, 1994], ceramics [Yoo, Cima, Khanuja, Sachs, 1993], and glass-ceramics [Nammour, 1995]. Using these materials, a wide variety of parts have been produced. This includes the direct printing of metal parts, injection molding tooling, casting shells, and structural ceramics. Figure 1.2 shows a miniature engine block which was fabricated from stainless steel powder demonstrating the ability of 3DP to make complex geometries. Figure 1.3 shows several injection molding tools fabricated using 3DP. The tooling can incorporate conformal cooling channels to decrease cycle time and residual stresses in the part. Figure 1.4 shows a ceramic casting shell for making knee implants along with the resulting part.

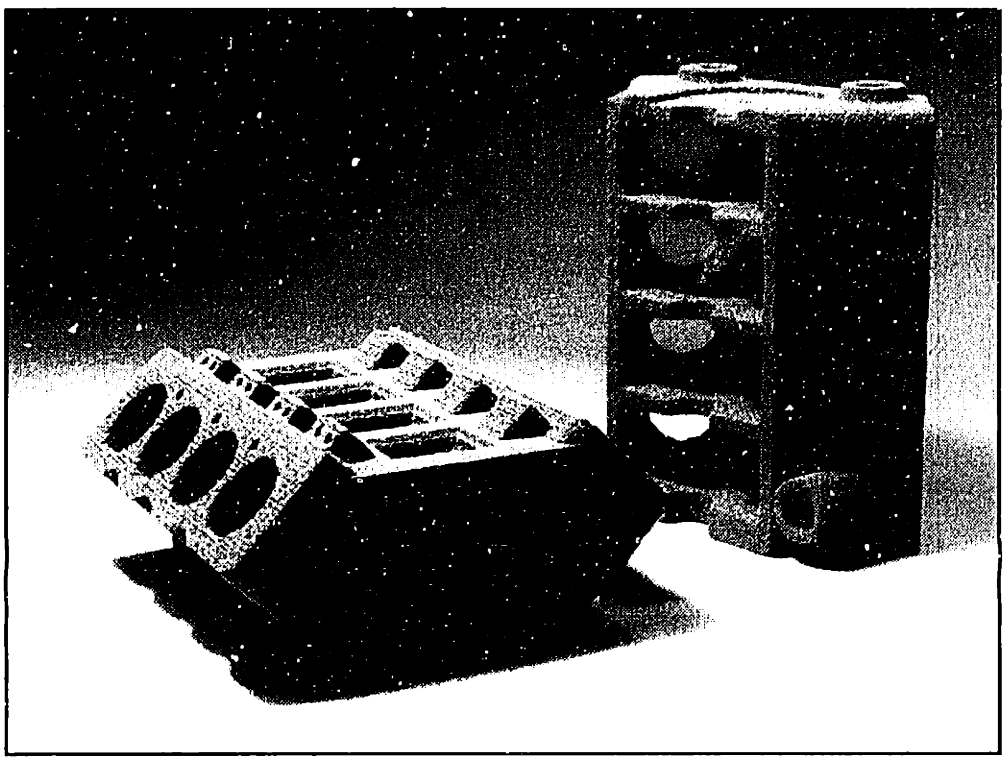

Figure 1.2: 3DP direct metal parts

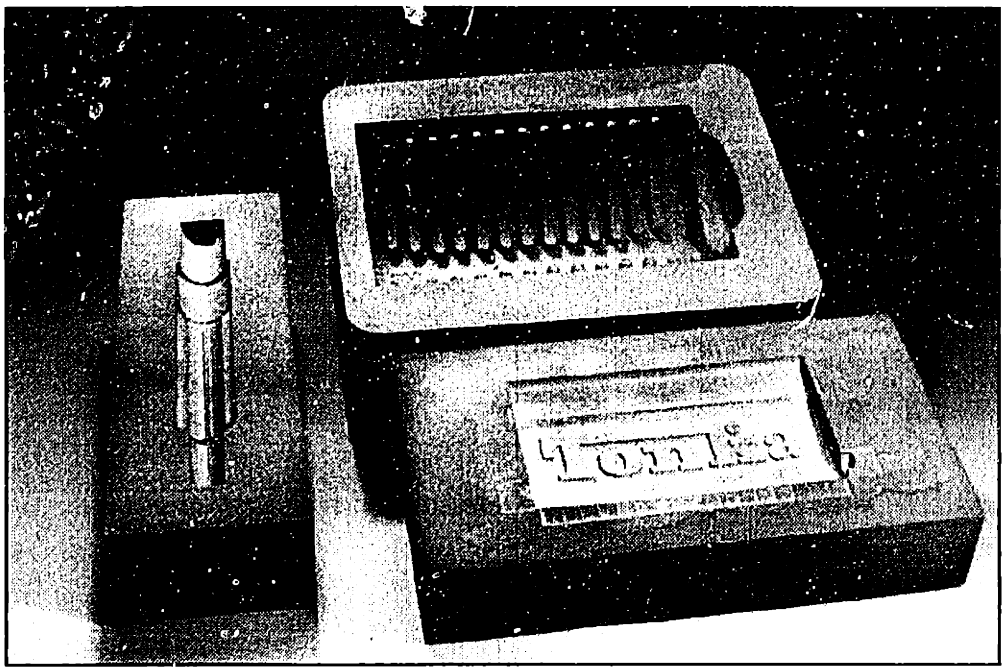

Figure 1.3: 3DP injection molding tools

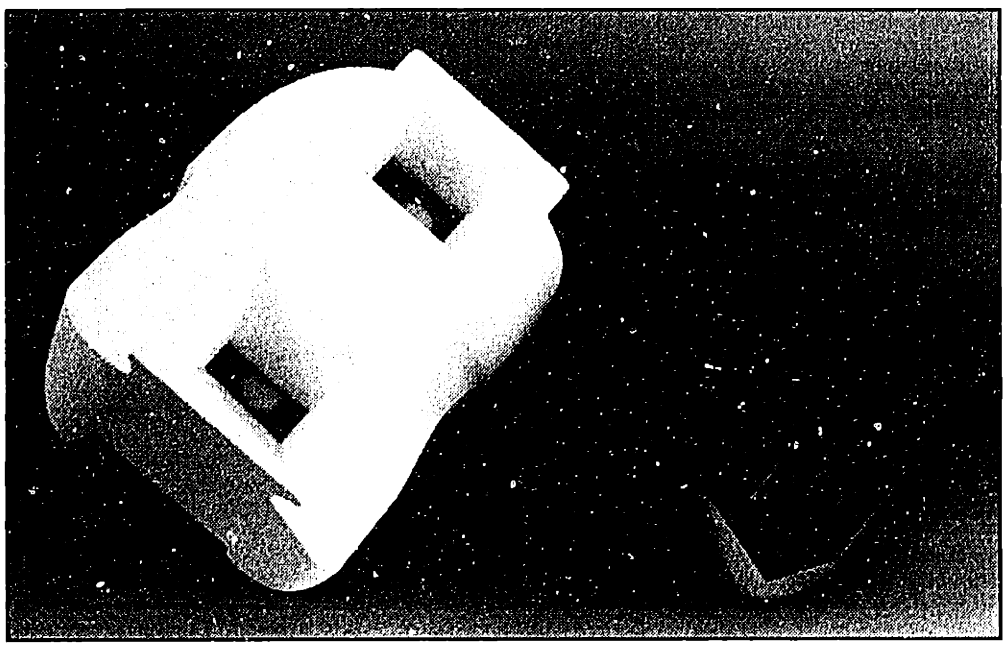

Figure 1.4: 3DP ceramic casting shell for knee implants

Using the 3DP process, it is also possible to make individual parts with regions composed of varying materials (functionally gradient materials). This can be achieved by ink-jet printing different materials into selected regions of an individual layer [Yoo, 1996]. This extra degree of freedom would allow designers to vary the material properties within a single part.

1.3: Previous Work on Fabricating Fully Dense Ceramics

Before the initiation of this research, several areas of structural ceramics had been explored. Most of the research has been focused on building parts by spreading alumina spray dried powders and ink-jet printing an aqueous-based polymer binder such as Acrysol WS-24 (Rhom & Haas, Philadelphia, PA). The spray dried alumina powder is made up of spherical granules typically ranging from 30-100 μm in size [Giritlioglu, 1996]. The granules are actually agglomerates of submicron powder bound together by an organic phase with a typical packing density of about 50% of theoretical [Yoo, 1996]. As a result, the packing density of the resulting green part will be too low to be sintered directly (typically 30 - 35% of theoretical). An iso-static pressing step will be required to increase the green body packing density. After iso-static pressing, alumina green parts fabricated with spray dried powders exhibit packing densities ranging from 59-63% of theoretical depending on whether the cold iso-static pressing (CIP) or the warm iso-static pressing (WIP) process is used [Giritlioglu, 1995]. This is adequate to achieve full density during sintering. With the alumina material system, complex geometries have been produced using such an approach [Giritlioglu, 1995]. An example of an alumina pre-ignition chamber printed using spray dried powder is shown below in Figures 1.5 and 1.6. These figures both show (from left to right) the as-printed green part, the part after the iso-static pressing step, and the resulting fully dense part after sintering.

Figure 1.5: Alumina pre-ignition chambers (photo courtesy Giritlioglu)

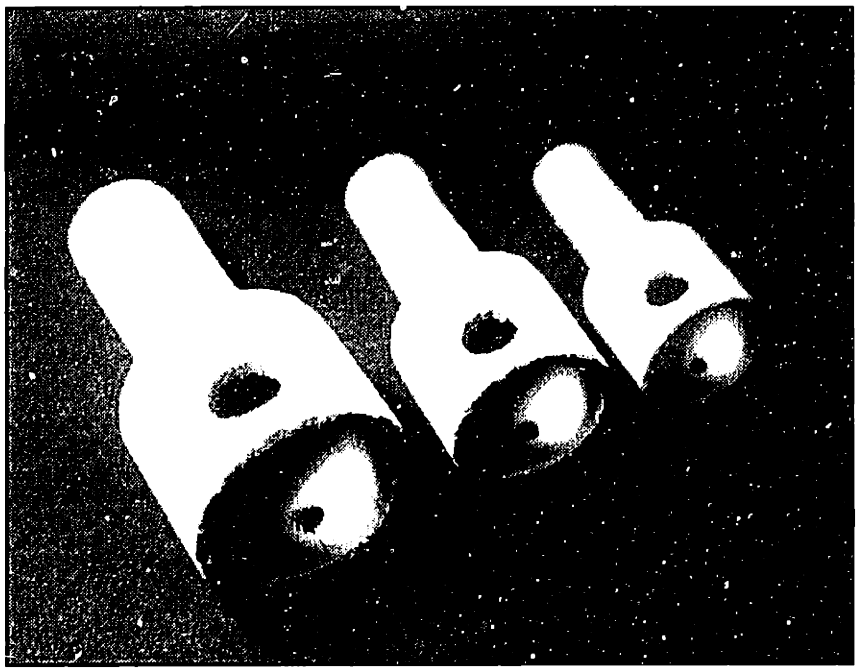

Figure 1.6: Alumina pre-ignition chambers (photo courtesy Giritlioglu)

Simple geometries using tungsten carbide/cobalt (WC/Co) spray dried powders have also been produced (see Appendix A). For this particular case, the resulting green body has a packing density which typically ranges from 25-30% of the theoretical density. Such green parts also require an iso-static pressing step. For the WC/Co spray dried material system, packing densities of about 50% of theoretical were achieved using the CIP step. This was adequate to achieve full density during sintering. Despite the disadvantages of the iso-static pressing step (discussed in the following paragraph), spray dried powders have excellent flowability and spreadability making them well suited to the 3DP process.

Although fully dense ceramic parts can be fabricated using a post-processing step such as CIP or HIP to raise the green density, use of these processes introduces several problems. First of all, before sintering, green parts are quite fragile and easy to damage. Iso-static pressing requires a relatively large amount of part handling. This includes placing the part in a pressing bag, the spring-back shock of the iso-static pressing step, removing the part from the pressing bag, etc. Secondly, the iso-static pressing step can introduce density gradients within the green part. This can cause problems during sintering such as warping and anisotropic shrinkage. This was in fact observed for the WC/Co material system. Anisotropic shrinkage during sintering was greater for parts which were iso-statically pressed than for those which were not. A final disadvantage of the iso-static

pressing step is that it raises production costs (lower part yields, more capital equipment and labor costs, etc.) which can make the use of 3DP printed ceramics economically unattractive when compared to ceramic parts fabricated from more traditional processing methods.

Attempts have been made to eliminate the iso-static pressing post processing step by increasing the printed part packing density. To date, the most feasible concepts which have been proposed have involved using slurries of the desired material to increase the as-printed green density. One possibility which has been suggested involves printing slurry into spray dried granules in order to increase the powder bed packing density [Khanuja, 1996]. Unfortunately, to date it has been difficult to get this to work successfully. Another proposal has involved the fabrication of powder beds entirely from a slurry. This wet powder approach or slurry-based 3DP approach is the main focus of this thesis.

1.4: Scope and Organization of this Thesis

The overall goal of this research was to work on producing fully dense ceramic parts which do not rely on an iso-static pressing step before sintering for the reasons mentioned above. Since the sintering step requires that the green part have a packing density greater than 50% of theoretical, the problem which was the main focus of this thesis was how to produce individual layers which result in powder beds with such packing densities. Along with good powder bed packing density, it was also considered important that the layers should have good surface finish in order to improve part definition, dimensional control, and resulting part surface finish.

This thesis is organized in the following manner. Chapter 2 describes the slurry-based 3DP process and several possible ways of fabricating layers for the process. Chapter 3 looks at the repeated tape casting approach to layer fabrication and reports some initial results. Chapter 4 examines the spray deposition approach to layer fabrication. Chapter 5 looks at the ink-jet slurry printing approach to layer fabrication and gives initial results. Chapter 6 briefly summarizes the results of approaches and suggests directions to be taken in order to actually fabricate complex structural ceramics using the slurry-based 3DP process.

Chapter 2 : The Slurry-Based 3DP Process

2.1: Use of Fine Powders To Fabricate Structural Ceramics

When fabricating structural ceramic parts, it is desirable to use fine powders (1.0 μm and smaller). Use of such fine powders offers several advantages. First of all, the use of fine powders is desirable since it enhances sinterability. The reason for this is that sintering is a solid state diffusion process and will be enhanced by increasing the surface area to volume ratio of the powder in the green part [Khanuja, 1996]. Another reason for using fine powders is that the overall part quality should be improved since the surface roughness can be no smaller than the powder size. Smaller powders also mean that the minimum feature size which can be specified by a designer and actually printed is also improved. Lastly, smaller powders allow thinner layers to be used which helps eliminate slicing defects such as stair-stepping [Arthur, 1996].

Despite the many advantages of using fine powders, they are difficult to use in the traditional 3DP process for a variety of reasons. Fine powders tend to stick to each other forming agglomerates since Van der Waal's attractive forces between the particles becomes significant in this size range [Khanuja, 1996]. The particles also tend to stick to any other bodies they come into contact with including powder piston walls and the spreader bar. This makes them difficult to work with. The low flowability of fine powders can also be attributed to the fact that very fine particles are typically irregularly shaped increasing friction. Poor flowability combined with the fact that the powder adheres to the spreader bar makes it difficult to spread smooth layers. The low flowability of the powder also inevitably leads to uneven densification within layers and consequently, the resulting green body. Another problem with fine powders is that they are difficult to print into without problems of ballistic ejection and erosion due to the binder jet impinging on the power bed surface [Arthur, 1996]. Despite these problems, ceramic parts have been printed (albeit with difficulty) using submicron alumina powder with the traditional 3DP techniques. The resulting green parts had packing densities of about 40% of theoretical which were well below the minimum necessary to achieve full density without iso-static pressing [Yoo, 1996]. Thus, if fine powders are to be used successfully, a new method must be found to deposit them which results in both smooth layers, uniform densification, and high packing density. One method which makes it possible to work with fine powders is the slurry-based 3DP process.

2.2: An Overview of the Slurry-Based Three Dimensional Printing Process

The slurry-based 3DP process is a significant change in the way powder beds are fabricated and parts are removed from the powder bed after printing. The traditional 3DP process (see Figure 1.1) uses dry powders which are spread with a bar to achieve smooth layers of uniform thickness. After spreading, the powder is held in place by the walls of the piston. This traditional 3DP layer generation technique relies on the powder being very flowable in order for smooth layers of uniform density to be created. As mentioned earlier, the traditional 3DP process is not well suited to the use of the fine powders due to their limited flowability. The slurry-based 3DP process basically makes layers by spreading a liquid dispersion of the desired material which then slip-casts onto the powder bed to make a new layer. This makes it possible to use fine powders without the flowability problem which exists when the powders are used dry. The problem of achieving high packing density is also taken care of by the fact that when fine particles in a slurry slip-cast onto a surface, the resulting cake will have typical packing densities of 50-65% of theoretical. The slurry-based 3DP process differs from the traditional process in both the way the layers are fabricated and the removal of the final part. The following is a brief overview of the slurry-based 3DP process which neglects many of the nuances and issues associated with the process. These will be examined in detail in later sections.

The slurry-based 3DP process can be broken down into several key steps. The first step of creating a layer is implemented by depositing slurry in an even fashion over the area of the powder bed (the actual method by which the slurry is delivered to the powder bed surface will be discussed later). Immediately after deposition, the slurry begins to slip-cast onto the powder bed to form a new layer. Because the actual thickness of slurry pooled on the powder bed surface is quite small, the new layer solidifies quite quickly. To prevent water trapped in the slip cast layer from interacting with the binder to be printed, a drying step is then performed to remove any water. This also helps prevent cracking of the powder bed [Khanuja, 1996]. After drying, the third step of printing binder into the new layer is performed. Depending on the binder used, drying may or may not be required after this step as well. This process is then repeated until the part to be printed is complete. A schematic which outlines layer fabrication in the slurry-based 3DP process is shown below in Figure 2.1.

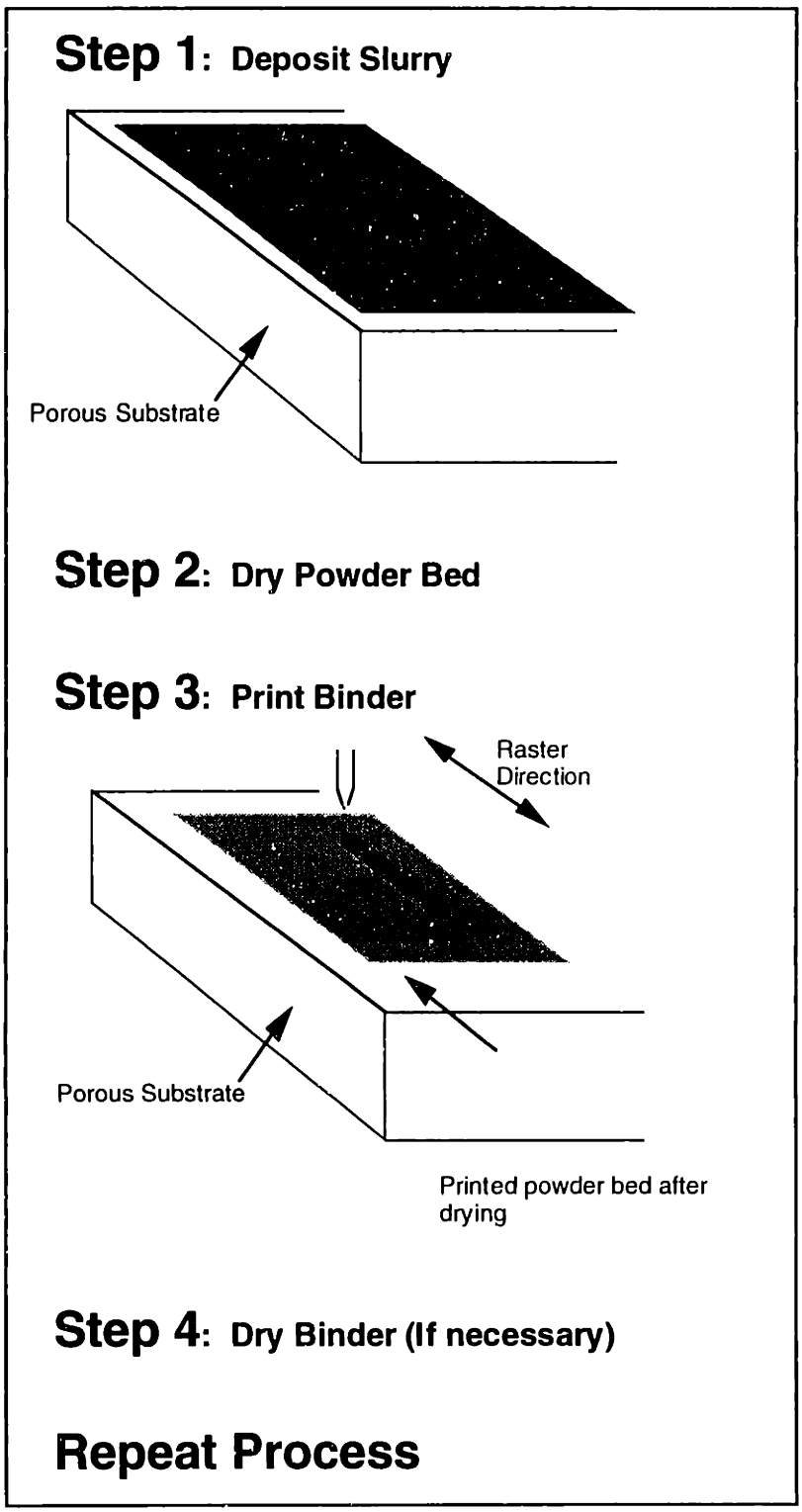

Figure 2.1: Slurry-based 3DP part fabrication

At this point, the result will be a cake of dried powder with binder printed in selected locations which defines a desired geometry. In the slurry-based 3DP process, part removal is a little more complicated than in the traditional 3DP process. In this case, the

cake of powder is immersed in a solvent (water in the case of alumina) to redisperse the unbound powder. This means that binder choices will be more limited since the binder must be insoluble in the solvent after drying. Furthermore, some form of mechanical agitation may be necessary to aid the redispersion process so the binder needs to be strong enough to resist this. After the excess powder is redispersed, the green part can be removed. Since the green part should have a packing density in excess of 50%, the part can then be sintered directly without the troublesome iso-static pressing step. The rest of the slurry-based process is illustrated in Figure 2.2 below.

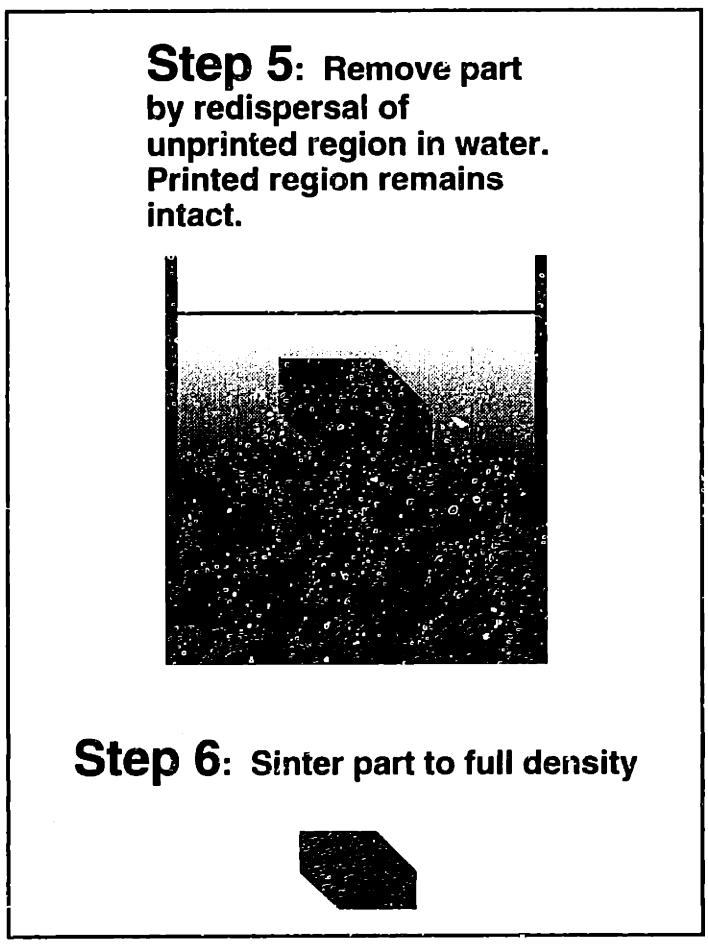

Figure 2.2: Slurry-based 3DP process part retrieval and sintering

The slurry-based 3DP process offers a number of key advantages over the traditional 3DP process. The most important advantage is the fact that green parts can be fabricated with packing densities exceeding 50% of theoretical without post-processing. This makes the process economically competitive with other manufacturing processes such as dry pressing which also produces green parts with high packing densities. The fact that

submicron powders can be utilized also means that parts with much finer details and much thinner layers can be fabricated. In industry, thin films can be produced by tape casting which are only several microns thick. Thus, it would be reasonable to expect that layers having a thickness of 10 microns or less could be made. Such small layers would significantly reduce surface irregularities due to slicing. It might also make it possible to use 3DP for new applications such as in the area of micro-mechanical devices. Finally, it is important to note that the slurry-based 3DP process can be used for any material which can be obtained as a fine powder and dispersed. Consequently, there are quite a few material systems which could be used.

2.3: Material System Selection

In developing the slurry-based 3DP process, there were a variety of material systems to choose from. Some of the candidates were alumina, silicon nitride, silicon carbide, and tungsten carbide/cobalt. For the ensuing process development, it was decided to use the alumina material system to develop and demonstrate the feasibility of the slurry-based 3DP process. This choice was due to several factors. The first of these is the fact that the alumina material system is already very well studied and understood. This makes it possible to focus on development of the process without being hindered by issues involved with developing a new material system. A second reason for using the alumina material system is that it can be dispersed easily using water as a solvent. This also speeds process development since relatively simple test hardware can be built while sidestepping machine design issues that come up when working with strong solvents necessary for some other material systems. Throughout this thesis, unless otherwise noted, the material being discussed in the slurry-based 3DP process is alumina.

2.4: The Alumina Material System

The alumina material system (Al_2O_3) is perhaps one of the most widely used ceramics today. Also known as corundum or emery, alumina finds many applications for both industrial applications (structural ceramics) and in the electronics industry (electrical insulation applications). Alumina powder is typically prepared using one of several powder processing methods. These include thermal decomposition of ammonium-alum, treatment of aluminum flakes by electric powder discharge in water, hydrolysis of aluminum alkoxides, and the Bayer process [Gauckler, 1988]. Alumina powder can be readily obtained in sizes down to 0.1 μm. Typically, the alumina powder will be doped with MgO to improve sinterability by inhibiting grain growth [Reed, 1988]. Grau studied several commercially available alumina powders. Of these, the powder manufactured by

Ceralox was the best in terms of making stable dispersions and being able to redisperse slip cast cakes. As a result, for the experiments described in this report, the alumina powder used was HPA and APA grades of alumina from Ceralox (Ceralox, Tucson, AZ). The powder is available in sizes of 0.5, 1.0, and 3.0 μm with or without MgO. The difference between the two grades is the purity levels. HPA grade alumina is 99.99% pure while the APA grade is 99.95% pure. Both grades contain trace amounts of sodium, iron, and silicon. For powder bed fabrication, the choice of HPA or APA grade does not matter. However, the impurities can make a difference during the sintering stage. A SEM photo of 0.5 μm APA Ceralox powder is shown below in Figure 2.3. The 1.0 and 3.0 μm have been observed to have a similar powder morphology.

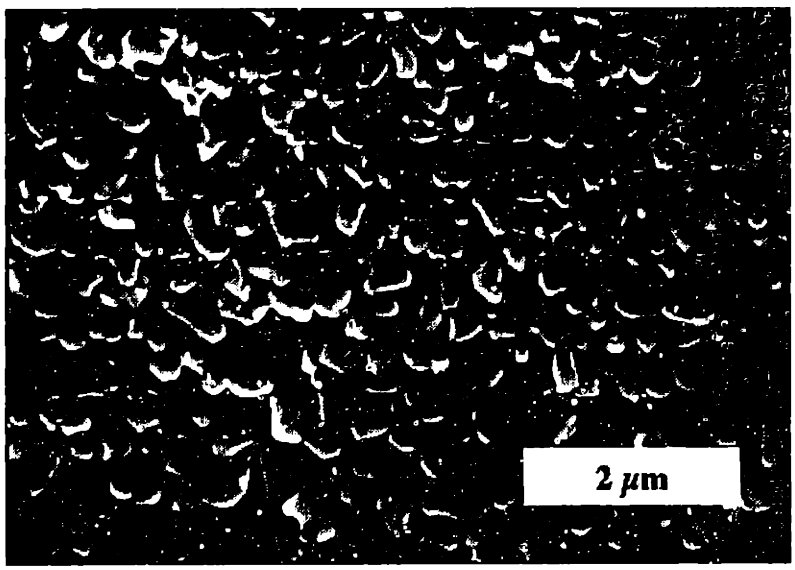

Figure 2.3: SEM photo of 0.5 μm APA Ceralox powder which has been slip cast to achieve high particle packing (courtesy Jason Grau)

2.4.1: Preparation of Alumina Slurries

Correct preparation of the material dispersion is vital to the success of the slurry-based 3DP process. The reason for this is that flocculated slurries pack to a lower density than well dispersed slurries [Khanuja, 1996]. Furthermore, a poorly dispersed slurry will be more difficult to work with depending on the delivery method used to deposit the slurry on the powder bed. Proper slurry preparation requires more than just mixing the correct proportions of powder, solvent, and surfactant. The order and rates in which the components are mixed can also significantly affect the quality of the resulting dispersion. A detailed description of a technique which consistently produces good alumina slurry is provided below.

Alumina powder can be readily dispersed using water as a solvent by forming an electro-static dispersion. This is accomplished by just keeping the pH of the alumina slurry at about 3.5 where the alumina dispersion is most stable [Khanuja, 1996]. The pH of the slurry is adjusted by adding the appropriate quantity of nitric acid. In practice, it has been found that it is not necessary to actually measure the pH of slurry directly. Instead, excellent results can be obtained by making sure that the slurry is prepared such that the molarity (moles per liter of solution) of the nitric acid in the slurry is between 0.05 and 0.1. The best amount of acid to used can depend on the powder size, impurities that are present, etc. However, Grau has found that a concentration of 0.05 M nitric acid usually produces excellent alumina slurry. Table 2.1 below lists the acid concentrations for several powders which have produced well dispersed slurries.

Powder	*Recommended Nitric Acid Concentration*
Ceralox APA-0.5 w/MgO	0.05 Molar
Ceralox HPA-1.0 w/MgO	0.05 Molar
Ceralox HPA-1.0	0.08 Molar
Ceralox HPA-3.0	0.05 Molar

Table 2.1: Recommended nitric acid concentrations

Alumina slurries of up to 40 v/o have been successfully dispersed using acid stabilization with powders that are 3.0 μm and smaller.

In order to successfully disperse powder, there are several important steps which should be followed. The procedure for preparing 200 cc of alumina slurry is outlined below. It is assumed that the following materials are available: 1.0 M nitric acid stock solution, 0.5 - 3.0 μm alumina powder, and deionized water. Deionized water should be used since the presence of charged impurities can cause the slurry to flocculate [Khanuja, 1996]. The following lab equipment is necessary for slurry preparation: 0.25 inch diameter alumina milling media (US Stoneware Corp., East Palestine, OH), a Nalgene polypropylene wide-mouth milling bottle, and a Nalgene polypropylene mixing beaker (Nalge, Rochester, NY). The bottle volume should be selected such that the total volume of milling media and slurry does not exceed about 2/3 the bottle volume. Overfilling the bottle will inhibit the effectiveness of ball milling. For instance, in the case of a 200 mL slurry, a 500 mL bottle would be used for milling. The use of a polypropylene beaker for mixing is preferred over glass since the slurry does not easily adhere to it.

Given the desired slurry volume in [cc], V_{slurry}, the necessary acid concentration in [M], AC, and a desired volume fraction of alumina (unitless), VF, the relative quantities of the nitric acid, powder, and water can be determined from the equations below:

$V_{alumina} = (V_{slurry})(VF)$ [cc] ($V_{alumina}$ is the volume of alumina) (2.1)

$M_{alumina} = (V_{alumina})(3.98)$ [g] ($M_{alumina}$ is the mass of alumina) (2.2)

$V_{acid} = (V_{slurry})(AC)$ [cc] (V_{acid} is the volume of 1.0 M nitric acid) (2.3)

$V_{water} = V_{slurry} - V_{alumina} - V_{acid})$ [cc] (V_{water} is the volume of water) (2.4)

The proportions of acid, water, and powder are shown below in Table 2.2 for a 200 mL alumina slurry for a variety of solid loadings assuming an acid concentration of 0.05 M is desired.

Desired Slurry Volume [cc]	200	200	200	200	200	200	200	200	200
Desired Solids Volume Fraction	0.5	0.45	0.4	0.35	0.3	0.25	0.2	0.15	0.1
Stock Nitric Acid Molarity	1.0	1.0	1.0	1.0	1.0	1.0	1.0	1.0	1.0
Volume Powder [cc]	100	90	80	70	60	50	40	30	20
Mass Powder [g]	398	358	318	279	239	199	159	119	79.6
Volume 1.0 M Acid Solution [cc]	10	10	10	10	10	10	10	10	10
Volume Water [cc]	84	94	104	114	124	134	144	154	164

Table 2.2: Acid, water, and powder proportions for a 200 mL alumina slurry

In order to prepare the slurry, the entire volume of acid to be used should be slowly added to the water in a polypropylene beaker and mixed thoroughly with a magnetic stirrer. Next, the powder should be slowly added in about 5 g increments with the magnetic stirrer operating at its highest setting where splattering does not occur. Between each powder addition, the powder should be allowed to fully disperse in the solvent. After enough powder is added so that the alumina volume fraction is between 0.15 and 0.2, the slurry should be milled for several hours to ensure proper mixing.

Before pouring the slurry in the mixing bottle, the bottle should first be filled about 1/3 full with the milling media. The slurry should then be poured into the milling bottle and placed on a ball mill. There is an optimal speed at which ball milling is most effective but it is not that critical that the exact optimal speed is used. The important thing is that the ball mill speed should not be set so high that the milling media just rolls with the milling bottle. This is illustrated below in Figure 2.4.

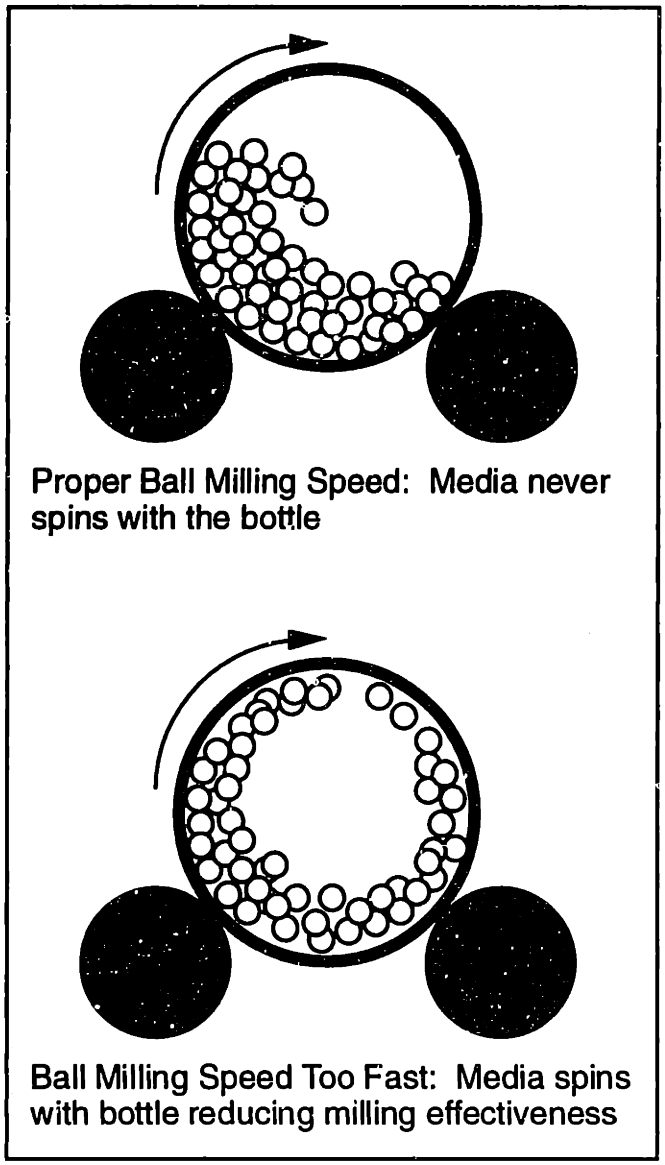

Figure 2.4: Proper and improper ball milling speeds

A speed setting which is too high reduces milling effectiveness since collisions between the balls which break up the slurry agglomerates will be minimized. Of course, a milling speed which is too low will also be ineffective since energy is needed to break up the agglomerates.

After milling the slurry for about 6-12 hours, the slurry should be poured back into the beaker. Occasionally, it may be noticed that the slurry exhibits a problem with foaming. This can easily be remedied by adding one small drop of octyl–alcohol (octonol) to the slurry. The rest of the powder required to reach the desired solids loading should then be added. Again, the powder should be added slowly so it can be dispersed

throughout the solvent. After adding the balance of the powder, the slurry should be poured back into the milling bottle. The slurry should then be milled for at least 48 hours. At this point, the slurry is ready to use. If the slurry is not needed right away, it can be kept on the ball mill with the milling media for another 48 hours. It is not a good idea to keep ball milling the slurry too long since this continually exposes new surface area of the powder and causes the pH of the slurry to change from its optimal value [Moon, private communication]. In order to keep a slurry longer, after about 80 hours of ball milling, the milling media should be removed. The ball mill can then be used just to keep the slurry mixed.

2.4.2: Alumina Slurry Properties

Once the slurry has been prepared and milled, good alumina slurry should have relatively low viscosity and be free of residue or other foreign matter. A significant increase in viscosity or the appearance of residue or "goo" in the slurry is a sign that flocculation has occurred and that the slurry is no longer usable. In practice, it has been found that the slurry is typically good for about 1 to 2 weeks after preparation. The viscosity of well-dispersed aqueous-based alumina slurry has been measured. A viscosity of about 10 centipoise (water is about 1 centipoise) has been reported for 30 v/o alumina slurry [Khanuja, 1996]. The viscosity of 35 v/o alumina slurry has been found to be about 12-15 centipoise [Moon, Private Communication]. Using a rotary viscometer, 30 v/o alumina slurry has been found to have a very newtonian rheology with little shear-thickening or dilatancy [Khanuja, 1996]. The density of alumina slurry as a function of the solids loading where water is used as the solvent is shown below in Figure 2.5.

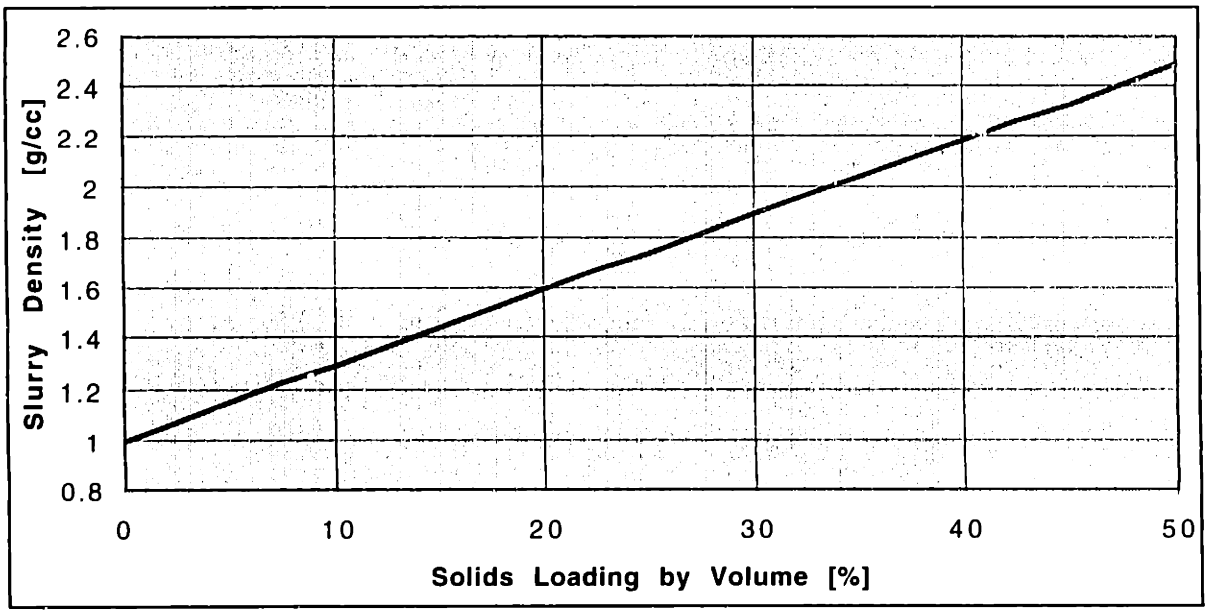

Figure 2.5: Alumina slurry density as a function of solids loading

2.5: Slurry Deposition in the Slurry-Based 3DP Process

Perhaps one of the most challenging parts of the slurry-based 3DP process is the development of a reliable method of delivering slurry to the powder bed such that a uniform layer with high packing density (at least 50% of theoretical) is formed. It is also important that when successive layers are made, no defects between the layers exist. Several approaches which have been proposed will be presented here at a level of detail to convey the concept. Those concepts which were investigated at an experimental level will be discussed in greater detail at a later point.

2.5.1: Layer Fabrication Using Repeated Tape Casting

One possible way deposit slurry onto the powder bed in order to create layers is to use a tape casting approach. In tape casting, a doctor blade is run along the surface upon which a thin layer is to be deposited. A pool of slurry is placed in front of the doctor blade so a constant supply of liquid is always available. In such an approach, the powder bed would be built up by repeatedly tape casting layers on top of one another. This approach is somewhat like the traditional 3DP process in the sense that a spreader bar is still used to set the layer height and smoothness. A schematic of the tape casting approach to making layers is shown below in Figure 2.6.

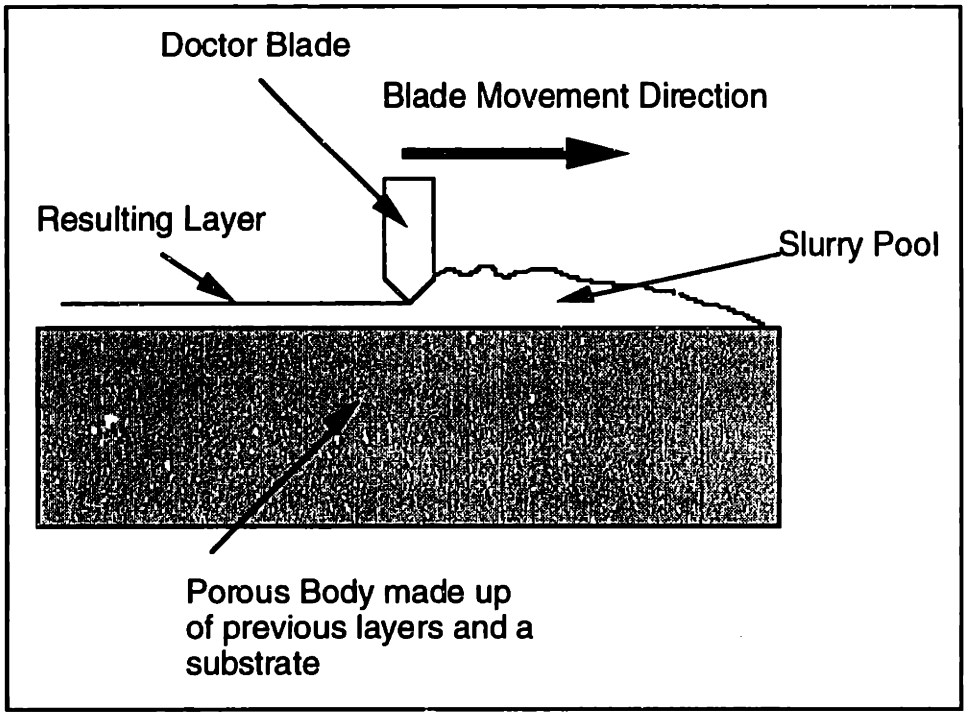

Figure 2.6: Side view of the tape casting approach

The tape casting approach has a number of advantages which make it a candidate for use in the slurry-based 3DP process. Tape cast films can be made with thicknesses of several microns. This means that such an approach would make it possible to create very thin layers. Another advantage of the tape casting approach is the possibility to get optical quality surface finishes over a relatively large area. This approach should also limit the possibility of errors in the build direction accumulating over time since the correct build height is set at each layer. The tape casting approach also has some disadvantages. The first of these is that tape casting requires a very high level of automation and control to get repeatable results. This includes controlling the slurry pool height before the doctor blade, the blade movement velocity, and the slurry rheology.

2.5.2: Layer Fabrication Using Spray Deposition

A second approach to producing layers with slurry is by spray deposition. A slurry mist can be created using an atomizing nozzle. This nozzle can then be rastered across the powder bed to create a layer. This is illustrated below in Figure 2.7.

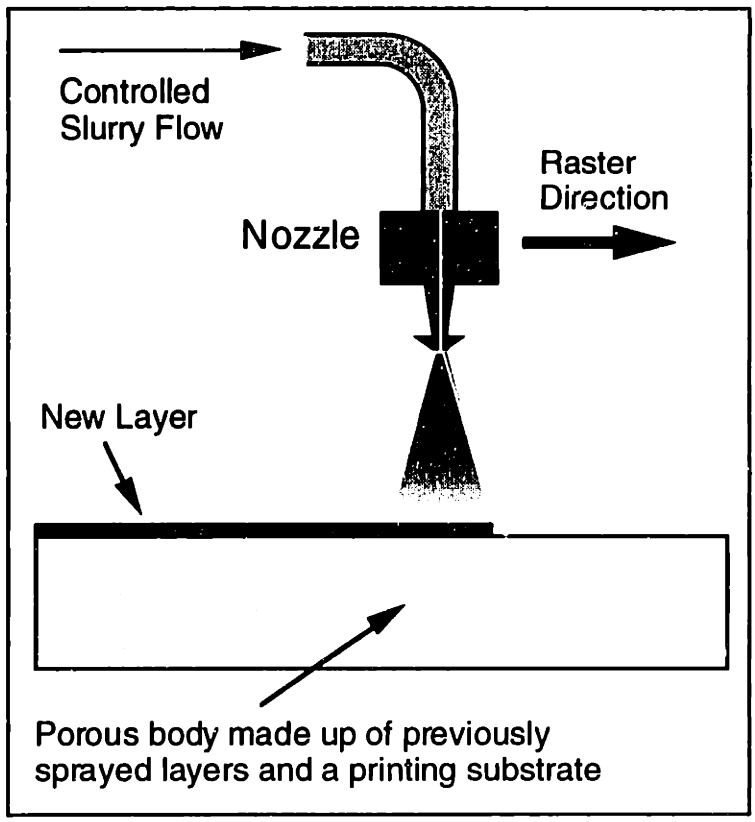

Figure 2.7: Spray deposition approach to layer fabrication

One apparent advantage of the spray deposition approach over the tape casting method is that the complexity of the motion hardware necessary to implement this scheme is reduced. Furthermore, equipment for moving the nozzle in a raster pattern is already available. However, control of the flow rate and resulting spray becomes critical in this approach since errors in the build direction will accumulate over time.

2.5.3: Layer Fabrication By Ink-Jet Printing

The last proposed method by which layers may be made is to ink-jet print the layers through a small nozzle. There is a relatively large range of nozzle sizes which could be used. Individual lines would be printed by rapidly rastering the nozzle across the powder bed until the layer is complete. This is illustrated below in Figure 2.8.

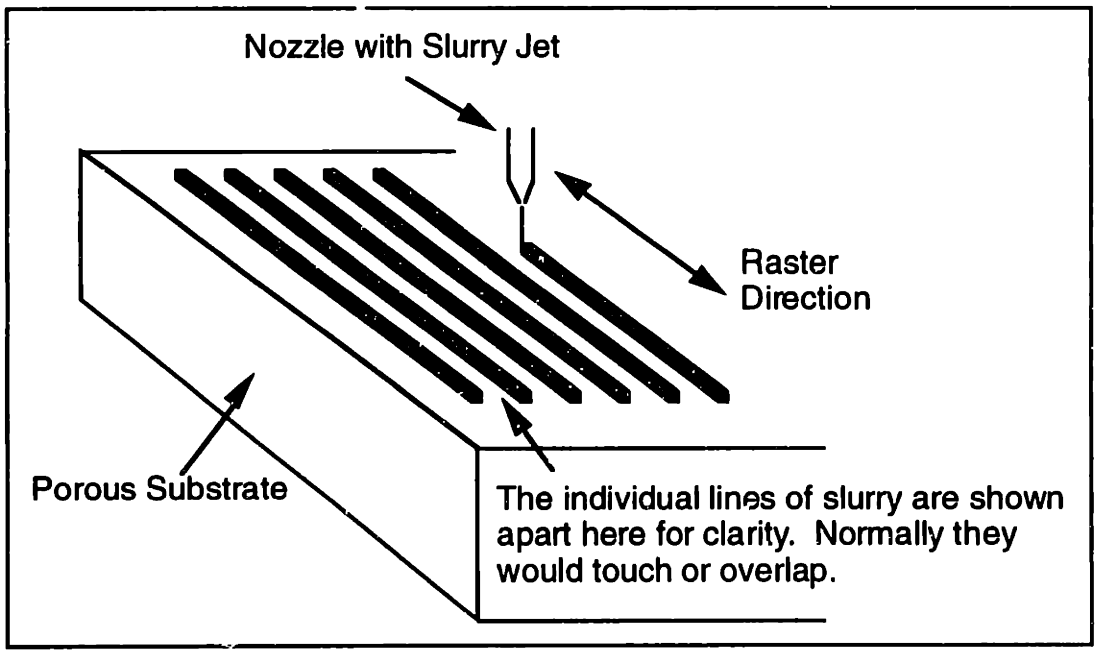

Figure 2.8: Layer generation by ink-jet printing of slurry

This approach offers a number of advantages. Ink-jet printing for use with 3DP has been extensively studied and a large amount of data and hardware is already in place. Ink-jet printing also makes it easier to control the deposition of slurry at any one local area in the powder bed. This is much more difficult to control in tape casting or in spray deposition. Ink-jet printing also has its drawbacks. The first of these is that jetting slurry through a small orifice can be difficult to do reliably. The difficulties of ink-jet printing slurry can be minimized by careful slurry processing and the use of larger orifice nozzles. Another disadvantage of this approach is that it is difficult to get optical quality surface finishes due to the fact that layers are made up of many individually printed lines. However, by carefully choosing printing parameters, layers with very good surface finish can still be obtained.

Chapter 3 : Feasibility Testing of the Repeated Tape Casting Approach

3.1: Tape Casting Approach to Layer Fabrication

One approach to creating layers for the slurry-based 3DP process is to use repeated tape casting. Such a process has some similarity to the traditional 3DP process in the sense that a spreader bar (doctor blade) is used to strike a layer of slurry. This process has the potential to create a layer with a thickness as little as several microns which has an optical surface finish.

3.2: Tape Casting Experimental Setup

In order to test the feasibility of the tape casting approach, a way of spreading the slurry at a known height above the powder bed was required. This problem was solved by using a moveable piston with fixed rails as shown on the following page in Figure 3.1. The piston height was set by adjusting a micrometer. The piston was equipped with a vacuum chuck which made it possible to easily fix a substrate to the piston. The rails ensured that the doctor blade would be kept at a known distance from the substrate.

In order to fabricate a layer, a pool of slurry was poured at one edge of the porous body. Then the doctor blade was slid along the rails by hand to spread the slurry out into a uniform layer. This technique is shown in Figure 3.2.

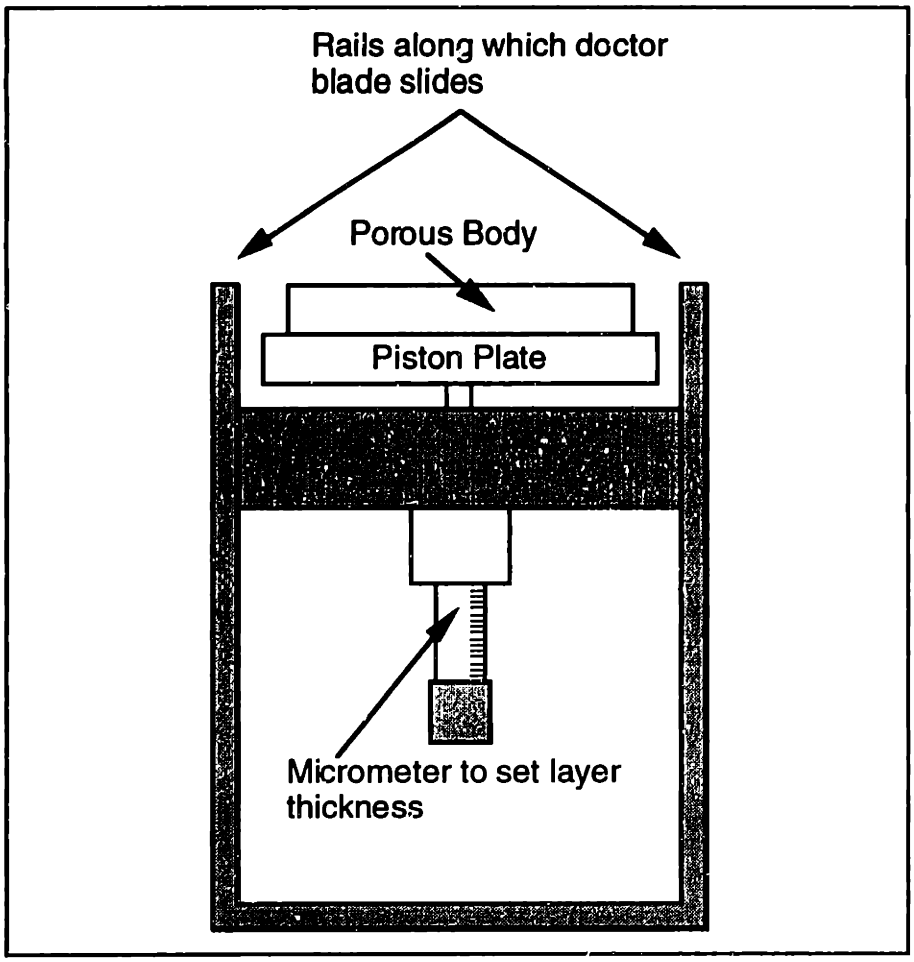

Figure 3.1: Schematic of the tape casting setup

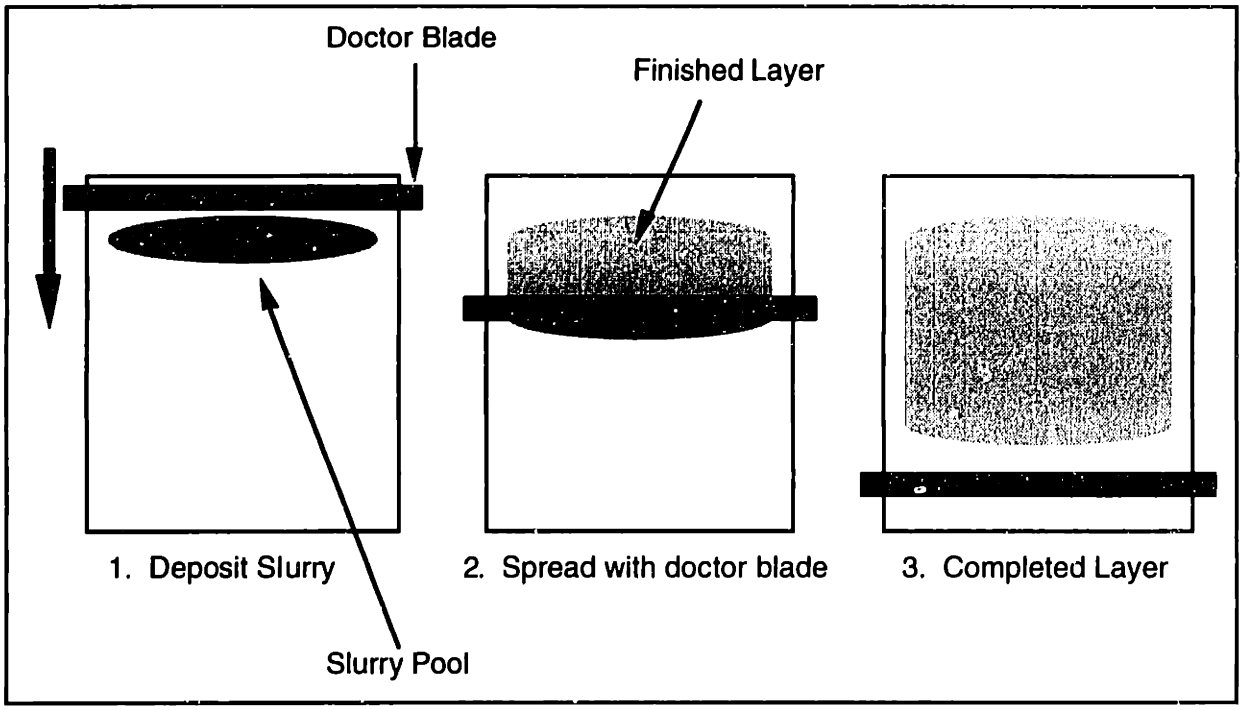

Figure 3.2: Top view of the approach used to tape cast layers

3.3: Brief Review of Process Physics of the Tape Casting Approach

The nominal layer thickness which will be generated by the tape casting approach will be set by the difference between the rail and substrate heights. However, there is a pressure imbalance between the pool of slurry in front of the doctor blade and the resulting layer. As a result, slurry will tend to flow under the doctor blade. If a layer is spread starting with a fixed pool of slurry, as the pool decreases in size, the flow rate will change. This results in a non-uniform layer thickness. This is shown in Figure 3.3 below.

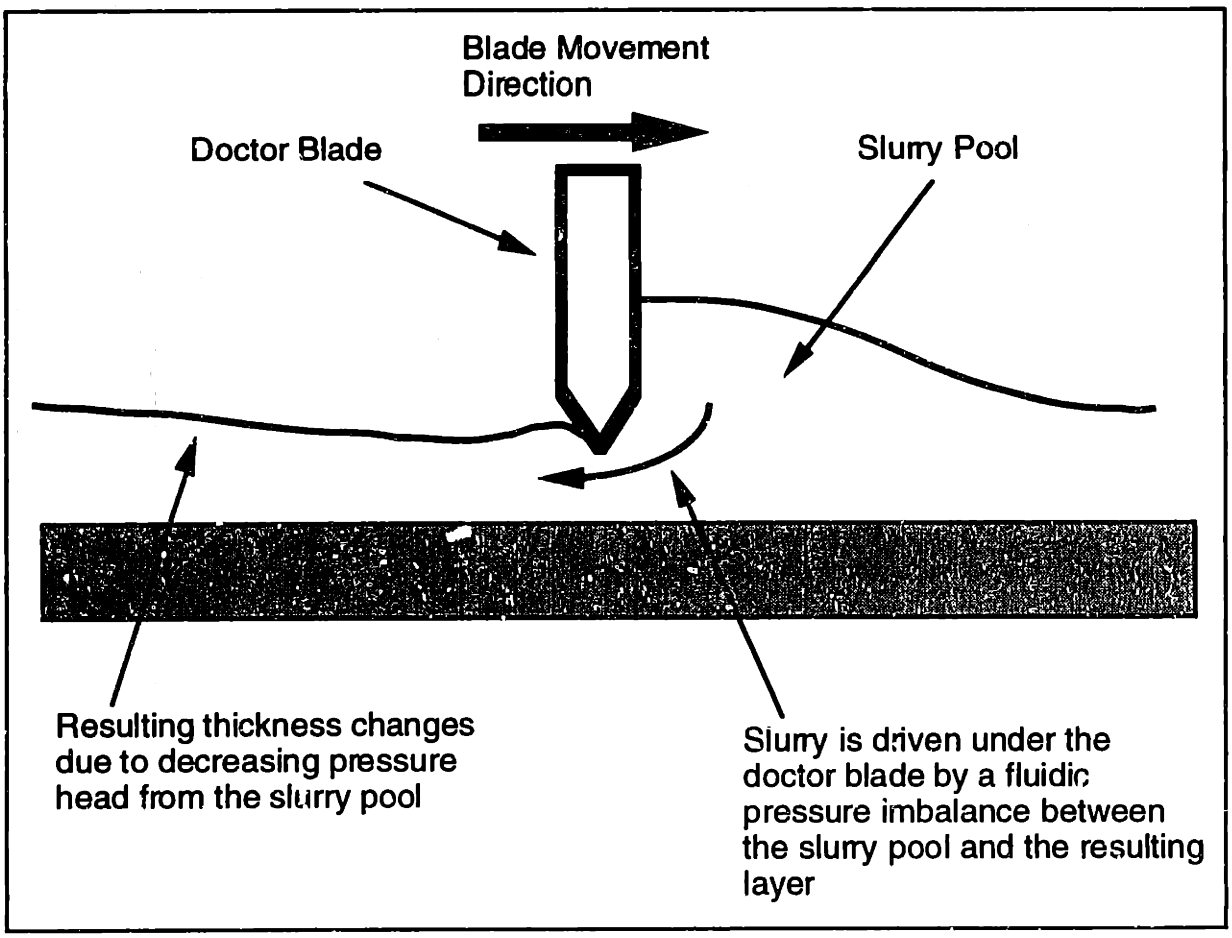

Figure 3.3: Determination of the tape casting layer height

The physics behind the actual layer height which will be created is a complicated function of many variables such as the doctor blade geometry, blade wiping speed, slurry viscosity, surface wetting characteristics of the slurry, etc. However, it is important to realize these potential sources of problems in generating uniform layers.

Another important part of the process physics is slip casting of the layer onto the powder bed. When alumina slurry is spread out on a porous body (either a substrate or previously spread layers), before the water in slurry is absorbed, the slurry will exhibit some wetting contact angle. If this wetting angle is less than 90 degrees, the liquid is said to wet the material in question. An example of wetting is water on glass. If this wetting angle exceeds 90 degrees, the slurry is said to be non-wetting. An example of non-wetting is mercury on glass. The concept of the wetting angle is shown below in Figure 3.4.

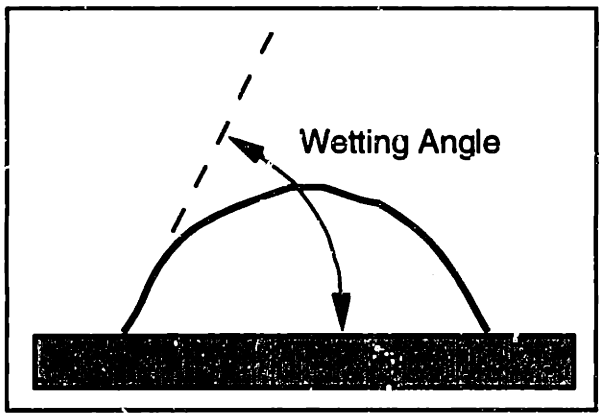

Figure 3.4: A liquid which wets a surface (wetting angle less than 90°)

When choosing a substrate upon which to slip cast layers, it is important to consider wetting characteristics. A substrate which the slurry wets poorly will result in non-uniform layers and poor surface finish. Assuming the slurry wets the material upon which it has been placed (alumina slurry wets the alumina powder bed), capillary suction will try to pull the liquid into the porous body. However, the pores in the substrate act as a filter letting the water pass and leaving the solids of the slurry on the surface. This cake which results typically exhibits high packing density if the slurry was well dispersed and agglomerate free. This process is known as slip casting. This is illustrated in detail in Figure 3.5 below.

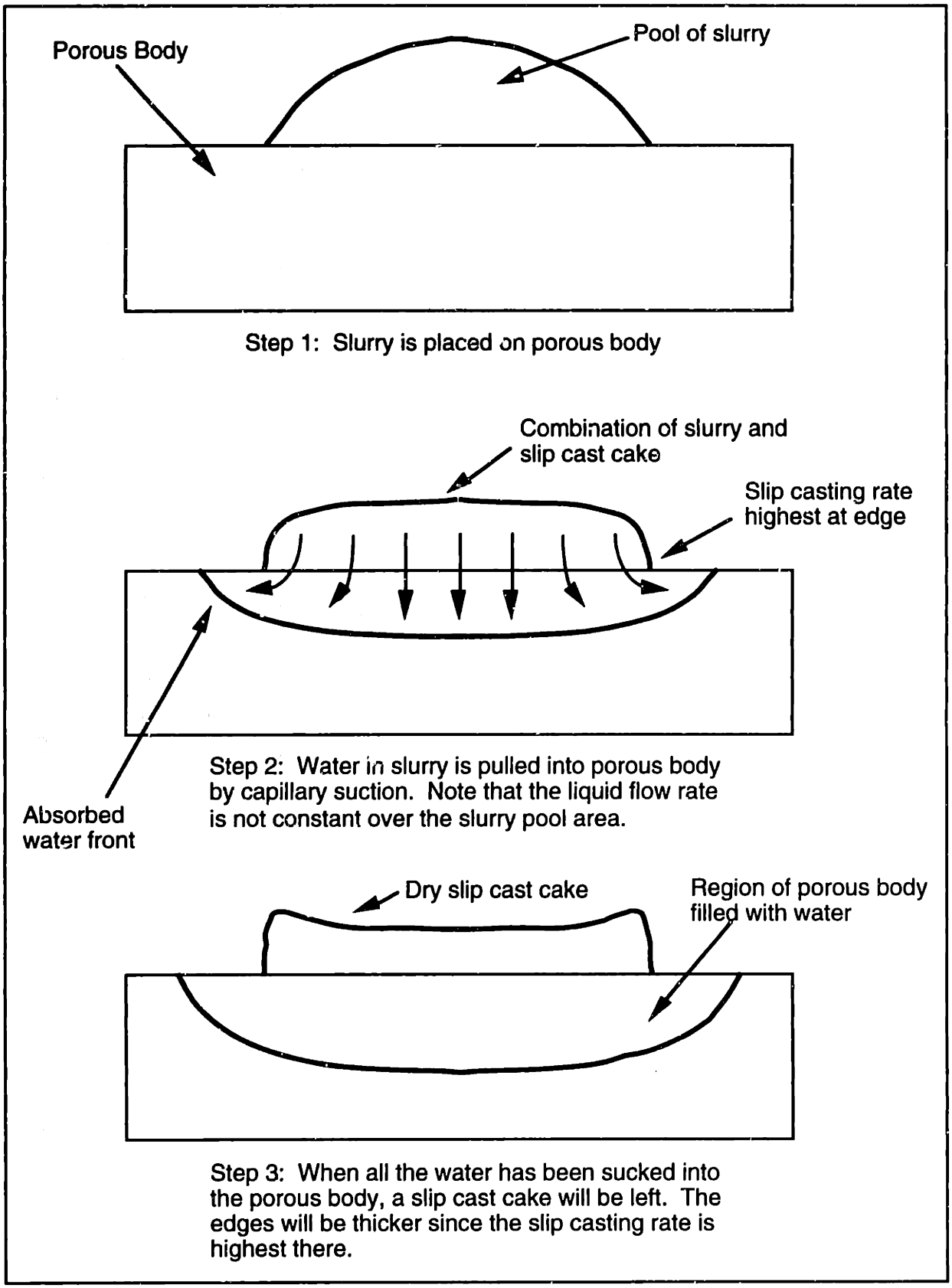

Figure 3.5: Slip casting process

It is important to take into consideration the slip casting process when studying the tape casting layer generation technique. If uniform layers are desired, steps to overcome the problems associated with different slip casting rates in a layer must be taken. Potential sources of problems include layer edge defects and uneven casting within a layer which might be caused by the presence of binder.

3.4: Experiments and Results from the Tape Casting Approach

Using the tape casting approach described above, several multi-layer powder beds were built. The surface finish of the resulting layers was optically smooth as expected. However, the uniformity of the layer thickness was not that good. These problems were probably a direct result of the fact that there was no automation in these experiments. Since the slurry was not precisely metered when poured onto the powder bed before spreading, there was usually a considerable amount of excess slurry. As mentioned above in the process physics, this had the potential to cause the layer to vary with the excess pool height. As a result, the layer thickness would be greatest at the start of a layer and thinnest where the layer spreading step was completed. Another source of problems was the fact that the doctor blade was moved by hand rather than with a controlled constant velocity. This caused uneven layer thickness and defects in the surface finish.

In order to see if a part could be extracted using this process, PAA (Mw = 5000, 20 w/o) bars were printed into the tape cast layers using a drop-on-demand (DOD) line printer. It was noted that where layers were tape cast over a printed region, some surface defects were visible at the interface of the printed and unprinted regions. Bars which were printed did not have sufficient green strength to be removed intact in the redispersal step.

The density of the powder bed created by tape-casting layers was measured by Grau using mercury porosimetry. The density of powder beds made with 0.5 μm powder was found to be 66% of theoretical. The density of powders beds made with 1.0 μm powder was found to be 60% of theoretical. The pore size distribution for 0.5 μm and 1.0 μm powder is shown below in Figures 3.6 and 3.7 respectively (data courtesy Grau).

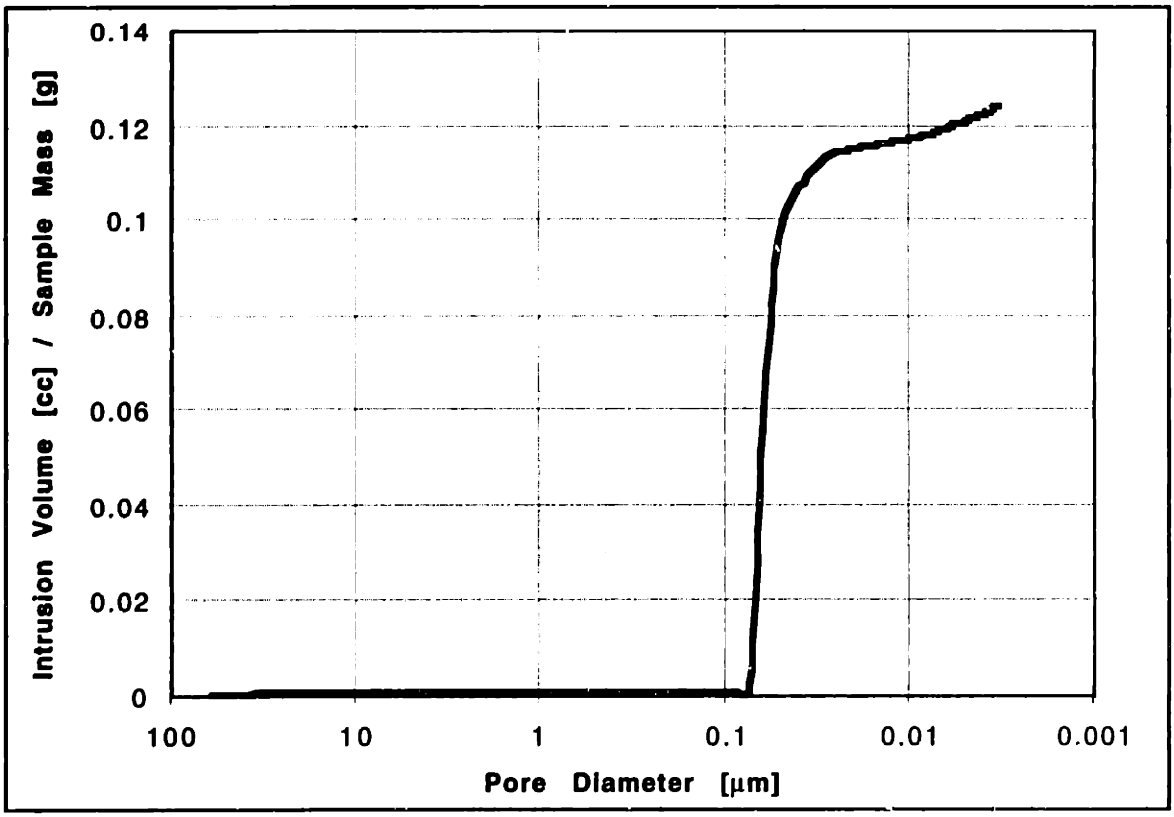

Figure 3.6: Tape-cast powder bed pore size distribution using 35 v/o 0.5 µm alumina

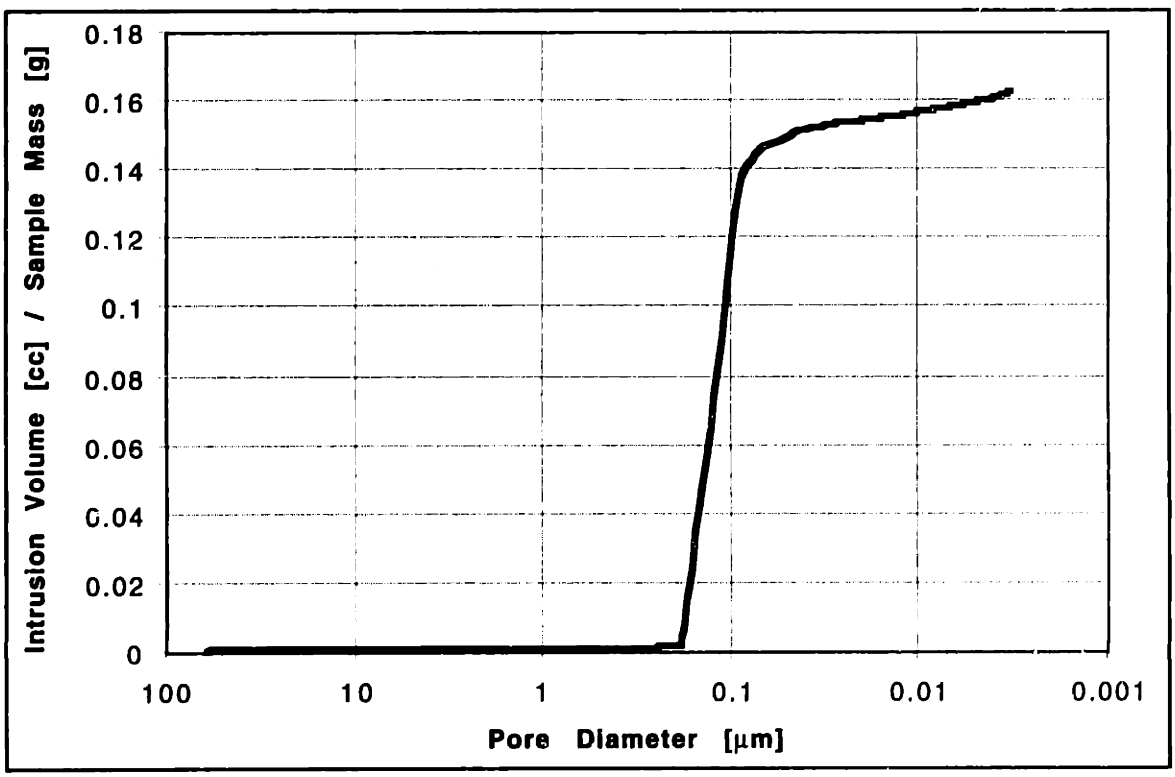

Figure 3.7: Tape-cast powder bed pore size distribution using 35 v/o 1.0 µm alumina

Although the powder beds formed using 0.5 μm powder had smaller pores, both powder beds should easily sinter to full density. The surface finish of the powder beds made by tape-casting was of optical quality. A photo of the surface of a tape-cast powder bed is shown below in Figure 3.8.

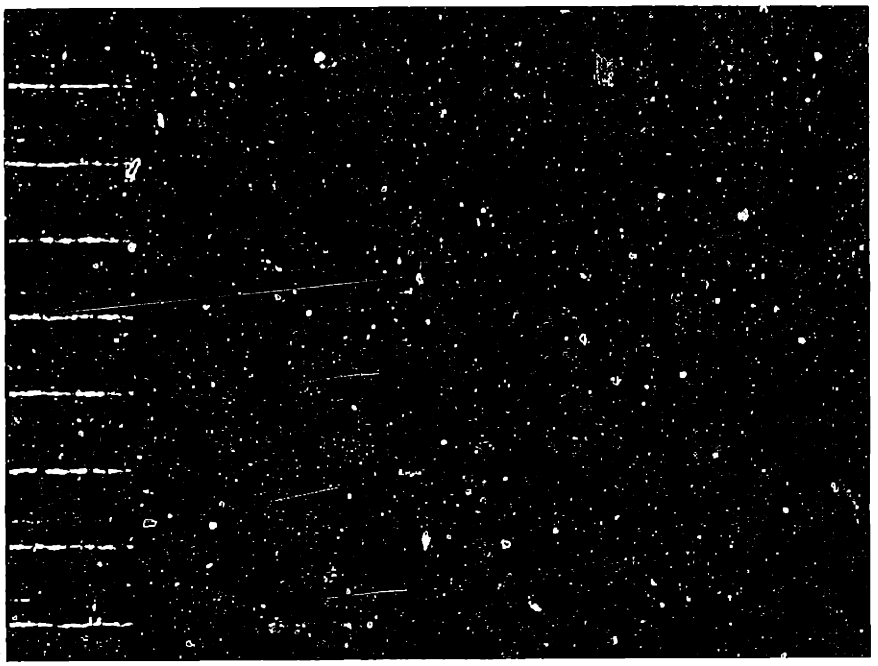

Figure 3.8: Photo of resulting surface finish of powder bed made using repeated tape-casting (scale divisions are 1/64 inch apart)

The defects are so small that it is hard to assess the surface finish optically. Using a Dektak-8000 profilometer (Veeco Instruments Inc., Santa Barbara, CA), the surface finish could be measured quantitatively. The profile is shown below in Figure 3.9.

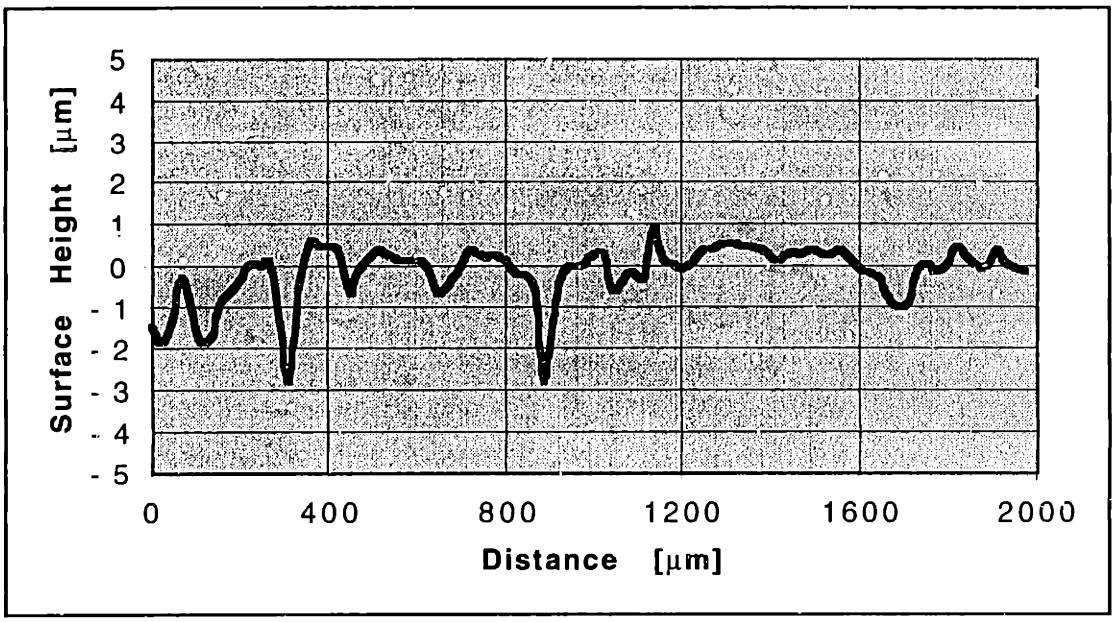

Figure 3.9: Surface profile of a powder bed using repeated tape casting

It can be seen in Figure 3.9 that the surface roughness is only about 4 μm peak-to-peak. This surface finish is better than that obtained by the spray deposition and the ink-jetting printing approach.

Initial results from the tape casting approach to making powder beds showed some promise. In order to better evaluate the tape casting approach, much of the process would have to be automated. Since the development of the necessary hardware to solve these automation problems could take some time, it was decided to suspend work on the tape casting approach in favor of other methods. However, it would still be worth examining this method at a later time since layers ranging from several microns to the cracking thickness limits of the powder used can be rapidly fabricated with excellent surface finish. The process speed advantage comes from the fact that rastering is not necessary in this method.

Chapter 4 : Feasibility Testing of the Spray Deposition Approach

4.1: Spray Deposition Approach to Layer Fabrication

A second approach which was examined for fabricating layers for the slurry-based 3DP process was spray deposition. In this approach, a fine mist of slurry droplets is created using an atomizing nozzle. By rastering such a nozzle, a fine layer of slurry can be deposited on the powder bed surface. Since there is no direct registration of the layer height in spray deposition, a high degree of spray control and motion automation will be required.

4.2: Spray Deposition Experimental Set-Up

A significant amount of effort was put into hardware development for the spray deposition approach to layer fabrication. This was due to the fact that without good control and automation, it would be impossible to assess the feasibility of such an approach [Khanuja, 1996]. Hardware development efforts focused on three areas: nozzle selection, flow rate controls, and nozzle motion control.

4.2.1: Spray Deposition Nozzle Selection

The nozzle used in spray deposition is an important factor in the quality of the resulting layers. A generic nozzle which could be used for the spray deposition application is shown below in Figure 4.1. This figure illustrates several factors which are important to consider when choosing a nozzle. These include the spray droplet velocity, droplet size, and range of usable flow rates. It is also important to consider the uniformity of the spray pattern. The spray flow profile at the surface is not uniform but instead appears to be roughly Gaussian as shown in Figure 4.1. However, whether this distribution is in fact Gaussian has not been verified. This flow profile at the substrate was measured for one nozzle spraying water and is shown in Figure 4.4. Another important factor in nozzle selection is the stability of the resulting spray. The mist should not be time varying. This would include effects such as spray pulsation or wandering of the mist direction.

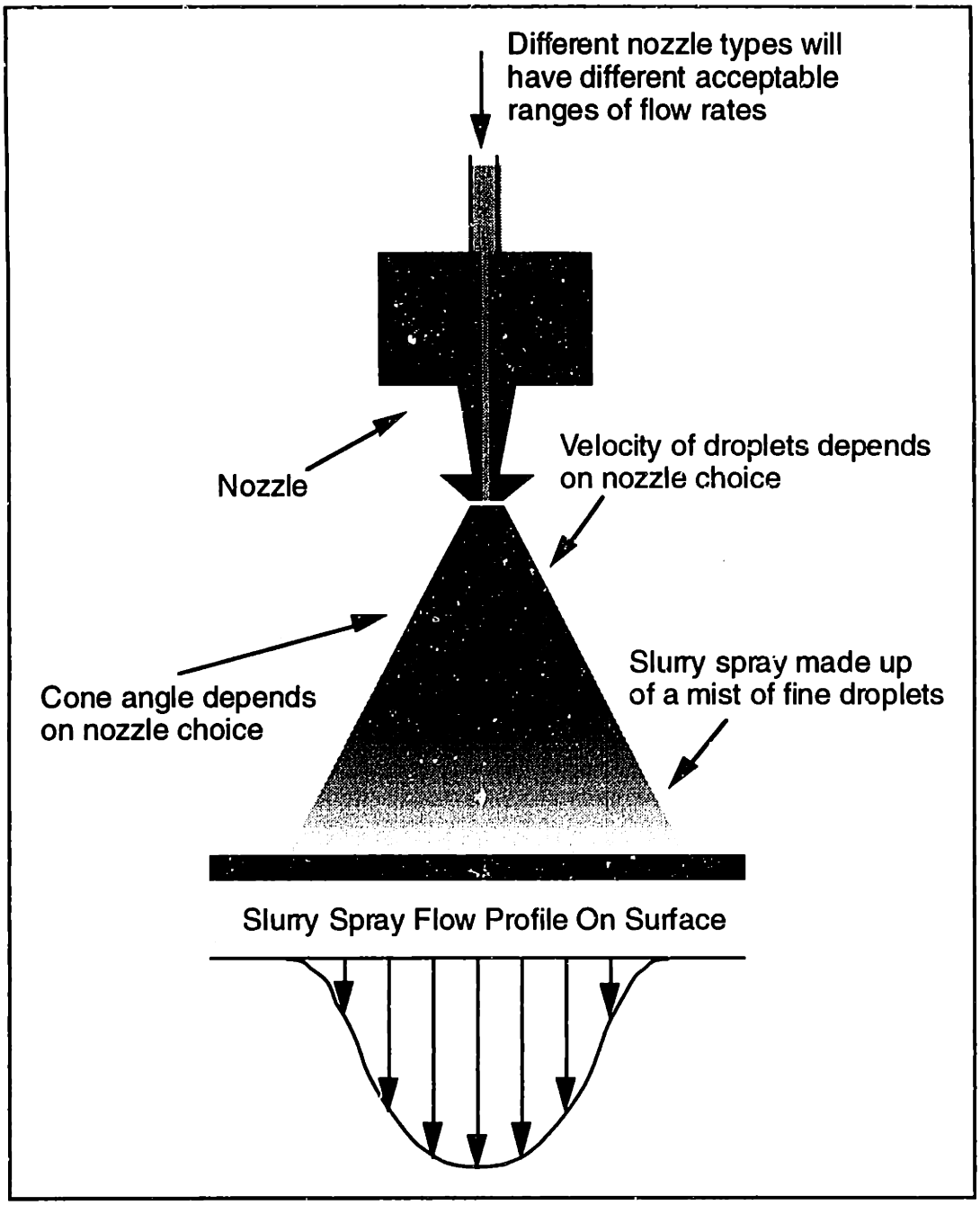

Figure 4.1: Generic spay nozzle

There are several ways which can be used to generate the slurry spray. The two methods which were investigated were air-atomizing nozzles and piezo-type spray nozzles. The air-atomizing nozzles generate a spray by mixing the slurry with a high velocity air flow. This causes a venturi effect which helps draw the slurry out of the nozzle and breaks it up into small droplets. The use of air-atomizing nozzles from two manufactures has been investigated. Grau and Khanuja investigated the use of an air-atomizing nozzle (part number MH#1) manufactured by Paasche (Paasche, Harwood Heights, IL). The use of an

air atomizing nozzle (part no. 1/4J+SU11 PA67147-SS) from Spraying Systems (Spraying Systems Co., Wheaton, IL) was also investigated. A cross-section of the nozzle from Spraying Systems is shown below in Figure 4.2.

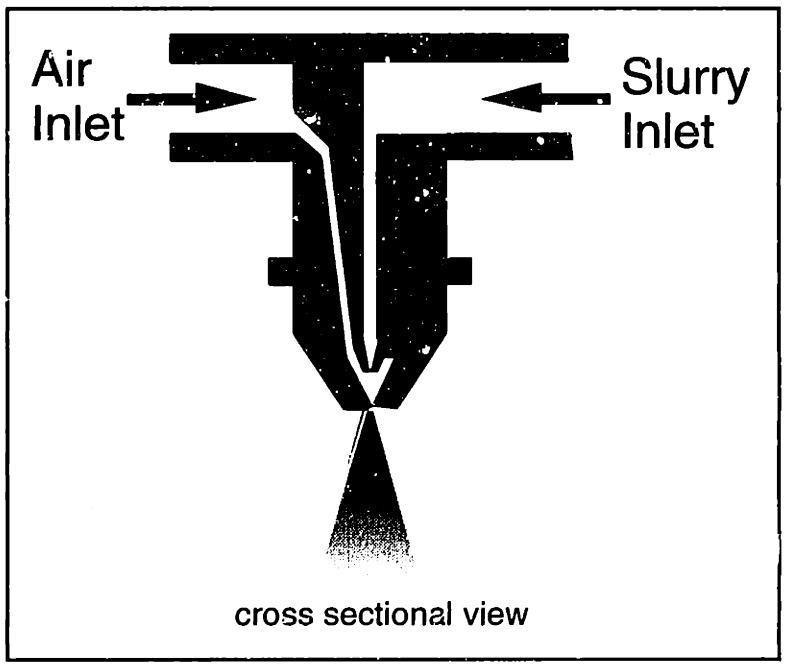

Figure 4.2: An air-atomizing nozzle

Both air-atomizing nozzles used exhibited several problems. The first of these problems was that the resulting spray had a high velocity. One manufacturer quoted the spray velocity from such nozzles as ranging from 5 to 20 m/sec. Such sprays are energetic enough to actually erode previously printed layers as new ones are deposited [Grau, private communication]. The high velocity droplets also leads to a significant amount of back-spray. This wastes material and can build up on the nozzle tip disturbing the spray pattern. Another disadvantage of the air-atomizing nozzles is that they need to have moderate flow rates in order to work properly. Flow rates typically have to be higher than 5 cc/min in order to have a stable spray for the very lowest capacity air-atomizing nozzles available. A final disadvantage of these nozzles is the fact that both the air and slurry inlet pressures need to be controlled. The main advantage of the air-atomizing nozzles is their cost. They are more than an order of magnitude less costly than piezo-atomizing nozzles. Although this is not important in a laboratory setting, it becomes very important when the hardware must be scaled for use in an industrial setting.

The alternative to the air-atomizing nozzle was piezo-atomizing nozzles (also known as ultrasonic atomizing nozzles). These nozzles work by mechanically vibrating an

atomizing horn at frequencies ranging from 20-120 kHz using piezo transducers. As the liquid flowing through the nozzle wets the atomizing surface of the horn, it is broken up into small droplets producing a low velocity spray. A piezo-atomizing nozzle is shown below in Figure 4.3.

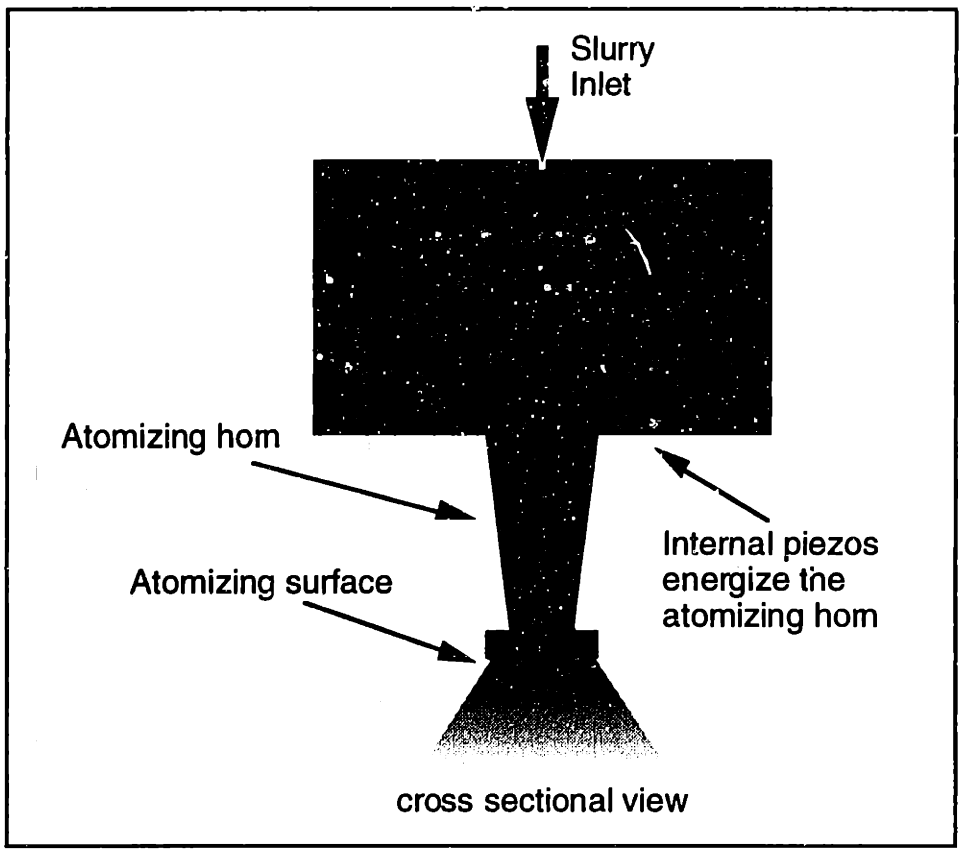

Figure 4.3: Piezo atomizing nozzle

Several manufacturers offer such piezo-atomizing nozzles. Models offered by three different manufacturers were examined to see which had the best performance. These were the Sono-Tek 8700-60 (Sono-Tek, Milton, NY), the Misonix Micromist™ (Misonix, Farmingdale, NY), and the Sonics & Materials wide dispersion atomizer (Sonics & Materials, Danbury, CT).

The Sono-Tek nozzle had already been purchased for a previous application. It had a custom drilled orifice diameter of 0.85 mm. According to the manufacturer, the mean droplet size for this nozzle should be about 40 μm. With 20 v/o aqueous-based alumina slurry, the nozzle was able to produce a spray with flow rates ranging from about 1 to 15 cc/min without difficulty. The mist which was produced by the Sono-Tek nozzle was very fine and low velocity as compared to the spray generated by the air-atomizing nozzles.

However, the mist generated by the Sono-Tek nozzle appeared to be less stable than the air-atomizing counterpart with the spray exhibiting pulsations. Originally, this was attributed to the fact that the pressure driven flow system being used was not providing a constant flow. In order to improve this, a syringe pump which enforces a constant flow rate was employed. This improved the nozzle performance slightly. However, the pulsations still appeared to be present. This pulsation could also be attributed to air being introduced into the nozzle by the atomizing action of the horn. The spray cone also seemed to wander. This could be due to the fact that the mist is very sensitive to air currents which may be present. This problem was mitigated by using an air-shroud accessory which creates an air curtain that entrains and directs the nozzle spray. For the Sono-Tek nozzle, the uniformity of the spray being deposited on a substrate at different heights was measured by Terrazzoni. A plot showing the liquid deposition rates at the substrate for different nozzle heights is shown below in Figure 4.4.

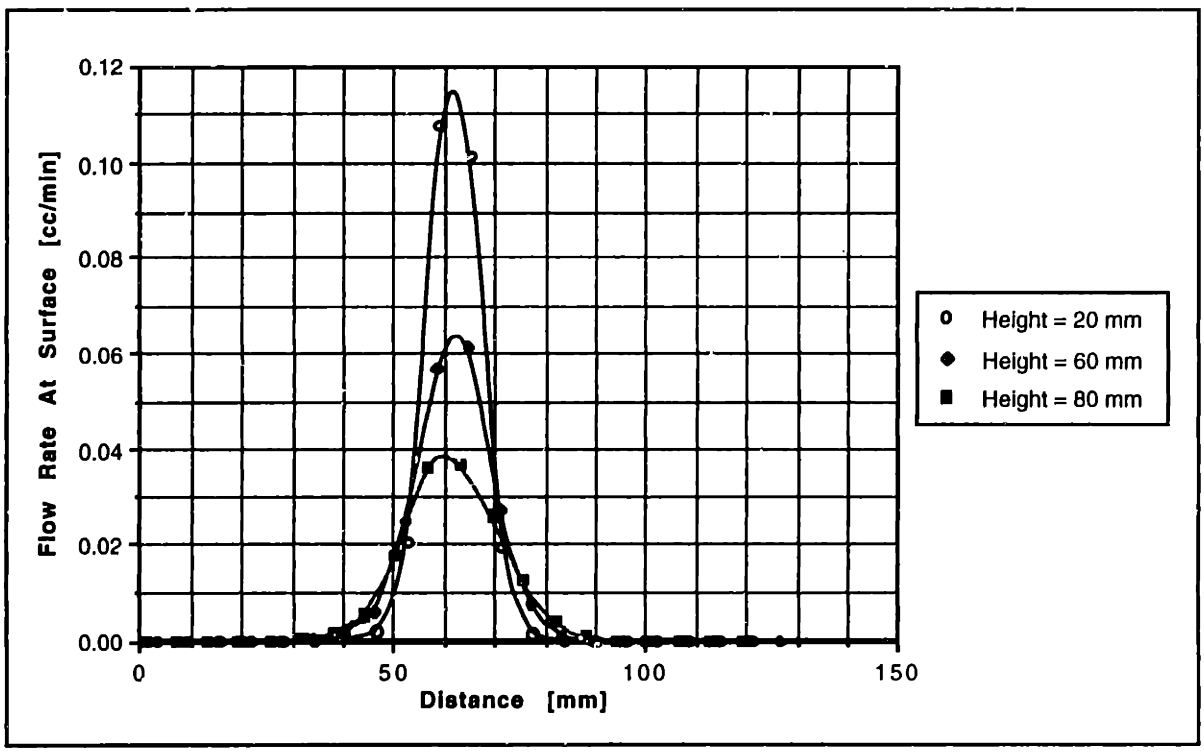

Figure 4.4: Spray deposition uniformity as a function of nozzle height

The Misonix nozzle exhibited very similar behavior as the Sono-Tek. It had an orifice size of 2.79 mm. The average droplet size for the unit was 20 μm as reported by the manufacturer. However, from observing slurry droplets which were printed on a substrate, the actual droplet size is more likely on the order of 60-100 μm for alumina

slurry. With 20 v/o and 35 v/o aqueous based alumina, the nozzle was able to produce mists with flow rates from 1 to 15 cc/min. Like the Sono-Tek unit, the Misonix nozzle also had problems with spray stability even when a syringe pump was used. In most respects, the Misonix and Sono-Tek nozzles gave the same level of performance. However, the Misonix unit did offer two distinct advantages: it is very small and lightweight (less than 1/4 the mass of the Sono-Tek nozzle) and it has a much easier start-up procedure than the Sono-Tek unit which lends itself well to automation.

The last piezo-atomizing spray unit which was looked at was the wide dispersion atomizer sold by Sonics & Materials. This unit cannot be accurately described as being a nozzle. The unit consists of a 6 inch wide plate upon which the liquid to be sprayed must be applied. As the liquid flows down the side of the plate, it is atomized and a mist is generated. This is demonstrated in Figure 4.5 below.

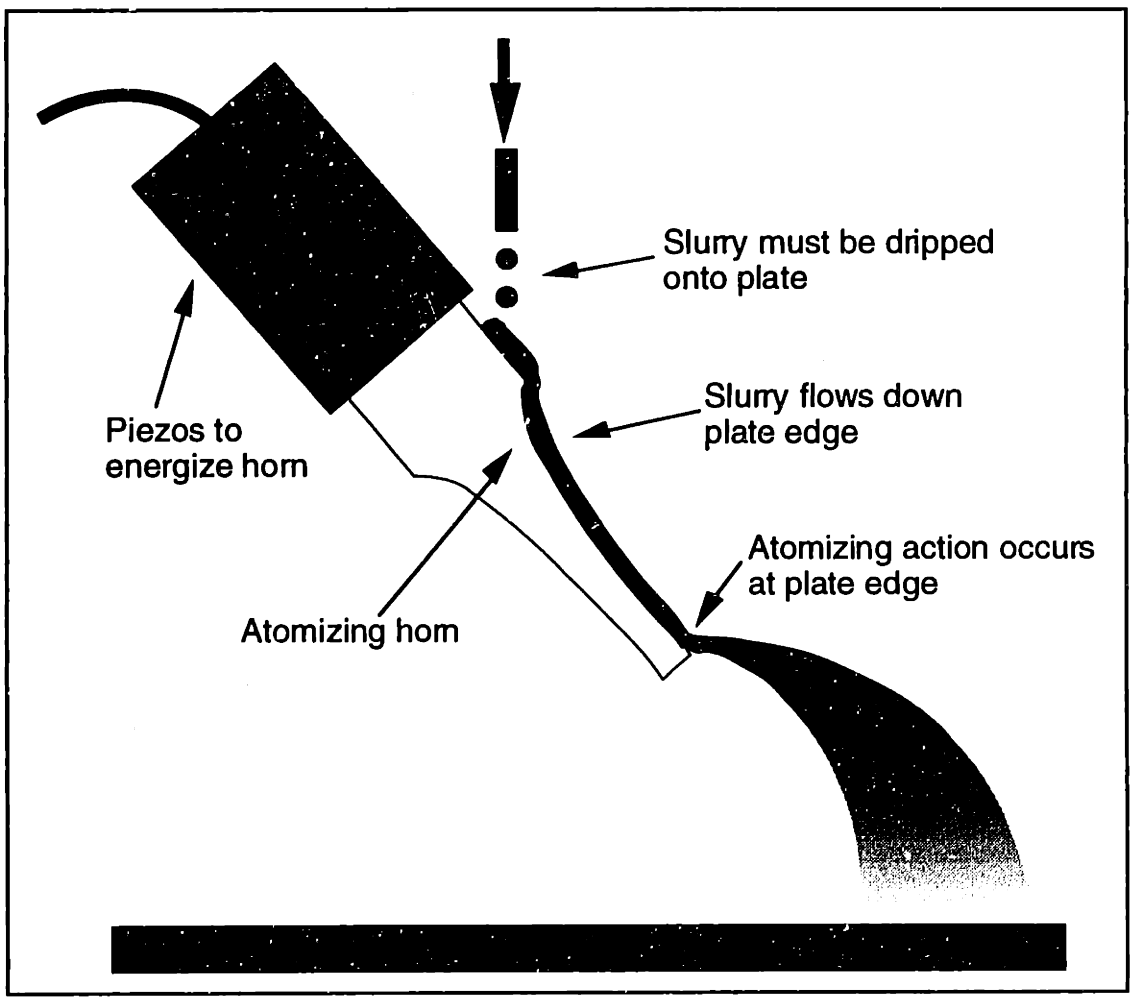

Figure 4.5: Schematic of the wide dispersion atomizer

The manufacturer specifies the median droplet size as 90 μm and the maximum flow rate as up to 100 cc/min per inch of plate width. The spray velocity was quoted as ranging from 0.2 to 0.4 m/sec (which is considerably less than the air-atomizing nozzles). The mist which was generated by this unit compared favorable with the Sono-Tek and Misonix units. As long as a steady dribble of slurry was applied to the plate, the resulting mist appeared to more stable than the other units. However, making a steady stream on the plate proved to be a challenging task. Furthermore, the piezo unit and atomizing horn were quite massive compared to the Sono-Tek and Misonix units making it difficult to use in existing motion equipment.

From the experiments performed with different piezo-atomizing nozzles, none seemed to stand out as being particularly better than the rest. As a result, most experiments were performed with the Sono-Tek unit since it had already been purchased for a different experiment.

4.2.2: Fluid Control Hardware

The second important piece of hardware which needed to be developed for the spray deposition experiments was a reliable fluid system which could deliver alumina slurry at a constant flow rate. There are many different ways of making a liquid delivery system. There are positive displacement pumps (syringe, gear, and peristaltic), centrifugal pumps, pressurized tanks, and gravity systems. The fluid system design was driven by several requirements: constant flow rates without pulsation, being able to work reliably at low flow rates down to 5 cc/min, and being able to change the flow rate easily. These requirements eliminated the use of gear pumps (wear issues), peristaltic pumps (pulsating flow), centrifugal pumps (pressure limited, not usually for low flow rate applications), and gravity driven systems (hard to change flow rate significantly). The remaining choices were pressurized tanks and syringe pumps. Syringe pumps provide extremely constant flow rates but the units which are available have limited capacity (typically 60 cc) and can cost several thousand dollars. Since the flow rates used would range from 5 to 15 cc/min, the capacity limitation of the syringe pumps resulted in the decision to use pressurized tanks to deliver a constant slurry flow rate to the nozzle.

Initially, the pressurized tank setup was configured as an open-loop control system. The slurry flow rate set-point was adjusted by changing the tank pressure. This is shown in Figure 4.6 below.

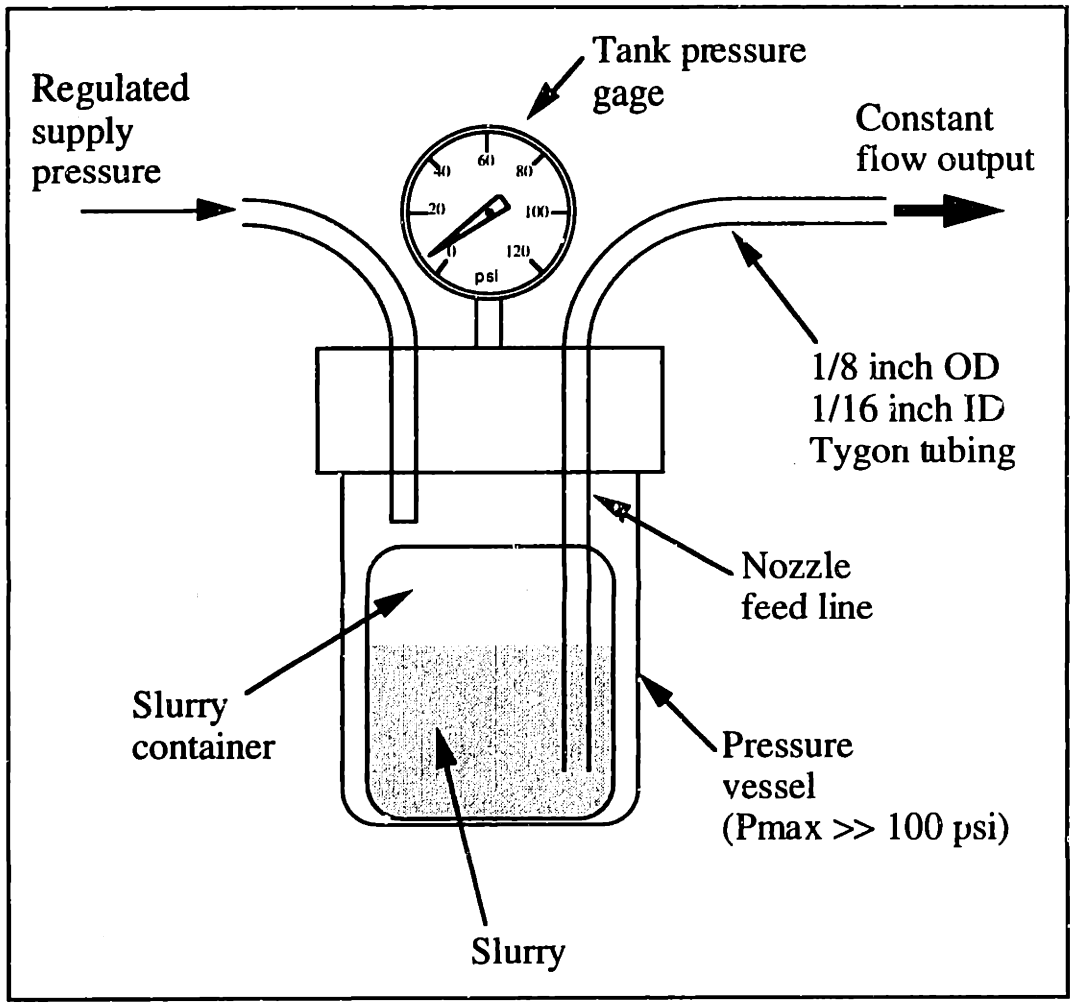

Figure 4.6: Pressurized tank flow control setup

A similar setup had been already been used as a flow source for jetting binder and slurry through very fine nozzles (typically 45 - 70 μm) at pressures ranging from 25 - 50 psi. For such applications, the above setup worked quite well. However, for the case of jetting slurry, the nozzle orifice is relatively large (850 μm for the Sono-Tek unit, 2790 μm for the Misonix unit). As a result, the pressure required to achieve the required flow rate is typically 1 - 3 psi. This means that the flow rate will be sensitive to small variations in the driving pressure. Initial experiments with the above open-loop flow control system showed that the flow rate was not constant. Flow rate measurements made over a 45 minute period using the above setup for a 20 v/o alumina slurry are shown below in Figure 4.7. It can be seen that the flow rate changes significantly over time. This would be unacceptable for the spray deposition process since the resulting layer thickness would also change over time.

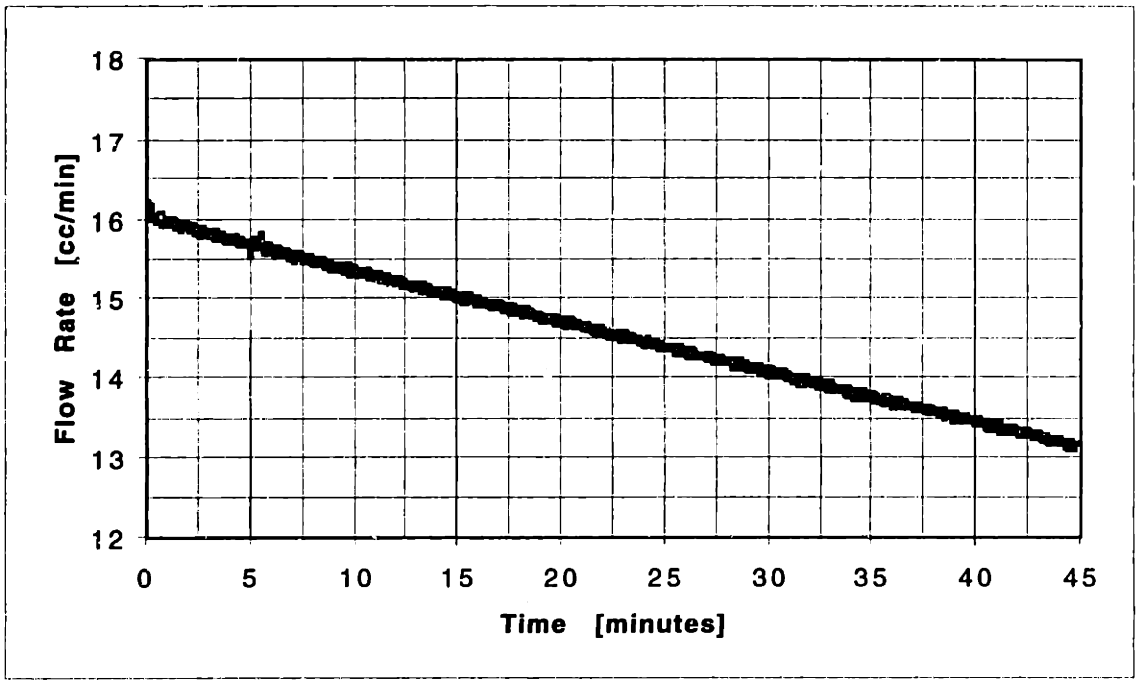

Figure 4.7: Open-loop flow control system performance

There are two sources of pressure variations which could cause the flow rate to change over time. These are the supply pressure and changes in the fluidic pressure head due to the reservoir height. Variations in the supply pressure were minimized by using a large gas cylinder as a pressure source (as opposed to the shop air supply which fluctuates considerably) and a high quality low pressure precision regulator (model no. 700 0-2 psi) from ControlAir (ControlAir Inc., Amherst, NH). The fact that the flow-rate decreases in such a linear fashion indicates that the problem source is not random fluctuations in the pressure supply. As a result, the problem source had to be due to the changes in the fluidic pressure head. In order to compensate for such changes, a closed-loop control system was required.

In order to design a closed-loop control system to maintain constant flow rates, it is important to first examine the relevant physics. A schematic of a pressurized tank system which shows the relevant physics is shown below in Figure 4.8.

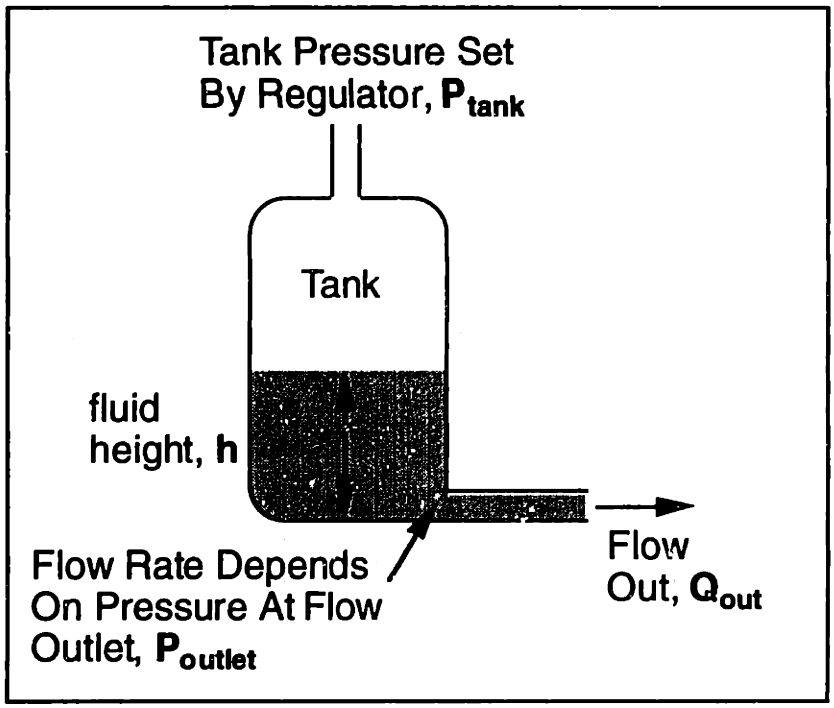

Figure 4.8: Pressure tank system physics

For the above system, without any kind of pressure adjustment during operation, the flow rate will decrease over time. For a slurry of density ρ, the flow rate should be governed only by P_{outlet} assuming the fluidic resistance is constant. P_{outlet} is given by

$$P_{outlet} = P_{tank} + \rho gh \tag{4.1}$$

For P_{outlet} to remain constant,

$$P_{tank} = P_{tank_0} + \rho g(h_0 - h) \tag{4.2}$$

Where P_{tank_0} and h_0 are the initial values of the tank pressure and fluid height respectively and h is the instantaneous height of the fluid column. Equations (4.1) and (4.2) assume the use of a consistent set of units. Although the change in the height of the fluid column cannot be determined by direct measurement, it can be easily determined if the flow rate, Q_{out}, and the reservoir cross-sectional area is known. The change in fluid height, Δh, over a known time period, Δt, is given by

$$\Delta h = \frac{Q_{out}\Delta t}{A} \tag{4.3}$$

where A is the cross sectional area of the reservoir. Methods of measuring the flow rate will be discussed later. Once the height change of the reservoir is known, P_{tank} can be adjusted periodically to keep the flow rate constant.

In order to implement a closed-loop flow control system, several pieces of additional hardware were necessary. The first of these was a way to electronically adjust the pressure with a high degree of resolution. A search of commercially available electronic pressure regulators which are designed to operate at low pressures with high resolution and repeatability was unsuccessful. As a result, a custom pressure regulator was built using a stepper motor and a low pressure high precision regulator (model no. 700 0-15 psi) from ControlAir. The advantage of using a stepper motor is that it can used without a feedback sensor which simplifies the design. Furthermore, since the step size is fairly repeatable, each step can be correlated with a known pressure change (assuming the regulator is linear). A diagram of the physical hardware and a photo of the actual electronic pressure regulator which was designed is shown below in Figure 4.9.

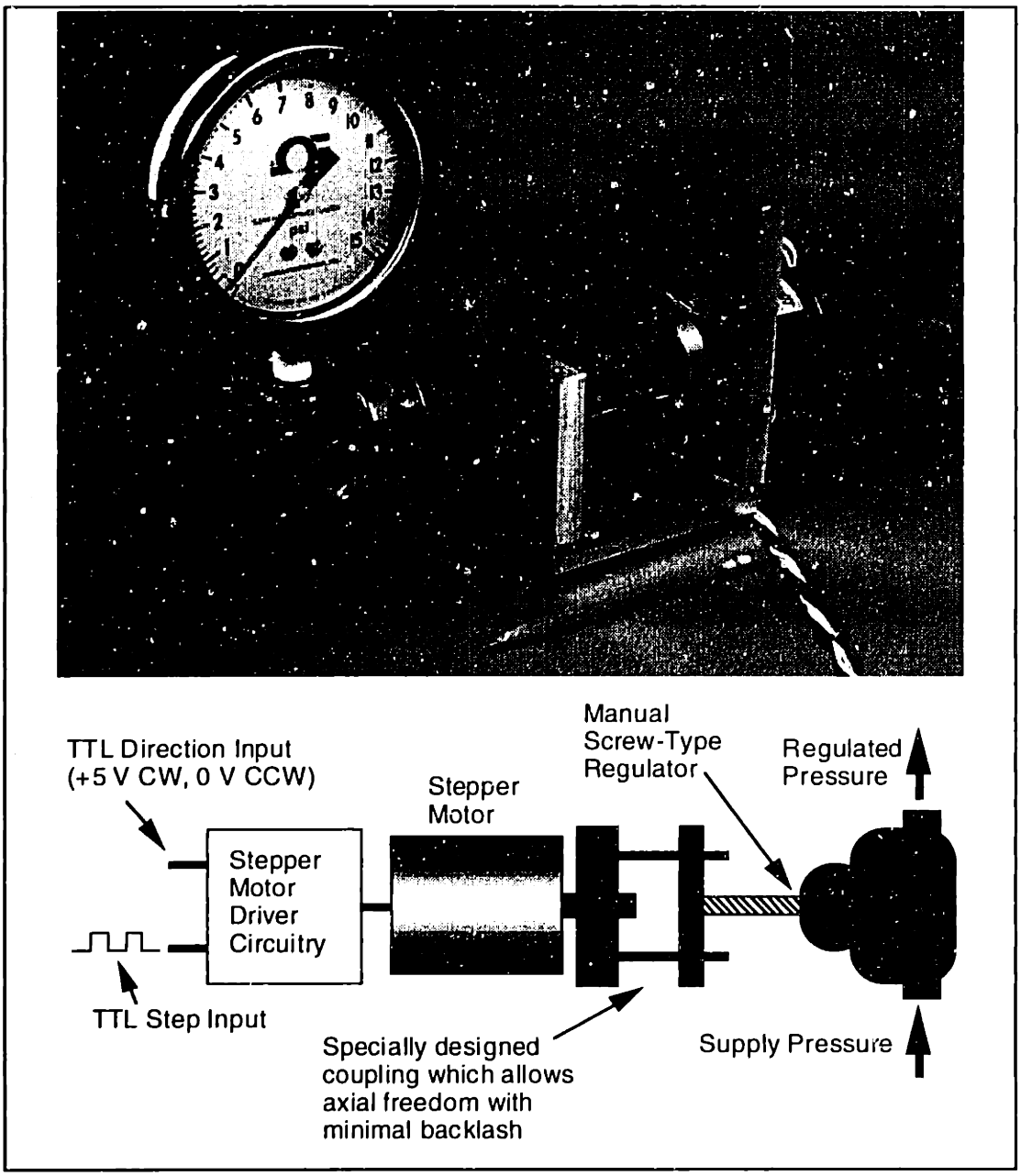

Figure 4.9: Electronically controlled pressure regulator schematic and photo of hardware

From a theoretical standpoint, a closed-loop flow controller only requires a flow rate measurement without any knowledge of the actual reservoir pressure. However, from a practical standpoint, it is useful to be able to directly measure and control the pressure for several reasons. The first of these is a safety standpoint. If the slurry line became clogged, the flow controller would keep increasing pressure without bound in an attempt to match the desired set-point. This could lead to a catastrophic failure of the system. With a pressure sensor, the system can be shut down automatically if the tank pressure becomes to high. The second reason for being able to measure and control pressure is that it turns out

that the closed-loop flow controller is quite slow to reach steady-state when given a step change in the set-point. If the pressure which results in roughly the correct flow rate is known *a priori*, then a pressure controller can be used to set the flow rate close to the desired value. When the flow controller is then activated, the time to reach steady-state can be reduced significantly. As a result, two entirely separate controllers were built: a reservoir pressure controller and a slurry flow controller. The reservoir pressure controller was to be used for setting the reservoir pressure to approximately the pressure required to achieve a desired flow rate. The pressure controller could then be switched off and the flow controller could be turned on to fine tune the flow rate and keep it constant.

In order to implement the pressure controller, a transducer was required to measure the reservoir pressure. A PX72-015GV piezo-resistive pressure transducer (Omega Engineering, Stamford, CT) was selected for its low cost ($15 each) and capability of measuring low pressures accurately. In order to use such a transducer, special custom signal conditioning electronics was designed. The schematic of the pressure transducer circuit is shown in Appendix B. Using a PC equipped with an AT-MIO-16E-1 data acquisition board [National Instruments, Austin, TX], the output of the pressure transducer could be measured by a computer. Using LabView (also a product of National Instruments), a simple proportional controller was implemented to control the pressure at a user defined set point. A block diagram of the pressure controller is shown below in Figure 4.10.

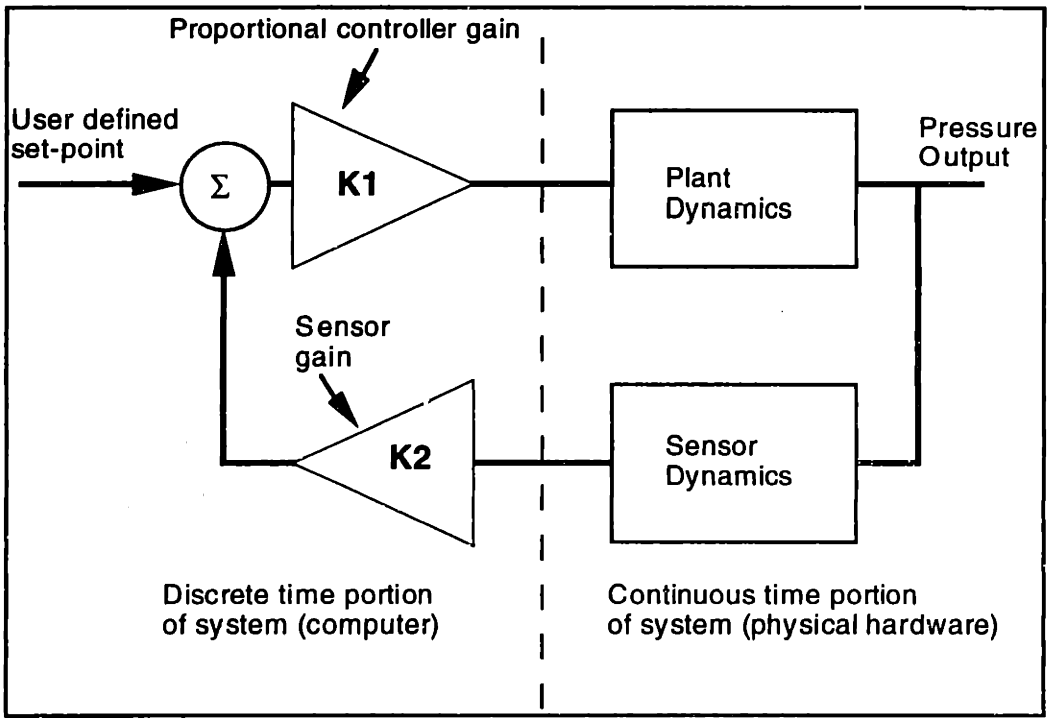

Figure 4.10: Pressure controller block diagram

Little effort was made to optimize the pressure control system since it had settling times which more than an order of magnitude faster than the flow controller (see below). The gain was chosen to give a good transient response without overshoot. In order to assess system performance, the step response was measured for controlling the pressure of an empty 1.6 L pressure vessel. It is shown below in Figure 4.11.

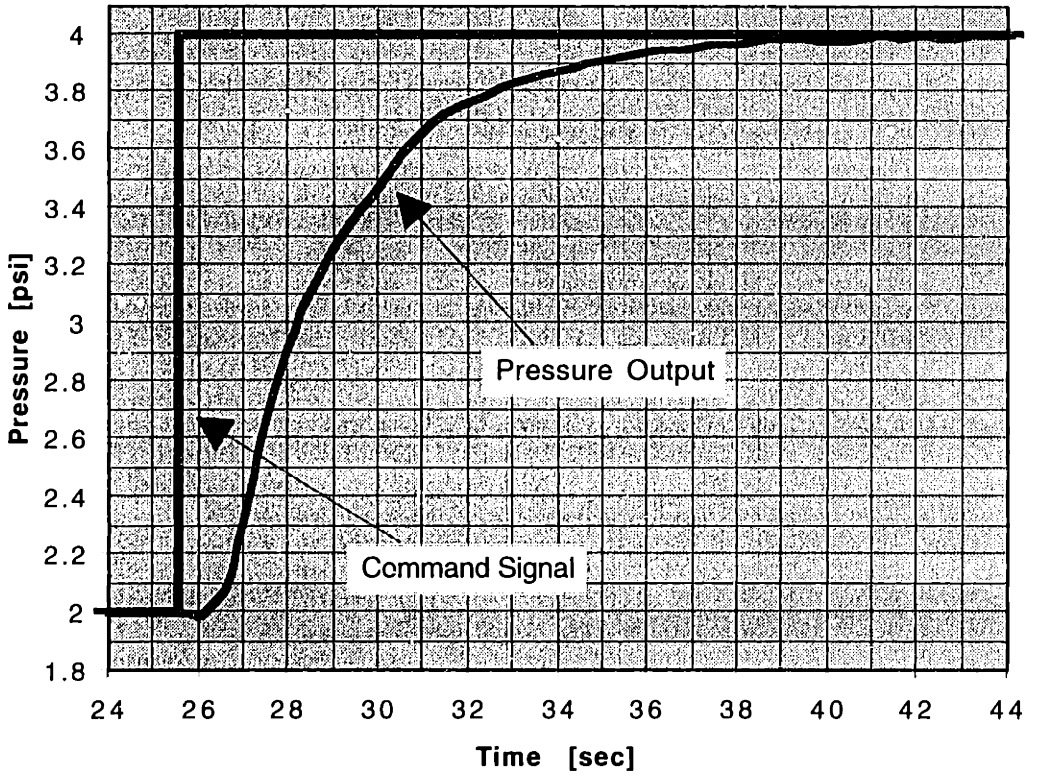

Figure 4.11: Pressure Control System Step Response

From the step response, the transient behavior of the system can be determined. The results of a transient and steady state analysis for the pressure control system are shown below in Tables 4.1 and 4.2. The analysis used to determine these values is described in detail in Appendix C.

Parameter	*Average Value*
Time Constant [sec]	3.2 seconds
1% Settling Time [sec]	13.1 seconds
10-90% Rise Time [sec]	5.8 seconds
Estimated Bandwidth [Hz]	0.06 Hz

Table 4.1: Pressure control system transient response parameters

Pressure Range	0-15 psi
Pressure Resolution	0.008 psi (sensor limited)
Accuracy over 0-5 psi	±0.05 psi
Accuracy over 0-15 psi	±0.15 psi
Errors due to the P-control scheme	negligible at steady state

Table 4.2: Pressure control system steady-state performance

Developing a closed-loop flow controller was much more challenging than the pressure controller. This was a direct result of the fact that it was difficult to make accurate measurements of low flow rates. The problem is complicated by the fact that a non-invasive measurement technique was required since the alumina slurry is abrasive and can destroy moving parts such as those found in turbine and paddlewheel flow meters. The only non-invasive flow meter sold which was able to measure low flow rates accurately (about ±1% in the range of 5-15 cc/min) was the D6 mass flow and density sensor sold by Micro Motion (Micro Motion, Inc., Boulder, CO). This meter works by measuring the coriolis forces induced by fluid flow as it passes through a curved sensor tube. Although the unit appeared to meet the requirements for use in a flow control system, the cost of the Micro Motion unit (about $5000) was reason to search for less costly flow measurement techniques.

Another way to measure the flow rate of the slurry is to measure the mass change of the slurry reservoir. Assuming incompressible flow, the rate at which the mass of the reservoir changes should also be the mass flow rate of the slurry. In order to make a flow rate measurement, the mass change of the reservoir between a known time interval is measured. The volume flow rate is determined by

$$Q = \frac{m_2 - m_1}{\rho \Delta t} \tag{4.4}$$

where Δt is the sampling interval of the balance. To determine the balance resolution required to make reasonably accurate measurements, the desired sampling rate must be known. A reasonable sampling interval would range between 0.5 and 10 seconds. Faster sampling times are not possible due to limitations in the balance update rate. The absolute error in a flow rate measurement is given by

$$\text{error} = \frac{60(\text{balance resolution})}{\rho \Delta t} \tag{4.5}$$

where the error is in [cc/min], the balance resolution is in [g], the fluid density, ρ, is in [g/cc], and the sampling interval, Δt, is in [sec]. A graph of the absolute flow error for a fluid with a density of 1.8 g/cc as a function of sample delay is shown for balances of ±0.1 g and ±0.01 g resolution in Figure 4.12.

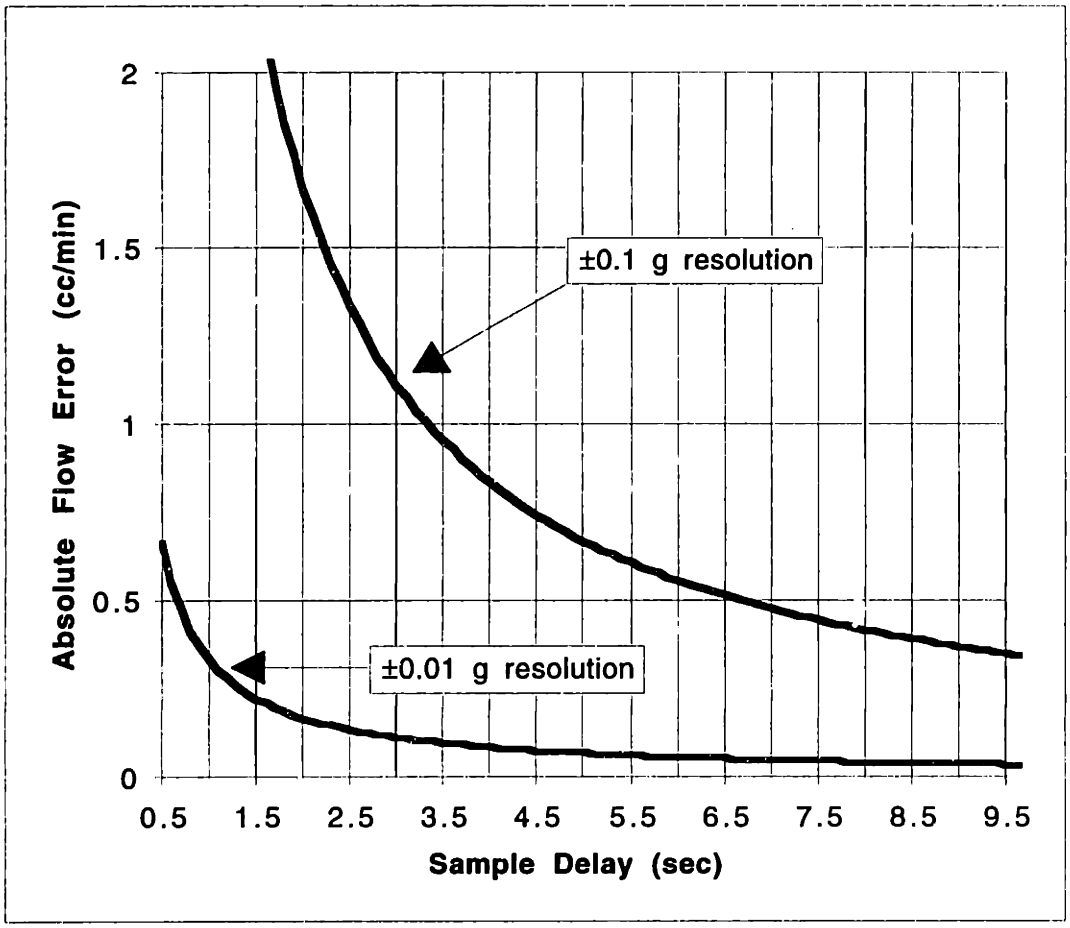

Figure 4.12: Flow error as a function of sample delay and balance resolution (ρ = 1.8 g/cc)

From the above figure, it is immediately apparent that a balance with a resolution of ±0.1 g will be insufficient for measuring flows rates below 10 cc/min accurately. As a result, a Mettler PM2000 high capacity balance with ±0.01 g resolution (Mettler-Toledo, Inc., Hightstown, NJ) was chosen for the flow measurement application. Balances exist which have resolutions of ±0.001 g and high capacity. However, such balances are poor for dynamic measurements since they use special internal filtering algorithms which result in slow update times.

In order to make mass measurements, the slurry reservoir was placed directly on the balance. The balance was then attached to a PC via a standard RS-232 serial connection. One problem that balances with high resolution have is that they are very sensitive to vibrations and air currents. In order to minimize such disturbances, the balance and reservoir was enclosed in a sealed box. The balance was also placed on a vibration isolation sheet. Using LabView, mass measurements could be made at known time

intervals. With this information, Eq. (4.4) could be used to determine the slurry flow rate. With knowledge of the flow rate, the change in the slurry reservoir height could also be determined using Eq. (4.3). Using the reservoir height change information, the pressure could be adjusted to maintain a constant flow rate. In addition, a proportional plus integral compensation algorithm (PI-control) was implemented to prevent flow rate changes due to unmodeled disturbances and allow easy change of the set-point. A diagram of the closed-loop flow control system is shown below in Figure 4.13.

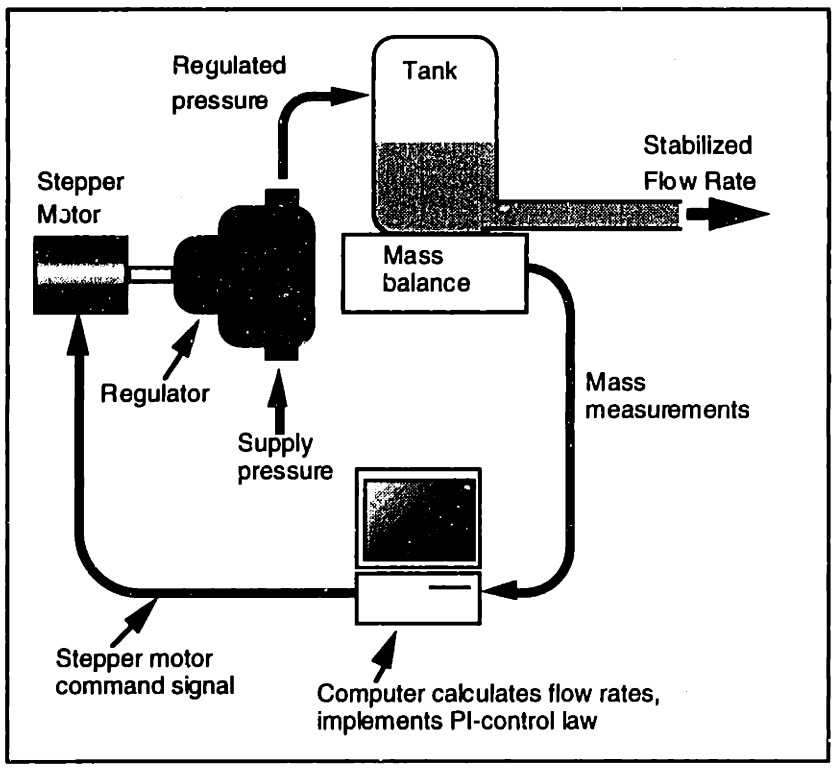

Figure 4.13: Diagram of the closed-loop control of slurry flow rate

The actual computer algorithm which was used to generate the required pressure change during each sampling iteration, ΔP, is listed below in Figure 4.14.

Δt = Sampling time
Qmeas = Measured value of flow rate for the iteration
Qset = Flow rate set-point
Sum = Integrator summation value
g = acceleration due to gravity
ρ = density of the fluid
A = Reservoir tank cross-sectional area
Kp = Proportional Gain
Ki = Integral Gain

$$\Delta P1 = \frac{\rho g \Delta t Qmeas}{A}$$ (pressure increase due to loss of fluid pressure head)

$\Delta P2 = Kp(Qset - Qmeas)$ (proportional control term)

$\Delta P3 = Ki[(Qset - Qmeas)\Delta t + Sum]$ (integral control term)

$Sum = Sum + (Qset - Qmeas)\Delta t$ (recompute integrator sum)

$\Delta P = \Delta P1 + \Delta P2 + \Delta P3$

Figure 4.14: Control algorithm to determine pressure adjustment, ΔP, during each sample iteration to maintain flow rate at a user defined set-point

The gains for the PI-controller, Ki and Kp, were chosen to minimize settling time. Initial performance of the flow controller was rather poor since good flow rate measurement accuracy required a slow sampling period (refer to Figure 4.12). In order to improve transient response and flow control accuracy, dynamic sampling was implemented. In such a scheme, the sampling rate of the controller is adjusted continuously based on the error signal. It is desirable to use short sampling times (about 1 sec) when the error signal is high. In such a situation, some error in the flow rate measurement due to the short sample duration is acceptable since it is desirable to get the flow rate near the set-point as fast as possible. A short sampling duration makes it possible to have a faster rise time. As the output approaches its steady state value, measurement error must be minimized so a slower sampling period (5 sec) is used to improve the flow rate measurement accuracy at the expense of the settling time. Such a scheme makes it possible to have a relatively quick rise-time without degrading steady-state accuracy. In order to assess system transient performance, the step response was measured. For the step response shown below in Figure 4.15, the fluid used was water.

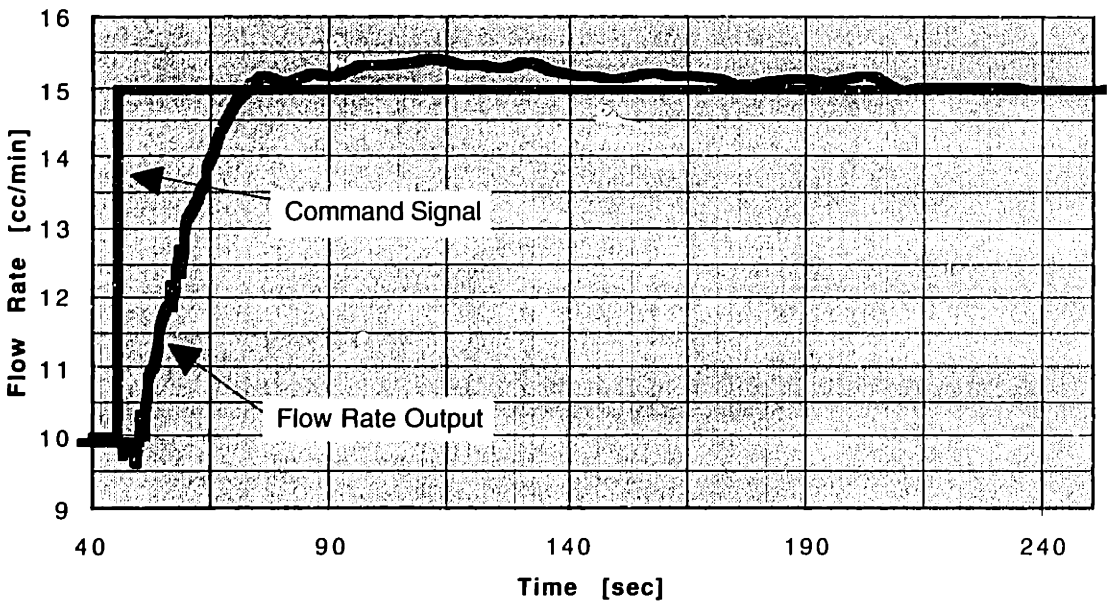

Figure 4.15: Flow control system step response using dynamic sampling

Although dynamic sampling improved the control system performance, the response is still quite slow. This is why it is useful to set the pressure explicitly before initiating the flow controller to speed up the time to reach steady state. The results of a transient and steady state analysis for the flow control system are shown below in Tables 4.3 and 4.4. The analysis used to determine these values is described in detail in Appendix C.

1% Settling Time [sec]	200 seconds
10-90% Rise Time [sec]	16.6 seconds
Estimated Bandwidth [Hz]	0.02 Hz
Percentage Overshoot	8.2%
System Damping	0.62

Table 4.3: Flow control system dynamic response parameters for water

Flow Rate Measurement & Control Range	5 - 75 cc/min
Absolute Maximum Error in Flow Measurement	±0.12 cc/min (at steady state operation)
Absolute Maximum Error in Flow Control	±0.20 cc/min (at steady state operation)

Table 4.4: Summary of steady-state flow control performance

To verify the improved performance, the steady state performance of the closed-loop flow controller was measured under the same conditions as the open-loop system performance showed in Figure 4.7. A graph which compares the open-loop (no compensation) and closed-loop (compensated) flow control systems is shown below in Figure 4.16.

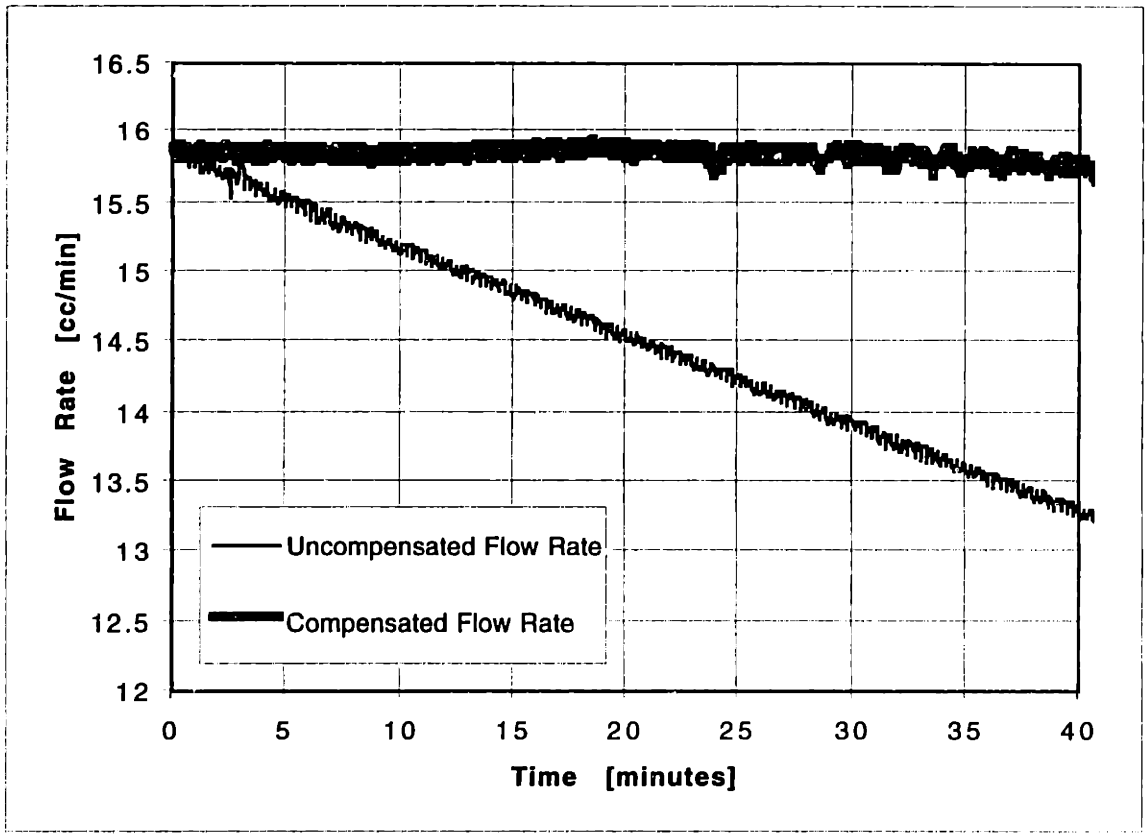

Figure 4.16: Compensated and Uncompensated Flow Control Performance

4.2.3: Motion Control Of Spray Nozzle

The last piece of hardware which was necessary for testing spray deposition was motion control of the nozzle. An X-Y overhead gantry type positioning table (Part no. MD2) using stepper motors (no feedback encoders) was purchased for this purpose (Arrick Robotics, Hurst, TX). The quality of the X-Y positioning table was marginal at best as the carriage had problems with vibrations, mysterious "hick-ups" in the motion, and the start and stop positions were typically not repeatable. Some of these issues were probably related to software problems while others were related to poor mechanical design (e.g. timing belt drive cogs on the motors held with set screws with no flats machined into the motor shafts). Despite the questionable quality of the X-Y table, its performance was adequate for printing several layers for evaluation purposes. However, such a setup would not be adequate for printing parts. Another X-Y overhead gantry type positioning table from Asymtek was evaluated after the purchase of Arrick Robotics unit (Asymtek, Carlsbad, CA). It was far better than the Arrick Robotics unit both in terms of the software, design quality, repeatability, and accuracy [Baker, 1997]. If an X-Y overhead

gantry positioning table were to be purchased in the future, the Asymtek unit would be well worth considering both for spraying and binder printing applications.

4.3: Brief Review of the Relevant Process Physics of Spray Deposition

In the spray deposition approach, the slurry is deposited on the powder bed surface in the form of a spray. It has been shown that the amount of drying which the slurry undergoes while traveling from the nozzle to the powder bed is minimal for aqueous based alumina slurry [Grau, private communication]. As a result, when the slurry reaches the powder bed, it can be assumed that there has been no water loss. It has been reported that the typical layer thickness created using the spray deposition process ranges from 30-60 μm [Khanuja, 1996]. Film thicknesses of this size are large enough that cracking can occur during drying. As a result, it is important to consider the factors which might lead to such problems.

Cracking of layers occurs when the drying stresses in a layer become too large. As the thickness of a deposited layer increases, the stresses during drying also increase. The threshold thickness at which a layer is thick enough for cracking to occur is known as the critical cracking thickness (CCT). The critical cracking thickness for films depends on the material, surface tension of the solvent, and particle size [Grau, private communication]. Smaller particles will have higher capillary stress and result in a lower CCT. The addition of organic additives into the slurry such as PEG and PVA can increase the strength and toughness of the film and result in a larger CCT. The CCT for a film made from pure 0.5 μm alumina has been reported to be about 65 μm [Chiu, Garino, and Cima, 1993]. However, this does not mean that cracking will not occur as long as the thickness of the deposited layer (before absorption into the powder bed) does not exceed the CCT. Because the water in a sprayed layer is absorbed by the underlying powder bed, this region can also contribute to the drying stresses. Thus, the critical dimension to consider is the thickness of powder bed which would be fully saturated by all the water present [Grau, private communication]. This distance is known as the saturation thickness. This is illustrated below in Figure 4.17.

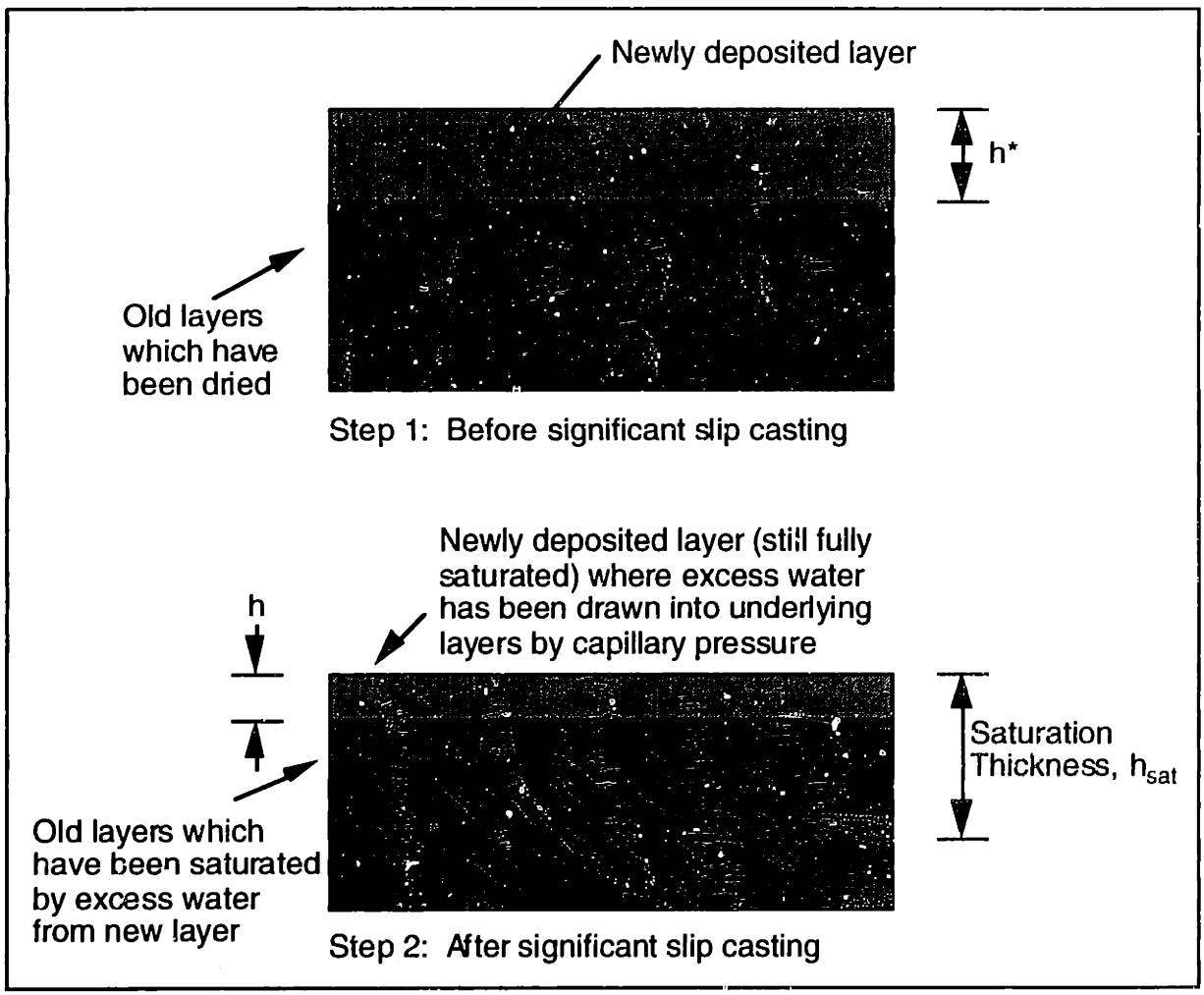

Figure 4.17: Determination of the saturation thickness for cracking analysis

In order to see if the CCT has been exceeded, the saturation thickness must be calculated. If the height, h^*, of a wet deposited layer is known before slip casting can occur, the saturation thickness, h_{sat}, can be shown to be

$$h_{sat} = \frac{1 - VF}{1 - PF}(h^*) \qquad (4.6)$$

where VF is the slurry volume fraction and PF is the packing fraction of the resulting layer. As an example, suppose a layer of 0.5 μm alumina is sprayed deposited resulting in a wet layer thickness (before slip casting) of 40 μm. If the slurry solids loading is 25% (VF = 0.25) and the packing density of the resulting layer cake is 55% (PF = 0.55), then the saturation thickness for cracking determination purposes would be 67 μm. Theoretically, such a layer might have cracking problems since it has exceeded the CCT. However, the

layer may not crack since the above calculation is a conservative estimate. It does not consider the fact that some of the water might evaporate before being absorbed by the powder bed. One might initially be concerned about residual stresses building up as several layers are sprayed. However, it has been shown that after drying, there are no residual stresses present in alumina films due to particle rearrangement during drying [Chiu, 1991]. This is why the drying step is very important. With sufficient drying, it is not important to worry about stresses building up with the spraying of successive layers. The preceding discussion on the CCT of alumina layers can be used as a guide to choose reasonable starting points for slurry spray dose choices but is by no means an exact analysis that can predict when cracks will or will not occur.

4.4: Experiments and Results from the Spray-Deposition Approach

Grau and Khanuja investigated different printing parameters and the ability to generate layers without cracking that exhibited high packing density. They conducted experiments using both the Paasche air-atomizing nozzle and the Sonotek piezo-atomizing nozzle. Parameter variation studies were made which examined raster speed (typ. 10-50 cm/sec), working distance between nozzle tip and powder bed (typ. 25-40 mm), raster spacing (typ. 10-20 mm), and solids loading (typ. 15-30 v/o) [Grau, private communication]. Resulting powder beds were evaluated for surface finish and packing density.

Using the spray deposition technique, powder beds with acceptable surface finish were fabricated. However, care had to be taken to prevent problems such as layer cracking (exceeding the CCT) and blistering (from drying to rapidly). The packing density of resulting layers printed using spray deposition was evaluated using mercury porosimetry. Mercury porosimetry gives both the packing density of a powder bed as well as a distribution of the pore sizes. Grau has quantified typical packing densities for sprayed powder beds using aqueous-based alumina slurry. The packing densities for 15 and 30 v/o alumina slurry was respectively 60% and 54% of theoretical [Grau, private communication]. The pore size distribution of powder beds using these solid loadings is shown below in Figure 4.18 (data provided by Grau). Typically, porosity much greater than 1 μm is difficult to remove during normal solid phase sintering operations of alumina. As a result, sprayed powder beds made using 30 v/o slurry will probably not sinter to full density as they have a significant number of pores ranging from 10-30 μm. On the other hand, powder beds sprayed using 15 v/o slurry exhibit almost no porosity above 0.1 μm and can be expected to achieve nearly full density during sintering.

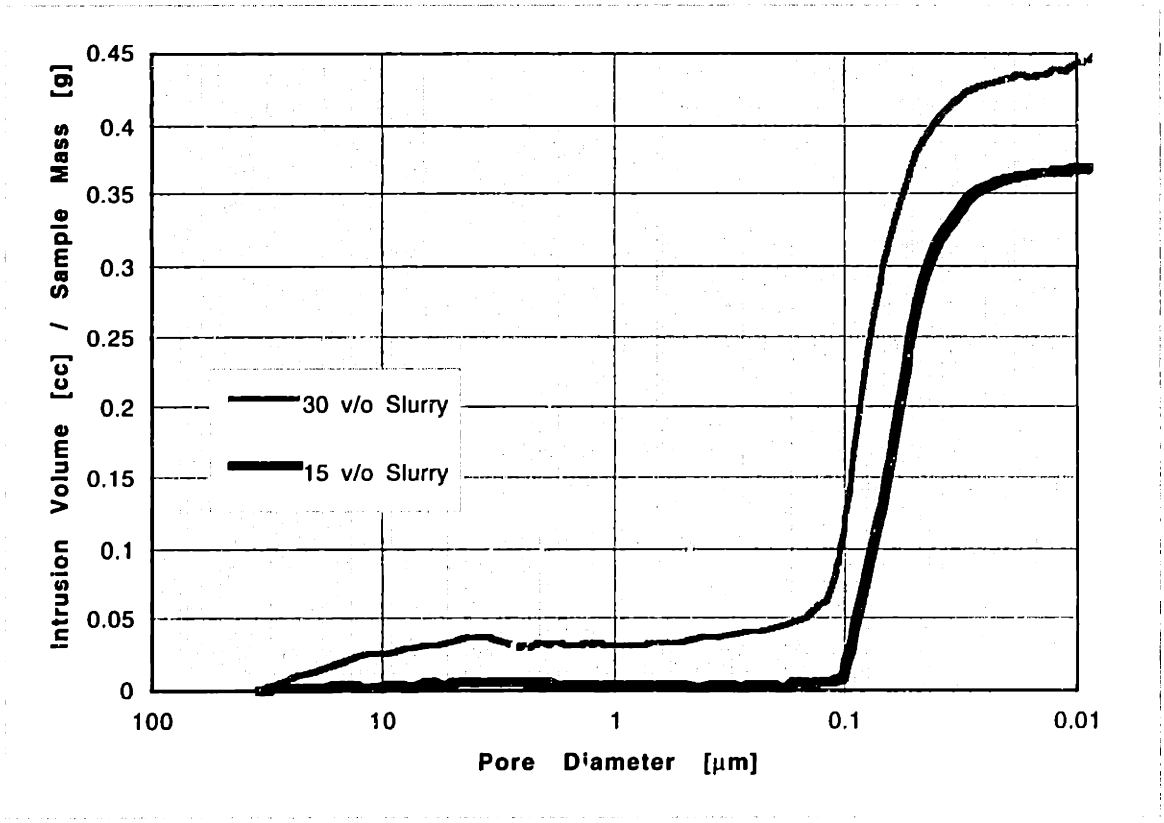

Figure 4.18: Spray deposition powder bed pore size distribution

The surface finish of the powder beds sprayed using 15 v/o slurry appeared to be better than those made using 30 v/o slurry. This is reasonable since the lower solids loading gives the slurry more time to combine on the substrate before slip casting is complete. A photo of the typical surface finish for a 15 v/o sprayed powder bed is shown below in Figure 4.19.

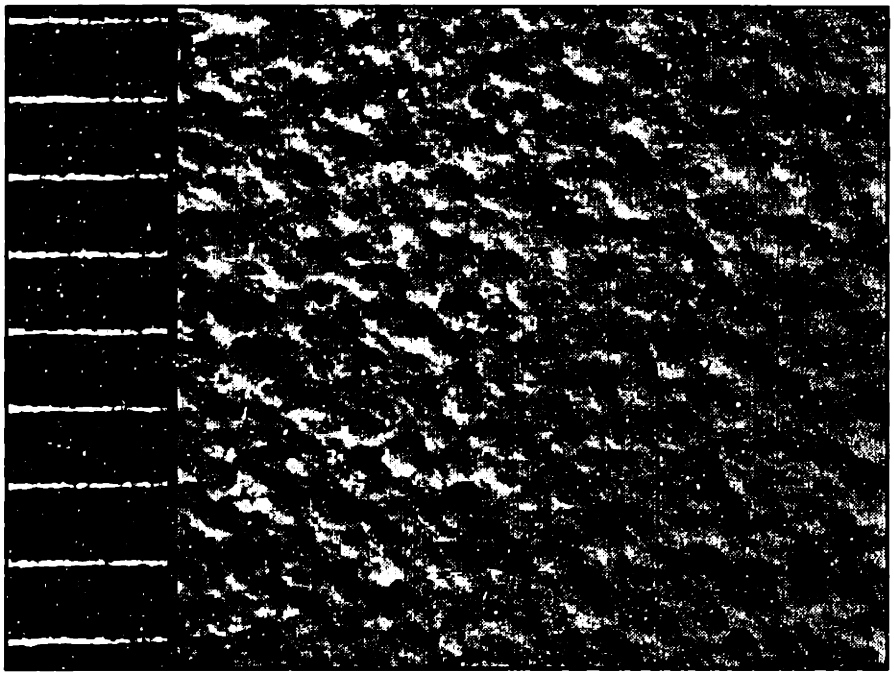

Figure 4.19: Typical sprayed powder bed surface finish using 15 v/o alumina slurry after 15 layers were printed (scale divisions are 1/64 inch apart)

The nozzle type used did not play a significant role in the results presented above. The main difference between the use of air-atomizing and piezo-atomizing nozzles was reliability and ease of use. The air-atomizing nozzles had poorer reliability and had problems with damaging previously sprayed layers due to the high droplet velocity.

Although initial powder bed samples exhibiting acceptable surface finish and packing density were made using the spray deposition approach, making powder beds large enough to print significant parts was not possible. This was due to repeatability and control problems with the nozzles. Even though the piezo-atomizing nozzle was more reliable, both nozzle types would periodically damage the powder bed. In the case of the air atomizing nozzles, erosion of the powder bed from the spray velocity and overspray problems dominated. The air-atomizing nozzle would also partially clog from time to time causing a non-uniform spray. For the piezo-atomizing nozzle, a large problem was slurry build up on the nozzle tip. Periodically, this build-up would be spit out as large drops ruining the powder bed. These problems were serious enough to look for another slurry deposition technique which offered a higher level of control. Although an improved nozzle might make the spray deposition process attractive, it appears that no nozzle which has the required spray reliability and uniformity currently exists.

Chapter 5 : Feasibility Testing of the Ink-Jet Printing Approach

5.1: Ink-Jet Printing Approach to Layer Fabrication

The third and final approach which was examined for fabricating layers for the slurry-based 3DP process was ink-jet printing of slurry. In this approach, a slurry jet is rastered back and forth across the powder bed. This is similar to spray deposition in some respects except that the use of a slurry jet offers a much greater degree of control. It is much easier to make sure the same dose of slurry is applied at all locations in a layer. Although this approach requires a high level of motion control, such hardware already exists because ink-jet printing is central to the 3DP process. As a result, the only step which was required to implement motion control was software changes to the already existing equipment.

5.2: Ink-Jet Printing Nozzle Choices

The biggest hardware issue was the choice of the ink-jet printing nozzle. The choices can be grouped into two categories: small nozzles (127 μm and less) and large orifice nozzles (greater than 127 μm). The nozzle type (small or large) will have important implications about the flow rates, filtration requirements, and jet on/off control. For jetting layers, it is advantageous to be able to operate at low flow rates since the CCT limits the permissible slurry dosage. Filtration is also a big issue with jetting slurries since filters usually build up sediments as time progresses resulting in a steadily but not necessarily predictable declining flow rate. Jet on/off control is important since the slurry nozzle will be mounted on the same motion carriage as the binder nozzle. As a result, it will be necessary to somehow prevent the slurry jet from reaching the powder bed during the binder printing step of the slurry-based 3DP process.

5.2.1: Small Orifice Nozzles

In the past, small orifice nozzles have been used to jet slurries and binder. Usually, ceramic wire-bonding tools sold by Gaiser are used as nozzles (Gaiser Tool Company, Ventura, CA). Such ceramic nozzles are available in sizes ranging from 25 to 127 μm. The ceramic nozzles have been used in the past for a variety of reasons. The first of these being that they are impervious to attack by all solvents currently used in the 3DP process. Secondly, such nozzles are physically robust. The ceramic nozzle orifice does not easily

erode even when abrasive slurries such as alumina are jetted. This can be a problem for other kinds of nozzles such as nickel and stainless steel orifices [Khanuja, 1996]. The main small nozzle selection criterion was the reliability of the resulting slurry jet. Besides never having full clogs where the jet stops completely, a reliable jet does not have partial clogs. Partial clogs can last as little as a second and result in changes in the jet angle or turn the jet into large sporadic droplets. Sometimes, the jet angle will even rapidly switch back and forth during a partial clog. After such disturbances, the jet will usually return to its normal behavior. The different partial clogs are illustrated below in Figure 5.1.

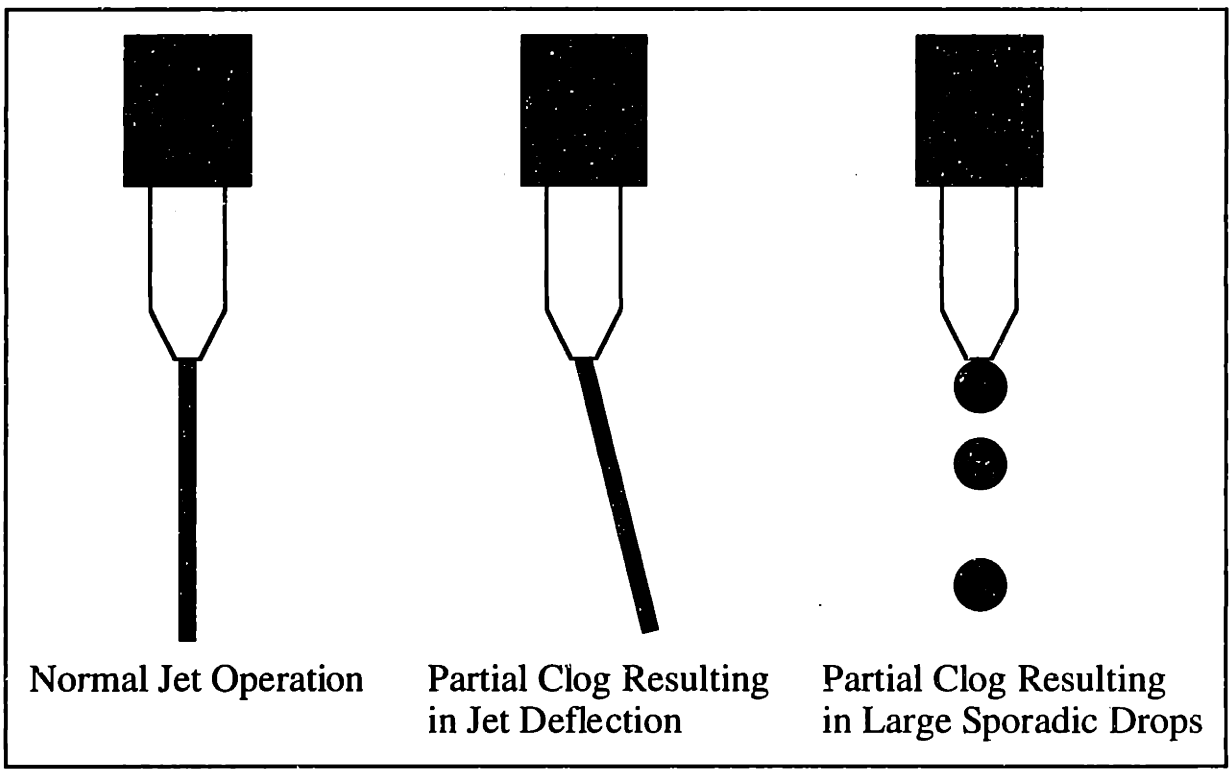

Figure 5.1: Different types of partial clogs

Obviously, such partial clogs are unacceptable since they will result in layers with surface defects. In order to make sure a reliable jet of alumina slurry could be made, experiments were performed to check the performance of different nozzle sizes. Although it is possible to jet alumina slurry through a 45 μm nozzle, it is difficult to prevent partial clogs when jetting slurries of high solids loading through such a small orifice. As a result, only 70 and 127 μm nozzles were tested for jetting slurry.

Experiments were made to check the operating parameters and reliability when jetting slurry through 70 and 127 μm nozzles. The experimental setup for the 70 μm nozzle is shown below in Figure 5.2.

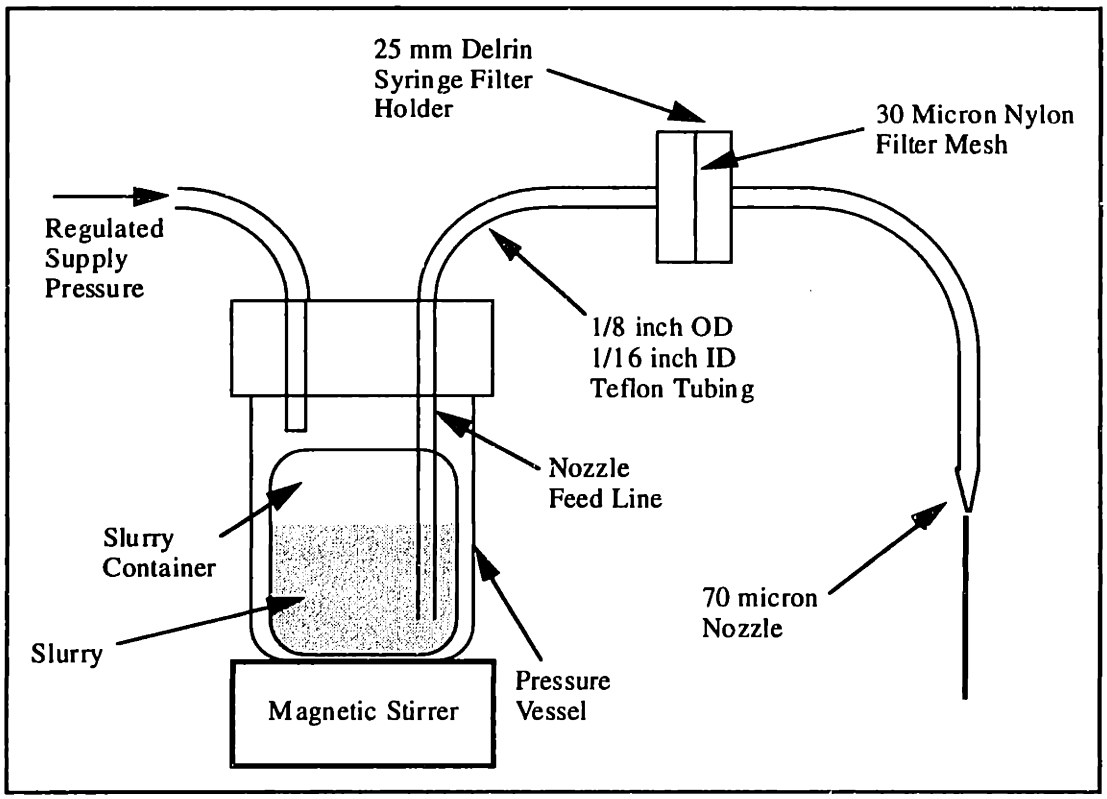

Figure 5.2: Setup for jetting alumina slurry

In order to avoid problems associated with the slurry settling, a magnetic stirrer was used. The stirrer was set at a slow speed to minimize the possibility of introducing air bubbles into the slurry. Since the powder size was 1.0 μm, a nylon mesh filter with 30 μm openings (Small Parts Inc., Miami Lakes, FL) was chosen in hopes that most agglomerates would be smaller than this and would be able to pass through the filter. For the 70 μm nozzle, slurry could be jet for periods of about 10 minutes without full clogging using 35 v/o slurry (1.0 μm Ceralox powder). However, partial clogs were observed every couple of minutes for periods lasting a few seconds or less. Typical flow rates for this case ranged from 0.8 to 1.2 cc/min. Typical pressures for the above experimental setup were about 40 psi. After about 15 minutes of jetting, the filter mesh would be full of sludge. This also presented a problem since the flow rate would gradually drop off as the filter became increasingly filled with particulates.

In order to alleviate the clogging and filtration problems, a 127 μm orifice nozzle was used. This made it possible to use a larger filter mesh which would not become clogged with particulates as rapidly. Using a filter mesh with 53 μm openings, the 127 μm nozzle was able to jet 35 v/o alumina slurry for long periods of time without full or partial

clogs. The limiting factor in this case was again the fact that the filter would eventually clog. However, the rate at which this happened was slowed considerably by the use of the 53 μm filter. For well dispersed slurries, the filter could be used from 30 minutes to an hour before cleaning was required. This problem could be further minimized by using a filter with a much larger surface area. The 127 μm nozzle exhibited flow rates ranging from 1.8 to 2.5 cc/min at pressures ranging from 24-30 psi. From these experiments, it was decided that the 127 μm nozzle would be the best choice of the small orifice nozzles since it offered reliable performance with reasonable flow rates.

Unfortunately, slurry jet on/off control is complicated with the small orifice nozzles. The slurry flow cannot be simply pinched for such a small orifice since this almost guarantees a full clog will occur upon attempting to start the jet again. Such small orifices must be left running continuously. As a result, there are only two options for turning the slurry jet on and off. The first of these is to employ an electro-static deflection scheme to deflect the slurry into a catcher when binder is to be printed. The second option is to use some kind of mechanical catcher with a solenoid which could be placed under the jet when it is to be shut off. Both of these approaches to slurry jet on/off control could be complex design challenges.

5.2.2: Large Orifice Nozzles

A second approach to the jetting problem was to use relatively large orifice nozzles ranging from 150 μm to 350 μm. In this case, fluid dispensing hypodermic needles (Small Parts Inc., Miami Lakes, FL) with blunt ends were used as nozzles. These needles were made of stainless steel and used a luer-lock fitting for fluid connections. Three large-orifice nozzle sizes were studied: 203 μm, 254 μm, and 330 μm. There were several reasons for pursuing the large orifice nozzle concept. The first of these being that if the orifice was large enough, no filtration would be required. This would eliminate the problem of clogging filters and changing flow rates. The second advantage was the jet on/off control. If a large enough orifice was used, the slurry jet could be turned on and off by simply pinching the slurry flow. This would be much simpler than the elaborate schemes necessary for turning the jet on and off if a small orifice nozzle was used. The downside to using the hypodermic needles would be relatively high flow rates.

It was discovered during layer printing experiments that the slurry jet must reach the substrate as a laminar jet (as opposed to individual droplets) in order to achieve good surface finish. In order for this to happen, the slurry jet needs to have a break-off distance of at least 3-5 mm from the needle tip (to be discussed further in Section 5.4.1). In order to make sure that the laminar region was long enough, the resulting jet from a hypodermic

needle was observed with a CCD camera and carefully characterized. A schematic of a typical alumina slurry jet exiting a hypodermic needle is shown below in Figure 5.3.

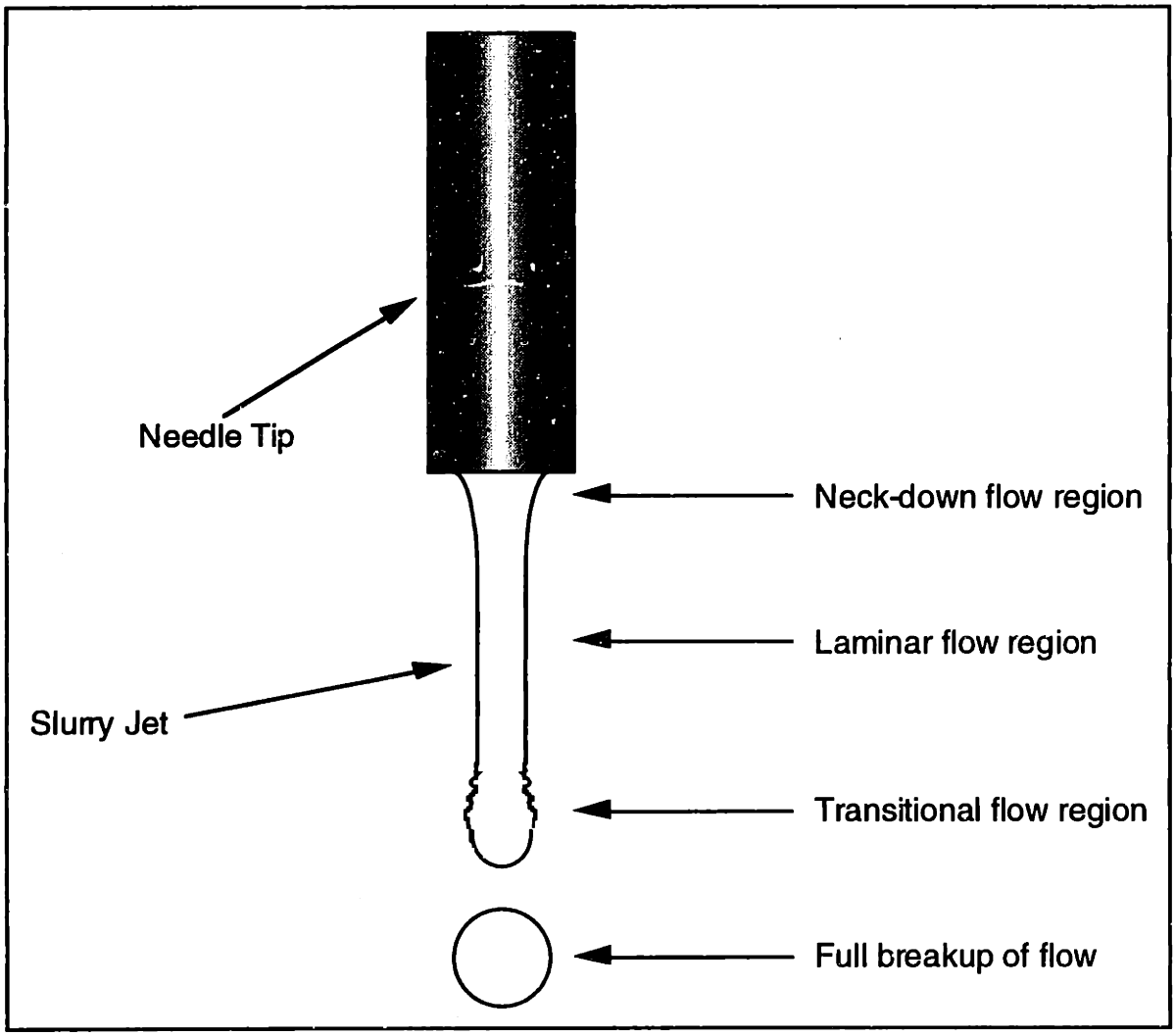

Figure 5.3: Regions of slurry jet from the needle tip

The four important regions of the slurry jet are the neck-down region, the laminar flow region, transitional flow region, and the full break-up (turbulent) region. The break off-distance is the point where individual droplets can be distinguished. For layer printing purposes, it is desirable to have a laminar flow region which extends at least 3-5 mm from the needle tip. In some cases for needle jetting, no laminar flow region exists (observed at very low flow rates). In other cases, the laminar flow region was more than 10 mm long (observed at high flow rates). To give an idea of the typical lengths of these regions, each was measured for the 254 μm needle (inner diameter) using a CCD camera. The results of these measurements are shown below in Table 5.1.

Needle Inner Diameter	254 μm
Slurry Description	35 v/o alumina, 1.0 μm powder
Volume Flow Rate	2.7 cc/min
Neck down region length	200 μm starting from needle tip
Laminar Flow region length	2000 μm starting from the end of the neck down region
Transitional Flow region	1300 μm starting from the end of the laminar flow region
Full Breakup of Flow	5000 μm from needle tip

Table 5.1: Typical slurry flow region lengths for a 254 μm needle

The parameter of greatest interest was the distance from the needle tip to the end of the laminar flow region. This would set the maximum distance between the needle tip and the substrate to be printed on. The neck down region is so short that it could be ignored since the needle tip should never be so close to the powder bed or else a crash might occur.

In order to determine a reasonably sized large-orifice nozzle, several parameters were studied. These were filterless jetting capability, laminar flow lengths, flow rates, and resistance to clogging when turned on and off. An advantage of the large orifice nozzles is the possibility of performing jetting without an in-line filter. In order for this to be successful, it is important to use fresh unflocculated slurry. It is also important to remove any large particulates immediately before jetting. To do this, a standard powder sieve with an opening size of 38 μm (W.S. Tyler Inc., Salisbury, NC) is placed over a large funnel with a beaker underneath to collect the slurry. The slurry is then poured into the sieve to remove large particulates. The sieve is then cleaned and the procedure is repeated again to ensure the removal of agglomerates. After filtering, the slurry is put under a vacuum of 25 inches of mercury to remove air introduced during the milling and filtering process. Increasing the vacuum more than this is not a good idea since it will result in foaming of the slurry. After preparing the slurry in the way described above, several filterless jetting capability tests were performed. Each needle was checked to see if it had a reliable slurry jet which was stable and did not clog when no filter was used. The 254 μm and 330 μm needles never clogged. However, the 203 μm needle clogged several times. As a result of this, the 203 μm needle was ruled out as a candidate for slurry printing.

The next set of experiments looked at flow rate and the laminar flow region length. These two parameters are measured together since the laminar flow region length is a function of the flow rate. The flow rate was measured at several points for each needle over a range of reasonable laminar flow region lengths (about 3 to 7 mm). Lengths below

3 mm require the needle to be precariously close to substrate (while traveling at 1.5 m/sec or higher). Laminar flow region lengths above 7 mm require flow rates which are too high. A plot of the measurements showing the flow rate necessary to create a certain laminar flow region length is shown below in Figure 5.4. Only one measurement was made for the 203 μm needle due to clogging problems.

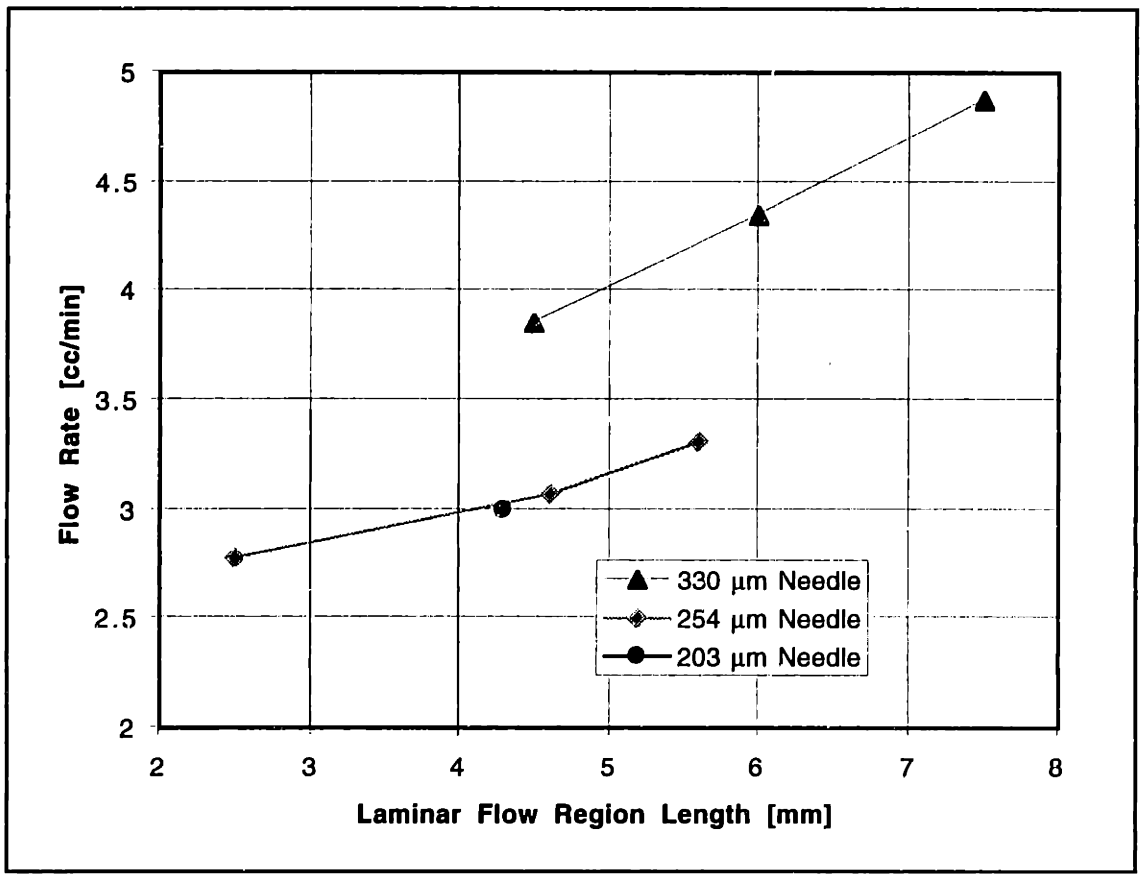

Figure 5.4: Laminar flow region length as a function of flow rate

The 254 μm needle exhibits flow rates which are close to those used for printing powder beds using wire bonding tools as a nozzle. The flow rates obtained with the 330 μm needles are probably too high and would flood the powder bed resulting in cracking problems. The flow rate is basically limited by the fastest raster velocity which can be used (see discussion of slurry dosage in Section 5.3).

For the 330 μm and 254 μm needles, experiments were performed to check if the slurry jet could be shut off for long periods of time and then revived by simply restoring the slurry flow. Two ways were considered for implementing such an on/off jet capability. The easiest way was to use a pinch valve to block the slurry flow. However, initial experiments revealed a problem with this approach. When the slurry flow was pinched, a

drop of slurry would form on the outside of the needle tip and dry. This is illustrated in Figure 5.5. Sometimes this drop could not be blown off with a large pressure increase. Sometimes, the droplet would also cause excess slurry to dry on the needle tip. When the jet was restarted, this dried slurry would perturb the jet departure angle.

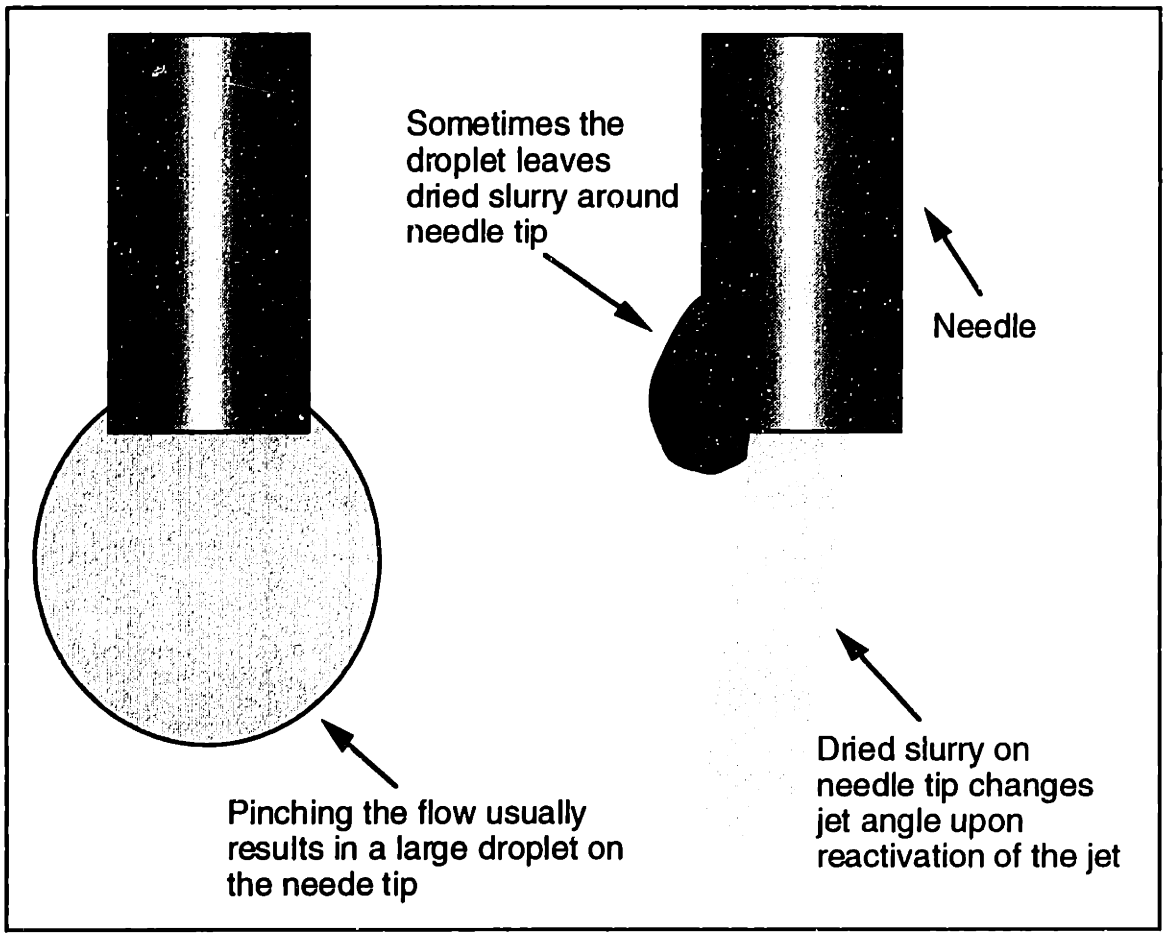

Figure 5.5: Problems with using pinch valves for jet on/off control

A second way to implement on/off control which avoids these problems is to control the tank pressure. Using several pressure sources, the jet could be turned on and off. The droplet formation problem on the needle tip could be eliminated by briefly drawing a vacuum to draw the droplet back into the needle tip. A schematic of the system which was implemented is shown below in Figure 5.6.

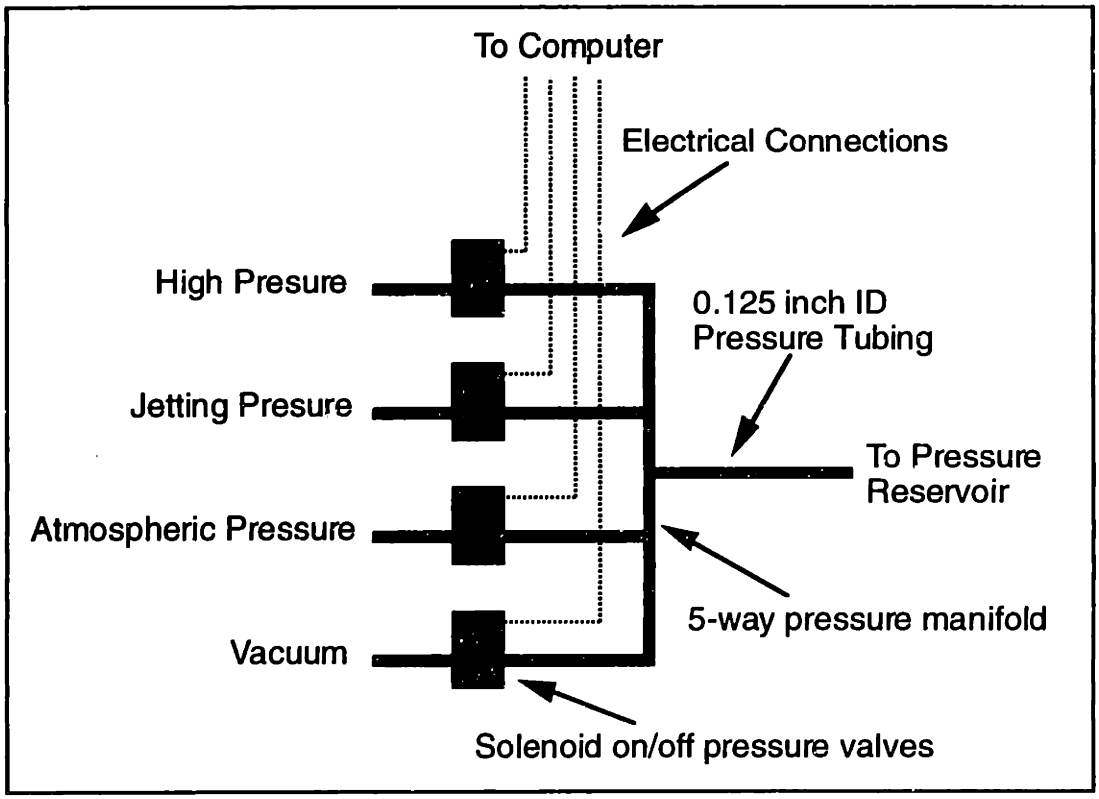

Figure 5.6: Schematic of the on/off needle flow control system

In order to turn the jet on, the high pressure switch was opened. This would blow out any slurry that might have dried in the nozzle. After several seconds, the normal jetting pressure switch was opened while closing the high pressure switch. To turn the jet off, the jetting pressure switch was turned off and the vacuum was briefly applied to suck any excess slurry into the needle. After that, the atmospheric pressure switch was opened. The 254 and 330 μm needles were tested to see how much boost pressure (above the normal jetting pressure) was required to revive the jet after being off for 2,4, and 5 minutes. The results are shown below in Table 5.2.

Duration of OFF period	*Pressure boost for 254 μm needle*	*Pressure boost for 330 μm needle*
2 minutes	1 psi	1 psi
4 minutes	6 psi	3 psi
5 minutes	8 psi	5 psi

Table 5.2: Jet activation pressure boost requirements

With large slurry tubing (1/16 inch ID), the slurry jet starts up and reaches steady state in a couple of seconds. With the thin slurry tubing that is commonly used (typical ID of 0.015

inch), it takes more than 10 seconds for the slurry jet to achieve steady state behavior once restarted. Once revived, the slurry jet behaved as it did before being turned off as long as no slurry dried on the outside of the needle. Although this did occur once in awhile, it happened much less frequently than with the pinch valve approach to on/off jet control.

From the results of the above experiments, the 254 μm needle was chosen as the best large orifice nozzle to use since it had good filterless reliability, reasonable flow rates, and could be turned on and off in a reliable fashion. Although the use of the hypodermic needles has several advantages, there are several drawbacks which should also be considered. The first of these is the limited physical robustness of the needles. Compared to the wire bonding tools, the hypodermic needles are easy to damage. This includes bending or marring the needle orifice as well as susceptibility to chemical attack. The fact that the nozzle is made of stainless steel is of some concern when jetting alumina slurry since there could be problems with erosion (from the abrasive nature of the alumina) and corrosion (from the acidity of the slurry). For nozzles which were used for several hours, no change in the orifice diameter could be observed. However, there were some problems with the needles starting to rust. Another problem with the needles is that there seems to be relatively poor dimensional control of the inner diameter. The inner diameter of a random sample of needles was measured and the result deviated from the nominal value as much as ±15% [Terrazzoni, private communication]. This is a concern since a variance in the geometry means the optimal printing parameters may change with a needle swap. However, the hypodermic needles are so inexpensive that a large supply could be purchased to select ones which have similar dimensions.

5.3: Brief Review of Relevant Process Physics in Ink-Jet Printing Layers

Unlike the spray deposition and tape casting approaches to layer fabrication, the ink-jet printing approach gives very localized control of the layer build process. In this process the most fundamental unit is the individual line. When a line is printed, it quickly slip casts on the powder bed (see Section 3.3 for a discussion of slip casting) before the next line is printed (see Section 5.4.9). The resulting nominal build height of a layer can be quantified with knowledge of the raster velocity, line spacing, flow rate, and packing density. A schematic showing the important parameters in building a layer are shown below in Figure 5.7.

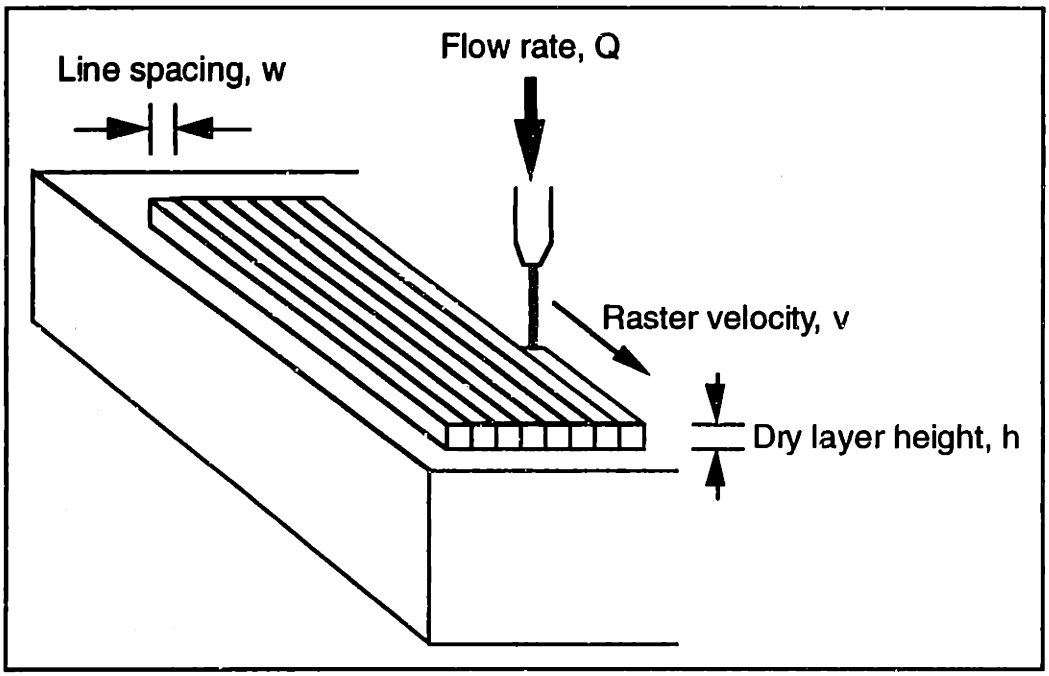

Figure 5.7: Important parameters in ink-jet layer fabrication

Assuming that the slurry printed in each pass is constrained by the neighboring lines, the wet height, h*, of a printed line before slip casting or drying takes place is given by

$$h^* = \frac{Q}{w \cdot v} \tag{5.1}$$

where the SI unit system is employed. Unfortunately, such units are not always the most convenient to use. Eq. (5.1) can be written in terms of more useful units where in this case, h* is in [μm], Q is [cc/min], w is in [μm], and v is [m/sec].

$$h^* = \frac{Q \cdot 10^6}{60 \cdot w \cdot v} \qquad \text{(see above for units)} \tag{5.2}$$

The final height of the resulting dry layer, h, will be determined by the solids volume fraction of the slurry, VF, and the packing fraction (packing density) of the resulting powder bed, PF.

$$h = \frac{VF}{PF} \cdot (h^*) \tag{5.3}$$

Since h is directly proportional to h*, any units can be used with Eq. (5.3).

It is important when picking printing parameters that the CCT is not exceeded. As discussed in Section 4.3, the saturation thickness, h_{sat}, should not exceed the CCT to avoid cracking. Substituting Eq. (5.2) into Eq. (4.6), we find the saturation thickness as a function of the printing parameters.

$$h_{sat} = \frac{Q \cdot 10^6}{60 \cdot w \cdot v} \cdot \frac{1 - VF}{1 - PF} \tag{5.4}$$

Keep in mind that Eq. (5.4) uses non-standard SI units where h_{sat} is in [μm], Q is [cc/min], w is in [μm], and v is in [m/sec]. Assuming the use of 35 v/o alumina slurry and a packing density of 55% (1.0 μm powder), plots of the saturation thickness as a function of line spacing are shown below in Figure 5.8 for a raster speed of 1.2 m/sec.

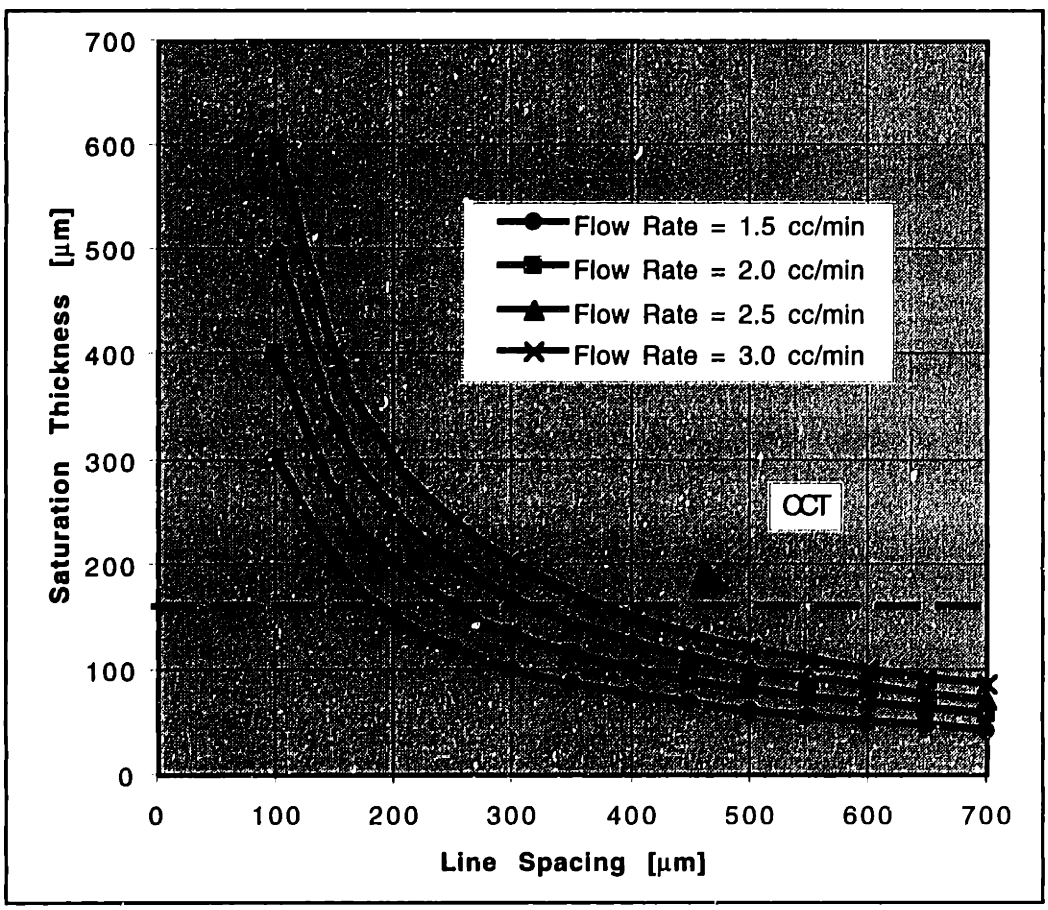

Figure 5.8: Saturation thickness as a function of printing parameters for 1.0 μm powder and a fast-axis speed of 1.2 m/sec

When choosing printing parameters, Eq. (5.4) should be used to check that the effective layer height does not exceed the CCT of the slurry type being used. Grau has investigated the dependence of the CCT on powder size for the Ceralox 0.5 and 1.0 μm powders. This data is shown below in Table 5.3.

0.5 μm Powder (Packing Fraction = 0.60)		*1.0 μm Powder (Packing Fraction = 0.55)*	
Saturation Thickness	*Result*	*Saturation Thickness*	*Result*
less than 60 μm	crack free	less than 133 μm	crack free
60 - 70 μm	cracks are possible	133 - 160 μm	cracks are possible
greater than 70 μm	will crack	greater than 160 μm	will crack

Table 5.3: Cracking results for different saturation thicknesses

In order to have some sense of how to determine an optimal set of printing parameters for attaining good layer surface finish, it is important to consider all the experimental variables. The most important experimental variables are listed below:

- Raster speed
- Line spacing
- Flow rate
- Intra-layer line placement
- Inter-layer line placement
- Nozzle orifice size
- Slurry solids loading
- Slurry particle size
- Slurry wetting angle
- Powder bed temperature
- Dwell time between lines in a layer

Although there are quite a few parameters listed above, they may not all independent. One way to attempt to predict the parameters which will result in good surface finish is to make some simplifying assumptions of how the layers will stitch together and stack on top of one another. The first simplifying assumption which can be made is that the shape and width of an individual line is mainly dependent on the slurry dose. The slurry dose, D, is defined as the volume of slurry deposited per length of printed line or

$$D = \frac{Q}{v} \tag{5.5}$$

where Q is the flow rate and v is the raster velocity. Originally, it was hypothesized that the cross section of an individual line should be roughly the same as long as the dose remained constant. This would reduce the number of necessary experiments since many combinations flow rate and raster speed would then result in a similar surface finish. In order to check this assumption, three lines were printed with the same dosage that had different combinations of fast-axis velocity and flow rate. The printing parameters of each line are shown below in Table 5.4.

Line Number	*Flow Rate*	*Raster Velocity*	*Dosage*
1	2.0 cc/min	2.5 m/sec	0.000133 cc/cm
2	1.8 cc/min	2.25 m/sec	0.000133 cc/cm
3	1.6 cc/min	2.0 m/sec	0.000133 cc/cm

Table 5.4: Printing parameters for line dosage experiment

The cross section of the printed lines was then measured using a Dektak-8000 profilometer. A plot which compares the profile of each of the printed lines is shown below in Figure 5.9.

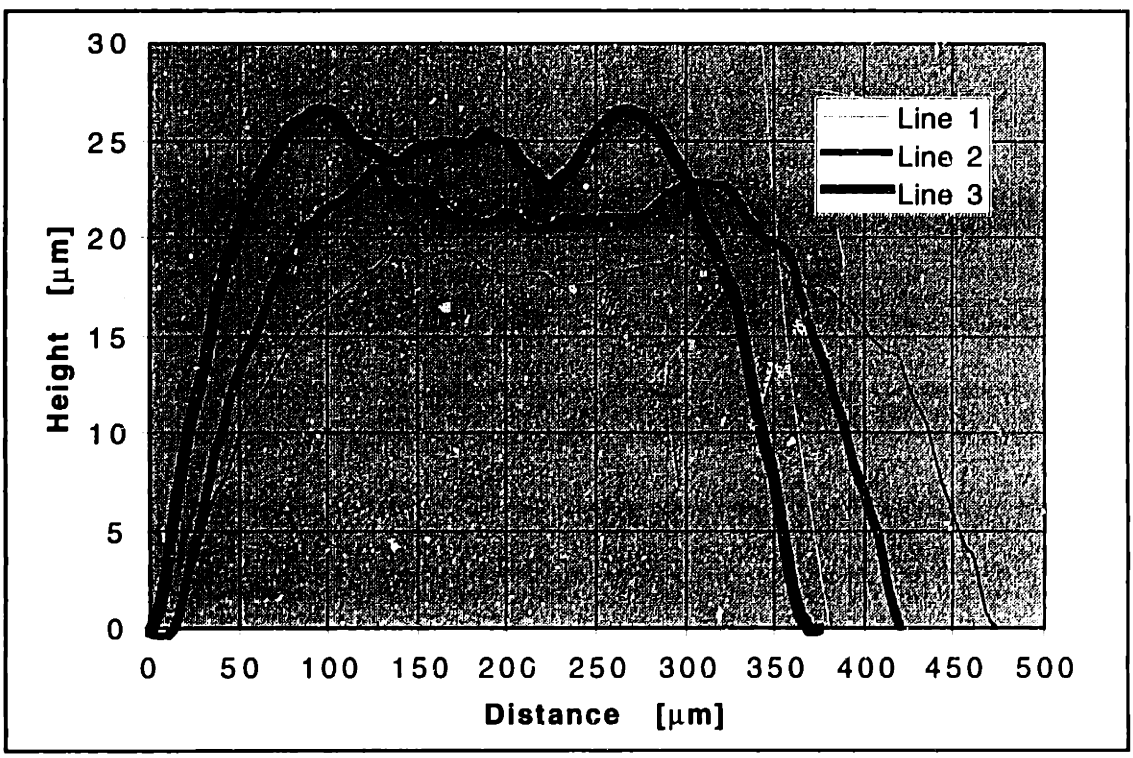

Figure 5.9: Comparison of lines printed with the same dosage (see Table 5.4 for printing parameters)

This figure clearly shows that lines of the same dosage do not have identical profiles. As the flow rate increased, the lines spread out more with a lower resulting height. The higher flow rate profile (Line 1) also had a smoother profile with less noticeable slip casting defects. Thus, it appears to be desirable to maximize the flow rate when picking a particular printing dosage in order to get lines with a smoother top profile. This data also shows that the assumption that surface finish is only a function of dosage is not valid.

Another assumption has to do with resulting surface profile perpendicular to the fast-axis direction. The surface profile results from the printing of individual lines. A first-order approximation which predicts the surface along the slow-axis direction is to assume that the resulting surface profile of a layer after printing can be determining by simple addition of heights. Thus, if we know exactly where the lines are placed and their profile, we will be able to predict the resulting cross-sectional profile of the layer. This is illustrated in Figure 5.10 with the following assumptions for illustrative purposes: 1) the lines have a triangular distribution 2) The lines are printed such that the ends of the triangular distributions meet 3) The lines in the second layer are printed on top of the lines in the first layer.

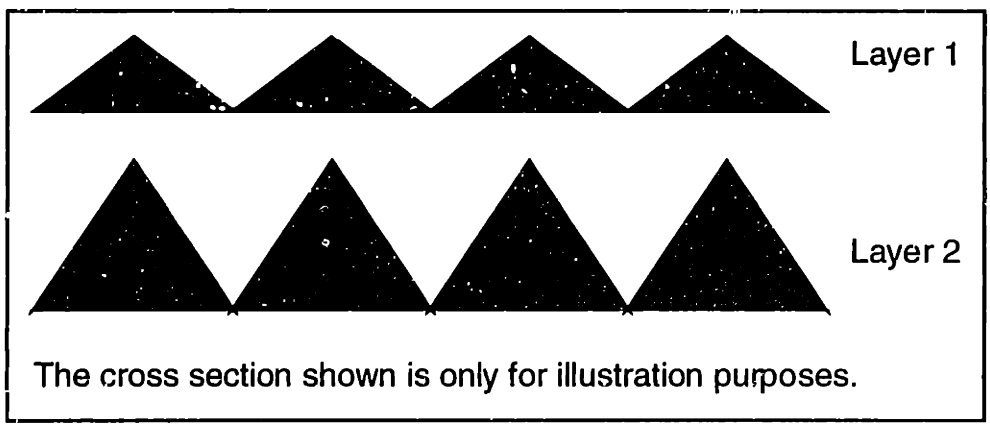

Figure 5.10: Resulting layer cross-sectional profile using additive model

Such an assumption would allow one to simply run simulations to determine which printing parameters would result in a good surface finish. The profile of a typical printed line is shown below in Figure 5.11.

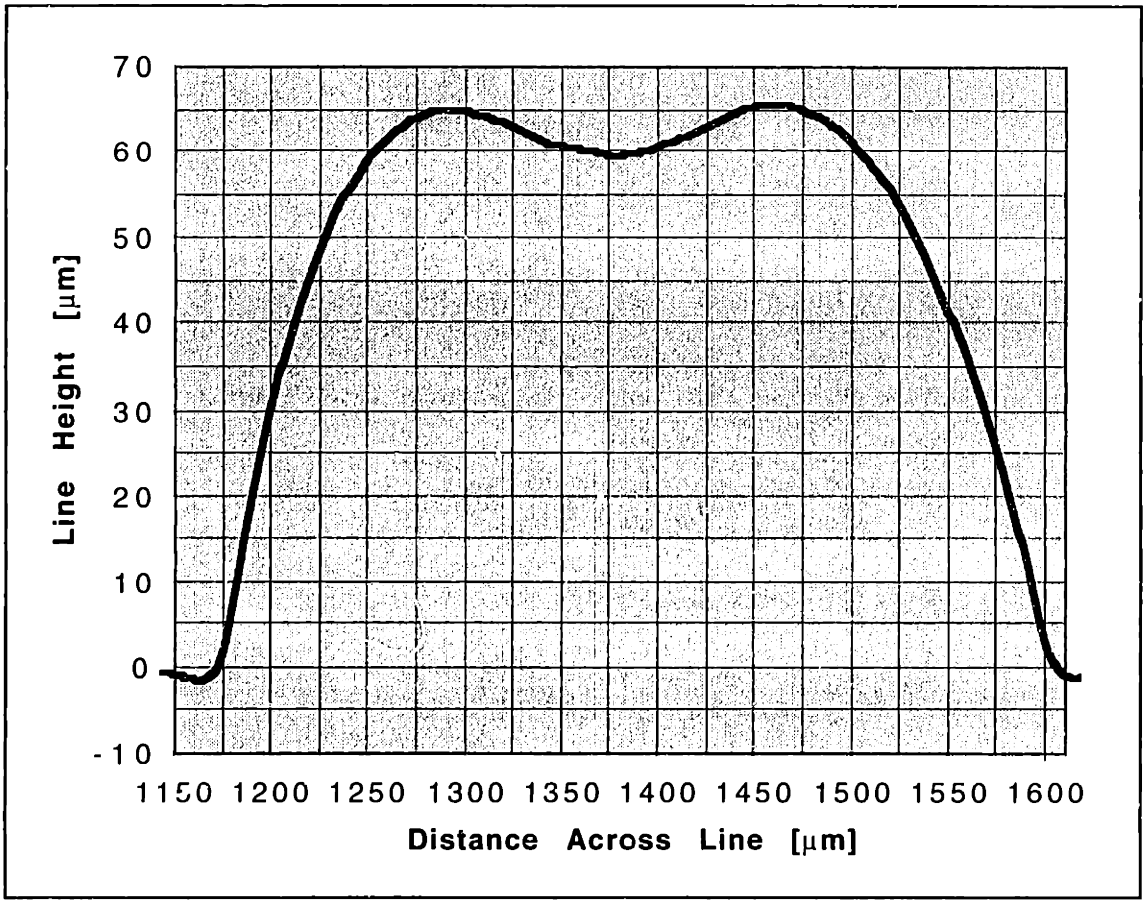

Figure 5.11: Typical printed line cross section using 35 v/o alumina slurry, 254 μm nozzle, fast-axis speed of 1.3 m/sec, and a flow rate of 3.1 cc/min

The profile was measured using a Dektak 8000 surface profilometer (Veeco Instruments Inc., Santa Barbara, CA). The fluid system used to generate the above line was 35 v/o slurry jetted through a 254 μm hypodermic needle. The printing parameters were a raster speed of 1.3 m/sec and a flow rate of 3.1 cc/min. Similar profiles were measured with the 127 μm nozzles except the height and width would usually be less. The depression visible at the top of the line cross section is not an abnormality. This was observed for all printed lines. However, the size of the depression grows with increasing slurry dose. It is the result of the fact that the slip casting rate is not uniform across the width of the line (refer to Section 3.3). The fact that the slip casting rate is the highest at the line edges results in the depression at the line center.

Although this assumption that surface finish can be predicted using an additive model would simplify the printing parameter search, this assumption does not appear to hold up very well. The troublesome factor is the uneven slip casting rates of a printed line. Although the effect of uneven slip casting is negligible for an individual line, the situation changes completely when a line is printed next to a previously existing one. In this case,

one side of the line now has significantly more area against which it can slip cast. This results in a very rough unpredictable surface finish. This is illustrated below in a Figure 5.12.

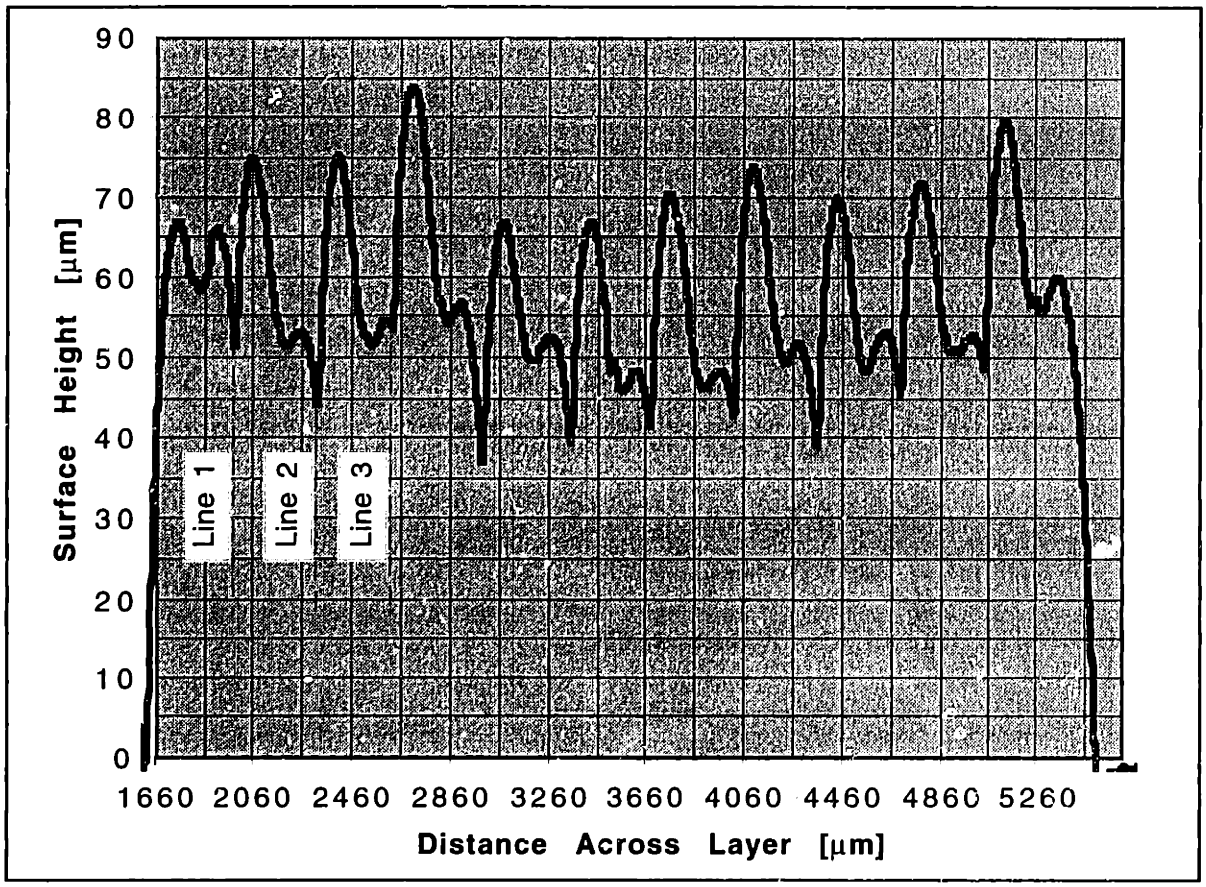

Figure 5.12: Surface profile of a single layer using 35 v/o alumina slurry, 254 µm nozzle, fast-axis speed of 1.3 m/sec, flow rate of 3.1 cc/min, and a line spacing of 340 µm

This figure shows the result of a surface profile scan by a Dektak 8000 profilometer. The fluid system used to generate the layer was 35 v/o slurry jetted through a 254 µm hypodermic needle. The printing parameters were a raster speed of 1.3 m/sec, a flow rate of 3.1 cc/min, and a line spacing of 340 µm. In this figure, the first line (marked as "Line 1") is printed at very left of the plot. Note that it has a symmetric profile like the one shown in Figure 5.11. However, the next line (marked as "Line 2") is no longer symmetric since the side next to the previously printed line slip casts much faster resulting in large peaks in the resulting surface. This phenomenon repeats throughout the entire layer resulting in a much larger roughness than would have been predicted by the additive model. If this slip casting effect could be lessened, then the additive model might be accurate enough to use to predict the resulting surface finish from a set of printing

parameters. However, the best way to currently determine a set of printing parameters which give a good surface finish is to determine these experimentally.

5.4: Experiments Using The Ink-Jet Approach to Layer Fabrication

Experiments were performed to assess the feasibility of the ink-jet layer fabrication approach. Experiments ranged from looking at the working distance, trying different printing parameters, studying individual lines, etc. Dimensional control of the powder bed over a large number of layers was also examined.

5.4.1: Experiments with the Nozzle Working Distance

Initially, the 127 μm wire bonding nozzle was used to create a slurry jet. The time to develop a device to turn the slurry jet on and off as discussed earlier was unavailable. Consequently, a very simple slurry printhead was built which incorporated a special catcher to prevent slurry from reaching the substrate when desired. This catcher was basically a small box with a volume of about 10 cc which could be easily placed under the slurry jet. In order to have room for the catcher box, the slurry jet had to be placed about 33 mm above the substrate. The large distance between the nozzle and the powder bed later proved to be a source of problems since the slurry jet had broken up into discrete droplets by the time it reached the surface.

For the first experiment, a 35 v/o alumina slurry (1.0 μm) was prepared. In the fluid system setup used, a 25 mm diameter syringe filter with a nylon mesh with 53 μm openings was used to filter the slurry before it passed through the 127 micron nozzle orifice. The slurry reservoir tank was pressurized to about 21 psi. As a substrate, a borosilicate filter disk (Ace Glass, Vineland, NJ) with a porosity of 10-20 μm was employed.

In the first attempt to print a powder bed with an alumina slurry jet, a fast axis speed of 1.25 m/sec was chosen and a slow-axis line spacing of 450 μm was used. At the beginning of the experiment, the flow rate was found to about 4.1 g/min (about 2.0 cc/min). The surface finish which was initially observed was quite poor. At first, it was not clear whether this was a wetting problem or a problem with the printing parameters themselves. To make sure that this was not a wetting problem, 5 layers were printed with the same parameters. Wetting problems disappear after several layers are printed because an alumina foundation is built. Thus, an improvement in the surface would indicate a wetting problem. Heat lamps were used after each layer to remove excess water. After the fifth layer, it was quite clear that the problem was not related to wetting since no improvement was noted. A photo of the surface after the fifth layer had been printed is

shown below in Figure 5.13. In this figure, the fast-axis was in the horizontal direction. It should be noted that the splatted droplets which were formed are about 400-800 microns in diameter which is quite big.

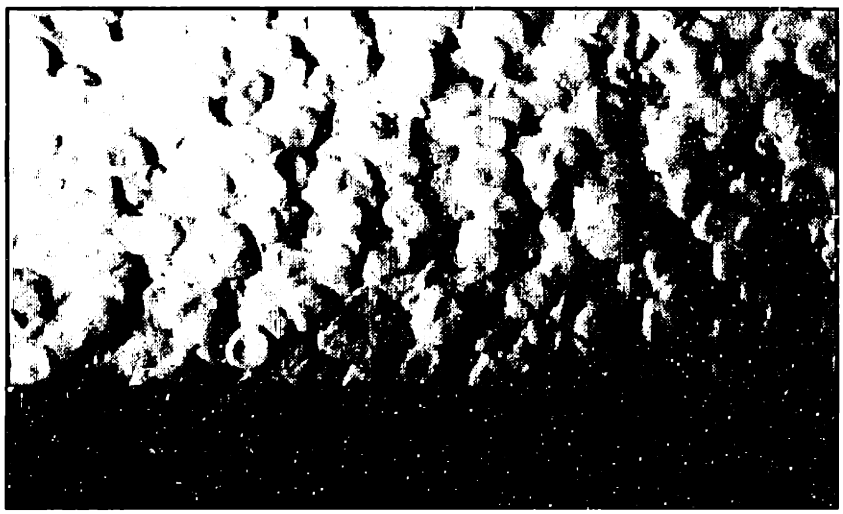

Figure 5.13: Powder bed with individual drops hitting surface using 35 v/o alumina slurry, 254 μm nozzle, fast-axis speed of 1.25 m/sec, flow rate of 2.0 cc/min, and a line spacing of 450 μm (scale divisions are 1/64 inch apart)

Since the working distance was so high (3 cm), the jet was certainly arriving at the powder bed as individual droplets. It was then checked to see if this could be improved by lowering the nozzle such that an unbroken laminar jet hit the powder bed surface. The printhead was modified to bring the nozzle within 5 mm of the powder bed surface. Unfortunately, this made it necessary to remove the catcher box so the nozzle had to be physically removed from the printhead to turn the jet off. With the nozzle now setup such that a laminar stream was hitting the powder bed instead of individual drops, much better results were expected. A line spacing of 450 μm was again used with a mass flow rate of 4.0 g/min (1.96 cc/min). The raster speed was kept at 1.25 m/sec. These parameters should produce dry layers which are 37 μm high assuming a packing density of 55%. The change in the nozzle height significantly changed the resulting surface finish of the powder bed. Eight layers were printed with the use of drying lamps after each layer. Figure 5.14 shows a photo of the resulting surface finish. The fast-axis is in the vertical direction of this photo.

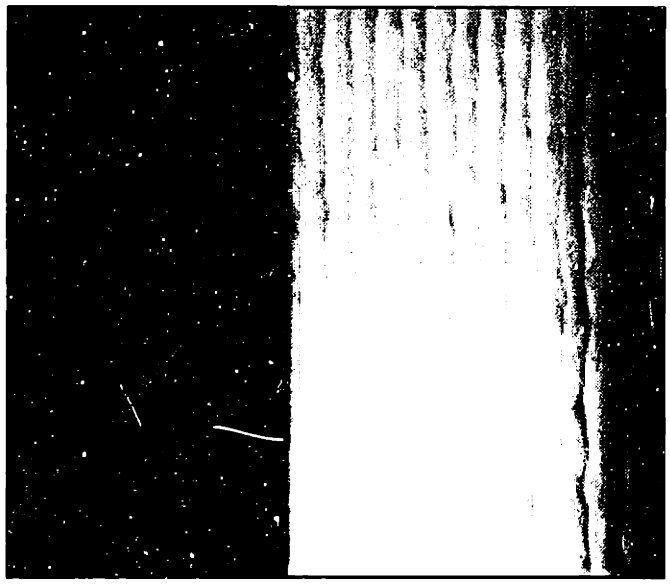

Figure 5.14: Powder bed with laminar flow jet hitting surface using 35 v/o alumina slurry, 254 μm nozzle, fast-axis speed of 1.25 m/sec, flow rate of 1.96 cc/min, and a line spacing of 450 μm (scale divisions are 1/64 inch apart)

The surface finish shown in Figure 5.14 was encouraging. From these results, it was considered critical that a slurry jet be an unbroken laminar stream when hitting the powder bed. The reason for the improvement can be easily explained. The volume of the droplets are so small that they slip cast almost instantaneously on the powder bed. As a result, it is impossible for the droplets to merge with one another and a poor surface finish results. By having a laminar stream hit the powder bed, even though slip casting occurs rapidly, a smooth line will result.

5.4.2: Experiments with the Printing Parameters

From the results of the working distance experiments, a more physically robust printhead which placed the 127 μm nozzle about 3 mm above the substrate was built. This new printhead allowed rapid removal of the nozzle from the printhead to make it easier to turn the jet on and off. Printing parameters were sought which gave the best layer surface finish. In order to prevent cracking, the fast-axis speed needed to be kept as high as practically possible and the flow rate had to be kept as low as possible. As a result, the parameter which was varied was the line spacing. The LabView program which controlled the motion of the printhead was reprogrammed so five powder beds could be printed with different line spacings in each layer printing iteration. Line spacings of 200, 300, 400, 500, and 600 μm were printed side by side. A fast-axis speed of 1.2 m/sec was chosen

since it was the fastest speed which was observed to have constant velocity over the printed region.

For the printing experiments, 35 v/o alumina slurry (1.0 μm) was prepared. The slurry also contained 2 weight percent PEG (Mw = 400) on the basis of the alumina used. The main purpose of the PEG is to aid in redispersing the powder bed after printing. Even though this was not of concern in the experiment, its presence may effect the slurry rheology. Heat lamps were applied at full intensity for about 1 minute after each layer was printed. This removes excess water from the powder bed so drying stresses will not increase as more layers are printed and cause cracking problems.

In the fluid setup used, a 25 mm diameter syringe filter using a nylon mesh with 45 micron openings removed large particles from the slurry before it passed through the 127 micron nozzle orifice. One problem that occurred was that the filter would slowly clog up over time and change the flow rate over time. To keep track of this problem, the mass flow rate was measured periodically. To keep the flow rate roughly constant, the filter was flushed every couple of layers. In Figure 5.15 below, the mass flow rate is shown as a function of the layer being printed. It is important to note that each layer represents the passage of anywhere from 5-10 minutes of time. The figure clearly shows the flow control problems associated with using filters.

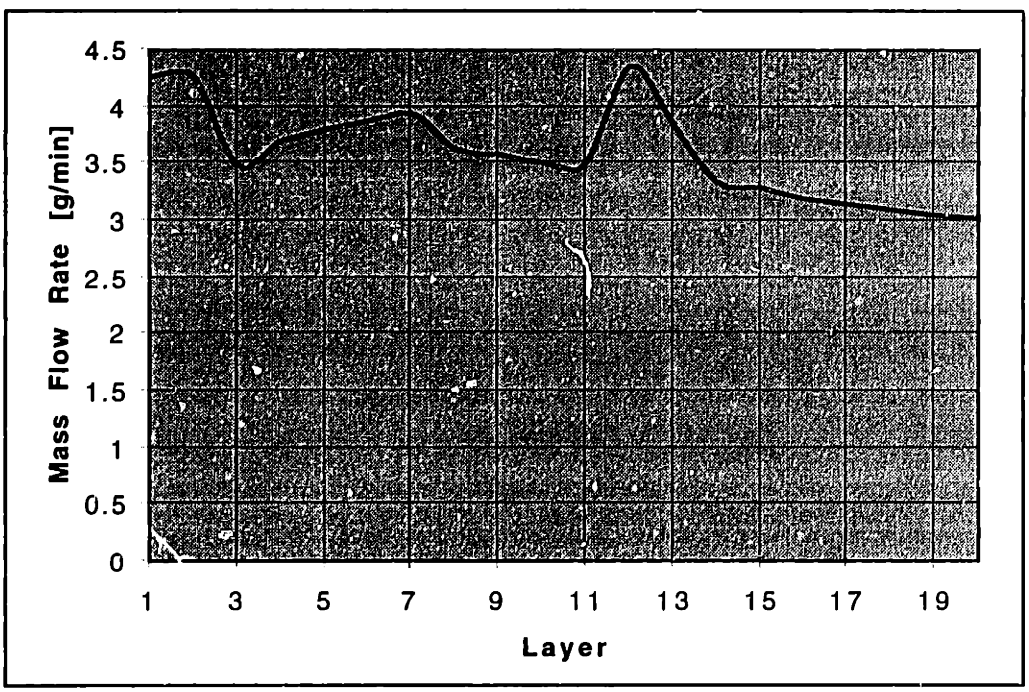

Figure 5.15: Slurry mass flow rate during line spacing parameter study

After printing 20 layers, the surface finish of the resulting powder beds was examined. Of the line spacings which were printed (200, 300, 400, 500, and 600 μm), the 200 μm line spacing exhibited the best surface finish. The resulting surface finish is shown below in Figure 5.16.

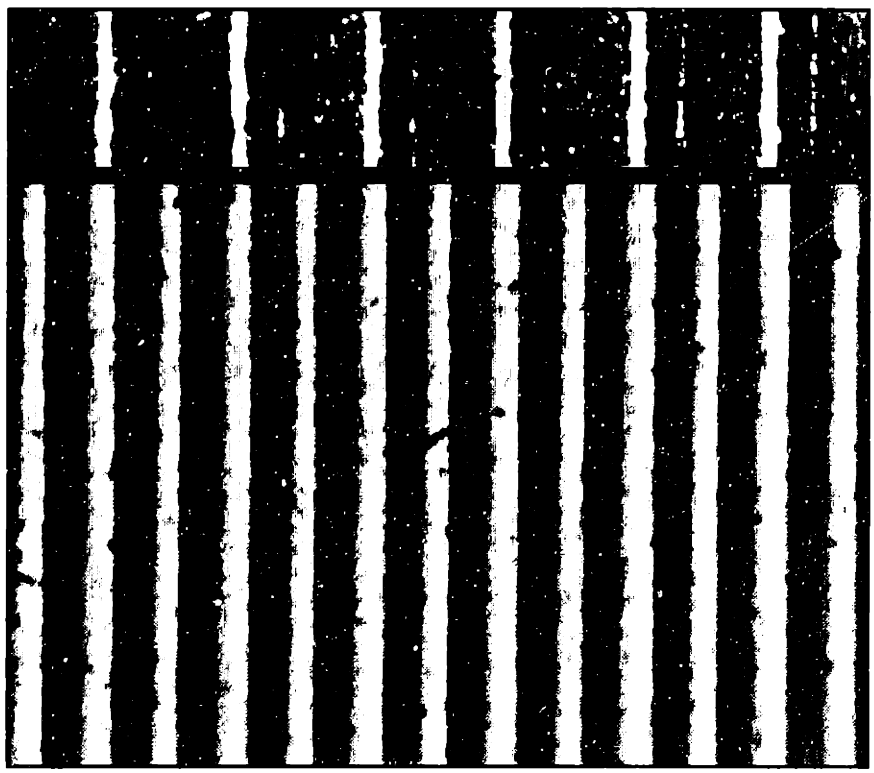

Figure 5.16: Powder bed surface using 35 v/o 1.0 μm alumina slurry, 127 μm nozzle, fast-axis speed of 1.2 m/sec, average flow rate of 1.8 cc/min, and a line spacing of 200 μm (scale divisions are 1/64 inch apart)

As the larger line spacings were used, gaps appeared between the lines leading to large valleys and peaks in the resulting surface finish. The case where 500 μm line spacing was used is shown below in Figure 5.17. Large gaps between the lines and deep grooves are clearly visible in this photo.

Figure 5.17: Powder bed surface using 35 v/o 1.0 μm alumina slurry, 127 μm nozzle, fast-axis speed of 1.2 m/sec, average flow rate of 1.8 cc/min, and a line spacing of 500 μm (scale divisions are 1/64 inch apart)

From these results, it was the smallest line spacing (200 μm) which gave the best surface finish. However, it may not always be possible to use such small line spacings. If the saturation thickness for critical cracking thickness purposes is calculated using Eq. (5.4) assuming a resulting packing density of 55% of theoretical (PF = 0.55), h_{sat} is found to be about 180 μm. This is above the CCT reported by Grau (see Table 5.3) for 1.0 μm powder. The reason that cracking was not observed might be the fact that not enough layers were printed. In order to use such line spacings reliably for powder beds with more layers, a higher fast-axis speed or lower flow rate will be necessary to reduce the saturation thickness. Later experiments confirmed the fact that small line spacing result in better surface finishes then large line spacings (see Figure 5.22). The limiting factors to using small line spacings are the build rate and the CCT.

5.4.3: Layer to Layer Print Styles

Looking at Figure 5.11, it can be seen that the surface finish of an individual line is quite good. The limiting factor in the surface finish is the way the individual lines are stitched together. Peaks are evident where the lines are printed and valleys can be seen between the printed lines. In order to reduce this effect, a layer shifting scheme was adopted. The idea behind layer shifting is to print the lines in the valleys so that the resulting surface will be smoother. This concept is illustrated below in Figure 5.18.

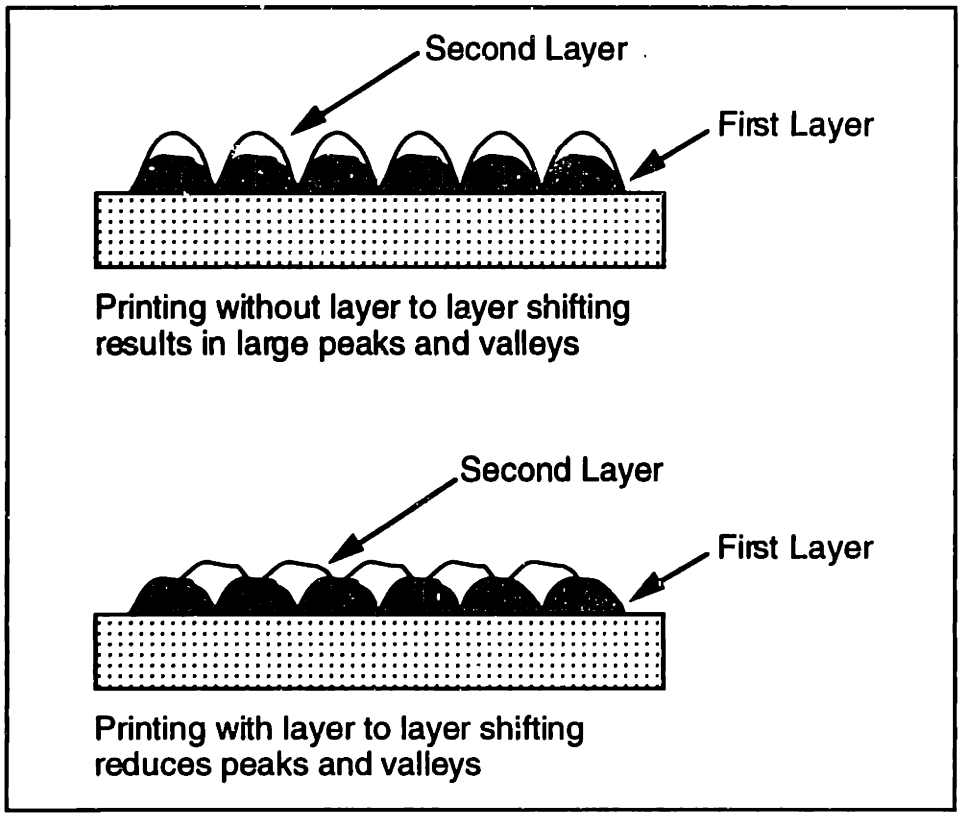

Figure 5.18: Layer to layer line shifting

Such a scheme can easily be implemented in software by shifting the slow-axis position where the layer is printed.

Use of the layer to layer shifting resulted in an improved surface finish. Uhland made measurements of powder beds printed using the shifting technique. Using a Dektak-8000 surface profilometer, the surface profile of two successive layers was measured and is shown in Figure 5.19 (data courtesy Uhland). The first layer shows prominent peaks and valleys while the second layer which has been shifted has filled the valleys resulting in a much smoother surface finish. It is important to realize that the distance scales of the axes are not equal. As a result, the peaks appear much sharper then they actually are. The printing parameters for the layers shown in Figure 5.19 were a flow rate of 2.3 cc/min, a line spacing of 350 μm, and a raster speed of 1.75 m/sec. The fluid system consisted of a 127 μm nozzle jetting 35 v/o alumina (0.5 μm).

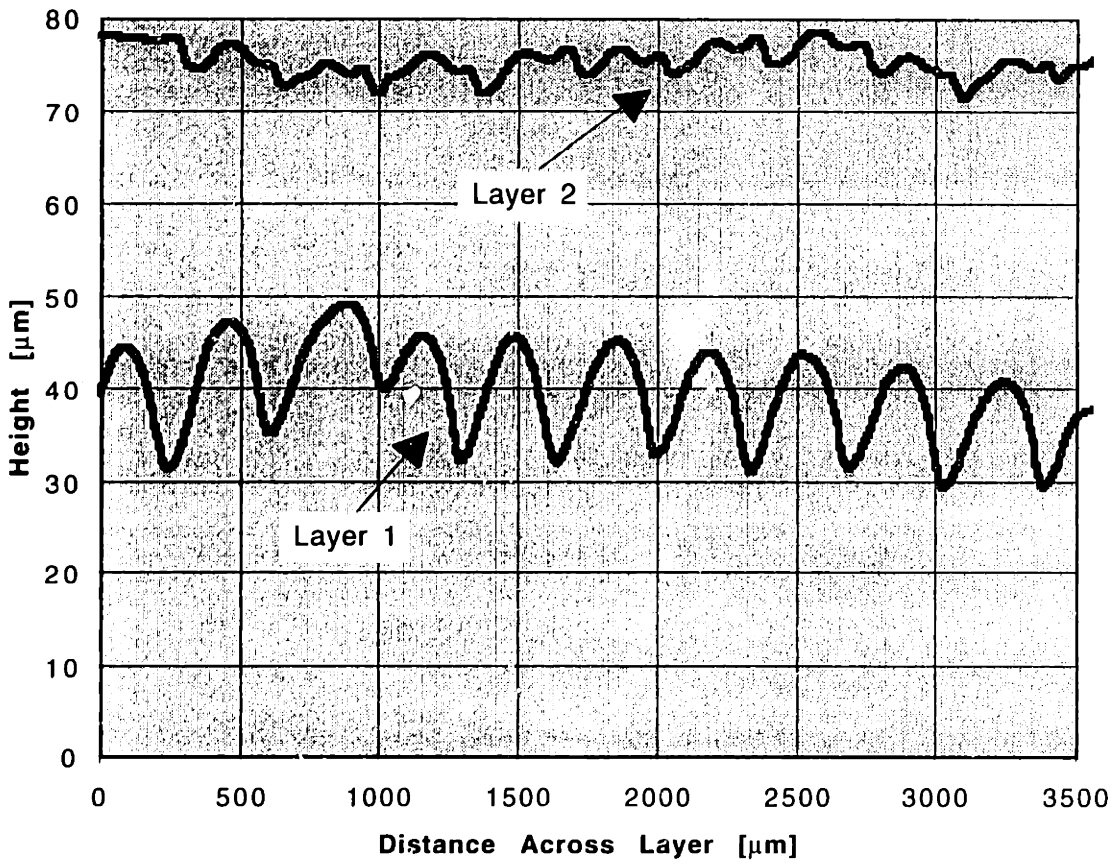

Figure 5.19: Surface finish with layer shifting using 35 v/o alumina slurry, 127 μm nozzle, fast-axis speed of 1.75 m/sec, average flow rate of 2.3 cc/min, and a line spacing of 350 μm

5.4.4: Print Styles Within A Layer

In Figure 5.12, it was demonstrated that uneven slip casting rates can result in a significant increase in the surface roughness. In this case, the surface roughness is increased due to the fact that when a new line is printed, one side of the line is against a previously printed line. Thus, one side of the line slip casts much more quickly than the other side. It was hypothesized that this effect could be reduced significantly by employing special print styles within a layer. A cross section of the proposed scheme is illustrated below in Figure 5.20 (lines in the figure are going into the page).

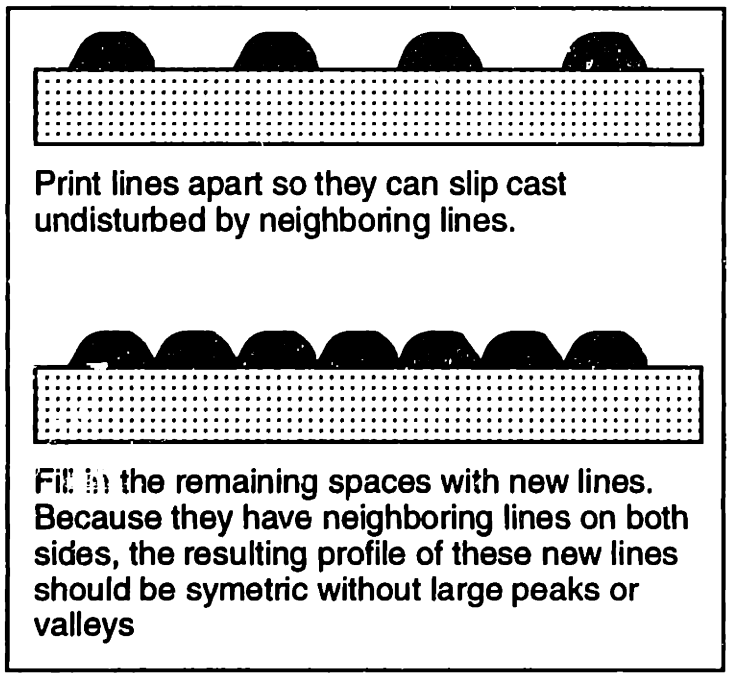

Figure 5.20: Proposed method of reducing surface roughness due to uneven slip casting of individual lines

This method was attempted by Uhland using a 127 μm nozzle and 35 v/o alumina slurry. Using the same printing parameters, three layer powder beds using the usual method (lines printed next to each other) and this new method (lines printed apart and then fill in). Initial results showed little significant difference in the resulting surface roughness between the usual and this new line print style. However, there might be more difference when powder beds with more layers are printed.

5.4.5: Comparison of Large and Small Orifice Nozzles

A significant number of powder beds were printed with both the large (254 μm) and small (127 μm) nozzles. The smaller orifice nozzle (127 μm) had the advantage of giving noticeably better surface finish. The simplest explanation for this is that poor surface finish is due to the way lines are stitched together. Big lines with a larger height have the potential for a rougher surface finish. It has been observed that as the slurry dose increases, the line height also increases. The typical slurry dose for the small orifice nozzle (flow rate of 1.8 cc/min and raster velocity of 1.3 m/sec) is about 0.00023 cc/cm. The typical slurry dose for the 254 μm hypodermic needle (flow rate of 3.1 cc/min and raster velocity of 1.3 m/sec) is about 0.00039 cc/cm. The slurry dose for the large orifice nozzle is almost double that for the small orifice nozzle. As a result, the large orifice nozzles will have lines which are significantly taller. This results in larger hills and valleys in the

resulting surface finish. Photos of the layers printed with 254 μm (Figure 5.21) and 127 μm (Figure 5.22) nozzles using parameters which give the best surface finish for each are shown below. Note how surface roughness for the 127 μm nozzle is considerable better than that of the 254 μm needle.

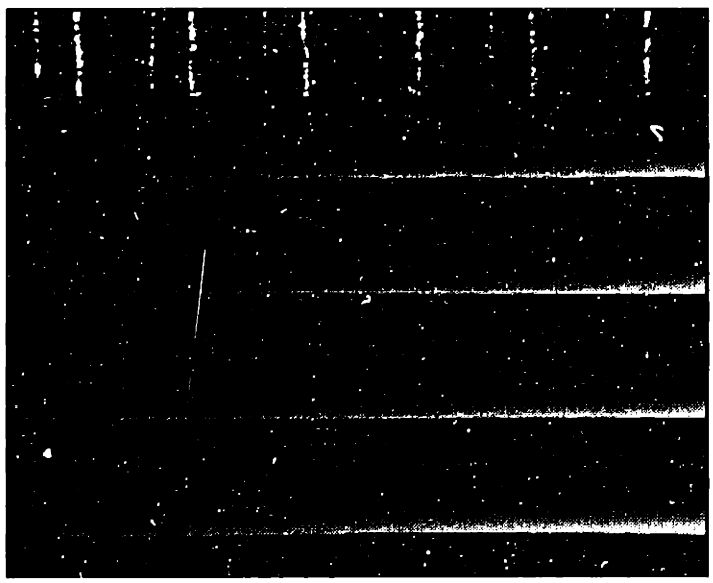

Figure 5.21: Best layer surface finish with a 254 μm hypodermic needle using 35 v/o alumina slurry, flow rate of 3.1 cc/min, raster velocity of 1.3 m/sec, and line spacing of 400 μm (scale divisions are 1/64 inch apart)

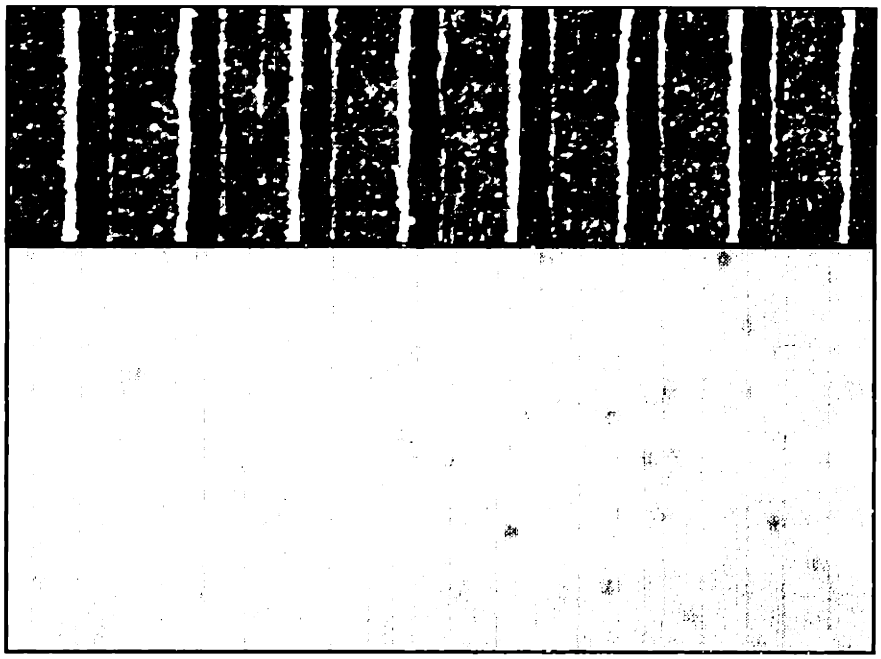

Figure 5.22: Best layer surface finish with a 127 µm nozzle using 35 v/o alumina slurry, flow rate of 2.0 cc/min, raster velocity of 2.5 m/sec, and line spacing of 150 µm (scale divisions are 1/64 inch apart)

From the above Figures, it is clear that use of the smaller orifice nozzle has an advantage in the resulting surface finish. However, this advantage could be minimized if the slip casting rate was slowed down so the individual lines could be stitched together better. The performance of the large orifice nozzles could also be improved by using increased fast-axis speeds. However, this can be difficult to do in practice. In Table 5.5 below, a simple qualitative comparison of the two nozzle types is made reviewing the advantages (denoted with a "+") and disadvantages (denoted with a "-") of each type.

Feature/Attribute	127 μm ceramic nozzle	254 μm needle
Filtering	Requires in-line filter which clogs over time (-)	No filter is required during jetting (+)
Flow Rates	Flow rates below 2.0 cc/min possible (+)	Flow rates much below 3.0 cc/min cannot be used (-)
Jet on/off control	Elaborate setup required to achieve jet on/off control (-)	Jet on/off control is relatively simple (+)
Surface Finish	Smaller lines appear to result in smoother surface (+)	Relatively large lines give a coarser surface (-)
Physical robustness	Resistant to chemical and mechanical attack (+)	Easily damaged and corroded (-)
Cost	$20-$30 each (-)	$0.20 each (+)

Table 5.5: Qualitative comparison of large and small orifice nozzles

At this point, there is insufficient information to make an absolute judgment as to which is the best kind of nozzle to use. The nozzle type to use depends largely on the end requirements. If surface finish is deemed to be of paramount importance, then smaller nozzles appear to be the best choice. However, if the surface finish resulting from the large orifice nozzles is acceptable, then the hypodermic needles would probably be a better choice since they are low cost, do not require filtering, and require very simple hardware for jet on/off control.

5.4.6: Effect of Slurry Solids Loading on Surface Finish

The solids loading of the slurry can have a noticeable effect on surface finish. The choice of the solids loading will be driven by competing factors. In order to reduce the possibility of cracking, to have a good layer build rate, and to decrease the amount of drying time, a high solids loading is desirable. Uhland compared the surface finish of layers printed using 40 v/o and 35 v/o alumina slurry with identical printing parameters. It was found that the surface finish of powder beds using 40 v/o alumina slurry was considerably rougher those printed with 35 v/o slurry. This is probably due to the fact that a high solids loading speeds up the slip casting rate making it more difficult for lines to spread out smoothly. Further improvement in the surface finish may possible by lowering the solids loading even more. However, cracking problems probably limit the solids loading to no less than 25 - 30 v/o [Grau, private communication].

5.4.7: Attempts to Improve Surface Finish Using an Air Jet

The reason that the ink-jet printed powder beds do not have a perfectly smooth surface finish is stitching defects between lines. By enhancing the amount that lines are able to flow into one another, the surface finish could be improved. Unfortunately, this is difficult since the slurry is unable to spread out fast enough compared to the speed that it slip-casts on the surface upon which it has been printed. One proposal for increasing the speed at which the slurry spreads out was to force the slurry with an air jet which immediately follows the slurry jet. This was implemented as shown below in Figure 5.23.

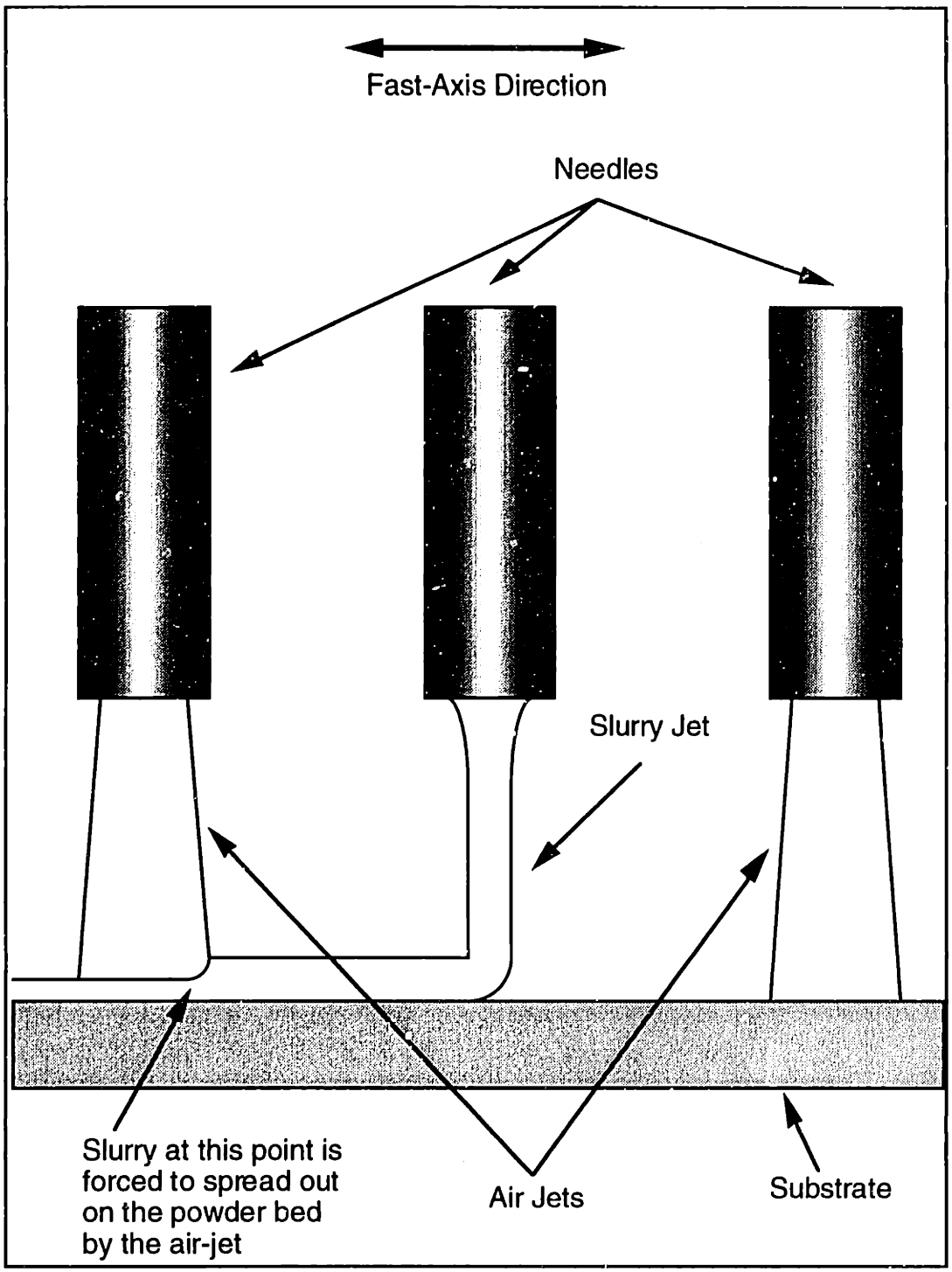

Figure 5.23: Air jet set-up for enhanced surface finish

Two air-jets are necessary since printing occurs in both raster directions. As a result, only one jet is actually helping to spread the slurry at any particular time during the printing process. The use of the two jets may help cancel out any tendency of air deflected by the substrate to disturb the slurry jet.

In order to check whether an air jet improved the surface finish, the set-up shown above was implemented with three 254 μm ID needles— one for the slurry jet and two for the air-jets. Although the air jet flow rate was not measured, the pressure across the needle was measured. The air jet needles had a length of 1.9 cm and an inner diameter of 254 μm. The slurry used was 35 v/o alumina slurry (1.0 μm) without PEG. Using a syringe pump, the flow rate was set at 3.1 cc/min. The fast-axis velocity was set to 1.3 m/sec and the line spacing was 200 μm. As a control, 6 layers were first printed with the air-jets off for comparison purposes. The resulting surface finish of this powder bed is shown below in Figure 5.24.

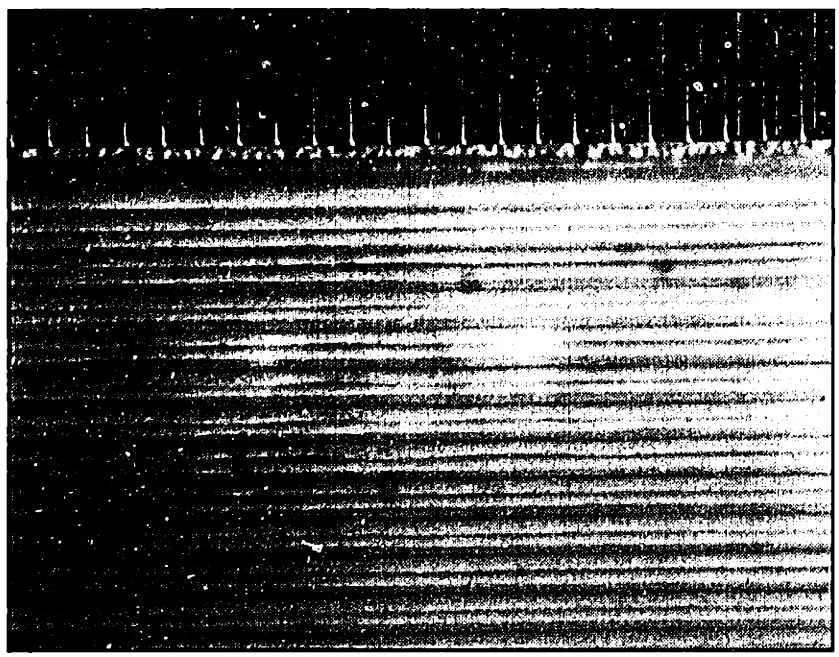

Figure 5.24: Surface finish without the use of an air jet using 35 v/o alumina slurry, 254 μm needle, fast-axis speed of 1.3 m/sec, flow rate of 3.1 cc/min, and line spacing of 200 μm (scale divisions are 1/64 inch apart)

After making the control sample, a powder bed was made with the exact same printing parameters except this time the air-jets were turned on by setting the air pressure source to 12 psi. A picture of the resulting surface finish after 6 layers is shown below in Figure 5.25.

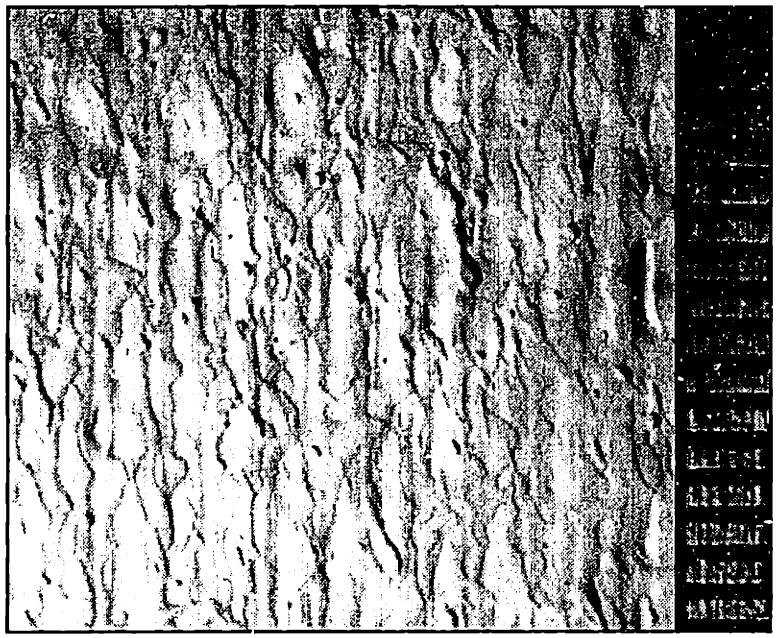

Figure 5.25: Surface finish with 12 psi air jet using 35 v/o alumina slurry, 254 μm needle, fast-axis speed of 1.3 m/sec, flow rate of 3.1 cc/min, and line spacing of 200 μm (scale divisions are 1/64 inch apart)

Although the amplitude of the surface roughness is approximately the same as the control, the imperfections are random and unpredictable. The air-jet seems to have caused splattering which suggests that the air-jet velocity is too high. As a result, the same experiment was tried with a lower air-jet velocity by setting the source pressure to 6 psi. A photo of the resulting surface finish is shown in Figure 5.26.

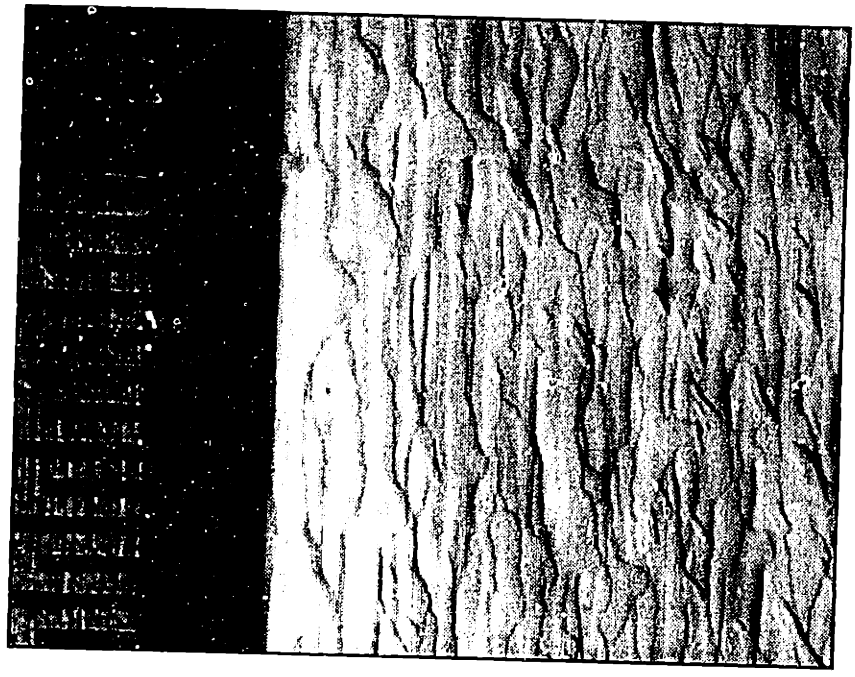

Figure 5.26: Surface finish with 6 psi air jet using 35 v/o alumina slurry, 254 μm needle, fast-axis speed of 1.3 m/sec, flow rate of 3.1 cc/min, and line spacing of 200 μm (scale divisions are 1/64 inch apart)

In this case, the amplitude of the roughness is less than that with the 12 psi air-jet. Also, splattering seems to have been virtually eliminated. However, it appears that the lines are not spread out in a repeatable fashion since the line width varies considerably in a chaotic fashion. This suggests that the air-jet which is impinging on the surface is in fact turbulent. This would explain why the line width is not constant. This could be improved by moving the air-jet closer to the substrate and perhaps lowering the pressure further.

Although the approach of using an air-jet does seem to help spread out the printed lines to some degree, it appears to be difficult to do so in a precisely controlled fashion. As a result, this approach to improving surface finish has been dropped for the time being. However, it is still conceivable that this could be used to reduce stitching defects between lines in an ink-jet printed layer.

5.4.8: Edge Effects in Ink-Jet Printed Powder Beds

When printing powder beds, it was observed that the substrate edge introduces defects into the powder bed. As a result, care must be taken to pick a powder bed which is large enough that these edge effects will not occur in regions where the part geometry will be printed. It was noticed that individual lines experience a disturbance when passing over the edge of the powder bed. This is shown below in Figure 5.27. The powder bed edge is at the left of the photo. The thickness of the resulting line can be seen to vary between 250

and 500 μm as a result of the disturbance. The printing parameters for this photo were a raster velocity of 1.3 m/sec, flow rate of 3.1 cc/min, and 35 v/o alumina slurry (1.0 μm) using a 254 μm needle. This transient behavior would last up to 25 mm from the powder bed edge before dying out. Thus, for these printing parameters, the printed regions of the powder bed must be more than 25 mm from the powder bed edge in the fast-axis direction. For other printing conditions, this distance may be different.

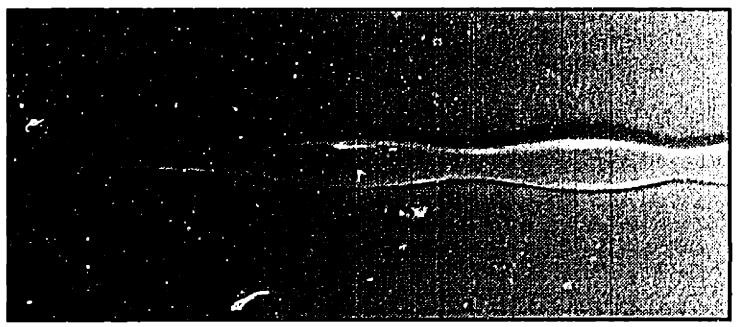

Figure 5.27: Jet disturbance caused by passing over the powder bed edge (line width varies from 250-500 μm)

This disturbance is most likely caused by aerodynamic effects as the jet begins to pass over the powder bed.

5.4.9: Effect of Dwell Time Between Individual Lines on Surface Finish

In scaling the ink-jet printing process to multiple nozzles or to print much larger powder beds, the time between each printed line will vary and can be relatively long. If the individual lines have not fully slip cast before the next line is printed, the duration between each printed line (the dwell) might effect the resulting surface finish. In order to check whether the dwell time between each line effected the surface finish, two 10 layer powder beds were printed (127 μm nozzle, Q = 2.0 cc/min, v = 2.5 m/sec, w = 200 μm, 35 v/o alumina 1.0 μm slurry). The first powder bed was printed normally. The second powder bed contained a 2.5 second pause after each line was printed to ensure sufficient time for complete slip casting to occur. The surface profile of each powder bed was then measured with a Dektak-8000 profilometer. The results are shown below in Figures 5.28 and 5.29.

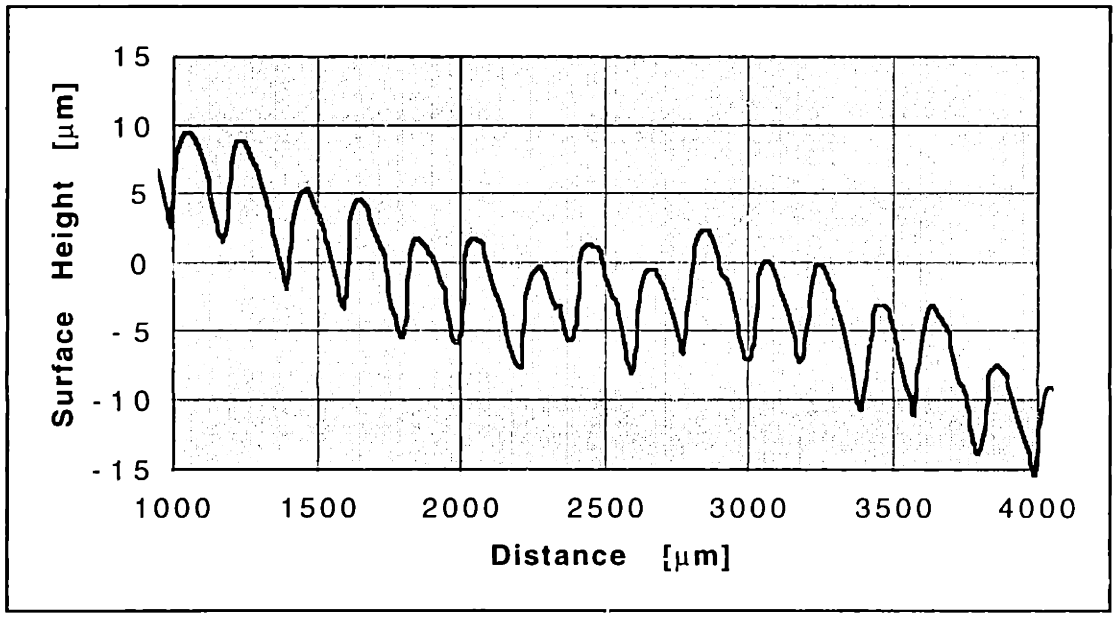

Figure 5.28: Powder bed surface finish with no dwell using a 127 μm nozzle, flow rate of 2.0 cc/min, fast-axis speed of 2.5 m/sec, and line spacing of 200 μm

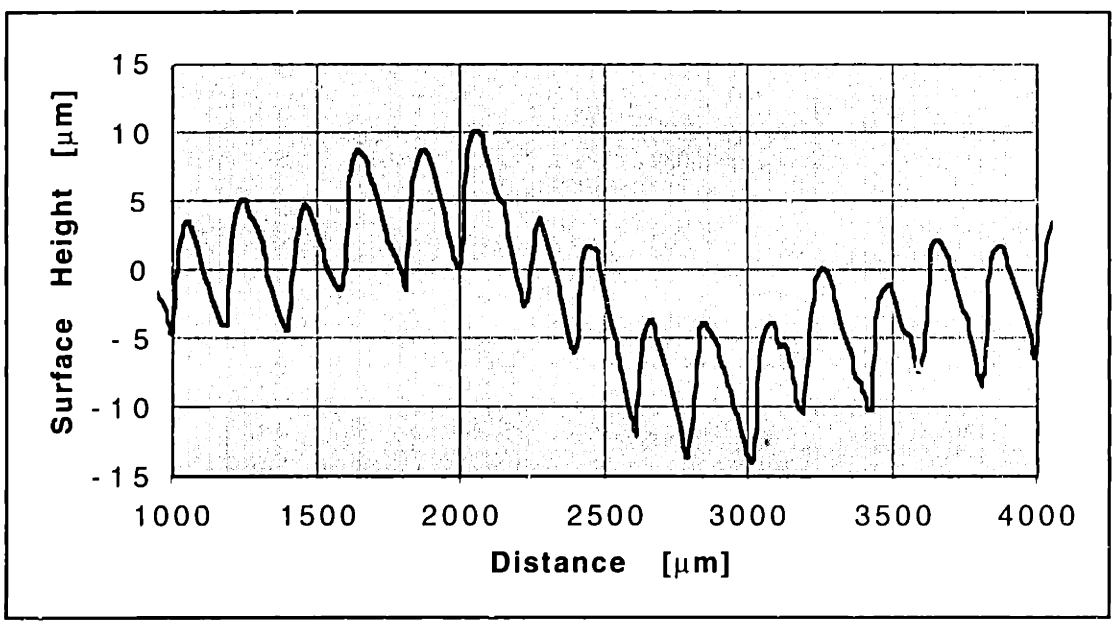

Figure 5.29: Powder bed surface finish with a 2.5 second dwell using a 127 μm nozzle, flow rate of 2.0 cc/min, fast-axis speed of 2.5 m/sec, and line spacing of 200 μm

In both of these figures, only the surface roughness is important. The fact that the overall surface is not flat is an artifact of the substrate upon which the printing took place. It can be seen that the surface finish is essentially the same for both cases which means that slip casting occurs before the next line is printed when the printing machine is operating normally. This means that the process can be scaled to print large powder beds where the

time between each line might be significantly longer than on the current prototype printing machines. The fact that the dwell time does not effect surface finish also means that multiple nozzle printheads could be used where sections of a layer may be joined after relatively long periods of time.

5.4.10: Microstructural Analysis of Ink-Jet Printed Powder Beds

Microstructural analysis of ink-jet printed powder beds before sintering has been performed by Grau. The three biggest areas of concern are the presence of inter-layer defects, packing density, and the pore size distribution. Using SEM photos, it can be seen that the ink-jet printed powder beds exhibit excellent stitching between layers. This can probably be attributed to the fact that underlying layers are being partially redispersed when a new layer is printed. This allows the layers to merge without defects. An SEM photo of a powder bed cross section is shown below in Figure 5.30. This photo shows about 4 layers of the powder bed. Note the absence of any interlayer defects.

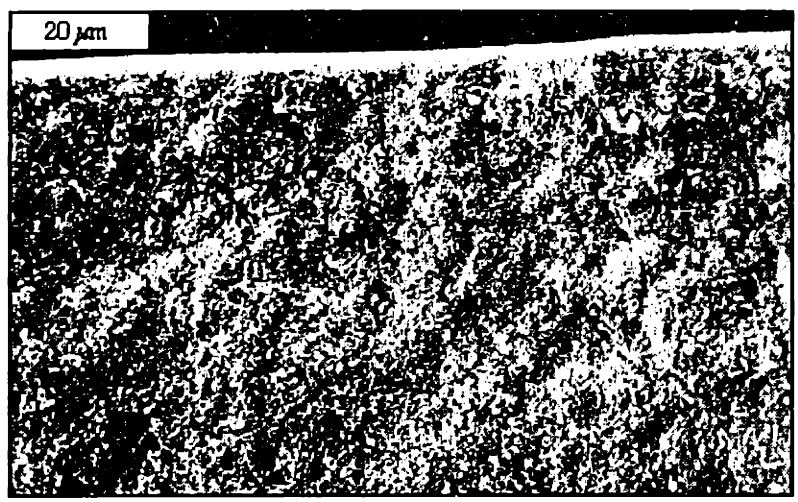

Figure 5.30: Cross section of an ink-jet printed powder bed (photo courtesy Grau)

Although the above photo shows no inter-layer defects, depending on the printing parameters used, it is still possible to have them. Defects have been observed when the layer surface finish contains deep valleys. When printing on such a layer, the slurry can slip cast before filling the valley completely resulting in large voids between layers.

Using mercury porosimetry, the typical packing density of ink-jet printed layers has been determined. For powder beds using 1.0 µm powder, a packing density of 55% of theoretical has been measured. In the case of 0.5 µm powders, the packing density is about 62% of theoretical [Grau, private communication]. Pore size distribution

measurements have also been made. Figure 5.31 shows the pore size distribution for 1.0 μm and 0.5 μm powders for powder beds.

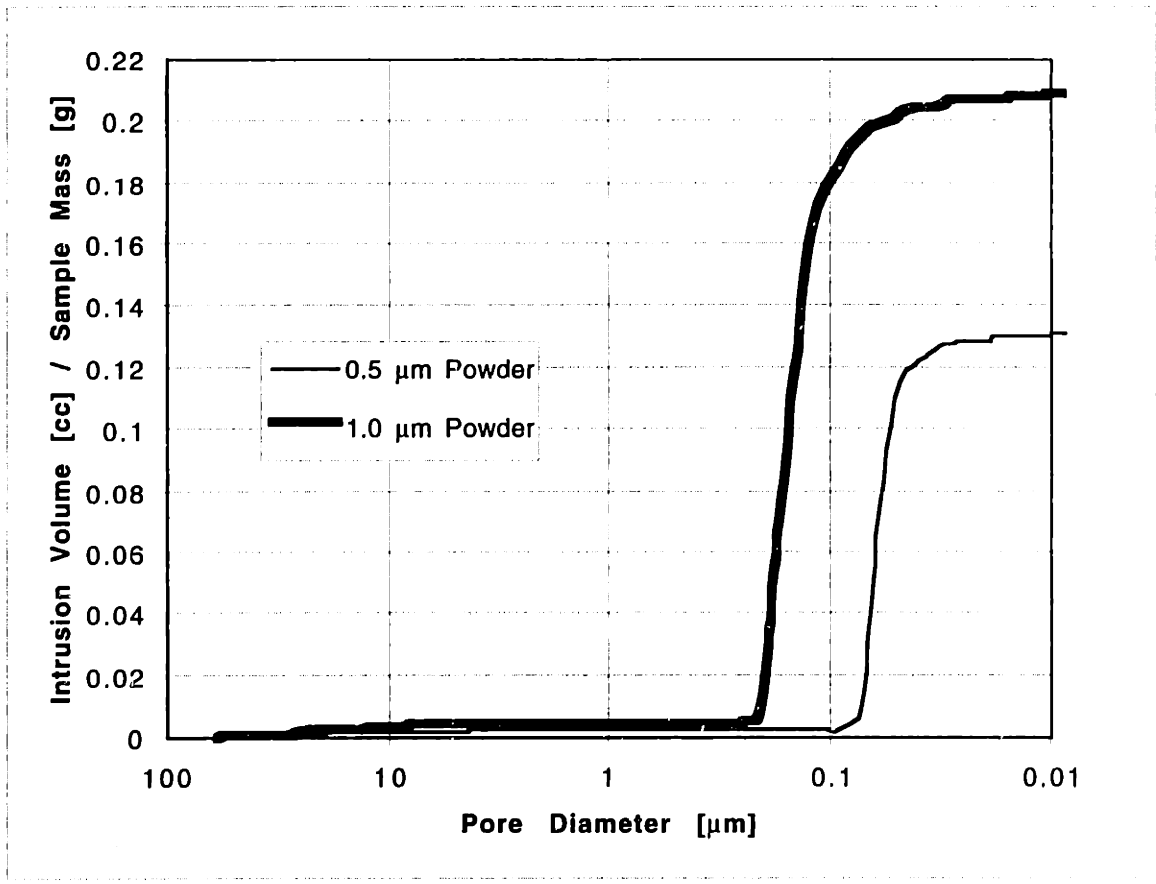

Figure 5.31: Pore size distribution of ink-jet printed powder beds using 35 v/o alumina slurry, 127 μm nozzle, fast-axis speed of 2.5 m/sec, line spacing of 400 μm, and flow rate of 2.0 cc/min

Both the 1.0 μm and 0.5 μm powder beds show pore sizes which should be able to be removed during normal sintering operations. This figure also shows a small percentage of large pores (greater than 1 μm) but these do not appear to be present for powder beds with narrower line spacing or slower fast-axis speed [Grau, private communication].

5.4.11: Examination of Powder Bed Dimensional Control

The use of ink-jet printing for fabricated layers of the powder bed differs significantly from the traditional 3DP process in the sense that there is no direct registration of individual layers to some known height reference. As a result, errors in the build direction can grow over time. Most of the powder beds which were printed while investigating the ink-jet printing approach to layer fabrication typically contained 20 layers

or less. It was important to check if the surface finish reaches a steady-state roughness and to find out when this occurs. It was also important to check the rat at which edge effects propagate as the powder bed height increases. In order to assess the surface finish, three powder beds of varying heights were fabricated with the same printing parameters. The parameters are listed below in Table 5.6. The nominal powder bed height is calculated from the theoretical layer thickness. Given that the slurry used was 35 v/o 1.0 μm alumina slurry (2 dwp% PEG Mw = 400) which has a typical packing density of 55%, the theoretical layer thickness is 56.6 μm. A 127 μm ceramic nozzle was used for jetting with an in-line filter using a nylon mesh with 53 μm openings. A syringe pump was used to maintain a constant flow rate. The slurry was prefiltered twice before printing by pouring it through a 38 μm opening powder sieve. A 40 second drying step was performed between each layer to remove excess water in the powder bed. The heat source was two 800 W halogen lamps operated at 60% of full intensity using a variac. The reason for not operating at full intensity is that the temperatures can get so high that the PEG will evaporate. This drying step removed most of the water from the powder bed.

Powder Bed	Raster Speed	Flow Rate	Line Spacing	Layers	Nominal Height
1	2.5 m/sec	2.0 cc/min	150 μm	20	1.13 mm
2	2.5 m/sec	2.0 cc/min	150 μm	56	3.16 mm
3	2.5 m/sec	2.0 cc/min	150 μm	152	8.59 mm

Table 5.6: Surface Finish and Edge Effect Experiment Printing Parameters

Since edge defects should increase as the powder bed thickness becomes larger, the powder bed widths used were 1.0 cm, 1.5 cm, and 2.5 cm for powder beds 1, 2, and 3 respectively. Figures 5.32 and 5.33 show several views of the ink-jet printed powder beds. A test powder bed which was printed (5 layers using the same printing parameters as the others) to verify the operation of the hardware is also shown in the figures.

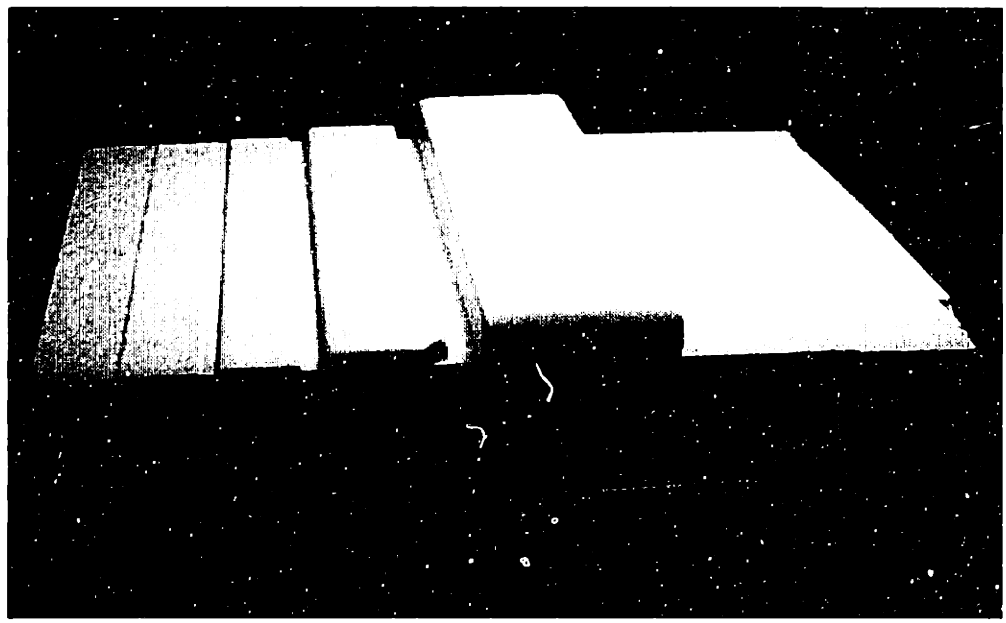

Figure 5.32: Ink-jet printed powder beds showing a test powder bed, powder bed 1, powder bed 2, and powder bed 3 from left to right (printing parameters for each bed is listed in Table 5.6)

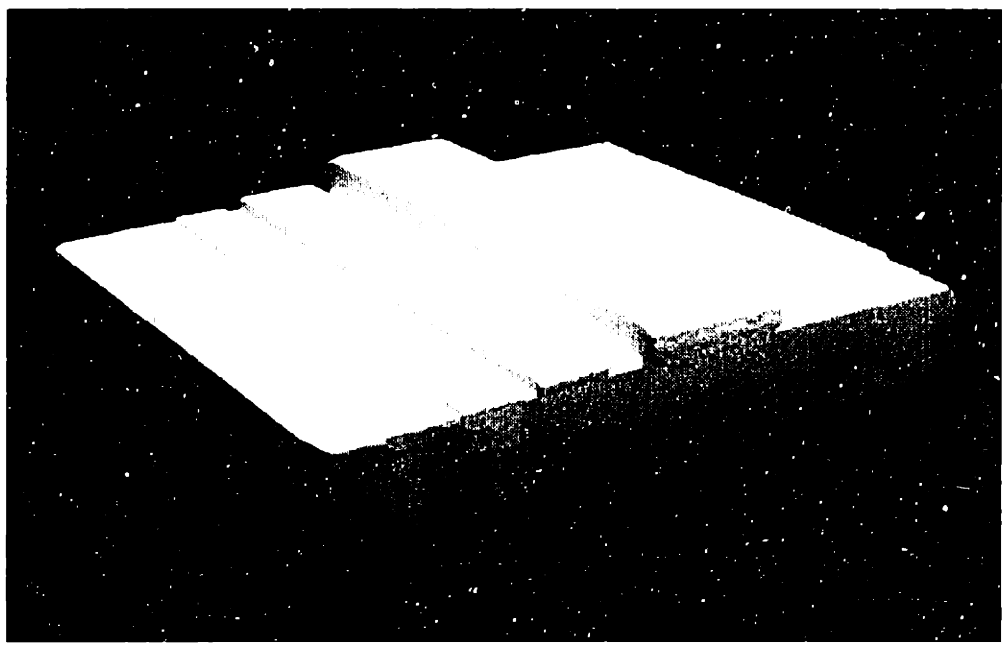

Figure 5.33: Ink-jet printed powder beds showing a test powder bed, powder bed 1, powder bed 2, and powder bed 3 from left to right (printing parameters for each bed is listed in Table 5.6)

The powder beds which were printed with the above parameters exhibited excellent surface finish (see Figure 5.22). Surprisingly, the powder bed edges were very smooth which was unexpected. This is shown below in Figures 5.34 and 5.35 for powder bed 3.

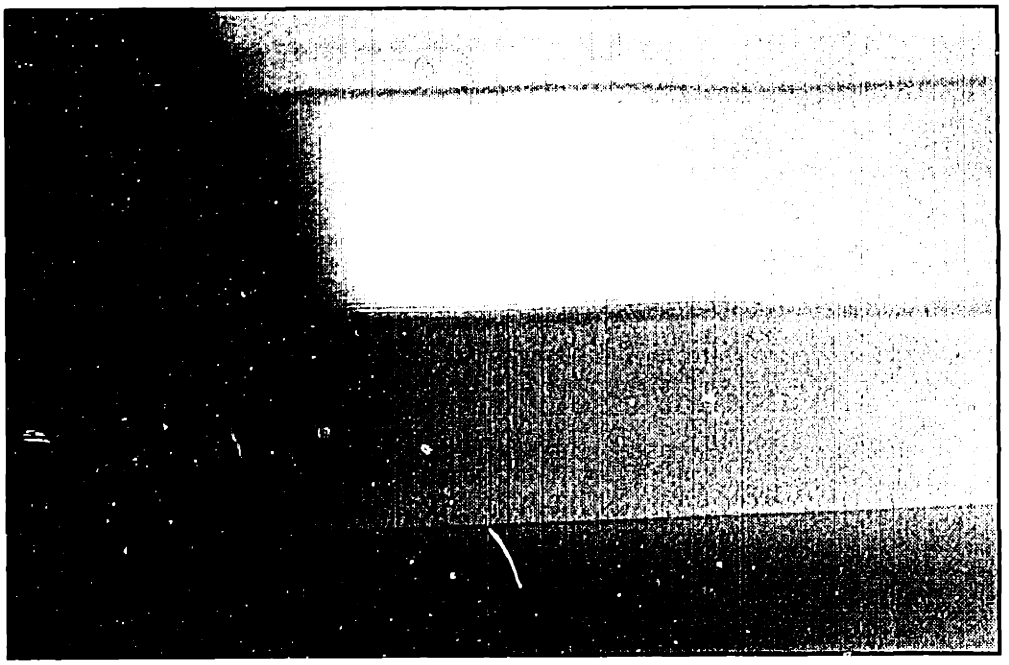

Figure 5.34: Photo of powder bed 3 (see Table 5.6 for printing parameters) showing the unexpectedly smooth powder bed edge (the height of the powder bed is about 8.5 mm)

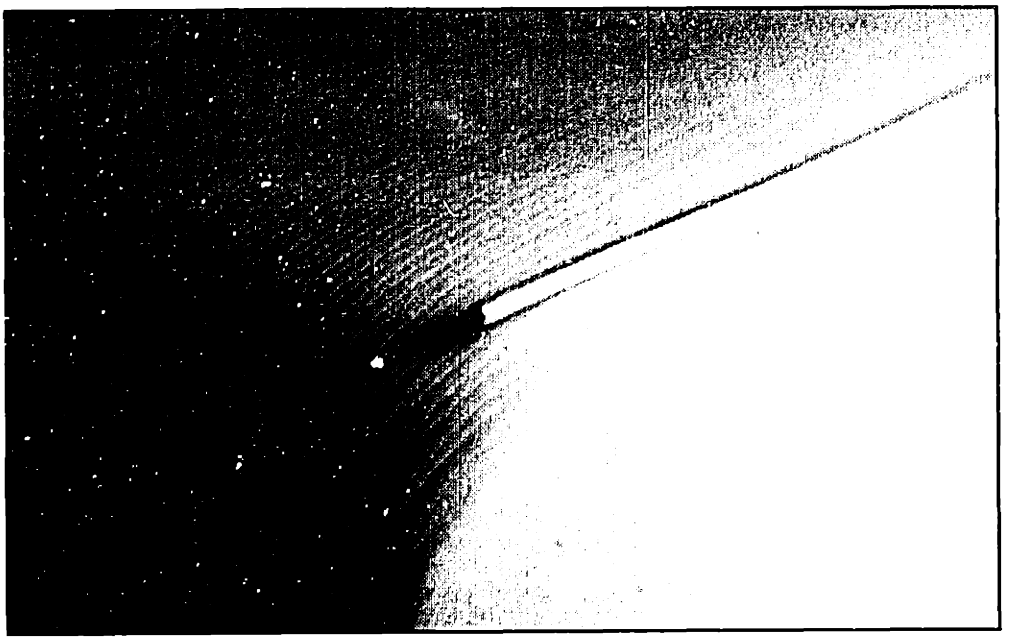

Figure 5.35: Photo of powder bed 3 (see Table 5.6 for printing parameters) showing the unexpectedly smooth powder bed edge and surface finish (the wire diameter is 250 μm)

There was a very regular surface aberration along the fast-axis direction which was almost certainly due to velocity ripple in the motion of the axis. This can be seen clearly in Figure 5.36 below.

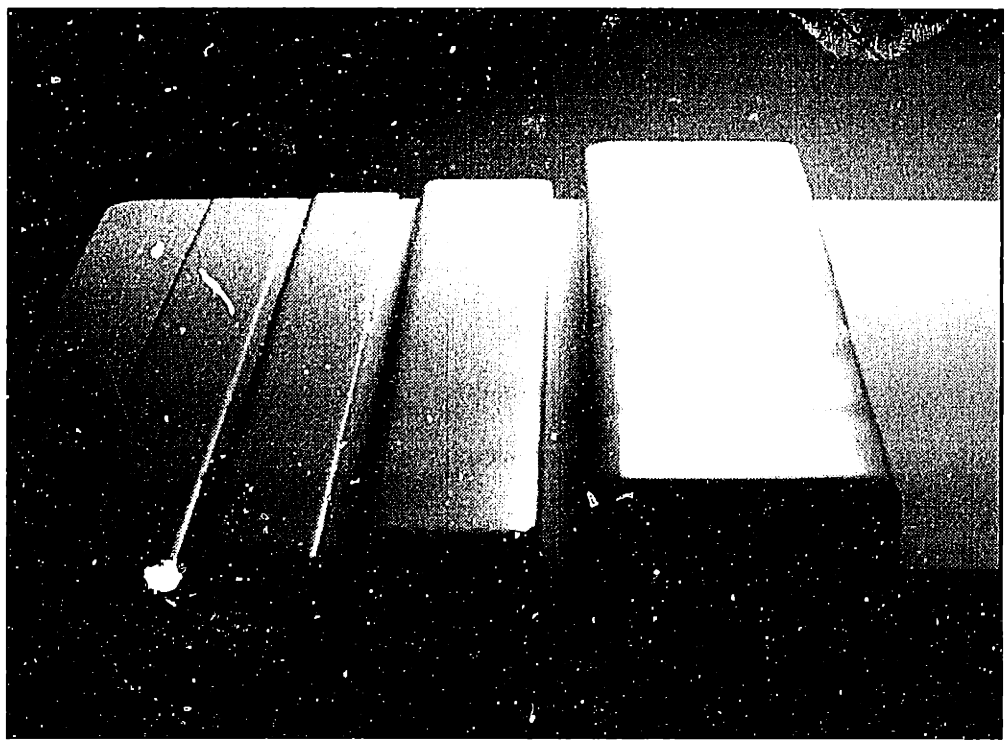

Figure 5.36: Photo of surface aberrations along the fast-axis due to velocity ripple where the test powder bed, powder bed 1, powder bed 2, and powder bed 3 are shown from left to right (printing parameters for each bed is listed in Table 5.6)

In order to assess the surface finish, profilometry scans were performed using a Dektak-8000. Figure 5.37 shows an overhead view of a generic powder bed where profilometry scans were made.

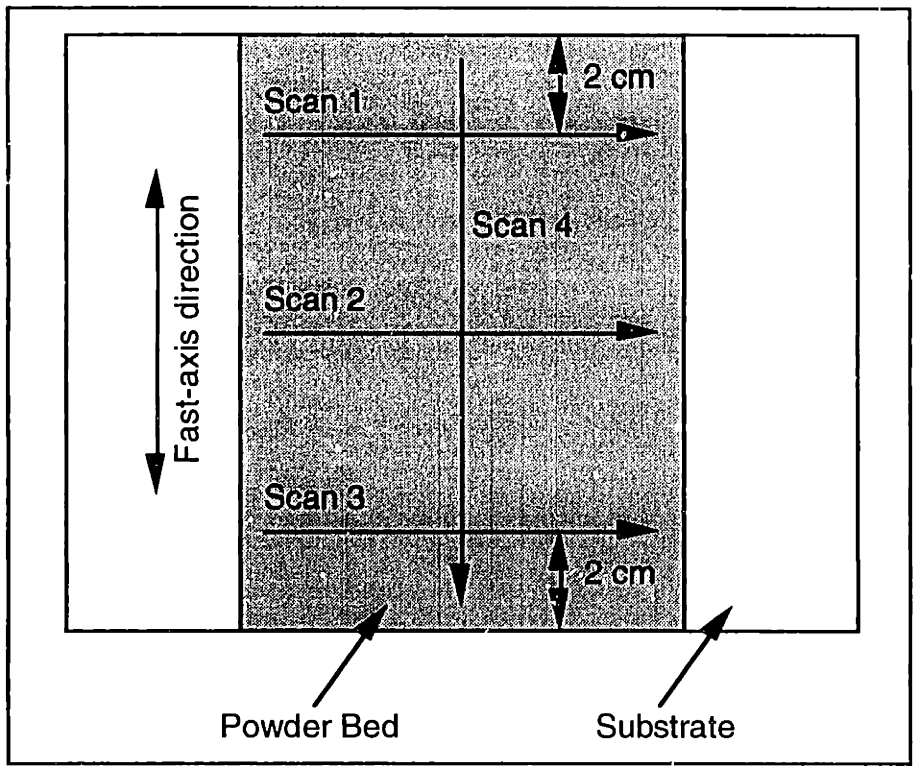

Figure 5.37: Overhead View of Powder Bed Showing Profile Locations

Three scans (Scans 1-3) were performed perpendicular to the fast-axis on each powder bed to assess the surface roughness. Scan 1 and Scan 3 were performed about 2 cm from the fast-axis edge of the powder bed to avoid measuring surface aberrations due to the edge. Scan 2 was made in the middle of the powder bed (in the fast-axis direction). The scans were all made in the middle portion of the powder bed (with respect to the slow-axis direction) where parts would actually be printed. The edges could not be captured due to a height travel limit of the profilometer of ±40 μm. Table 5.7 summarizes the results of the profilometry scan perpendicular to the fast-axis for the three powder beds. The peak-to-peak values stated in the table below are the local roughness as opposed to the absolute roughness over the entire scan.

Powder Bed 1			*Powder Bed 2*			*Powder Bed 3*		
Fig.	*Profile Scan*	*Local Pk-to-Pk Roughness*	*Fig.*	*Profile Scan*	*Local Pk-to-Pk Roughness*	*Fig.*	*Profile Scan*	*Local Pk-to-Pk Roughness*
5.38	Scan 1	6 μm	5.41	Scan 1	8 μm	5.44	Scan 1	8 μm
5.39	Scan 2	6 μm	5.42	Scan 2	8 μm	5.45	Scan 2	8 μm
5.40	Scan 3	6 μm	5.43	Scan 3	8 μm	5.46	Scan 3	8 μm

Table 5.7: Summary of profilometry scans perpendicular to the fast-axis

Figures 5.38, 5.39, and 5.40 show the profilometry scans for powder bed 1 which were taken perpendicular to the fast-axis direction (see Figure 5.37 for scan locations on the powder bed).

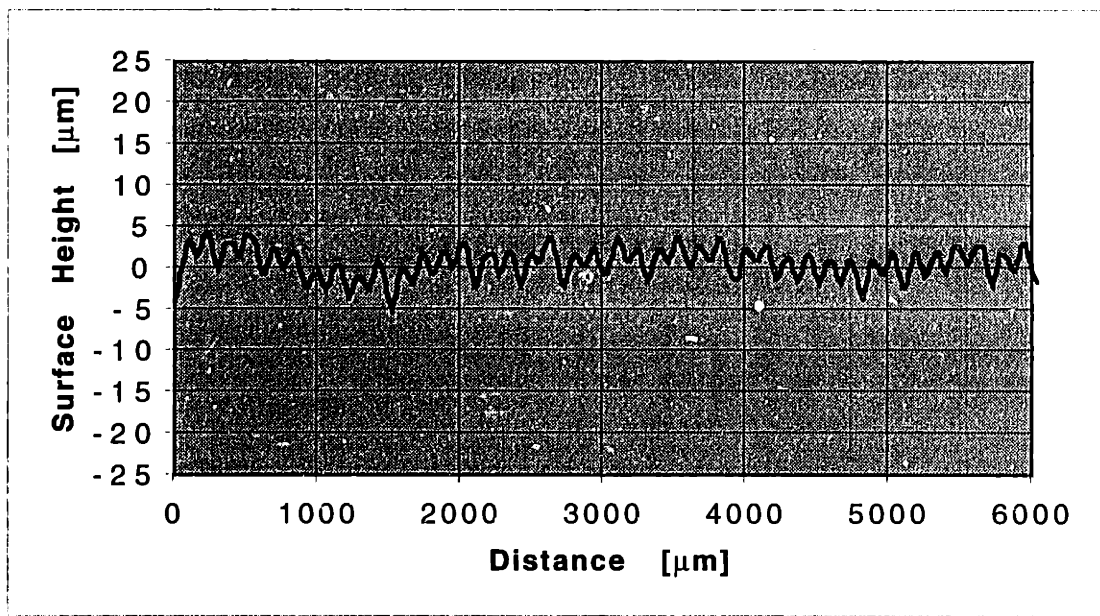

Figure 5.38: Scan 1 of powder bed 1 (see Table 5.6 for printing parameters)

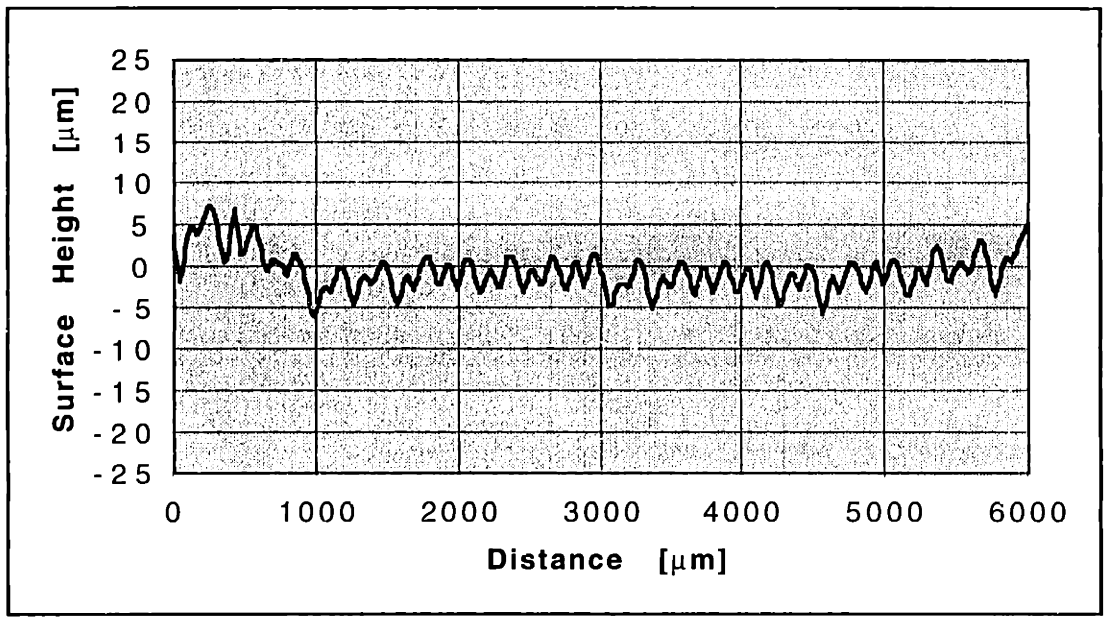

Figure 5.39: Scan 2 of powder bed 1 (see Table 5.6 for printing parameters)

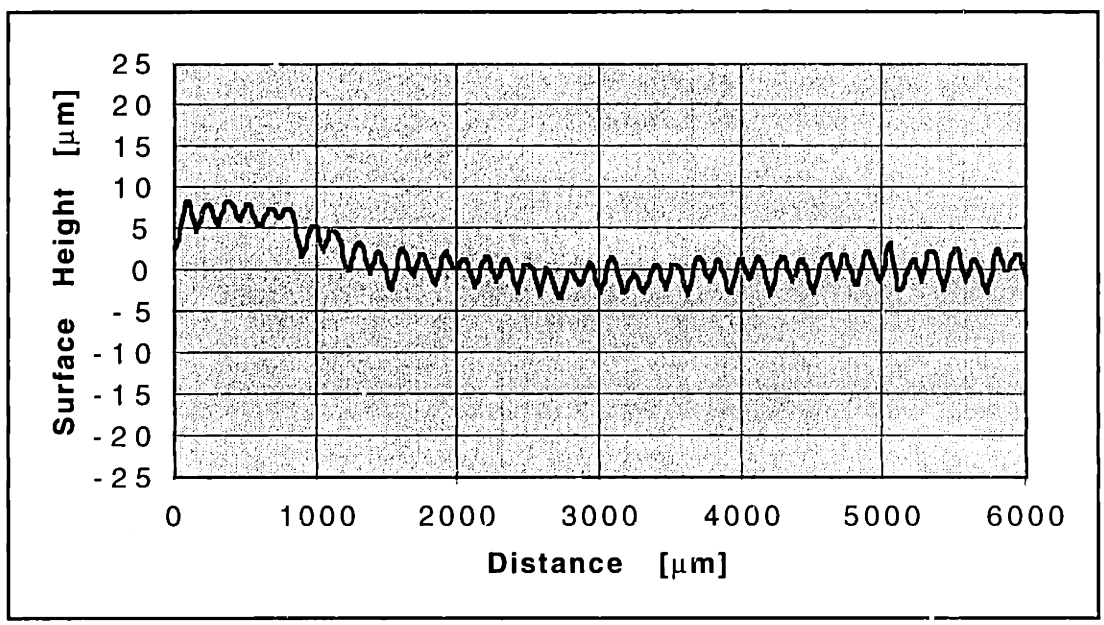

Figure 5.40: Scan 3 of powder bed 1 (see Table 5.6 for printing parameters)

Figures 5.41, 5.42, and 5.43 show the profilometry scans for powder bed 2 which were taken perpendicular to the fast-axis direction (see Figure 5.37 for scan locations on the powder bed).

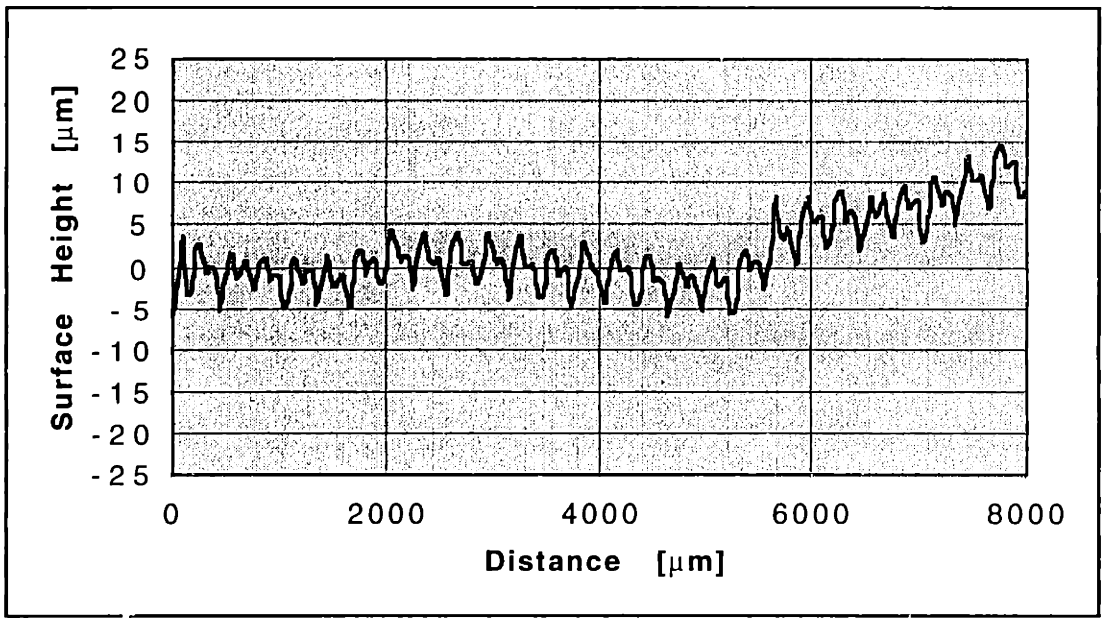

Figure 5.41: Scan 1 of powder bed 2 (see Table 5.6 for printing parameters)

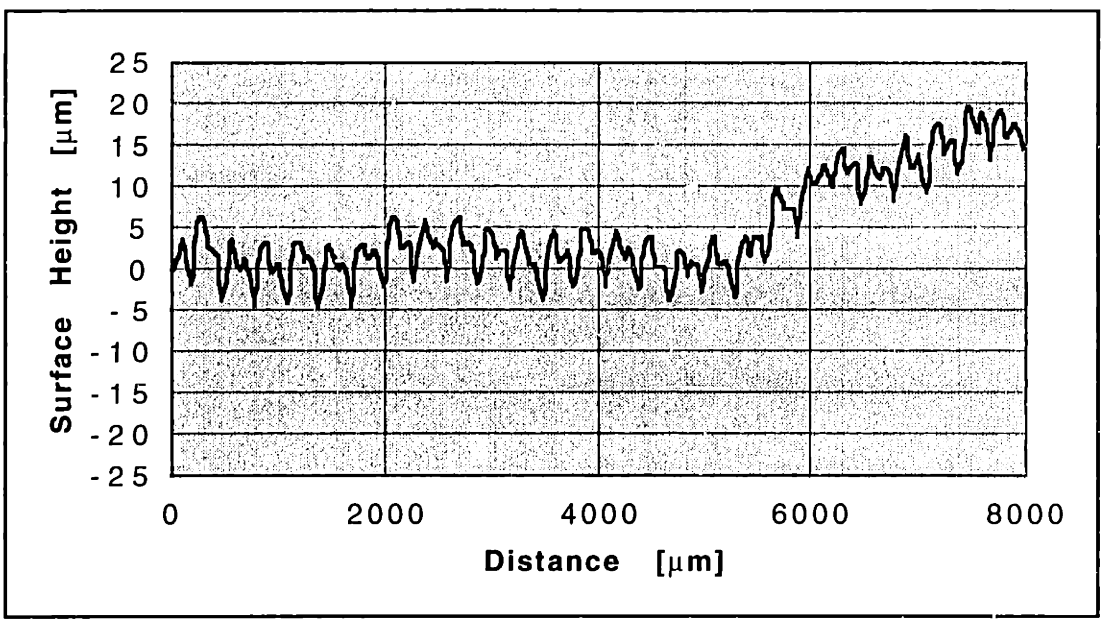

Figure 5.42: Scan 2 of powder bed 2 (see Table 5.6 for printing parameters)

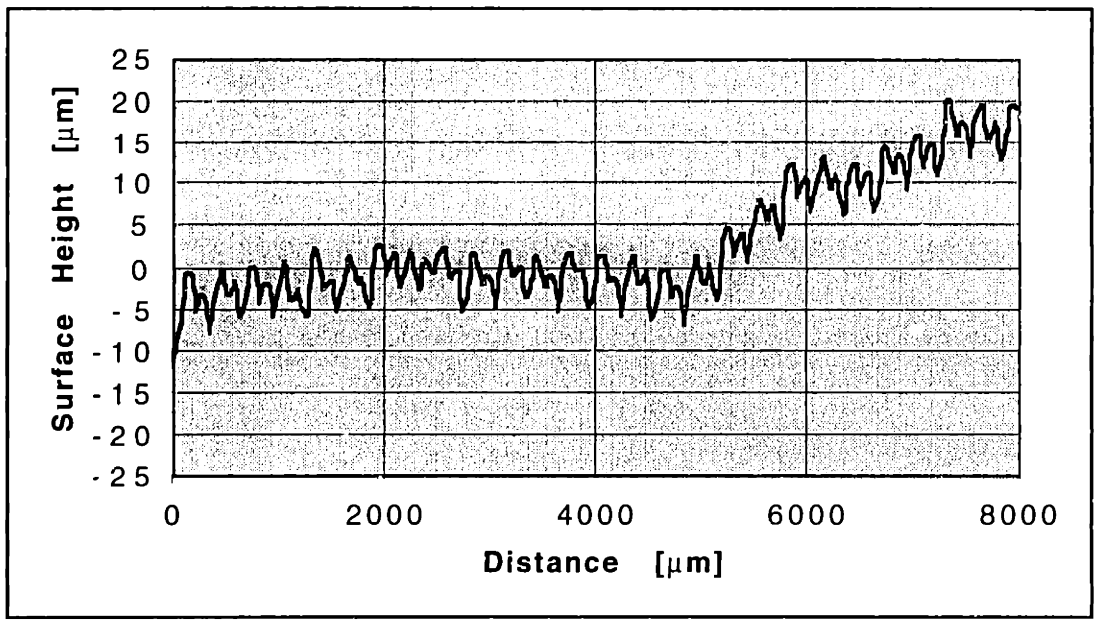

Figure 5.43: Scan 3 of powder bed 2 (see Table 5.6 for printing parameters)

Figures 5.44, 5.45, and 5.46 show the profilometry scans for powder bed 3 which were taken perpendicular to the fast-axis direction (see Figure 5.37 for scan locations on the powder bed).

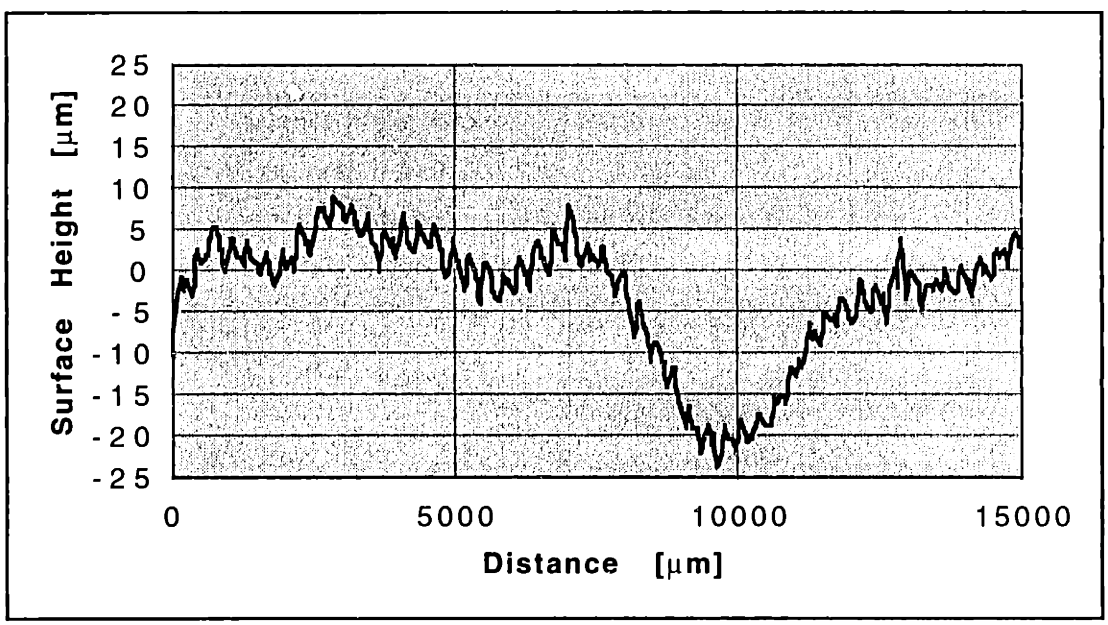

Figure 5.44: Scan 1 of powder bed 3 (see Table 5.6 for printing parameters)

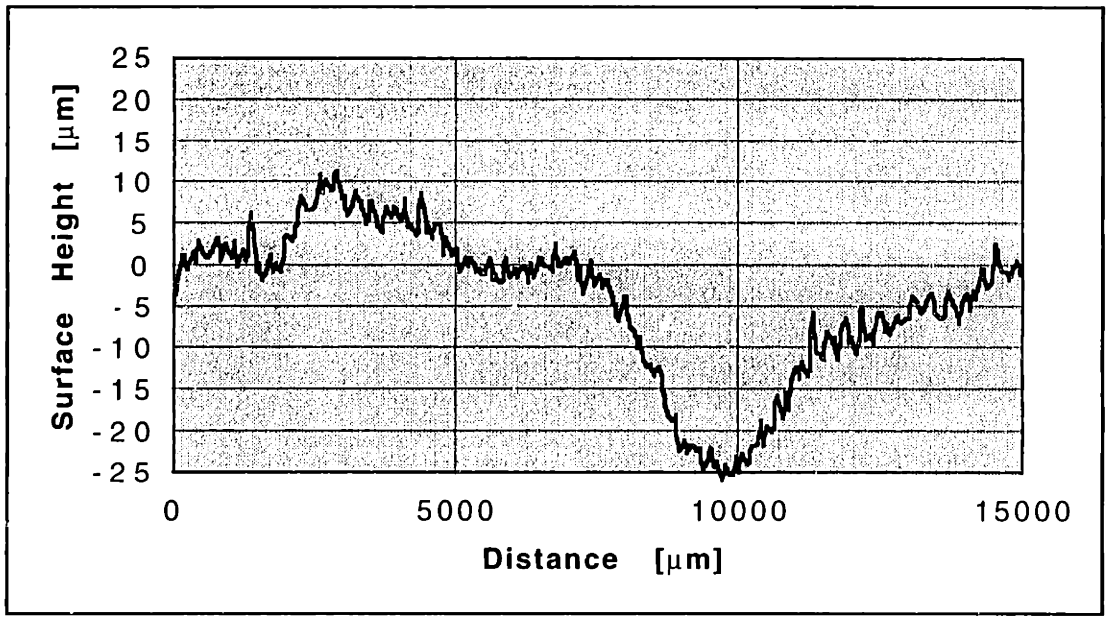

Figure 5.45: Scan 2 of powder bed 3 (see Table 5.6 for printing parameters)

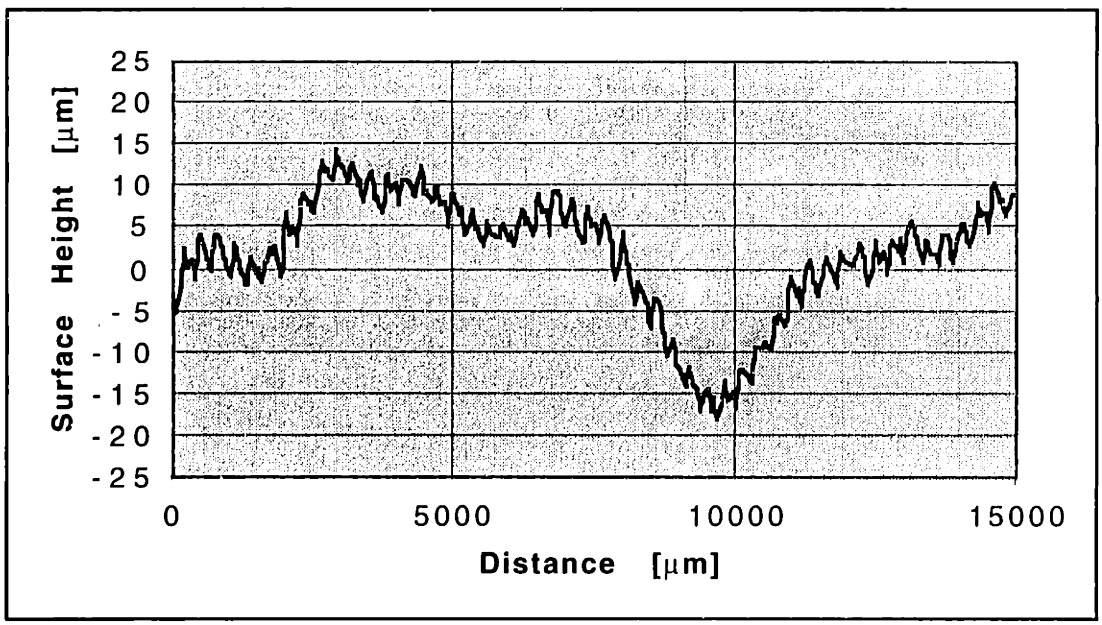

Figure 5.46: Scan 3 of powder bed 3 (see Table 5.6 for printing parameters)

It appears that the surface finish reaches a local steady state roughness of about ±4 μm in the direction perpendicular to the fast-axis. There are some larger aberrations along this direction which are probably due to nozzle problems (brief clogs or changes in jet angle). These aberrations are very repeatable along the fast-axis direction of the powder bed as can be seen in the above figures.

In order to assess the surface finish along the direction of the fast-axis, the surface roughness of an individual line in powder bed 3 was measured using the Dektak-8000 profilometer. As shown in Figure 5.47, the surface finish is about ±1 μm which corresponds to the particle size of the alumina in the slurry used for printing.

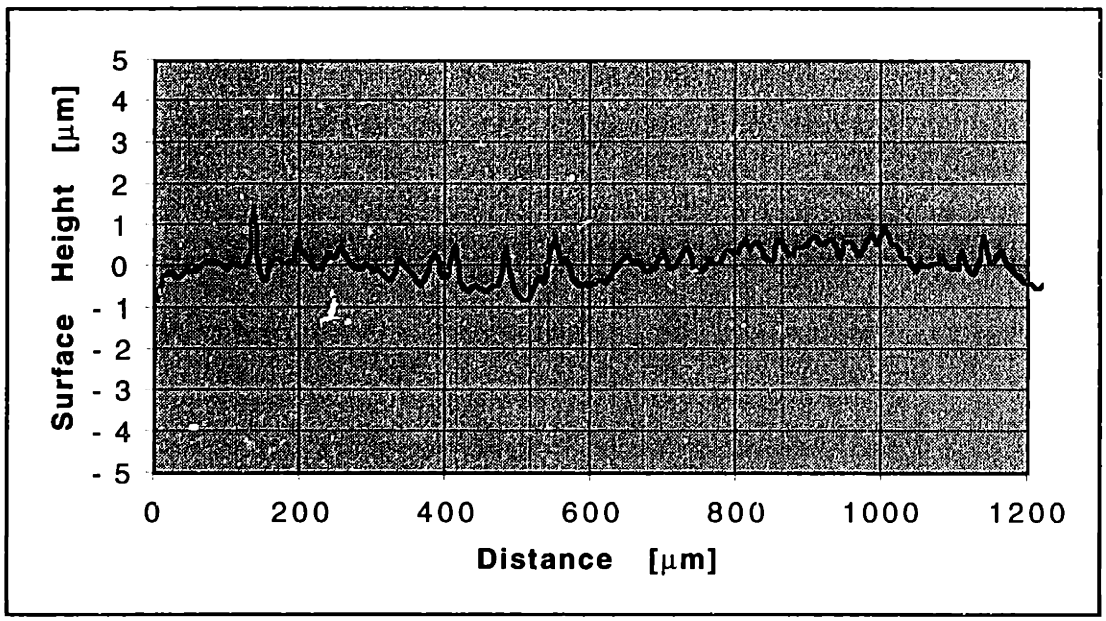

Figure 5.47: Surface finish along an individual printed line in the powder bed

It was discovered that there was a peak-to-peak velocity ripple of about 6% in the fast-axis of the carriage used for printing. This resulted in a wavy surface along the direction of the fast-axis. In order to assess the surface aberration due to the velocity ripple, the surface profile was measured along the fast-axis direction (Scan 4 in Figure 5.37). A profilometer measurement was only possible on powder bed 1 since the amplitude of the aberration was too large to be measured for the other powder beds. Peak-to-peak roughnesses were measured for powder beds 2 and 3 using a calibrated optical microscope. It was noted that although the amplitude of the aberrations along the fast-axis of the three powder beds was different, the frequency of the aberrations was identical. Figure 5.48 shows this velocity ripple surface effect for powder bed 1. As can be seen in the figure, the ripple is about 50 μm peak-to-peak.

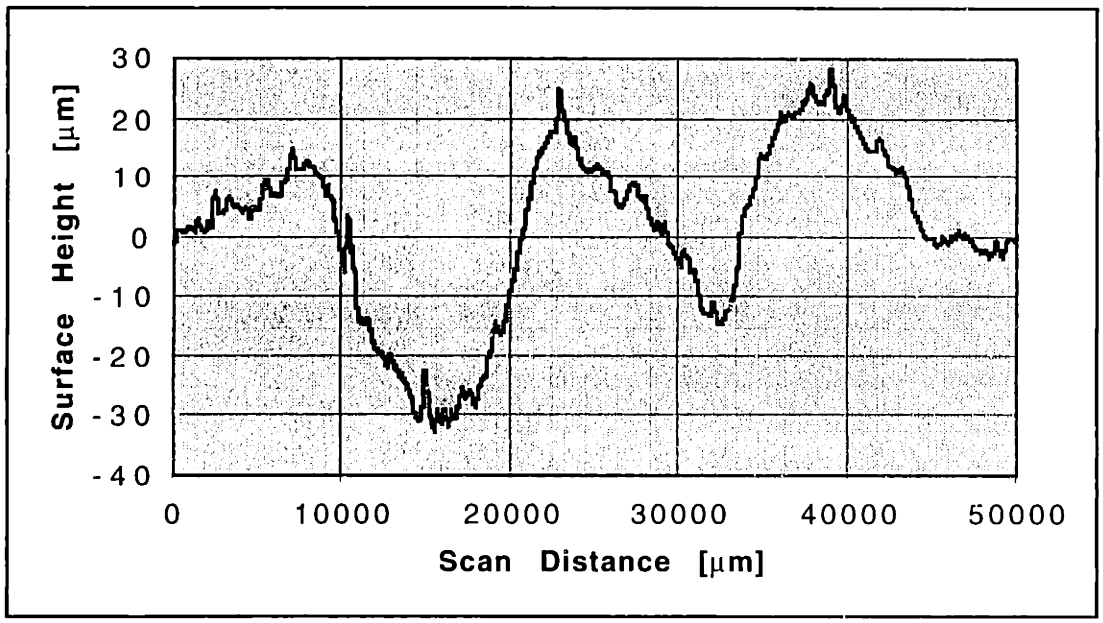

Figure 5.48: Surface aberration along fast-axis direction due to velocity ripple for powder bed 1 (see Table 5.6 for printing parameters)

Using a calibrated microscope, the peak-to-peak ripple was measured to be about 130 μm and 400 μm for powder beds 2 and 3 respectively. Assuming that such small variations in the height can be correlated directly with the velocity ripple, the ripple in velocity is about 4.4%, 4.1%, and 4.7% for powder beds 1 - 3 respectively. The peak-to-peak height ripple along the fast-axis direction as a function of powder bed thickness is shown below in Figure 5.49.

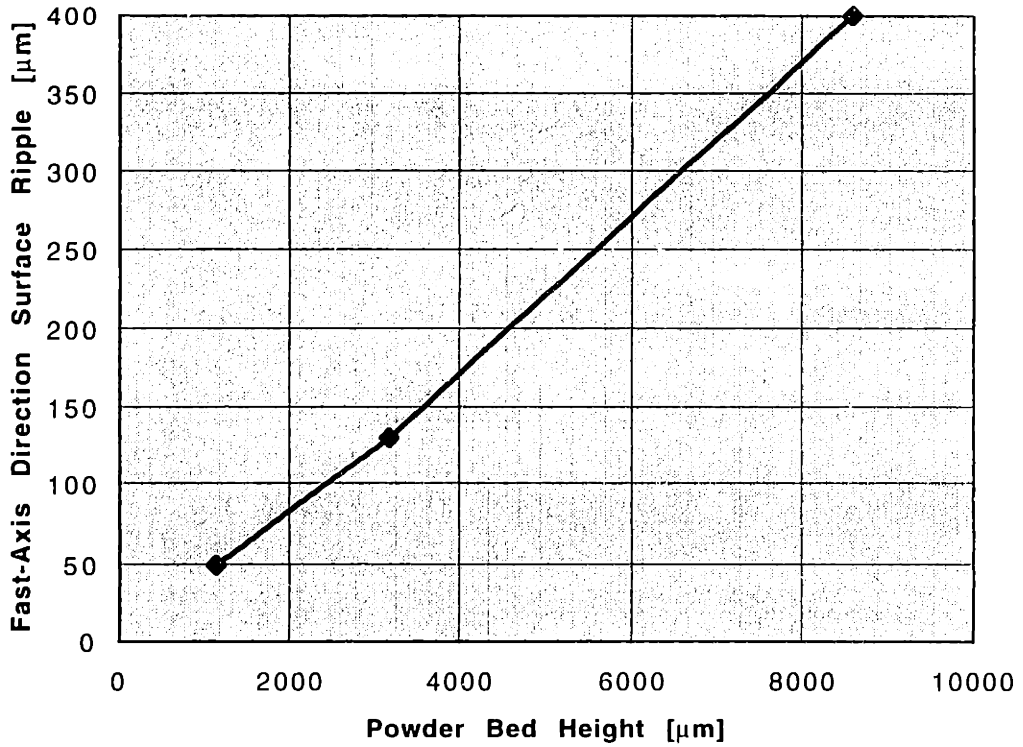

Figure 5.49: Peak-to-peak ripple amplitude as a function of the powder bed thickness

The slope of the line shown in the above figure should correspond to the velocity ripple as well. A best line fit gives a slope of 0.045 (4.5%) which roughly corresponds with the measured velocity ripple of 6%. Although the ripple height is large, it can be reduced considerably by improving the velocity ripple of the fast-axis.

Chapter 6 : Summary and Future Work

6.1: Brief Summary of the Investigation

The 3DP process has been used to create structural ceramic parts by spreading dry powder to create layers. Although fully dense parts have been made using this technique, it has been necessary to use an iso-static pressing step before sintering to achieve fully dense parts. Such a step has many disadvantages such as causing anisotropic shrinkage, warping, and lower part yields due to increased handling. These factors can make the use of 3DP as a manufacturing process for fabricating structural ceramics both technically and economically unattractive. Using the slurry-based 3DP process, the iso-static pressing step can be eliminated by producing green parts with as-printed densities exceeding 50% of the theoretical value. An important part of the slurry-based 3DP process is creating the layers which make up the powder bed using slurries instead of dry powders. Three approaches to fabricating layers using slurry were examined at various levels of detail. These were the repeated tape-casting approach, the spray deposition approach, and the ink-jet printing approach to layer fabrication.

Although the repeated tape-casting approach was not studied very extensively, it had several advantages which might make it worth examining further in the future. The first of these is the fact that layers can be made with an optical surface finish using only a single pass. This means that thick parts can be built relatively quickly compared to the other approaches. The resulting powder beds had high packing density of 60-66% of theoretical (depending on powder size) with pores which can easily be eliminated during the sintering process. The main disadvantage of this method is that tape-casting operations can be difficult to control. One particular control problem is errors in the build height during initiation of layer spreading. The doctor blade velocity will not be constant during startup and this will result in a layer of greater thickness than desired since the slurry will have more time to slip-cast on the surface. Over a large number of layers, this error could become quite significant.

The spray deposition approach was examined in a fair amount of detail. Significant efforts were put into controlling the spray by trying different commercially available nozzles and building dedicated flow controlling equipment. Unfortunately, the reliability and consistency of the resulting spray of the commercially available nozzles does not appear to be good enough to print large powder beds. Besides this fact, the surface finish resulting from spray deposition was considerably worse than that attained using tape-casting or ink-jet printing (although it is still good as compared to spreading dry powders).

From these results, the spray deposition approach does not seem to be a viable candidate for use with the slurry-based 3DP process at this time.

The ink-jet printing approach was also examined in detail. Although similar to spray deposition in some respects since a slurry jet is used instead of a spray, many of the nozzle control problems are eliminated. Large powder beds were printed using the ink-jet printing approach which demonstrated good surface finish and dimensional control. The packing density of ink-jet printed beds is typically 55-62% of theoretical (depending on powder sized used) which is adequate for sintering to full density. Several small parts have been printed by Grau demonstrating the feasibility of this approach for the slurry-based 3DP process.

6.2: Future Work

Although both the ink-jet printing and repeated tape-casting approaches to layer fabrication appear feasible, the fact that ink-jet printing has been actually used to fabricate parts makes it the leading candidate for future work. The repeated tape casting approach does have slightly better surface finish and faster build rates but these advantages could be made insignificant with further refinement of the ink-jet printing method. Ink-jet printing also offers the potential for varying the material composition throughout a layer which is not possible with repeated tape casting.

In order to produce complex parts of significant size using the ink-jet printing approach, several hardware improvements should be implemented. The first of these is that the fast-axis velocity ripple on the machine used to print layers must be minimized. This would help eliminate defects along the fast-axis of the powder bed which have been observed. The second hardware issue which needs to be addressed is slurry jet on/off control. The most feasible approach to solving this problem is to use a mechanical catcher. The challenge with doing this is that the catcher needs to operate between the nozzle tip and the powder bed (about 3 mm). Another hardware improvement which is vital to building large powder beds with good dimensional control is to devise a way to detect problems with the slurry jet. This would allow the process to be immediately suspended if the jet stopped or became crooked while printing a layer. Some kind of optical detector might be able to solve this problem. Again, the challenge here is that the space between the nozzle tip and the powder bed is very limited. A final area which should be investigated is multiple nozzle printheads which would allow faster build rates. The challenge with such printheads is determining how the layer should be stitched together to give a uniform surface finish.

References

Arthur, Tara L., "Factors Limiting the Surface Finish of Three Dimensional Printed Parts", M.S. Thesis, MIT, June 1996.

Chiu, R., "Drying of Granular Ceramic Films", Ph.D. Thesis, MIT, 1991.

Chiu, R., Garino, T.J., Cima, M.J., "Drying of Granular Ceramic Films: I, Effect of Processing Variables on Cracking Behavior", Journal of the American Ceramic Society 76 (9) pp 2257-2264 (1993).

Cima, M.J., E. Sachs, L.G. Cima, J. Yoo, S. Khanuja, S.W. Borland, B. Wu, and R.A. Giordano (1994). Computer-Derived Microstructures by 3D Printing: Bio and Structural Materials, in *Proceedings of the SFF symposium*, pp. 181-190, University of Texas, TX.

Gauckler, L.J., (1988). Processing and Properties of Advanced Structural Ceramics, Ch. 5 in *High-Tech Ceramics*, edited by Gernot Kostorz.

Giritlioglu, Bugra, "The Effect of Print Style on Mechanical and Microstructural Properties of Structural Ceramic Parts Via Three-Dimensional Printing", M.S. Thesis, MIT, September 1995.

Kalpakjian, S., (1992). Manufacturing Processes for Engineering Materials, Addison-Wesley Publishing Company, NY.

Khanuja, Satbir Singh, "Origin and Control of Anisotropy in Three Dimensional Printing of Structural Ceramics", Ph.D. Thesis, MIT, February 1996.

Reed, James S., (1988). Introduction to the Principles of Ceramic Processing, John Wiley & Sons, NY.

Yoo, Jaedeok, "Fabrication and Microstructural Control of Advanced Ceramic Components By Three Dimensional Printing", Ph.D. Thesis, MIT, September 1996.

Appendix A: Research on Fabricating WC/Co Parts Using Spray Dried Powders

Introduction

One of the numerous applications of Three Dimensional Printing is the ability to make tooling for industrial applications. Currently, tooling is produced by 3DP with stainless steel powder. Although this material is adequate for many applications, it is not good enough for situations where high hardness is required such as in cutting tools and dies. Typically, tungsten-carbide tooling is used in these applications. As a result, adapting 3DP so as to allow the printing of carbide tooling would increase the flexibility of the process.

Difficulties With Printing Carbide Tooling

The main problem in adapting 3DP to allow the printing of carbide parts is achieving high green density. Typically, stainless steel parts are first sintered and then infiltrated with bronze to achieve full density. Tungsten carbide parts undergo liquid phase sintering where the part should achieve full density during firing. Infiltration would be undesirable because it would lead to parts with degraded material properties. The problem with liquid phase sintering is that the green parts must have a green density of greater than 50% of theoretical in order to achieve full density after sintering. Also, liquid phase sintering can lead to significant part shrinkage. As a result, it is very important to have carbide green parts of high density to minimize shrinkage and porosity.

First Attempts at Printing Carbide Parts

In order to assess what issues would be important in printing carbide parts, an initial printing attempt was made. A simple bar geometry was chosen for printing to simplify shrinkage measurements and make it possible to use the CPRL hood machine which uses simple masks to control where binder is deposited in the powder bed. The printing specifications for the initial test bars are shown in Figure A.1.

Figure A.1: Initial Printing Specifications

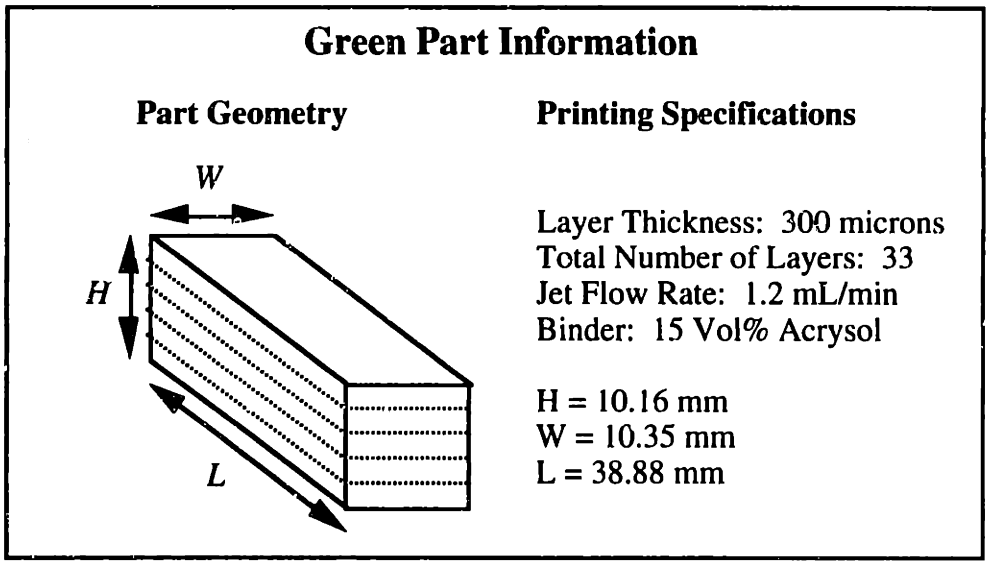

Three powders were available for printing which are listed as follows:

Submicron WC powder

This powder which has an average size of 0.8 microns is not very useful for 3DP because it is not flowable and not easy to spread. Instead it is used for making WC slurries which can serve as a binder for other powders. A picture of the powder is shown in Figure A.7.

WC spray dried VC101 powder

This powder which was supplied by Valenite has the following composition: 9.8% Co, 0.2% VC, 2.0% paraffin wax type R-25, and 88.0% 0.8 micron WC. The theoretical density of this powder is approximately 15 g/cc. This powder is difficult to use since aqueous based binders do not wet paraffin wax well.

WC spray dried VC2 powder

This powder which was supplied by Valenite has the following composition: 6% Co, 2% PEG 2000 wax, 92% 3.0 micron WC. The theoretical density of this powder is approximately 15 g/cc. This powder was produced by Osram-Sylvania. This powder was studied to determine its properties. The following photos in Figures A.2 and A.3 are SEM pictures showing the PEG spray dried granules.

Figure A.2: SEM of VC2 Spray Dried Powder

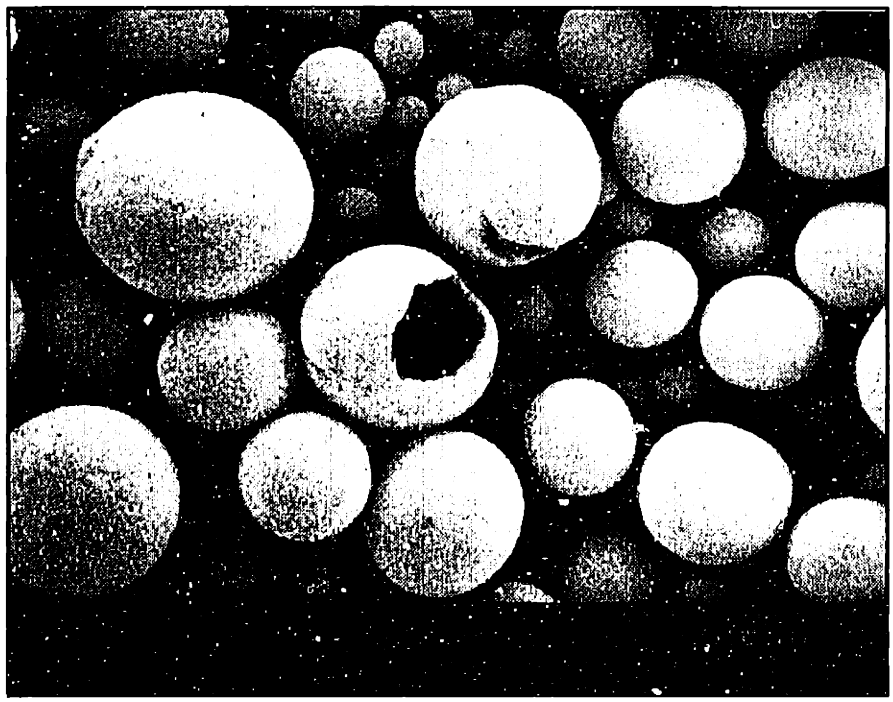

Figure A.3: SEM of VC2 Spray Dried Powder

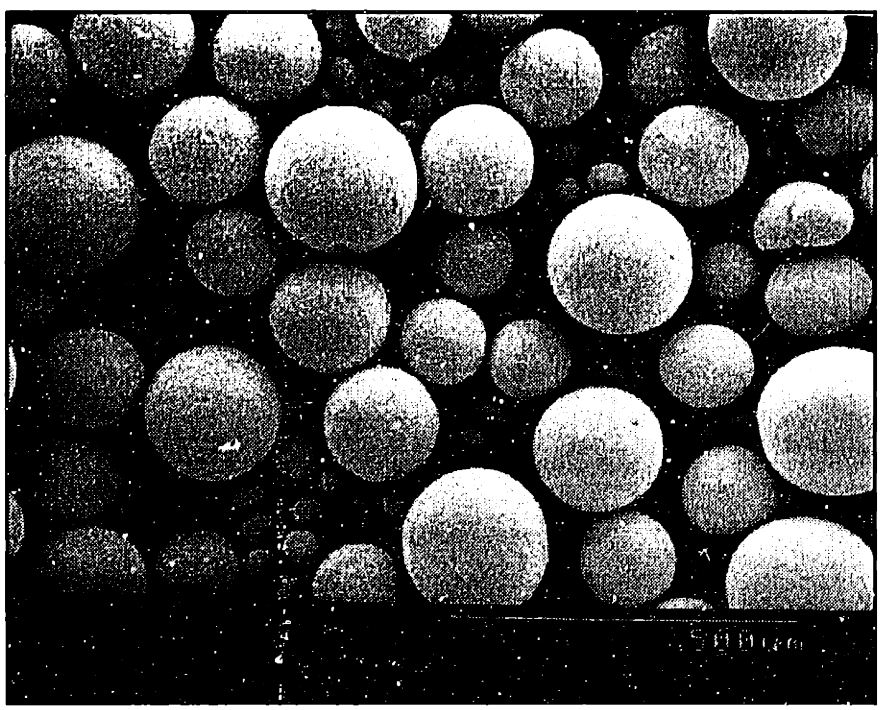

Note the fact that some of the granules are hollow and that there is a great deal of variety in the granule size. It was determined that the granules vary in size from 30 to 300 microns.

Paraffin Wax Spray Dried Powder Printing

It was decided to remove the paraffin wax from the VC101 powder before printing. This helped improve the wettability of the power. This was done by binder burnout in a tube furnace. The powder was heated to 400 degrees Celcius in flowing nitrogen for 6 hours. The nitrogen is important or else the cobalt will react with oxygen at elevated temperatures forming cobalt oxide which is a hazardous material. By checking the mass of the powder before and after the treatment, it was verified that the wax had been removed.

Initial printing attempts on the hood machine proved very difficult with the paraffin wax spray dried powder. Because the wax had been removed, the spray dried granules fell apart when spread. This caused the powder to spread poorly. Using 15 v/o acrysol as a binder, attempts were made to print bars using a 200 micron layer thickness. Whenever it was attempted to spread a layer on top of a previously printed layer, the part was damaged. Because of these problems, printing into paraffin wax spray dried powder was abandoned.

PEG Wax Spray Dried Powder Printing

Working with the PEG powder was much simpler than the paraffin wax powder. Since acrysol will wet the PEG spray dried granules, the powder could be used as supplied. Using 15 v/o acrysol, initial attempts were made to print bars with a 200 micron layer thickness. The PEG spray dried powder spread very well. However, when it was attempted to spread layers on top of previously printed regions, the underlying part was damaged. In order to rectify this problem, it was later determined that some of the spray dried granules were as large as 300 microns in diameter. As a result, this spreading problem was fixed by using a 300 micron layer thickness and by very carefully spreading the powder. Higher and lower concentrations of acrysol were also tried. Higher concentrations of acrysol (20-25%) resulted in too much warping. Lower concentrations of acrysol (5-10%) did not have warpage problems but had low green strength. As a result, 15 v/o acrysol was determined to be the best for the PEG spray dried material system.

Once these printing problems had been solved, several bars were printed using the PEG spray dried powder. The specifications of the green parts is listed below. Note that these measurements were taken after the bars had been removed from the powder bed and allowed to dry. The density of the parts was determined from the dimensions and mass of the bar and as a result, is certainly lower than the true density. When the density is determined in this fashion, it will be termed "apparent density" in this report.

Green Part Information	
Typical Valenite Sintered Density [g/cc]	14.9
Mass (g)	15.657
length (mm)	38.88
width (mm)	10.35
height (mm)	10.16
Apparent Density (g/cc)	3.82
% Sintered Density	0.25

It can be easily seen that the green density of the as-printed bars is well below that needed to achieve full density after sintering. In order to achieve better green density, one of the green bars was cold isostatically pressed (CIP) at 40 kpsi to achieve a higher packing density before sintering. The specifications of this bar is listed below.

CIP Green Part Information	
Mass (g)	15.431
length (mm)	31.75
width (mm)	8.275
height (mm)	7.78
Apparent Density (g/cc)	7.54
% Sintered Density	0.506

With the CIP step, the green density is just barely high enough to sinter to full density. These bars were shipped to Valenite and were sintered to see how close each would come to full density. The sintered parts were then returned to MIT for analysis. The results are shown below.

Returned Part #1 (No processing of green part)

Received 1/12/96

Firing Schedule

Sinter HIPed 45 minutes @ 1440 degrees Celcius

600 psi Argon HIP for 30 minutes @ 1440 degrees Celcius

Returned Part #1 Data		%Change from Green Part
Mass (g)	15.172	-3.098
length (mm)	28.85	-25.8
width (mm)	7.67	-25.89
height (mm)	7.56	-25.59
Apparent Density (g/cc)	9.06942716	136.83

Returned Part #2 (No processing of green part)

Received 1/12/96

Firing Schedule

Vacuum Sintered for 60 minutes at 1440 degrees Celcius

Returned Part #2 Data		%Change from Green Part
Mass (g)	15.229	-2.734
length (mm)	28.88	-25.72
width (mm)	7.76	-25.02
height (mm)	7.62	-25
Apparent Density (g/cc)	8.91779542	132.87

Return Part #3 (Iso-Statically Pressed)		
Received 2/20/96		
Firing Schedule		
Sinter HIPed 45 minutes @ 1440 degrees Celcius		
600 psi Argon HIP for 30 minutes @ 1440 degrees Celcius		
Returned Part #3 Data		%Change from Green Part
Mass (g)	14.814	-5.384
length (mm)	25.78	-33.69
width (mm)	6.75	-34.78
height (mm)	6.35	-37.5
Apparent Density (g/cc)	13.4063925	250.08

After these measurements of the sintered bars were made, the bars were again returned to Valenite for cross-sectioning and polishing to look at the part microstructure and porosity. The following photograph in Figure A.4 shows the cross section of a bar which was sintered without any post processing. This photo is shown at 100x magnification. Large areas of open porosity are clearly visible in this specimen. This can be expected from the fact that the green density was so low.

Figure A.4: Sintered bar without post processing (courtesy Valenite)

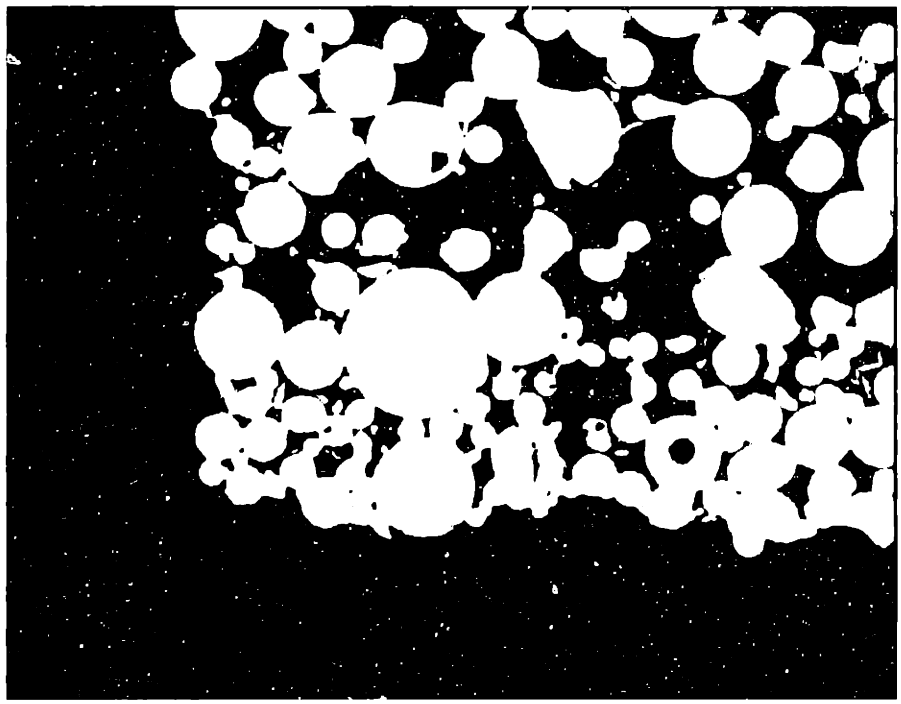

In Figures A.5 and A.6, cross sections of the iso-statically pressed bar are shown at 100x and 1500x magnification respectively. The specimen reveals no open porosity. Stephen Bennet, a research metallurgist at Valenite who took these photos, found this specimen to be excellent in terms of porosity issues. Thus, the apparent density measurement was significantly lower than the true value. This is probably due to the edges of part which are not smooth and the fact that the part geometry was not perfectly rectangular. One concern which was raised was the homogeneity of the microstructure. In Figure A.6, some inhomogeneity is visible. This could be due to the presence of acrysol in the part during sintering.

Figure A.5: Sintered Bar with CIP step at 100x (courtesy Valenite)

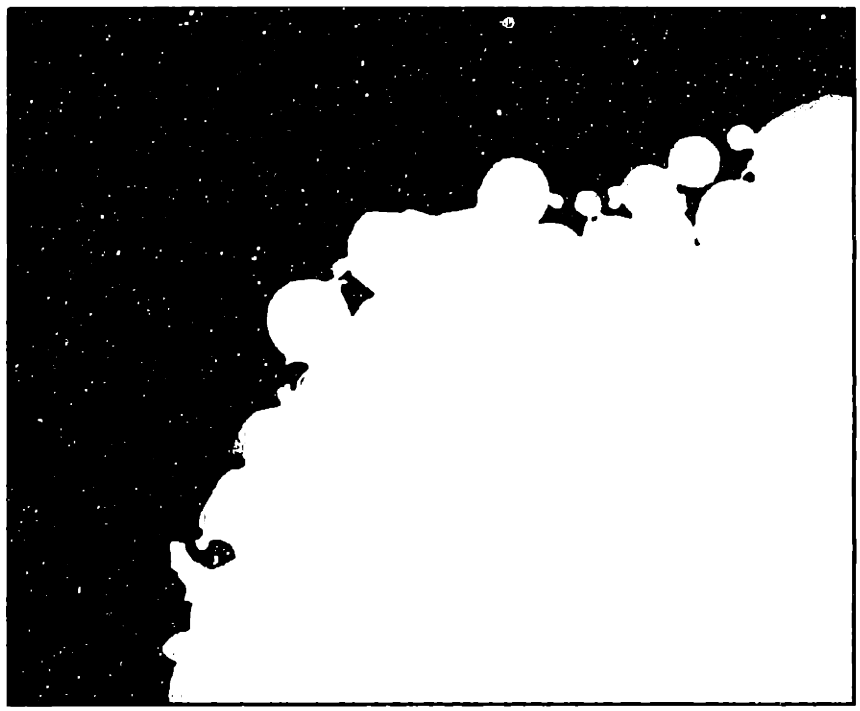

Figure A.6: Sintered Bar with CIP step at 1500x (courtesy Valenite)

Conclusions From the First Printing

There were a couple of important findings in this initial printing of carbide parts with 3DP. First of all, the green density of the bars must be over 50% to achieve full

density. Secondly, iso-static pressing may not be a desirable way of increasing the green density since it results in anisotropic shrinkage during sintering. In fact, Valenite has indicated that they would not want to use this post-processing step in making parts because of the increased costs. Another disadvantage of iso-static pressing is how it affects shrinkage during sintering. The bars which were not iso-statically pressed had very uniform shrinkage. The bar which was pressed did not shrink as uniformly in all dimensions.

As a result, a different printing approach was required to achieve green parts with higher green density. The next idea which was tried was to use a slurry made up of carbide particles which would be printed into the a WC spray dried powder bed. This would allow green parts of higher packing density to be fabricated.

WC Slurries

Making WC slurries and jetting them through a nozzle turned out to be a challenging task. The greatest obstacle in using metallic slurries as a binder is that they easily can clog lines, filters, and the printing nozzles. As a result, any metallic slurry to be used must have very small particles. In order to prevent clogging problems, the slurry must be well dispersed. The dispersability of a material is related to how fast it will fall out of a solution. According to Stokes Law, the settling velocity due to gravity on a particle in solution is given by

$$v = Kd^2(\rho - \rho_O)$$

where K is a constant of the solvent (related to viscosity), d is the particle diameter, $(\rho - \rho_O)$ is the difference between the particle and solvent densities. For fabricating carbide parts, the three materials which could be incorporated into the binder are tungsten carbide, titanium carbide, and tantalum carbide. The density chart below gives some idea of how dense the carbide particles of interest are.

Material	*Density*
Tungsten Carbide	15 g/cm^3
Titanium Carbide	4.9 g/cm^3

All work with metallic slurries was conducted with WC. Since this material has the highest density, it was also the most difficult to disperse. For a first attempt at making binders with metallic particles, 0.8 μm WC powder was added to water and prepared in the following ways:

- •Mixed with a magnetic stirrer
- •Sweeco vibratory mill
- •Sonication with a sapphire horn

To assess how well each dispersing method was able to reduce the size of the particles in solution, two tests were performed: filtering and jetting.

- •Filtering Test: Does the solution go through a 30 μm and a 10 μm nylon filter?
- •Jetting Test: Can the solution be jet through a 70 μm nozzle without clogging?

The filtration test results are listed below for 10 v/o WC slurries

Filtration Test Results for 10 v/o WC Slurries

Dispersing Media	Dispersing Agent dwp%	Dispersing Method	Filtration 30μm	Filtration 10μm	Stokes Diameter
Water	none	Mixed	flows	clogs	~ 20μm
Water	none	Sonicated	flows	clogs	~ 20μm
Water	none	Milled	flows	clogs	
Water	.2% Darvan	Mixed	flows	clogs	
Water	.2% Darvan	Sonicated	flows	clogs	
Water	1% Darvan	Sonicated	flows	clogs	
Water	1% Darvan	Milled	flows	clogs	~ 20μm

Mixed = magnetic stirring

Milled = sweeco vibratory milling (1.5 hours)

Sonicated = sapphire horn (1 minute at maximum intensity)

Filtration = nylon mesh

Later work with such slurries has shown that the milling times and methods used were inadequte. Much better results have been found using ball-milling for periods of 24 hours or more. The results from jetting are shown below.

Jetting Test Setup

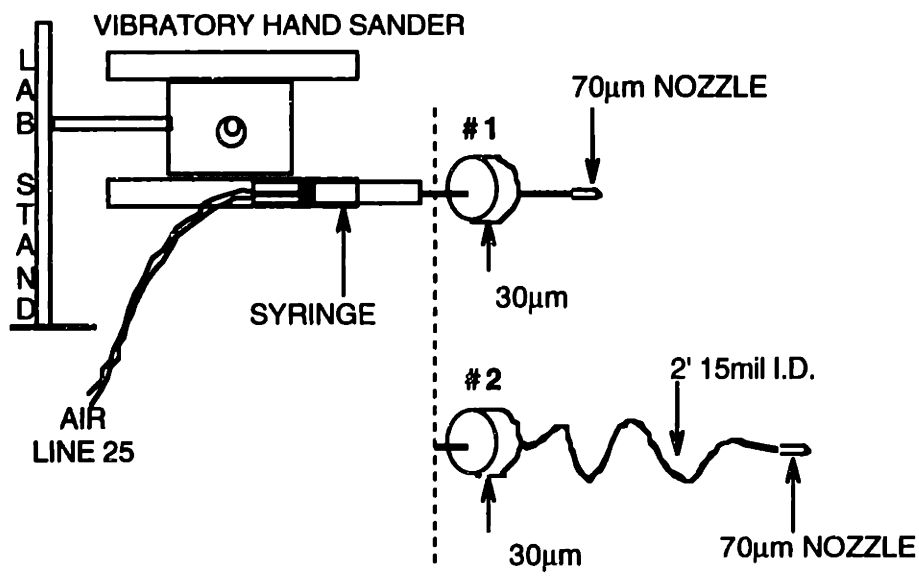

Results for 10 Volume% WC in Water (No dispersant)

Test Setup #1: Able to jet for short periods of time without nozzle clogging
Filter remained clear

Test Setup #2: Able to jet for short periods of time without nozzle clogging
Density of jetted solution was 1.75 g/cc (10 Vol% is 1.67 g/cc)
Filter remained clear

These initial tests were not very successful. Furthermore, when making parts of variable composition, the slurry must have a sufficient amount of metal particle content to significantly change material properties. A target of 40 v/o WC was chosen as the necessary metal particle content. When the jetting test was attempted with 20 v/o WC, both the filter and nozzle clogged almost immediately. This combined with the fact that the solutions were very poorly dispersed led to a search for a new solvent/dispersant system.

In previous work by Bruce Bishop and Richard Adams at the CPRL, silicon carbide and copper powders had been dispersed successfully using heptane as a solvent and OLOA-1200, an automotive crankcase oil additive, as a dispersant. Assuming that the

amount of dispersant required is directly related to the surface area of the powder to be dispersed, the amount of OLOA-1200 dispersant used by Bishop and Adams could provide an estimate for the amount required to disperse tungsten carbide. In order to determine the correct amount of OLOA necessary, the powder properties of the 0.8 micron WC being used was studied. The study included SEM photos of the powder as well as a BET surface area measurement of the powder. A photo of the powder is shown below in Figure A.7.

Figure A.7: SEM Of 0.8 micron WC powder supplied by Valenite

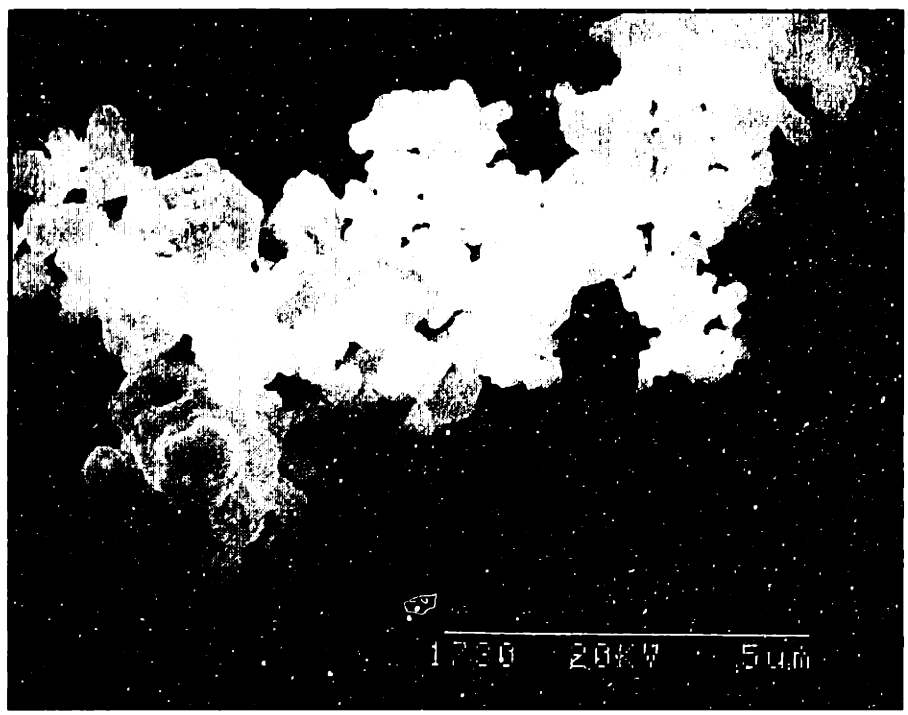

A BET measurement revealed the powder had a surface area of about 1.0 m^2/g. With this data, an estimate of the required amount of dispersant could be made. Although Bishop and Adams did not work with WC, their data could be used to estimate the amount of OLOA needed to disperse WC. Two estimates of the necessary amount of OLOA for WC were made by relating surface area and surfactant concentration used for SiC and Cu powders. Their results and the estimates made for WC is shown below.

Composition of OLOA-1200/Heptane System

Material (powdered)	Surface Area (m^2/g)	Density (g/cm^3)	dwp% OLOA Content
Betarundum b-SiC (Bishop)	18.3*	3.1	2.5
Cerac Cu (Adams)	0.85*	8.9	1.5
Valenite WC 0.8 μm	1.0*	15.0	1.8 (estimate based on Adams) 0.16 (estimate based on Bishop)

*From BET Nitrogen Absorption Test

From these estimates, three heptane/WC slurries were made:

- 5 Volume% WC in Heptane, no dispersant
- 5 Volume% WC in Heptane, 0.16 %wp OLOA-1200
- 5 Volume% WC in Heptane, 1.8 %wp OLOA-1200

As suggested by Bishop and Adams, ball milling was used to mix the solutions. The table below shows the results of this experiment and Figure A.8 shows data from a particle size analysis.

5 v/o WC Dispersions using Heptane and OLOA

Solvent	Dispersant (%dwp)	Dispersing Method	Filtration @ 30μm	Filtration @ 10μm	Stokes Diameter
Heptane	none	Ball-Mill 48 hrs	does not flow		~ 20 micron (stokes)
Heptane	0.16% OLOA	Ball-Mill 48 hrs	flows poorly		~ 8 micron (stokes)
Heptane	1.8% OLOA	Ball-Mill 48 hrs	flows	flows	~ 0.8 micron (Horiba)

Figure A.8: Particle Size Analysis of WC Dispersion

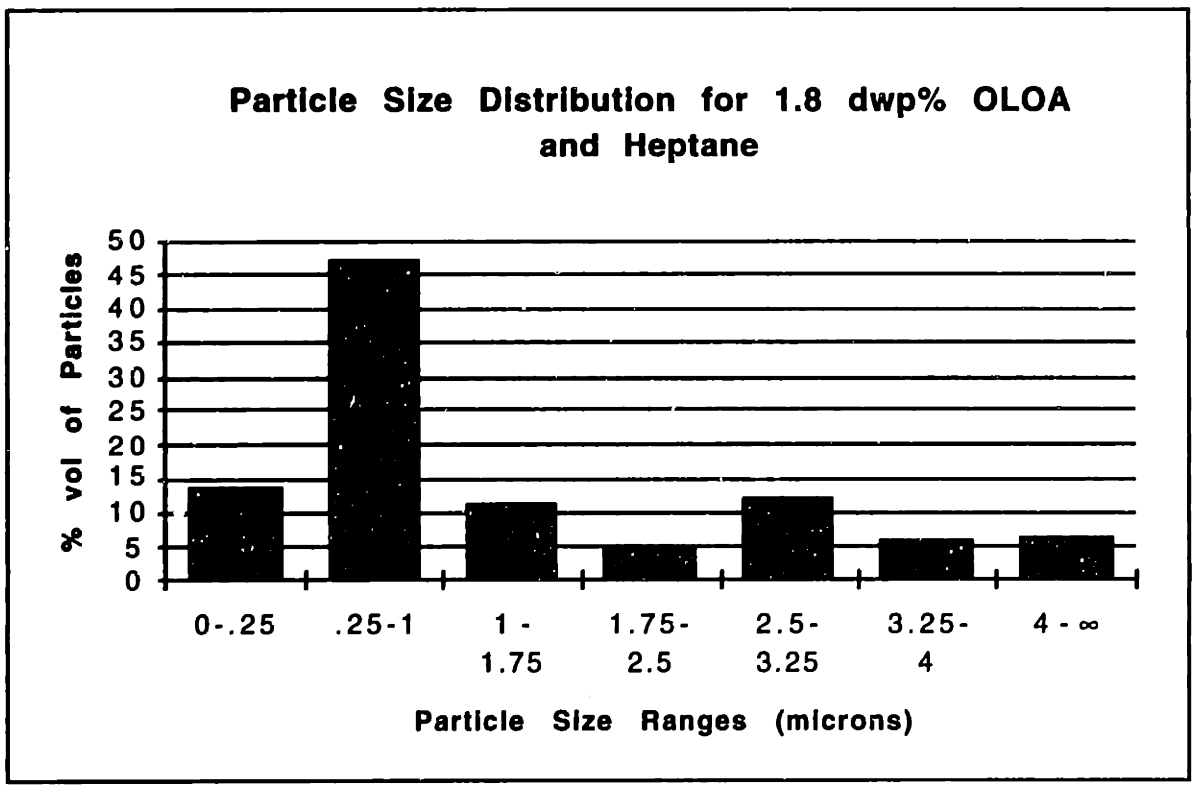

The 1.8 %wp OLOA-1200/Heptane system dispersed the tungsten carbide very well. However, new problems emerged. When the jetting and filtering tests were tried with the heptane, they failed. This was most likely due to the following:

•Heptane attacked plastics in the jetting apparatus
•Heptane was swelling the nylon filter

From these observations, it was pretty clear that heptane was not a good candidate solvent for use with printing since it is a strong solvent which will chemically attack most plastics. This makes it difficult to use on the existing 3DP hardware. Furthermore, heptane needs to be used under a hood since it is both a health hazard and quite volatile.

Search for a New Solvent/Dispersant System

Because using Heptane as a solvent posed some formidable obstacles, several alternative solvent/dispersant systems were considered. Possible candidates were the following:

•Light Mineral Oil and 1.8 dwp% OLOA-1200

•MultiTherm 503 Heating Oil and 1.8 dwp% OLOA-1200
•Water and 1 dwp% Darvan C with Ball Milling
•Water and Ball Milling

Except for the mineral oil which was too viscous to be jetted, the new candidate solutions were prepared at a solids loading of 5 v/o. Then they were tested with filtering and jetting tests. Before jetting, the slurries were pre-filtered using a buchner funnel and a 18 μm stainless steel filter. The results are shown in the table below.

Filtering Test Results

Solution	*18 μm filter and pipet*	*9 μm filter and pipet*	*18 μm filter and buchner*
Water[1]	visible deposits	visible deposits	not tried
Water and Darvan C[2]	easily passes	easily passes	.1 g residue for 50 cc
MultiTherm and OLOA[3]	easily passes	easily passes	.07g residue for 75 cc

[1]Milled 7 days
[2]Milled 3 days
[3]Milled 2 days

Both the water/Darvan C and Multitherm/OLOA systems performed well in the filtering tests. WC and water without a dispersant filtered very poorly. Stoke's diameter measurements of the particles in each slurry were measured and the following results shown in the table below were observed.

Stokes Diameter Measurements

Solution	*Settling Velocity*	*Stokes Diameter*
Water	153 μm/s	4.4 μm
Water and Darvan C	21 μm/s	1.6 μm
MultiTherm 503 and OLOA-1200	interface not visible	n/a

It was impossible to measure the settling velocity of the Multitherm/OLOA slurry because there was no visible interface formation in a reasonable amount of time. After prefiltering each slurry, jetted was attempted. The results for the water/Darvan C jetting is shown below.

Jetting Results: 5 Vol% WC / Water / 1 dwp% Darvan C

Tank Pressure [psi]	Jet Flow Rate [cc/min]	mass WC/slurry volume [g/cc]
12	1.1	.773
25	1.4	.786

Notes: •Average Volume% WC Jetted: 5.2 Volume% WC
•No nozzle clogs over 20 minutes of jetting
•The 30 μm filter was clear after jetting

The fact that the water with Darvan C worked well was surprising since previously there had been no difference between water alone and water with Darvan C. It appears that ball milling is a significantly better way of preparing slurries than sonication, sweeco vibratory milling, or plain magnetic stirring. The question remains if this aqueous based system can be used for higher tungsten carbide concentrations. Recent work by others on the WC material systems suggests that aqueous based 20 v/o WC dispersions are possible.

After testing the water/Darvan C system, the Multitherm/OLOA slurry was jetted. The following measurements were made and are shown below.

Jetting Results: 5 v/o WC with MultiTherm & OLOA

Tank Pressure [psi]	Jet Flow Rate [cc/min]	mass WC/slurry volume [g/cc]
20	0.8	.72
23	0.9	.88
29	1.1	.84
34	1.3	.68
39	1.4	.86
43	1.6	.78
45	1.7	.81

Notes: •Average Volume% WC Jetted: 5.3 Volume% WC
•No nozzle clogs over 55 minutes of jetting using a 70 μm nozzle

•The 30 μm filter was clear

The MultiTherm-OLOA system shows considerable promise as a viable alternative to water based systems. It is non-toxic and does not attack plastics so it could be used in the current alpha machine. Later tests showed that 20 v/o WC slurries using this system can be jetted reliably for hours.

Printing WC slurry into Tungsten Carbide Powder

Once it had been discovered how to jet relatively high concentration slurries of WC for long periods of time, the next step was checking the interactions between the different powders available and the binder (WC slurry). The powder/slurry interactions which were of interest included the absorption time and the strength of primitives formed by the slurry and powder. Both the PEG and Paraffin wax spray dried powders were tested with a variety of binders. Since it is difficult to quantify the strength of the primitives, qualitative strength measurements were made. The results of this test are shown below.

Powder/Slurry Interaction Results

Slurry	PEG WC/Co Powder		Paraffin WC/Co Powder	
	Absorption Time	Relative Strength	Absorption Time	Relative Strength
Water	0.5 sec	weak	does not wet	—
5 Vol% WC in Water	0.5 sec	strong	does not wet	—
MultiTherm	1 sec	very weak	2 sec	very weak
5 Vol% WC in MultiTherm	1.5 sec	strong	3 sec	very weak
20 Vol% WC in MultiTherm	35 sec	very strong	15-20 minutes	weak
35 Vol% WC in MultiTherm	160 sec	very strong	does not wet	—

From this experiment, it appears that paraffin wax spray dried powder is not a good candidate for slurry printing. The paraffin wax powder performed very poorly with low green strength. The PEG spray dried powder demonstrated good wetting properties. It also had good green strength when the WC slurries were used as a binder. As a result,

PEG spray dried powder is currently the best choice for use in printing WC slurries into powder.

Later, an SEM cross section of a large primitive was taken. As shown in Figure A.9, there is a region which is has very few voids. This is a good indication that printing slurry will increase the green density of printed parts.

Figure A.9: PEG Powder and Slurry Primitive Cross Section

Printing Slurry into Powder on the Hood Machine

Using the hood machine, 20 v/o WC slurry was jetted in an attempt to print bars of the same geometry as in the initial printing attempt. Although the jet worked very well and there was little ballistic ejection, the green strength of the layers was extremely low. It was too low to spread layers without damage to the part already in the powder bed. Even with 2, 3, and 4 passes in a single layer, although the green strength improved, it was still inadequate for printing multiple layers. One possible solution to this problem is using acryloids in the slurry as a binder which would do a better job bonding the spray dried granules together.

Increasing Green Density With Granules Which Collapse

An idea which was completely different from the first idea of printing either acrysol or slurry into spray dried powder was to print a solution into special granules which could

collapse on contact with the binder resulting in higher green density. The first attempt at making collapsing granules was to spray dry a heptane/OLOA WC slurry and then print heptane into this powder. The idea was that the heptane should redisperse the WC granules causing them to collapse into high density primitives.

The first step in making WC spray dried granules was to prepare a slurry which could be jet through a nozzle. Furthermore, it was important that amount of OLOA in the slurry was minimized since the OLOA does not evaporate and would remain a part of any granules created. A study was made to determine the minimum amount of OLOA necessary to disperse 5 v/o WC in heptane. Typically, 1.8% dwp has been used when dispersing WC in multitherm or heptane. It was found that the lowest amount of OLOA which could be used was 0.5 dwp%. When less OLOA than this was used, the slurry was unable to pass through an 8 micron filter.

Once the minimum amount of OLOA necessary to disperse WC in heptane was determined, a 5 v/o WC slurry was prepared for jetting (0.5 dwp% OLOA, 5 v/o WC, heptane as solvent). This slurry was then jetted through a 70 micron nozzle using the setup shown in Figure A.11. By directing the jet vertically towards the ceiling, the slurry dried in the air resulting in granules by the time the slurry had reached the floor. These granules were collected and a photo of them is shown below in Figure A.10. The granules were approximately 300 microns in diameter and many of them looked like donuts with a hole in the middle.

Figure A.10: "Homemade" Spray Dried WC Powder

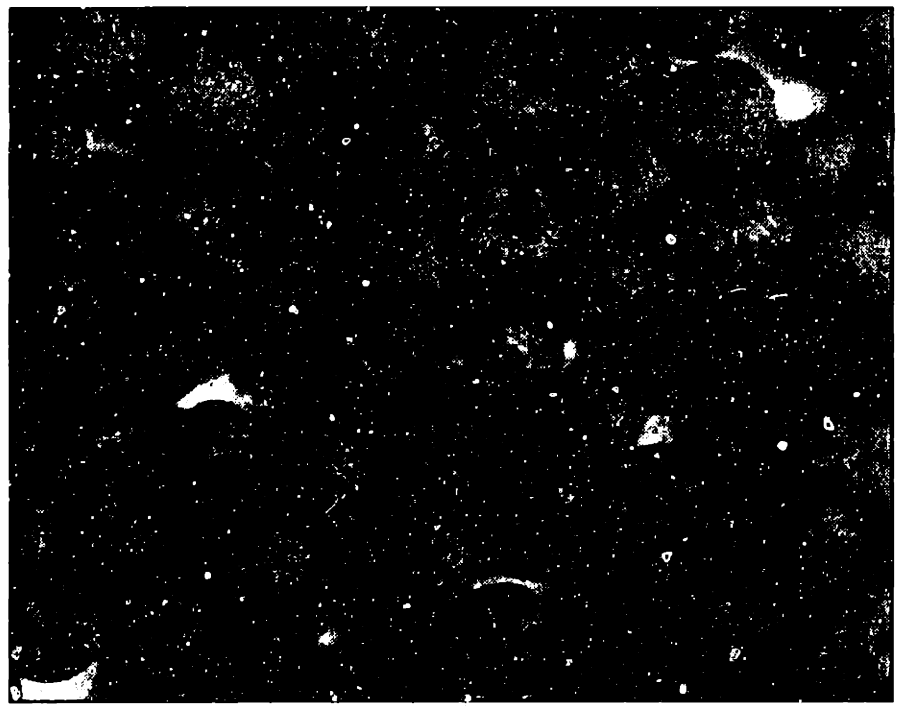

After enough powder had been spray dried, heptane was added to the granules to see if the granules would collapse to provide a higher packing density. Although the heptane seemed to disperse the granules, it did not appear to provide higher packing.

Because the heptane/OLOA spray dried powder failed to create the desired packing effect when the solvent was added, a different binder/powder reaction was needed to collapse the granules. A new idea was to use physical force to try to break apart the granules in hopes that they would then pack to a higher density. The physical force was created by adding a chemical to the powder which would rapidly evolve gas when the binder was added to the powder. In this case, household baking soda (carbonate hydrogen, $NaHCO_3$, specific gravity = 2.159) was added to the WC powder. By using an acidic binder which reacts with the baking soda, gas is evolved which breaks the granules apart. It was hoped that the resulting primitives would then have a higher packing density. Furthermore, the salt formed in the reaction could give green strength to the resulting primitives.

The WC/baking soda powder was prepared in the following manner. First, a slurry consisting of WC, baking soda, and water as a solvent was prepared (5 v/o WC, 2.2 v/o baking soda, 92.8 v/o water). This slurry was then mixed on the ball mill for 24 hours. The resulting slurry was then painted onto glass sheets with a disposable sponge paintbrush and allowed to dry. When the film had dried to the glass, it was scraped off with a razor blade and collected.

To assess how well the WC/baking soda mixture could help increase the packing density, the packing density of different kinds of primitives was measured using mercury porosimetry. The first type of primitive tested was that formed using the WC/baking soda powder and an acid solution. Several acid solutions were tested to see if it caused a strong reaction and resulted in good green strength. Three solutions which were tried were dilute nitric acid, citric acid, and polyacrylicacid (PAA). The table below lists results of combining the different solutions and the WC/baking soda powder.

Results of Acid and WC/Baking Soda Powder Combination

Acid Solution	*Strength of Reaction*	*Dry Green Strength*
Dilute Nitric Acid	Strong	Acceptable
Citric Acid	Strong	Very Weak
PolyAcrylicAcid (PAA)	None	Acceptable

From these results, dilute nitric acid was chosen as the best binder to use since it had a strong reaction with the powder and had some strength after drying. Tests were performed to determine the lowest concentration of nitric acid necessary to effect a strong reaction. The reason for this included both safety concerns and the fact that it is preferable to minimize the amount of non-WC matter in the resulting primitives. After trying a wide range of nitric acid concentrations, it was found that a concentration of 2 v/o reagent nitric acid (the acid was Mallinkcrodt 70.4% nitric acid by mass) in water was optimal. Using this as a binder, primitives were made. For comparison, primitives were also made using water with WC/baking soda powder, and water with plain WC powder. Using mercury porosimetry, the density of each kind of primitive was measured and is listed below.

Density Measurements of Different Powder Primitives

Sample	*Density*
Dilute Nitric Acid & WC/Baking Soda primitive	7.6 g/cc
Water & WC/Baking Soda primitive	7.4 g/cc
Water & plain WC powder primitive	5.8 g/cc

The results of this test are not completely clear. Although adding baking soda to WC powder seems to improve the packing density of the primitives, the mechanism which causes this to occur does not seem to be the evolution of gas when the binder and powder interact because the water with WC/baking soda sample (which produces no bubbles) had

almost the same density as the sample which used nitric acid as a binder (and evolves gas rapidly).

General Conclusions

Two basic methods of creating tungsten carbide parts using three dimensional printing have been identified and explored to some degree at this point. The first method is printing either a polymeric (e.g. acrysol) binder or slurry into spray dried powder. Using acrysol as a binder and iso-static pressing, fully dense parts have been made. However, this method of production is only economically feasible for very special value-added parts which can undergo the CIP process. Such an approach would not be feasible for a high volume manufacturing process.

The second idea which has been explored is that of creating a spray dried powder which reacts with the binder in such a way that the granules collapse to provide a higher packing density. Using mercury porosimetry, primitive packing densities of about 50% have been measured using baking soda as an additive to the WC powder. One problem with baking soda is that the residual baking soda would cause inhomogeneity in the microstructure of the resulting sintered part.

WC Processing Procedures

The following section discusses the procedures related to making slurry, assessing dispersions, and jetting slurry.

Slurry Preparation

In order to prepare WC slurry, the following materials are needed: dispersant (OLOA-1200, Darvan-C, or Duramax), WC milling media, submicron WC powder, a clean nalgene bottle, and solvent (distilled water, multitherm, heptane, etc.).

Dispersants

Several dispersants have been tried so far. For aqueous based slurries, the best choices are Darvan-C and Duramax. Darvan-C slurries have had the most testing and have successfully dispersed WC at concentrations of up to 10 v/o.

For non-aqueous based slurries, OLOA-1200 is the best dispersant. OLOA-1200 is only compatible with non-polar solvents such as multitherm, heptane, hexane, etc. Multitherm based slurries using OLOA-1200 have been dispersed at concentrations of up to about 35 v/o. Multitherm has been used extensively because it does not interact with most materials. It is also non-toxic.

Theoretically, similar results could be obtained for heptane based slurries (heptane has been used to make WC slurries with concentrations of up to 15 v/o). However, heptane is undesirable because it is a hazardous chemical (flammable and carcinogenic) as well as the fact that heptane attacks most plastics and rubbers except for Teflon.

A good rule of thumb for WC slurries as far as the mass of dispersant to use is that it should be approximately 1.5-2.0% the dry weight of the powder being dispersed. This rule is only for WC slurries and is not necessarily the optimal amount of dispersant.

WC milling media

The WC milling media provided by Valenite has been effective in dispersing slurries using the ball mill. When not in use, it should be cleaned and stored in isopropyl alcohol to prevent corrosion. To clean WC media, put the dirty media into a nalgene bottle and put it on the ball mill for a few hours. Every few hours, the dirty IPA should be poured off and replaced. After several cycles, the media should be clean.

WC powder

Valenite has supplied very fine 0.8 micron WC powder for making dispersions. This powder should be handled in a hood to prevent inhalation of the fines.

Nalgene Bottles

Nalgene wide-mouthed polypropylene bottles have been very useful for preparing slurries. A good rule of thumb for picking a bottle size is that the bottle should have at least 2 times the capacity of the slurry to allow room for the media and allow proper mixing. The nalgene bottles are capable of taking quite a bit of abuse on the ball mill. However, they do not hold up well when used with Heptane.

Solvents

The two solvents which have been used extensively are water and Multitherm 503 (Multitherm Corp.). Water based slurries are convenient to work with since they are not very messy. However, water only disperses WC well at low concentrations (less than 10 v/o WC) using a dispersant (Darvan C or Duramax). Furthermore, even these low concentration slurries are unstable and need to be kept agitated.

Multitherm is the other solvent which has been used extensively. It disperses WC very well even at high concentrations and is very stable (the slurries do not require agitation). However, these slurries are messy since Multitherm is an oil (these slurries are very similar in color, consistency, and cleanliness to used motor oil).

Some work has been done using heptane as a solvent. It does as good a job as Multitherm in dispersing WC but reacts with many plastics making it difficult to work with.

WC Slurry Recipe

Once the necessary materials have been gathered, the actual slurry preparation steps are pretty straight forward. The amount of solvent to be used should be measured out and poured into a Pyrex beaker. The dispersant should then be added to the solvent and several minutes allowed for a magnetic stirrer to fully mix the solution until it is homogenous.

While waiting for the solvent and dispersant to mix, the mass of powder to be used should be weighed out. When the solvent is satisfactorily mixed, the powder should be slowly added to the solvent while the stirrer is running. The powder should be added slow enough so dry powder does not float on the surface of the solvent. When all the powder is added, allow the mixture to stir for several minutes.

While the mixture is stirring, fill the clean nalgene bottle which is being used for ball milling approximately 1/3 to 1/2 full of clean, dry WC media (media which was in IPA can be dried in a glassware drying oven). When the slurry is adequately mixed, pour it into the nalgene bottle with the milling media. Make sure the cap is put on tightly and place the bottle on the ball mill.

There are a couple of rules of thumb for using the ball mill. First of all, make sure the speed of the mill is not too high. It should never be so high that the media is unable to tumble in the bottle. Theoretically, there is a maximum ball milling time after which the slurry degrades. In practice, this has never been observed for making WC slurries. The minimum time for water based slurries using Darvan-C or Duramax as dispersants is approximately 24 hours although 72 is more desirable. A week is even better but sometimes impractical. For slurries which use OLOA as a dispersant, 24 hours is usually fine. However, the dispersion improves with longer milling times. Slurries which have been milled for long times (such as a week or more) have been easier to jet and clog less than those which are milled for shorter times. The table below shows slurries which have been tested and how well they succeeded in dispersing WC.

Summary of Solvent/Dispersant Systems For WC Slurries

Vol% WC	Solvent	Dispersant	Dispersing Method	18 micron filter test	8 micron filter test	Jetting Results
5	Heptane	None	Ball Milled at least 24 hours	Clogs	Clogs	not tried
5	Heptane	.16% dwp OLOA	Ball Milled at least 24 hours	Passes	Clogs	not tried
5	Heptane	1.8% dwp OLOA	Ball Milled at least 24 hours	Passes	Passes	not tried
5	Multitherm	1.8% dwp OLOA	Ball Milled at least 24 hours	Passes	Passes	Jets Well
15	Multitherm	1.8% dwp OLOA	Ball Milled at least 24 hours	Passes	Passes	Jets Well
20	Multitherm	1.8% dwp OLOA	Ball Milled 7 days	Passes	Passes	Jets Well
25	Multitherm	1.8% dwp OLOA	Ball Milled 2 days	Passes	Passes	not tried
35	Multitherm	1.8% dwp OLOA	Ball Milled 2 days	Passes	Passes	inadequate pressure to jet
5	Water	None	Ball Milled 2 days	Clogs	Clogs	Clogs
5	Water	1% dwp DarvanC	Ball Milled 2 days	Passes	Passes	Jets Well
15	Water	1% dwp DarvanC	Ball Milled 2 days	Clogs	Clogs	not tried
15	Water	2% dwp DarvanC	Ball Milled 2 days	Passes	Clogs	not tried

TiC Slurries

Several slurries have been prepared using titanium carbide as a solute and Multitherm with OLOA as a solvent. The preparation procedure is identical to that used for making WC slurries. An optimal amount of dispersant has not been determined but 2 dwp% OLOA has been satisfactory. One problem with dispersing titanium carbide is that it is that it is more difficult to break TiC into submicron fines. As a result, the powder tends to have larger particles which do not disperse as readily.

Assessing The Degree of Slurry Dispersion

There are several ways to asses how well a slurry is dispersed. One can perform a stokes settling velocity test, a centrifuge test, or use the Horiba particle size analyzer. The

stokes settling time test is hard to perform and not very repeatable. The centrifuge test is time consuming and only provides indirect results--not absolute measurements. The Horiba particle analyzer also suffers the same problems as the centrifuge tests. Rather than go into detail about tests which have not yielded much useful information, the best test to perform when checking whether a slurry is dispersed or not is too just apply a sample to an 8 and 18 micron stainless steel filter mesh. If the slurry passes through readily without residue, it is safe to say the majority of the particles are smaller than the filter mesh size. This test provides a very quick measurement which can easily provide answers of whether the slurry is jettable or not. It the slurry passes through the 8 and 18 micron meshes without residue (the Multitherm/OLOA slurries will do this), the slurry should be fine for jetting. If the slurry only passes through the 18 micron mesh without residue, the slurry is borderline as far as jetting is concerned. If the slurry passes through neither mesh well, it is highly unlikely that the slurry can be jet reliably through a 70 μm orifice.

Jetting WC Slurry

Jetting WC slurry is somewhat of a magical process. Nozzles can clog constantly and then suddenly run without trouble for hours. As a result, there are only empirical guidelines to follow which come from hours of jetting and attempted jetting. If problems with inexplicable clogging occur, it is best to be willing to try different things and have lots of patience!

Currently the best set up for jetting is shown in Figure A.11 below.

Figure A.11: WC Slurry Jetting Setup

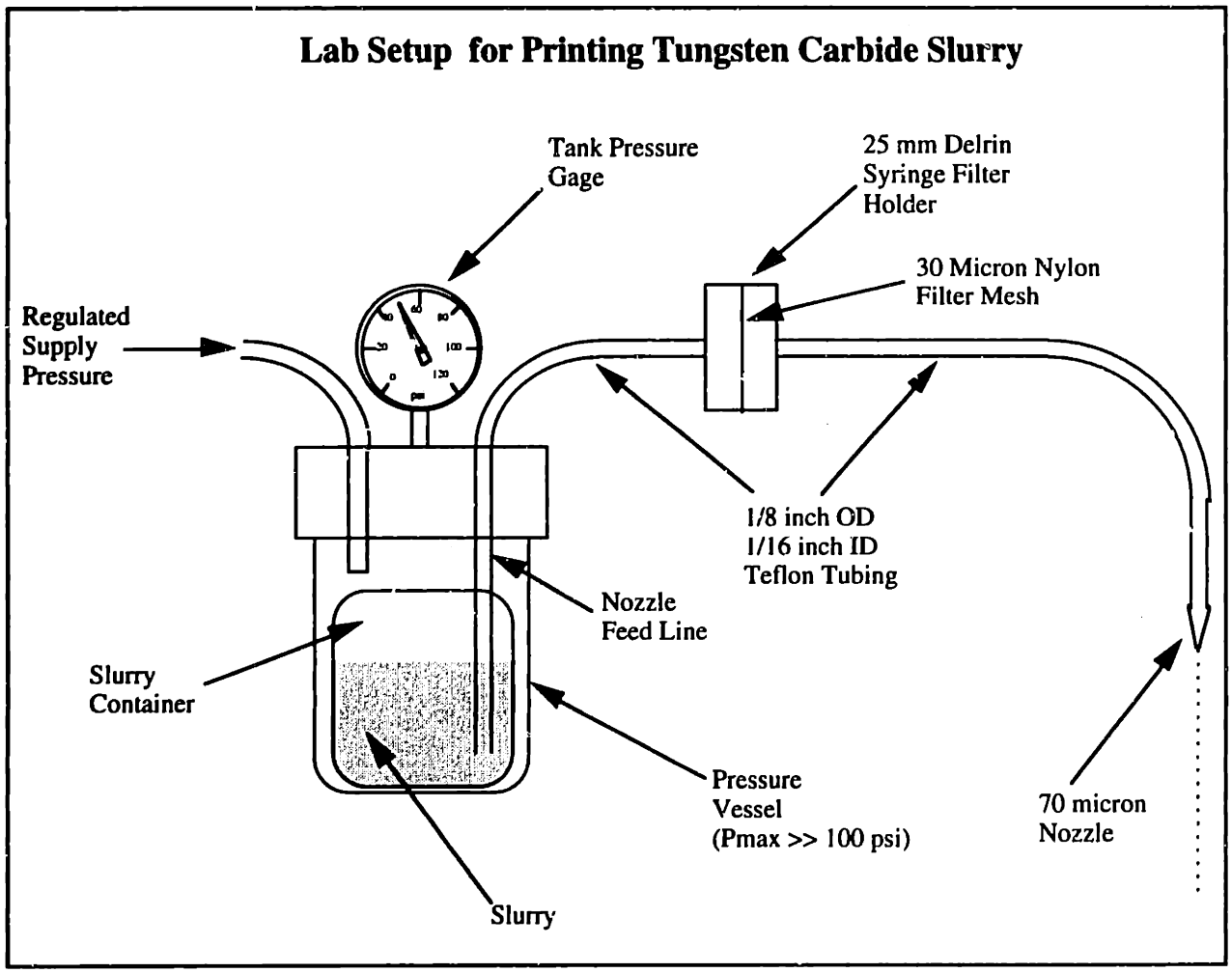

There are four main components to the jetting apparatus: The supply tank, the lines, the filter, and the nozzle.

Supply Tank

The best supply tank to use are the tanks used with the hood machine. A 500 mL bottle filled slurry readily fits inside and the tank can be placed on a magnetic stirrer to provide agitation of the slurry.

Lines

The best lines as far as chemical resistance and cleanability are Teflon lines. Although different sizes can be used, 1/16 ID tubing has been used quite successfully with lure-locks to connect tubing to the filter and the nozzle. Swage lock compression fittings

can also be used with the tubing. They offer better resistance to leaking or failure when high pressures are used.

Filter

The filter is probably the most important component in the jetting apparatus. It is needed to remove agglomerates from the fluid which will always exist. However, it appears that poor filter choice can actually cause agglomerates in the fluid! Quite a few different filter types have been tried including stainless steel sintered filters, stainless steel mesh, and nylon mesh filters. Sintered stainless steel filters have performed very poorly even though they have a very small pore size. They also cause significant pressure drops in the lines. Stainless steel mesh filters have worked acceptably but these filters are relatively expensive. The best success has been with using 30 micron opening nylon mesh filters (25mm diameter) using Gelman syringe filter holders. These are fairly easy to clean and have performed well continuously for hours. However, the filtration question is by no means a settled issue. Any attempted improvements in the jetting setup should include looking at other filtration choices. One thing to try would be to use a larger diameter filter holder.

Nozzle

So far, all successful jetting work has been performed using 70 micron diameter nozzles. Attempts at using 50 micron nozzles have been unable to result in long sustained jetting times.

Jetting Recipe

Again, there are no hard rules for successful jetting. The following notes are only things that have worked in the past. There are almost certainly improvements which could be added to the following procedures.

Before jetting slurry, be sure to use fresh slurry which has just been taken off the ball mill and been sufficiently mixed. Make sure that the filter and filter holder is clean by sonicating them. Also, make certain that all the lines are clean. Before trying to jet slurry, first try running the solvent through the system. After jetting solvent for at least 30 seconds, switch over to the slurry. It is quite normal for the jet to clog almost immediately when doing this. Clear the clog from the nozzle and try the jet again. It sometimes takes several tries before the nozzle starts running consistently. This seems to have something to do with the fact that it takes the filter some time to reach steady state operation. Once the nozzle starts running well, it will typically run long periods of time with no problems (well

over an hour). The best results for jetting have been found with the Multitherm/OLOA 1200 system at concentrations of 20 v/o WC. However, water based slurries using Darvan-C of 5 v/o WC have also been jet for long periods of time.

Whenever shutting the jet off, be sure to immediately flush the lines and filter with solvent. Otherwise, WC particles will agglomerate in the lines causing problems when the slurry jet is turned back on.

Appendix B: Pressure Transducer Electrical Schematic

Below in Figure B.1 is the electrical schematic for the piezo-resistive pressure transducer circuit which was designed. This circuit includes both the current source required to drive the transducer as well as a differential amplifier for noise reduction and signal amplification for the A/D converter of the DAQ board. Rather than build a discrete differential amplifier, the Burr-Brown INA102KP instrumentation amplifier chip was used.

Figure B.1: Signal Conditioning Electronics for the Pressure Transducer

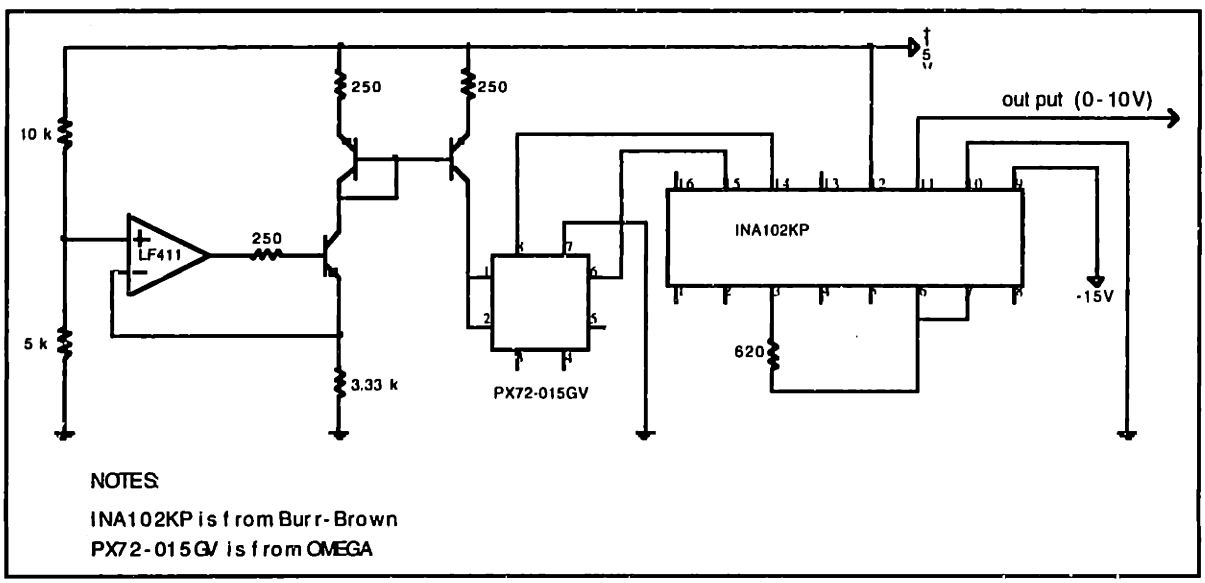

Appendix C: Pressure and Flow Control Performance Assessment

Brief Hardware/Software Review

A closed loop slurry flow control system was designed and built (refer to Chapter 4). This system was necessary to eliminate problems in the spray deposition approach to layer fabrication due to disturbances in the flow rate. Besides giving a steady flow rate, the set-point also needed to be easily set and changed to allow parameter studies. The hardware used included a custom designed electronic pressure regulator (refer to Chapter 4), an electronic mass balance, a pressure transducer, and a PC equipped with a data-acquisition board (DAQ). A schematic of the entire system is shown on the next page in Figure C.1. A digital control algorithm was implemented using Labview. Since the algorithm is fairly basic, the code is not shown here. A copy of the front end user interface for the flow controller is shown in Figure C.2. This appendix reviews the performance of the resulting system.

Figure C.1: Closed Loop Flow Control Schematic

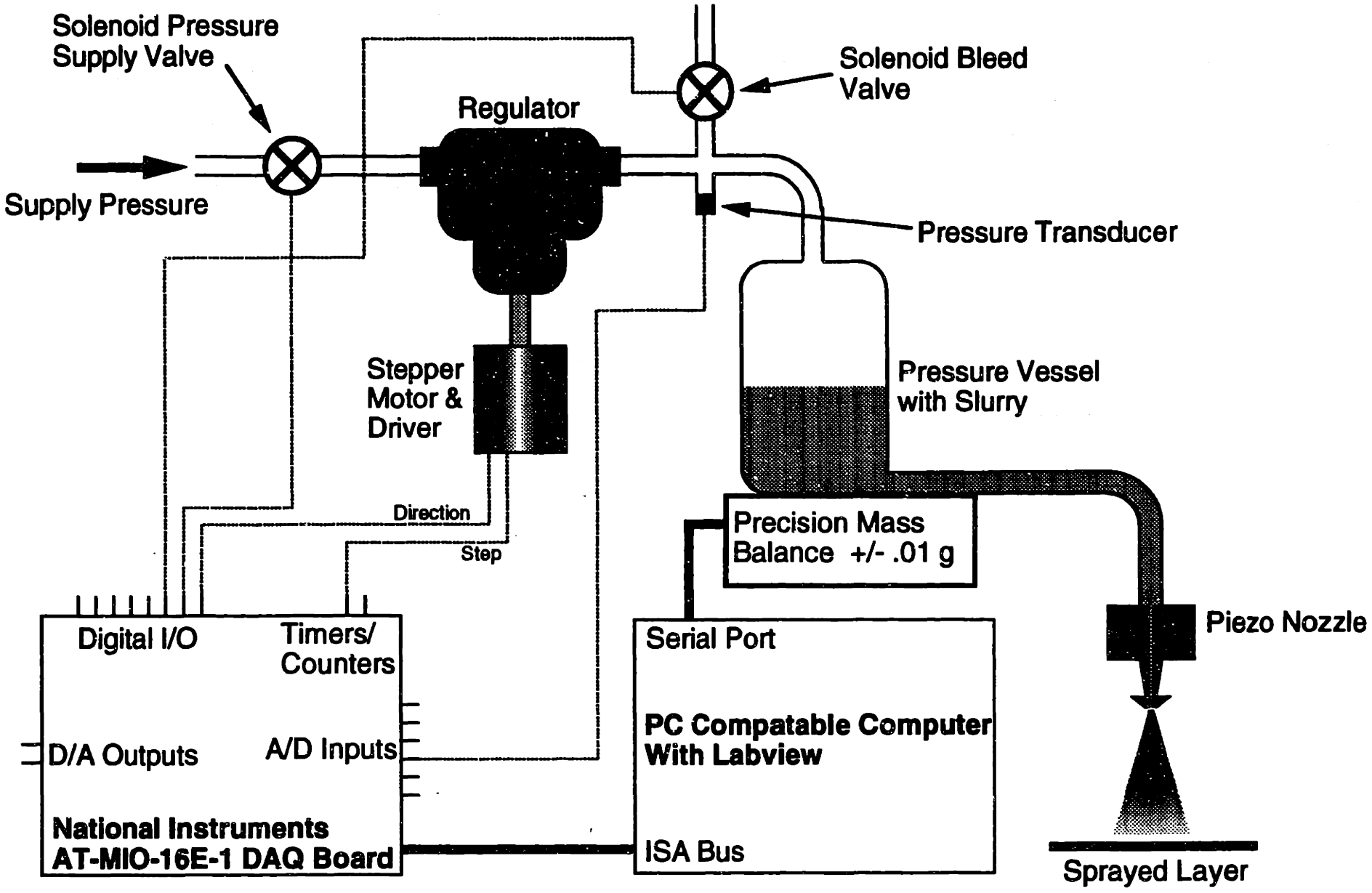

Figure C.2: LabView User Interface for Flow Control

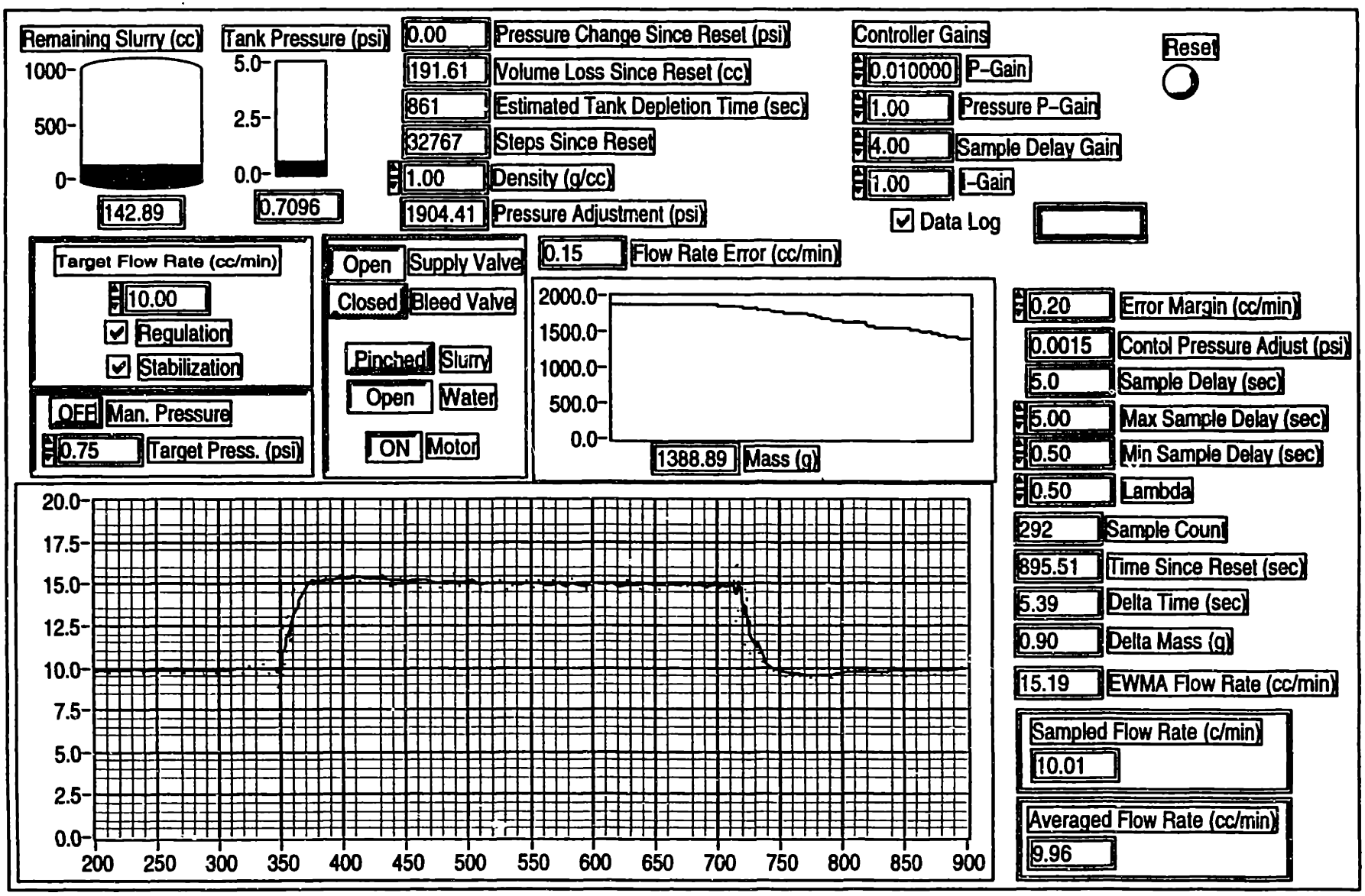

Pressure Control System Dynamic Performance Assessment

In order to make an assessment of the dynamic performance of the pressure control system, the step response was measured. From the step response, several important parameters used to characterize the dynamic response of a linear system can be determined. The parameters of interest here were the rise time, settling time, and overshoot.

In this case, the pressure of nitrogen in an empty slurry pressure vessel with a volume of approximately 1.6 liters was being controlled. The sampling rate of the control loop was set to about 1.6 Hz. Faster sampling times were not possible due to performance limitations of the computer being used. The proportional gain for the pressure controller was set to 1.0. In this test, the pressure command signal was initially set to 2 psi at t=0 seconds. At t=25.5 seconds, the command signal was changed to 4 psi and the resulting dynamic response was measured. The system was then allowed sufficient time to settle. The set point was then changed to 3 psi at t=90.5 seconds. Again, the dynamic response of the tank pressure was recorded. This data is shown below in Figure C.3.

Figure C.3

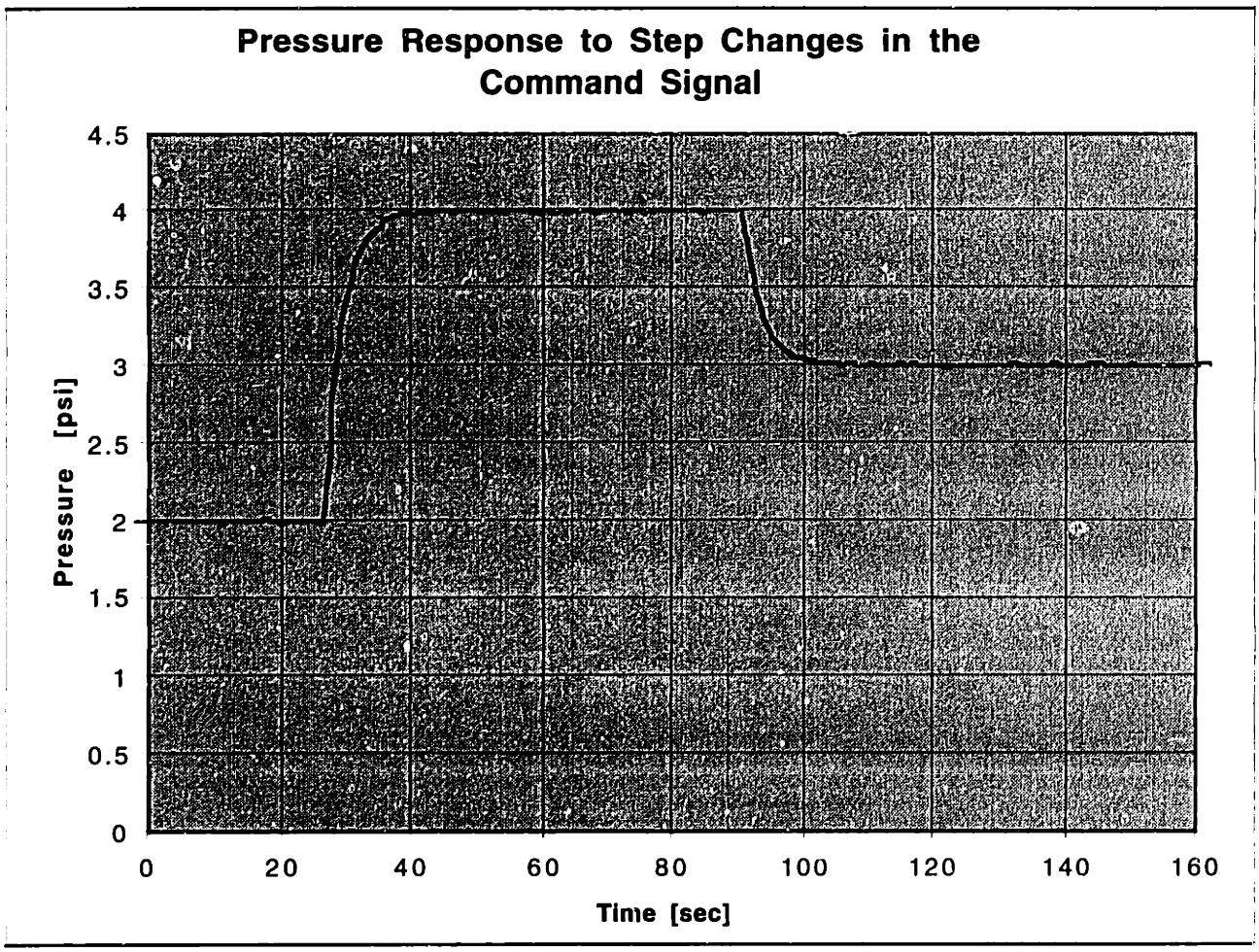

In order to make it easier to assess the step response, magnified views of the step responses from 2 psi to 4 psi (Magnified Step Response #1) and from 4 psi to 3 psi (Magnified Step Response #2) are shown below in Figures C.4 and C.5 respectively.

Figure C.4: Magnified Step Response #1

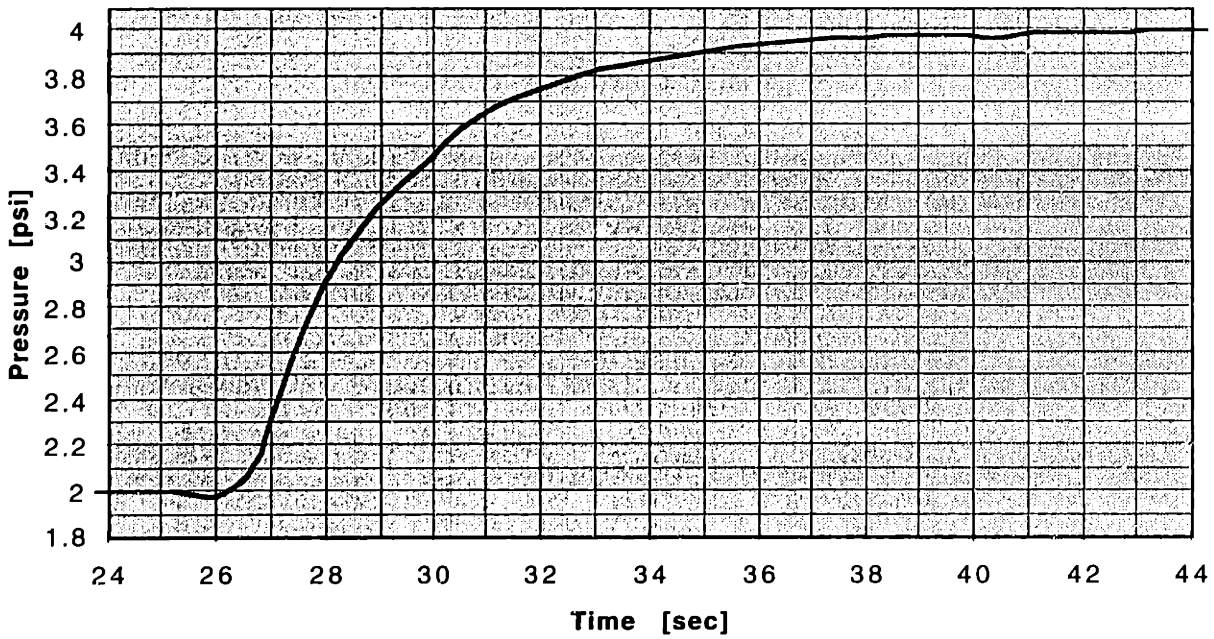

Figure C.5: Magnified Step Response #2

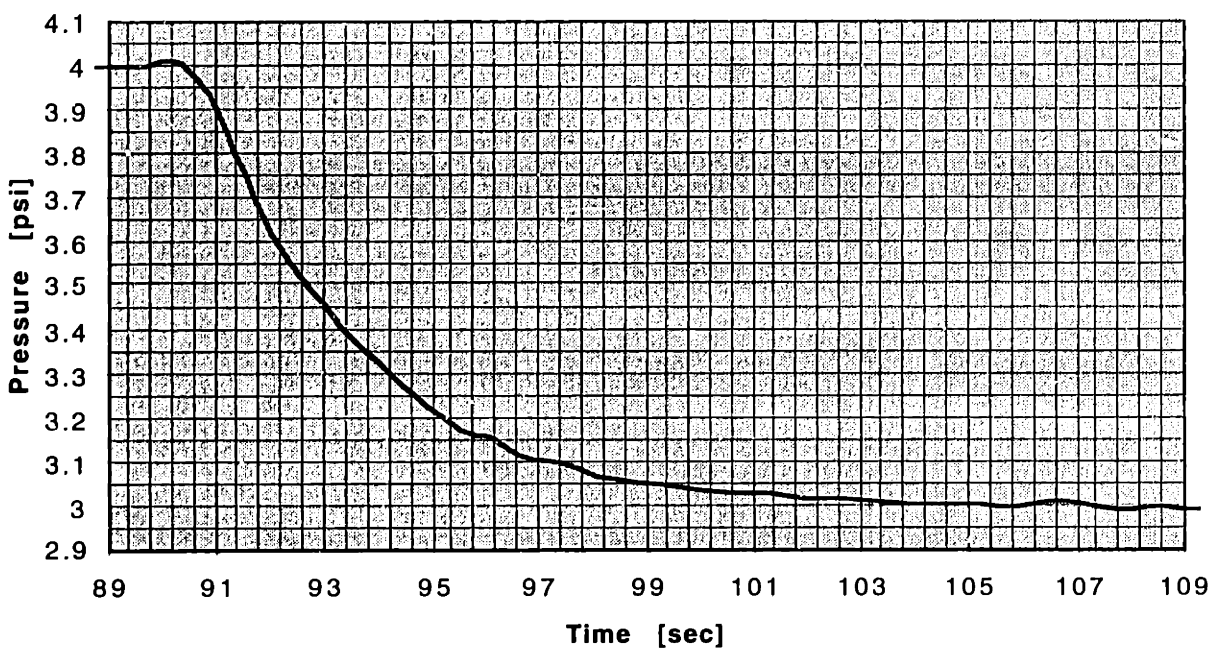

From the step response of a system, several system performance parameters can be determined. Ideally, the magnitude of the step should not have any effect on the performance parameters as long as the system is linear and operates in the small-signal regime (no slew-rate limiting effects). From a qualitative assessment, the behavior of the system is first-order dominant. However, there is some second-order behavior which can be seen in the magnified step response figures. The initial slope of the transient response is close to zero. There is also a small amount of oscillation visible as the response nears steady-state. However, these effects are negligible so the system was treated as first order. It is interesting to note that the system exhibits non-minimum phase behavior. This occurs when the parameter under control (in this case, pressure) initially changes in the wrong direction before asymptotically approaching its steady state value. In both step responses, the pressure can be observed initially changing in the incorrect direction before approaching its steady-state value. Although physically, it is not apparent what is causing this behavior, non-minimum phase systems result when there are zeros in the right half plane of the closed loop transfer function. However, in this case the behavior is fairly benign and was ignored.

Since the system was being treated as first order, the response can be parameterized by the system time constant, τ. The natural (transient) response of a first order system is given by

$$y(t) = Ae^{\left(\frac{-t}{\tau}\right)}$$

where τ is the time constant of the system. It gives a direct measure of how long the transient response of a system will last. The time constant is the amount of time in seconds that it takes the transient response to decay to 36.78% of its initial value. In this case, it is the time for the pressure to reach

$$P(\tau) = (1 - e^{-1})(P_f - P_i) + P_i$$

P_i and P_f are the initial and final pressures respectively. In this case, the time constant was measured to be 3.3 seconds for step response #1 and 3.15 seconds for step response #2. The rise time of the system was also measured. The rise time is the time it takes the transient response to go from 10% to 90% of its steady state value. In this case, the rise time for step responses #1 and #2 was found to be about 5.85 seconds and 5.75 seconds respectively. It is quite common in practice

to estimate the bandwidth of a system from the rise time. The most commonly used rule of thumb relating the bandwidth of a system to the rise time is

$$\text{BW [Hz]} = \frac{0.35}{\text{rise time [sec]}}$$

In this case, the bandwidth of the system is about 0.06 Hz. This basically means that this pressure control system could track a *sinusoidally* changing command signal with a frequency of up to about 0.06 Hz. The bandwidth can also be interpreted as meaning the system can reject sinusoidal disturbances up to 0.06 Hz. In the case of the pressure controller, the main interest is to keep the pressure constant. The last figure which was measured was the 1% settling time. This parameter measures the amount of time it takes the system to settle within 1% of its steady-state value. In this case, the 1% settling time was measured to be about 13.1 seconds and 13.0 seconds for step responses #1 and #2 respectively. A summary of the system performance is shown below in Table C.1 along with averages rounded to the worst case value.

Table C.1: Pressure Control System Response Parameters

Parameter	*Step Response #1*	*Step Response #2*	*Rounded Average*
Time Constant [sec]	3.3 seconds	3.15 seconds	3.2 seconds
1% Settling Time [sec]	13.1 seconds	13.0	13.1 seconds
10-90% Rise Time [sec]	5.85 seconds	5.75	5.8 seconds
Estimated Bandwidth [Hz]	0.060 Hz	0.061 Hz	0.06 Hz

Steady State Performance of the Pressure Control System

The steady state performance of the pressure control system will be set by two factors: the performance of the sensor being used to measure pressure and the ability of the control system to eliminate steady state error.

In the case of the piezoresistive sensor performance and associated signal conditioning hardware, the two important parameters are the sensor resolution and the sensor linearity (no hysteresis data was given by the manufacturer so this was assumed to be negligible). Because the sensor has an analog voltage output, the resolution limit will come from the analog-to-digital (ADC) converter used by the computer to poll the sensor. In this case, the AT-MIO-16E-1 I/O board employed had 12-bit ADC capability over a +10 to -10 V range. This means that the smallest detectable change in voltage is

$$\frac{20\ \text{V}}{2^{12}} = 4.88\ \text{mV}$$

For the PX72-015GV pressure transducer used (from Omega Engineering), the sensitivity was given as 9.5 mV/psi. Obviously, without any signal conditioning, the resolution would be quite poor. With the use of an instrumentation differential amplifier (the INA102 manufactured by Burr-Brown) to reduce noise and to amplify the voltage output of the sensor, the sensor output was boosted to 0.622 V/psi. This means that theoretically, the smallest detectable change in pressure, and therefore the resolution of the sensor and associated ADC is

$$\frac{4.88\ \text{mV}}{622\ \frac{\text{mV}}{\text{psi}}} = 0.008\ \text{psi}$$

The linearity of the sensor was given as ±0.5% of full scale. In this case, the full scale range of the sensor was 15 psi so the maximum error due to non-linearity of the sensor should be 0.075 psi. The non-linearity and other errors (except resolution) associated with the ADC are negligible compared to this and were ignored. From these error sources in the sensor system, the pressure measurement will have a maximum error of about ±.085 psi when properly calibrated. Since the non-linearity of the sensor is the greatest source of error in the pressure measurement, this figure can be improved significantly. The easiest way to improve the performance is to perform a two-point calibration about the region where it will be making measurements. Assuming the sensor exhibits a mild non-linearity, this can reduce the error a great deal. The second way to improve sensor performance is to map the sensor output. This can effectively eliminate errors associated with non-linearity assuming there is minimal hysteresis and drift. The approach of just doing a simple two-point calibration about the region of 2-4 psi was performed. From this, it was estimated that the total error over 0-5 psi was about ±.05 psi. It is important to remember that such an approach will mean that performance away from the calibrated pressures may be considerably worse than the manufacturer specification.

Besides having a good sensor, the steady state performance of the pressure system will be limited by the ability of the controller to eliminate steady state error. Although only proportional control is employed, no steady state-error was measured. A summary of the steady state pressure control system performance is shown in Table C.2 below.

Table C.2: Summary of Steady-State Pressure Regulation Performance

Pressure Range	0-15 psi
Pressure Resolution	0.008 psi
Accuracy over 0-5 psi	±0.05 psi
Accuracy over 0-15 psi	±0.15 psi
Accuracy over 0-15 psi	±0.15 psi
Errors due to the controller	negligible at steady state

Flow Control System Dynamic Performance Assessment

In order to make an assessment of the dynamic performance of the flow control system, the step response was measured. In this case, the liquid being used was water. The sampling rate of the control loop ranged from 1.6 Hz to 0.2 Hz (the sampling rate is set dynamically to help address some resolution problems with the balance). The proportional gain for the flow controller was set to 0.01. In this test, the flow rate command signal was initially set to 10 cc/min at t=0 seconds. At t=45 seconds, the command signal was changed to 15 cc/min and the resulting dynamic response was measured. The system was then allowed sufficient time to settle. The set point was then changed back to 10 cc/min psi at t=413 seconds. Again, the dynamic response of the flow rate was recorded. This data is shown in Figure C.6.

Figure C.6: Flow Rate Reponse to Step Changes in the Command Signal

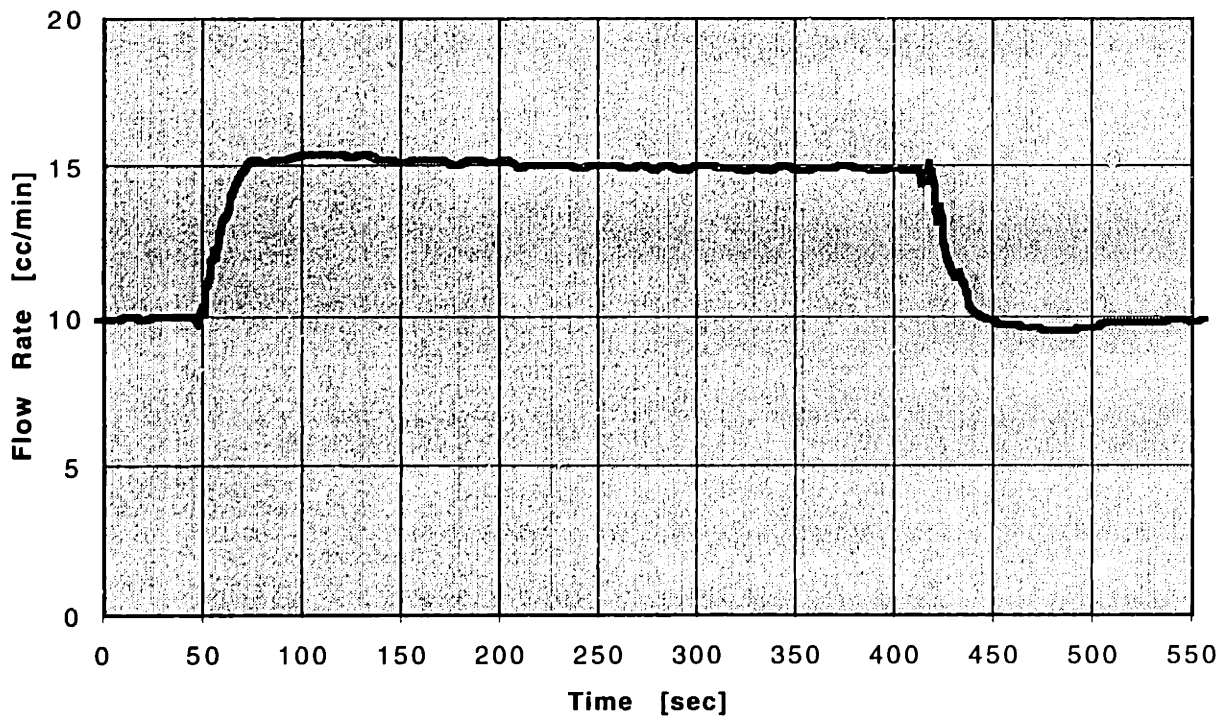

In order to make it easier to asses the step response, a magnified view of the step response from 10 cc/min to 15 cc/min is shown below in Figure C.7.

Figure C.7: Magnified Step Response

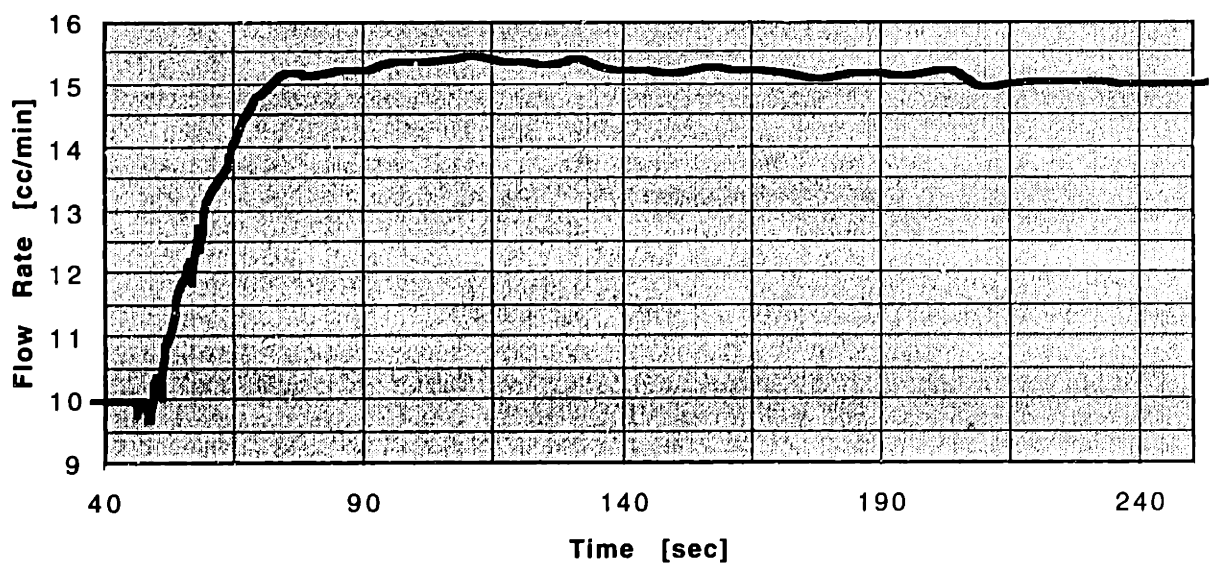

From a qualitative assessment, the behavior of the system is not first order. However, this is expected. Since the pressure control system alone was predominately first order, the dynamics of the transfer function relating pressure and flow rate will clearly introduce new poles to the system. There is a small amount of oscillation visible as the response nears steady-state. Again, the system exhibits non-minimum phase behavior. The response is also marked with a very long settling time.

The 10-90% rise time of the system was measured. In this case, the rise time was found to be about 16.6 seconds. From this, the bandwidth of the flow-rate control system was estimated to be about 0.021 Hz. The percent overshoot of the system was also measured. It was found to be about 8.2%. From the percent overshoot, the damping of the system can be estimated. For a second order system, the percentage overshoot is related to the damping coefficient, ζ, by the following equation:

$$\text{Percentage Overshoot} = 100e^{\left(\frac{-\pi\zeta}{\sqrt{1-\zeta^2}}\right)}$$

With the experimentally measured percentage overshoot value, the damping coefficient was estimated to be about 0.62. This is a reasonable value and is high enough that the system should not easily go unstable. The last parameter which was measured was the 1% settling time. In this case, the 1% settling time was measured to be about 200 seconds. The fact that the settling time performance is so poor is undoubtedly due to the integral action of the controller. This is one drawback of using integral compensation. It can slow down system performance significantly but is necessary to eliminate steady state error. It is important to note that these results are only valid for water or of liquids of nearly the same density and viscosity. Using a different fluid changes the dynamics of the plant and will require different gains to be employed.

Since the main purpose for this controller was to maintain the flow rate at a steady rate, the poor dynamic performance was acceptable. However, there is certainly room to improve the dynamic performance of the controller. The biggest obstacle in improving performance is the low loop sampling time. Unfortunately, this is currently limited by the speed of the hardware (both the balance and the computer) but with better equipment, this problem could be assuaged. Adjusting the integral gain might result in some improvement in the settling time with a possible trade-off in

the rise time or stability of the controller. A summary of the dynamic system performance of the flow-controller is shown below in Table C.3.

Table C.3: Flow Control System Dynamic Response Parameters For Water

1% Settling Time [sec]	200 seconds
10-90% Rise Time [sec]	16.6 seconds
Estimated Bandwidth [Hz]	0.02 Hz
Percentage Overshoot	8.2%
System Damping	0.62

Steady State Performance of the Flow Control System

Like the pressure control system, the flow control system steady state performance will be determined by the controller and the sensor. The steady state performance of the flow control system will again be set by two factors: the performance of the sensor being used to measure flow rate and the ability of the control system to eliminate steady state error.

Unlike the sensor used in the pressure control system where the measurement was relatively straightforward, measuring the flow rate both accurately and quickly is a challenging problem. The largest source of error in the sensor is the limited resolution due to the electronic balance. In this case, the balance used had a resolution of ±0.01 gram. The resolution of the measured flow rate will be

$$\text{Flow Rate Resolution} = \frac{60 \cdot \text{Balance Resolution [g]}}{(\text{Fluid Density [g/cc]})(\text{Sample Time [sec]})}$$

A plot of the flow rate resolution as a function of the sample period for water ($\rho = 1$ g/cc) is shown below in Figure C.8.

Figure C.8

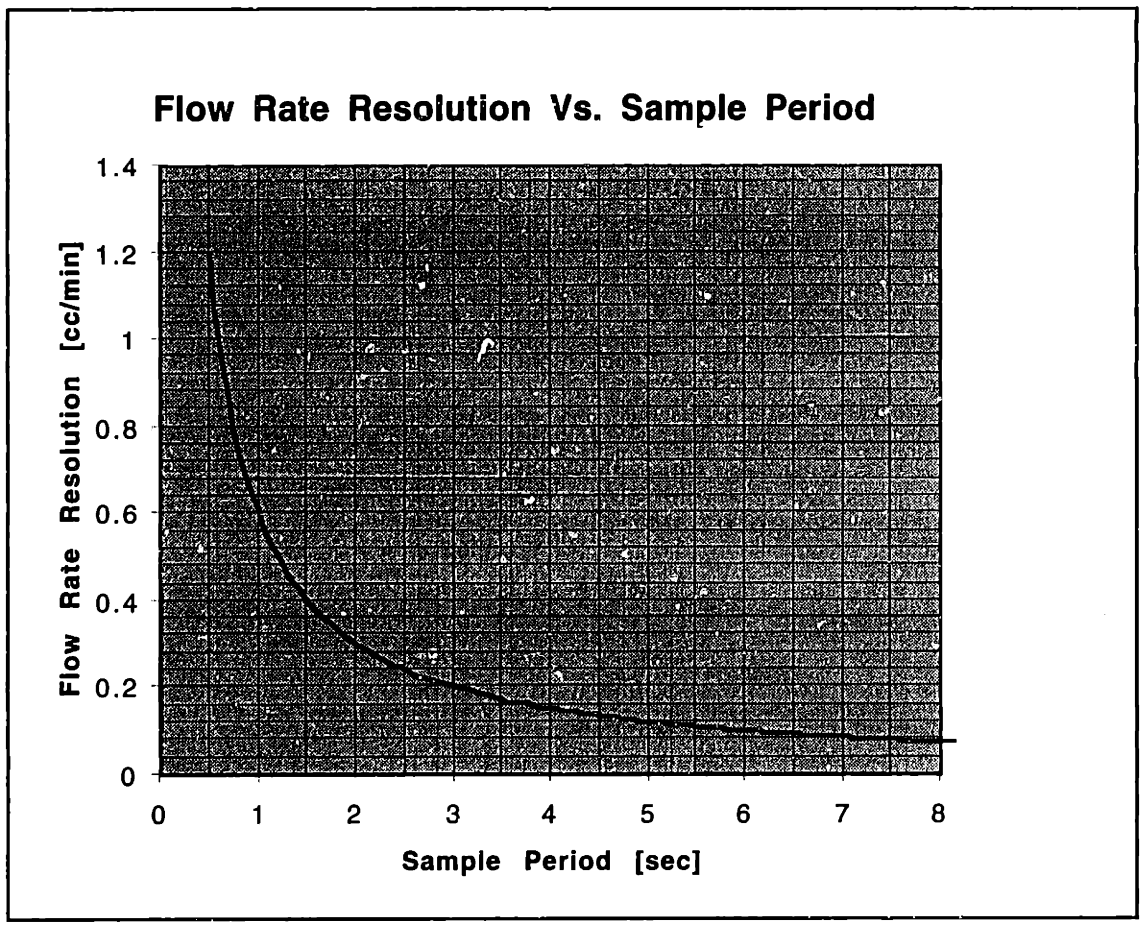

Obviously there is a trade-off between having good dynamic performance which requires a short sample period and good flow rate resolution (long sample period). The approach of dynamically changing the sampling time as discussed earlier was one way of dealing with this problem. The controller was set so that when the flow rate was within 2% of the desired steady state value, the sample period was about 5 seconds (0.2 Hz sampling rate). This provided a flow rate resolution of about 0.1 cc/min. Higher sampling periods did not make much sense since the improvement in resolution drops off rapidly while the ability to respond to disturbances worsens. When the measured flow rate was more than 2% from the set point, the sampling period would be decreased in proportion to the error until the minimum sample period of 0.5 seconds (2 Hz) was reached to improve the dynamic performance. At this point, the flow rate measurements were subject to a resolution error of ±1.1 cc/min. This sizable error could lead to instability or limit cycling if trying to control very low flow rates that are on the same order as the flow rate resolution.

For the flow rate measurement, the other sources of error are hard to quantify. These other errors are noise picked up by the balance which can be due to vibrations in the table the balance sits on, air currents in the room, slurry sloshing around in the reservoir, etc. Although steps were taken to minimize these errors, the flow rate measurement was still subject to random noise from these sources. The plot in Figure C.9 below shows the flow rate measurement data (dots) at steady state and a simple moving average of 4 data points (solid line). In this case, the flow rate is nominally 10 cc/min.

Figure C.9

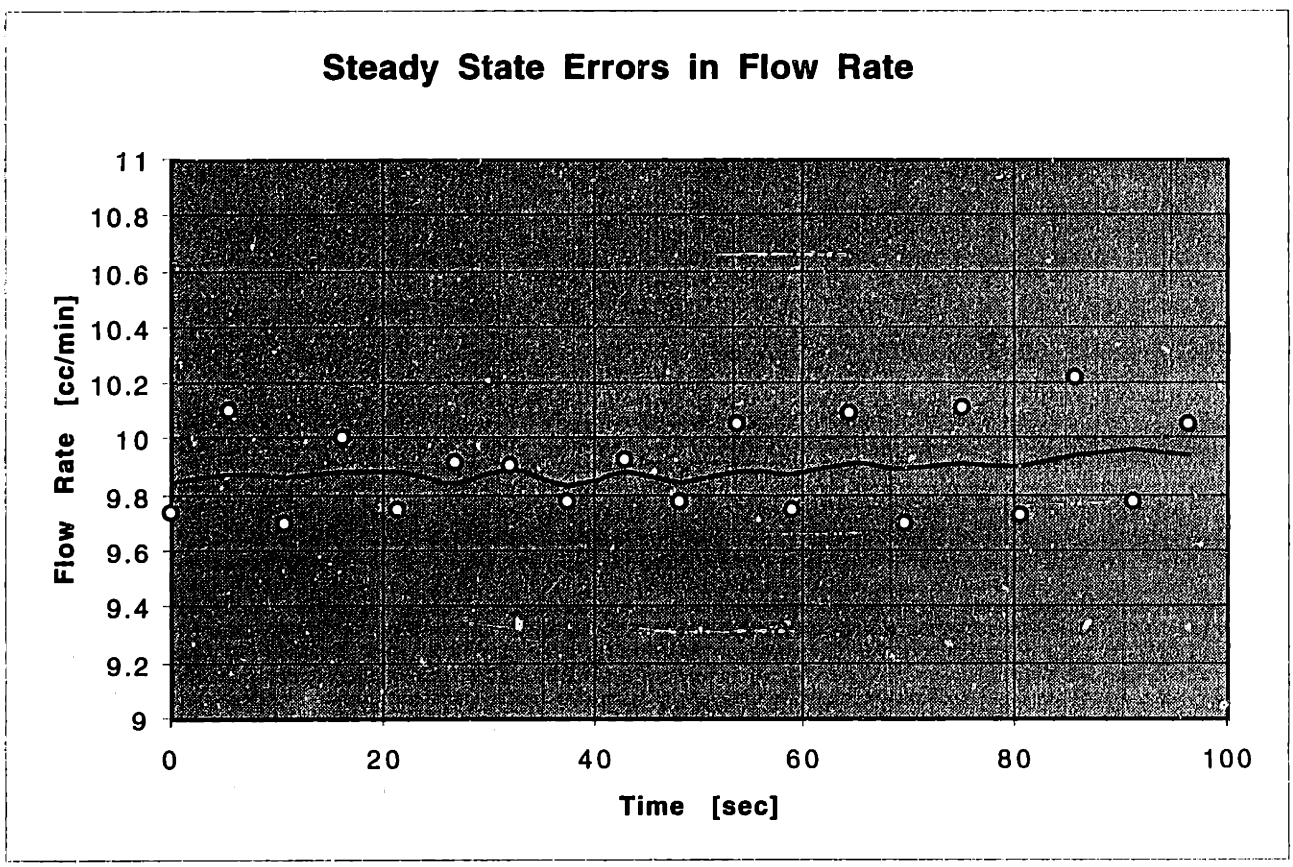

There is some scatter about the apparent mean flow rate which can be smoothed using the moving average. Of course, the moving average also adds a time delay which makes the dynamic response worse. By taking the standard deviation of measurements made during steady state operation, the error due to random noise was estimated to be about ±0.15 cc/min. From this random error and the resolution error, a reasonable estimate for the maximum error in a *flow measurement* at steady

state is about ±0.25 cc/min (note that this has nothing to do with the set-point — just the error in any particular flow measurement).

Despite the use of integral compensation, the flow rate seems to exhibit some steady state error. This may be due to the fact that there are disturbances which are of a higher frequency than the bandwidth of the system (this is quite possible when the bandwidth is 0.02 Hz). In this case, the steady state error will be non-zero but roughly constant.

It is important to note that all the errors in flow rate discussed above were for the case when the flow rate of water is being measured. Fluids with higher density (such as slurry) will actually have smaller resolution errors and noise errors which should be adjusted as follows:

$$E_{resolution} = \frac{\pm 0.10 \text{ [cc/min]}}{\text{specific gravity of fluid being measured}}$$

$$E_{noise} = \frac{\pm 0.15 \text{ [cc/min]}}{\text{specific gravity of fluid being measured}}$$

A summary of the steady state performance of the flow control system is shown below in Table C.4. Again, these values are for water and will have to be adjusted for fluids of a different density.

Table C.4: Summary of Steady-State Flow Control Performance

Flow Rate Measurement & Control Range	5 - 75 cc/min
Absolution Maximum Error in Flow Measurement	±0.25 cc/min (at steady state operation)
Absolute Maximum Error in Flow Control	±0.35 cc/min (at steady state operation)